DA-32

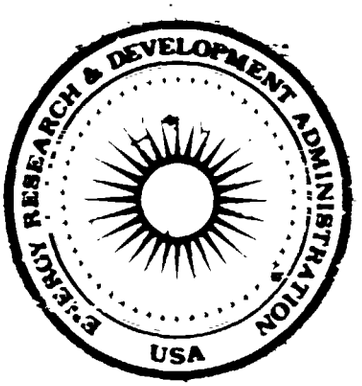

TEC-75/007

HYDROGEN-ENRICHMENT-CONCEPT ?PRELIMINARY EVALUATION

Final Report

Date Published—December 15, 1975

Jet Propulsion Laboratory
California Institute of Technology
Pasadena, California (USA)

UNITED STATES ENERGY RESEARCH & DEVELOPMENT ADMINISTRATION
OFFICE OF PUBLIC AFFAIRS ● TECHNICAL INFORMATION CENTER

NOTICE

Printed in the United States of America
Available from National Technical Information Service, Oak Ridge, Tennessee

Distribution Category UC-96

HYDROGEN-ENRICHMENT-CONCEPT PRELIMINARY EVALUATION

FINAL REPORT

Prepared by:

Jet Propulsion Laboratory
California Institute of Technology
Pasadena, California 91103

December 15, 1975

Interagency Agreement
EPA-IAG-D4-0548
dated May 1974

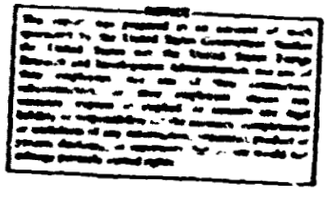

JPL Document 1200-237

EPA Project Officer:

E. Ecklund

This project was initiated by the Alternative Automotive Power Systems Division, Environmental Protection Agency, (now the Transportation Energy Conservation Division, Energy Research and Development Administration) and conducted under Interagency Agreement EPA-IAG-D4-0548.

Prepared for:

U.S. ENVIRONMENTAL PROTECTION AGENCY
Office of Air and Waste Management
Office of Mobile Source Air Pollution Control
Alternative Automotive Power Systems Division
Ann Arbor, Michigan 48105

BLANK PAGE

EXECUTIVE SUMMARY

The Jet Propulsion Laboratory (JPL) has previously investigated the feasibility of supplementing automotive engine gasoline/air mixtures with a hydrogen rich gas in order to permit the combustion of gasoline under ultralean conditions. It is desirable to operate an automobile engine in the ultralean region because the thermal efficiency is increased and the peak combustion temperatures are decreased. Increased engine thermal efficiency leads directly to improved fuel economy, while lower combustion temperatures result in less NO_x formation.

The JPL concept for producing the hydrogen avoids the hazard of carrying stored quantities of the gas in the automobile by generating the desired amount on a demand basis. This is accomplished by using a hydrogen generator in conjunction with a standard IC engine.

The implementation of the hydrogen-enriched fuels concept consists of the addition of a hydrogen generator to an internal combustion engine system (see Figure 1). Some of the fuel normally provided to the engine is diverted to the hydrogen generator. In the hydrogen generator, the fuel is vaporized and mixed with pre-heated air after which it is partially oxidized – i.e., reacted at an overall rich condition – on the surface of a low-cost nickel catalyst. The products of this reaction are predominantly hydrogen and carbon monoxide. Diluent nitrogen from the air also comprises a significant fraction of the product gas. Other products are H_2O, CO_2, and unreacted hydrocarbons. (For a detailed description of the product gas composition, see Table 1, page 37.)

The product gas is mixed with primary fuel and air and is then inducted into the engine. This resulting mixture undergoes combustion in the engine at

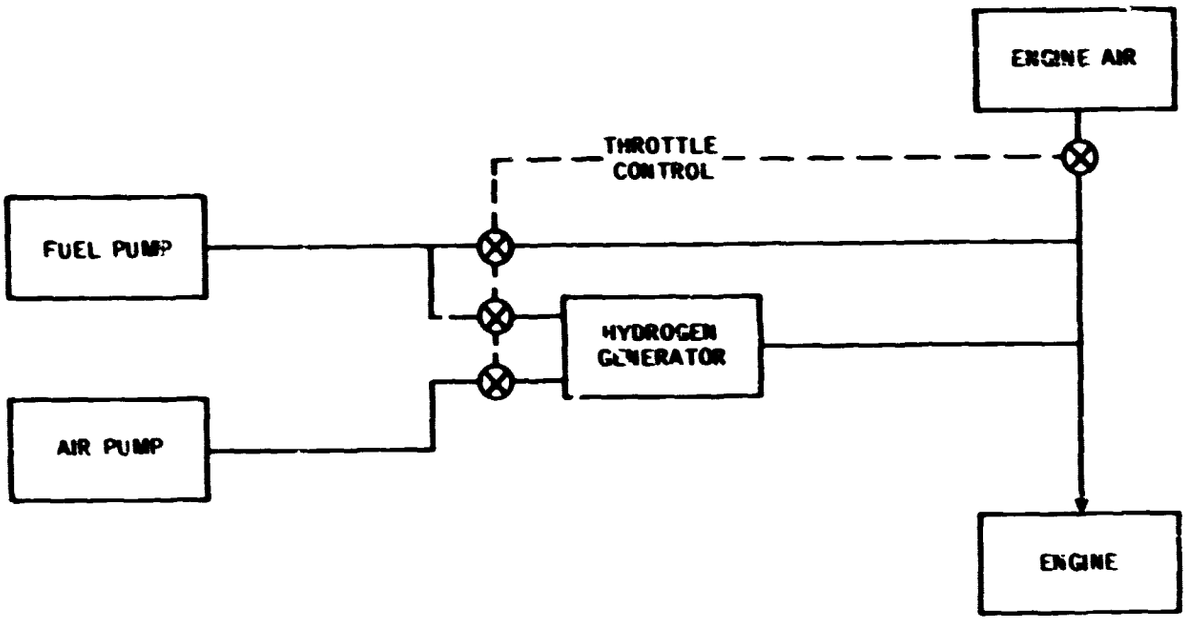

Fig. 1. System schematic

an air/fuel ratio much leaner than that which could be supported by gasoline alone. This ultra-lean combustion is accomplished as a result of the lean flammability limit extension provided by the use of hydrogen in the fuel mixture for the engine.

The results of this ultra-lean combustion are the reduction of NO_x emissions and the improvement in engine thermal efficiency. These benefits are the results of decreased combustion temperatures in the engine which cause:

1) Reduction in the rate of formation of NO_x.

2) Reduction in the heat loss to the engine cooling system.

3) Reduced heat content of the engine exhaust.

4) Reduced energy losses due to dissociation during the combustion process.

Control of the flowrates of fuel and air to the engine and the hydrogen generator is expected to be provided by an electronic controller activated by a driver-operated foot pedal. The complexity of this system is anticipated to be on the same order as that of current production, electronic, fuel injection systems.

The hydrogen enrichment concept requires that a part of the gasoline fuel be used to operate the generator. The total usage of gasoline by the generator and the engine has been shown to be less than an engine operating without hydrogen enrichment because the increased engine efficiency more than offsets the generator-associated losses.

In the current work for the EPA, the JPL system has been evaluated in terms of fuel consumption and engine exhaust emissions through multicylinder (V-8) automotive engine/hydrogen generator tests, single cylinder research engine (CFR) tests, and hydrogen-generator characterization tests. Analytical predictions have been made of the fuel consumption and NO_x emissions which would result from anticipated engine improvements. The hydrogen-gas generator, which was tested to quantify its thermodynamic input-output relationships, was used for integrated testing of the V-8 engine and generator.

Engine (V-8) tests, using gasoline alone as the fuel, were conducted with the stock, carburetted engine and with the engine modified with the Autotronics induction and ignition systems. These provided a well-defined baseline from which to make comparisons. The results of these tests were used to draw contour maps of brake specific fuel consumption (BSFC) and brake

specific emissions as functions of brake mean effective pressure (BMEP) and engine speed (RPM). Tests of the modified engine combined with the hydrogen generator provided data from which similar maps were made for three hydrogen-generator flow rates. Engine operation on the mixture of generator products and gasoline was excellent and generally trouble free. No problems reflecting a safety hazard were encountered. Post-test inspection of the heads, pistons, and intake manifold showed no adverse affects from operation with this fuel mixture.

Tests with a single-cylinder research (CFR) engine were made to evaluate the effect of "leanness of operation" and of hydrogen supplementation on critical compression ratio. Operation at ultra-lean conditions does result in a higher critical compression ratio. This suggests that either a higher compression ratio may be used with the mixed fuels (with an attendant increase in efficiency), or a lower octane fuel may be used at the current levels of compression ratio. This would, in turn, result in some reduction in maximum engine power.

An analytical model of a hydrogen-generator subsystem, consisting of the generator, a compressor, pump and heat exchangers, was used to estimate the additional engine power required to operate this subsystem. These estimates were then used with an analytical model of the combined engine/hydrogen generator subsystem to provide predicted system fuel consumption and emissions performance. The performance of the existing system was predicted and found to compare favorably with that actually observed. The effect on system performance then was predicted for engine improvements that will allow engine operation at a leaner condition and for increased compression ratios.

The Federal Driving Cycle was analytically simulated, and a parametric study of vehicle fuel consumption and NO_x emissions was performed. These studies showed that engine modifications, associated with state-of-the-art hardware and techniques, will result in the hydrogen generator/engine system giving a simultaneous mileage improvement of 26% and NO_x emissions of 0.2 gm/mile when compared to a stock vehicle.

Other significant achievements included determining that the energy content of the generator output stream is sufficient, in very preliminary startup tests, to start the (V-8) engine only 20 seconds after the generator is turned on, and that the systems simulation computer model predicts BSFC within a few percent of measured data.

BLANK PAGE

CONTENTS

CONTENTS (contd)

CONTENTS (contd)

SECTION I

INTRODUCTION

A. PURPOSE AND SCOPE

The Environmental Protection Agency (EPA) has sponsored a critical evaluation of the JPL hydrogen enrichment concept. This evaluation included the characterization of a hydrogen gas generator, the testing of a V 8 automotive engine operated with the gas generator, and an analytical prediction of the performance of an engine/generator system in a 1973 Chevrolet Impala sedan.

To best perform this evaluation, six objectives were established. These objectives were met by completing technical tasks designed for each objective. The entire effort may be divided into two parts: an experimental test effort and an analytical effort. Both are highly interdependent and each of the broad categories are discussed in more detail below.

The experimental effort had three objectives which are listed below. The supporting technical tasks for each objective are also discussed.

OBJECTIVE 1: To determine the input-output relationship of a hydrogen generator and to estimate the engine/generator startup characteristics.

Task (EPA Task A. Complete information on Task A is found in Section II. B. of this report): A characterization of the hydrogen gas generator was completed to determine the generator product composition over a range of generator fuel flow rates and reaction chamber pressures. The operating characteristics for the primary components of the generator subsystem were identified and this information and these data were used to estimate the time required for the generator to produce sufficient chemical energy to start

the automobile (V-8) test engine in a cold condition. Related startup characteristics of the generator, itself, were also determined.

OBJECTIVE 2: To measure the performance and emissions of a multi-cylinder (V-8) test engine fueled by a mixture of gasoline and hydrogen generator products.

Task (EPA Task D. See Section II. C.): An automobile engine mounted in a dynamometer test stand and operated with a gasoline/hydrogen-generator products mixture was used to gather the required (V-8) engine performance data. Continuous emissions data were measured for NO_x, CO and the HC pollutants using emission analysis equipment operated simultaneously with the engine dynamometer.

OBJECTIVE 3: To evaluate the effects of ultra-lean engine operation, resulting from hydrogen addition, on the critical compression ratio.

Task (EPA Task E. See Section II. D.): Tests were conducted using a single cylinder, Cooperative Fuels Research (CFR) engine to evaluate the relationship between critical compression ratio, the degree of lean operation, and hydrogen flow rate.

The analytical effort also had three objectives which are listed below along with a brief discussion of the supporting technical tasks.

OBJECTIVE 4: To develop an engineering definition of the hydrogen-generator subsystem and the operational characteristics of its subassembly components.

Task (EPA Task B. See Section III. B.): A hypothetical hydrogen generator subsystem was synthesized in engineering terms. This subsystem was based on test data generated in EPA Task A and estimated accessory component performance from the technical

literature. The effect of variations in this accessory load on system fuel economy and emissions was examined, using the hydrogen generator/engine model described in objective number five, below.

OBJECTIVE 5: To develop computer simulations of (a) the hydrogen-gas generator subsystem, (b) a combined engine/gas generator, and (c) the Federal Driving Cycle (FDC).

Task (EPA Task C. See Section III. C.): Three computer programs were developed. The first simulated and predicted the loads as a function of generator throughput which would be imposed on a vehicle by the generator subsystem. The second simulated engine/generator combination and predicted both fuel consumption rates and NO_x emissions as functions of engine operating conditions and generator throughput. The third simulated a vehicle being driven over the FDC, and predicted the vehicle performance in terms of gasoline mileage and NO_x emissions per mile.

OBJECTIVE 6: To utilize the computer simulations developed to achieve Objective 5, and to estimate the effects of engine improvements on engine/generator system performance over the FDC.

Task (EPA Task F. See Section III. D.): Data were generated using the engine/generator performance prediction model which, in turn, were used as inputs to the FDC simulation for determining fuel economy and NO_x emissions over the driving cycle. This process was repeated for several alternative engine configurations.

B. TECHNICAL HISTORY

1. Overview

The wide flammability limits of hydrogen make it a unique fuel. Small amounts of hydrogen, when mixed with other fuels, can be used to extend the flammability limits of the mixture. Fuel/air cycle calculations have long indicated that very lean operation of an internal combustion engine would result in improved engine efficiency and reduced emissions of NO_x by reducing combustion temperatures. To achieve these advantages, however, it was necessary that the engine operate at a fuel/air ratio leaner than the lean flammability limit of gasoline. The National Aeronautics and Space Administration (NASA) provided the facilities and sponsored a program to demonstrate by analyses and experiments that the addition of small amounts of hydrogen to gasoline resulted in ultra-lean operation with an attendant reduction of NO_x emissions and improvements in engine efficiency.

The use of molecular hydrogen as a fuel for automotive use has serious drawbacks. No nationwide distribution system for this fuel exists and its storage as a high pressure gas or cryogenic liquid requires vehicle capabilities which do not now exist. To eliminate these difficulties, JPL proposed that the needed hydrogen be obtained from gasoline already on board the vehicle. This would be done in a hydrogen generator in which the rich combustion of gasoline in air would result in a product gas rich in hydrogen plus various residual hydrocarbons, CO, and diluents.

The maximum theoretical hydrogen yield for a hydrogen generator using water, gasoline, and air is 29% by volume. When no water is used, chemical equilibrium calculations indicate that the generator air/fuel mass ratio must be greater than 5 to avoid soot formation. Under these conditions the maximum

theoretical hydrogen yield is 24% by volume. The catalytic generator used for the tests described in this report yields 22% by volume hydrogen without producing soot. This operation is achieved with only gasoline and air as inputs; no water is used. The catalytic generator has a chemical energy ratio of 80%. That is, the chemical energy content of the generator output is 80% of the energy content of the input stream. The remaining 20% is in the form of sensible heat not useful to engine operation. A schematic of the JPL hydrogen generator system currently in use is presented in Figure 1 below, with an explanatory narrative.

The implementation of the hydrogen enriched fuels concept consists of the addition of a hydrogen generator to an internal combustion engine system as

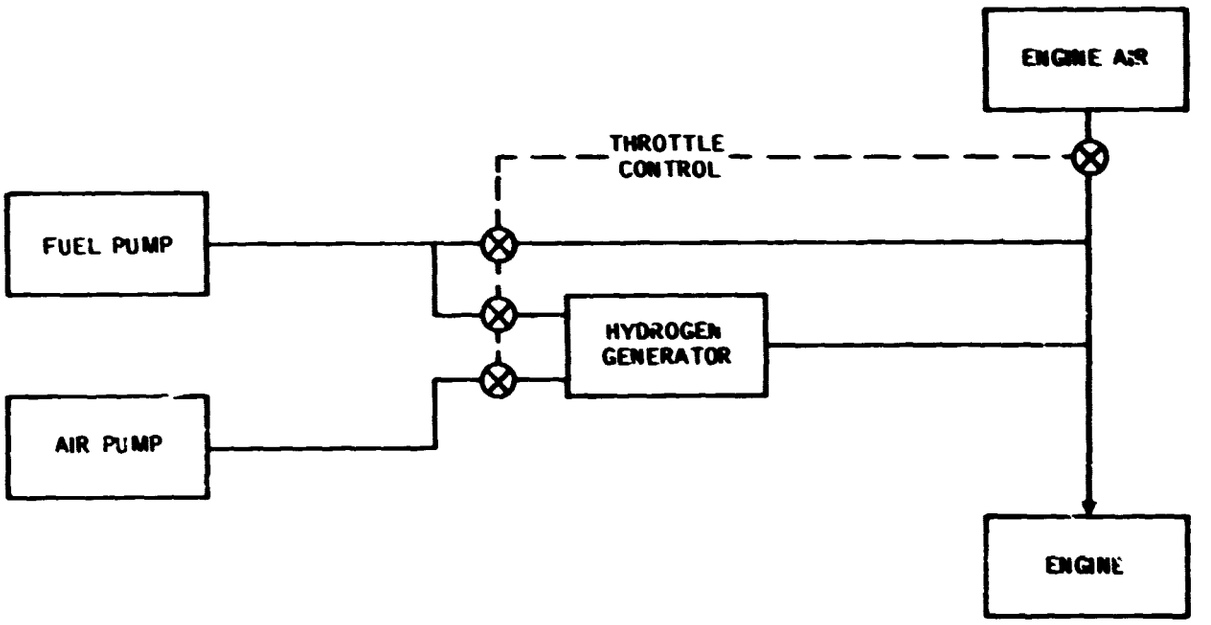

Fig. 1. System schematic

shown in Figure 1. Some of the fuel normally provided to the engine is diverted to the hydrogen generator. In the hydrogen generator the fuel is vaporized and mixed with pre-heated air after which it is partially oxidized - i.e., reacted at an overall rich condition - on the surface of a low cost nickel catalyst. The products of this reaction are predominantly hydrogen and carbon monoxide. Diluent nitrogen from the air also comprises a significant fraction of the product gas. Other products are H_2O, CO_2, and unreacted hydrocarbons. (For a detailed description of the product gas composition, see Table 1.

This product gas is mixed with primary fuel and air and is then inducted into the engine. This resulting mixture undergoes combustion in the engine at an air/fuel ratio much leaner than that which could be supported by gasoline alone. This ultra-lean combustion is accomplished as a result of the lean flammability limit extension provided by the use of hydrogen in the fuel mixture.

The results of this ultra-lean combustion are the reduction of NO_x emissions and the improvement in engine thermal efficiency. These benefits are the results of decreased combustion temperatures in the engine which cause:

1) Reduction in the rate of formation of NO_x.
2) Reduction in the heat loss to the engine cooling system.
3) Reduced heat content of the engine exhaust.
4) Reduced energy losses due to disassociation during the combustion process.

Control of the flowrates of fuel and air to the engine and the hydrogen generator is expected to be provided by an electronic controller activated by a driver operated foot-pedal. The complexity of this system is anticipated to be on the same order as that of current production, electronic, fuel injection systems.

2. Early CFR Engine Studies

The hydrogen enrichment concept was conceived during the course of a series of experiments conducted with a single cylinder CFR engine. In the initial single cylinder CFR engine work, NO_x emissions from various fuels were compared in terms of grams of emission per indicated horsepower-hour produced. Fuel consumption was measured in terms of engine-indicated thermal efficiency, and combustion conditions were expressed in terms of equivalence ratio. Equivalence ratio is the actual fuel/air ratio divided by the chemically correct (i.e., stoichiometric) fuel/air ratio. In these CFR engine experiments, is was shown that NO_x emissions from gasoline could be reduced slightly by lean operation. With gasoline fuel, levels equivalent to the EPA 1978 standard could not be achieved because engine misfire limited the minimum equivalence ratio (ϕ) to about 0.59 (see Figure 2). With hydrogen, however, the engine was operated down to equivalence ratios of ~0.1 where the NO_x emissions were less than 1/100 of the EPA Standard and are approximately equal to the EPA ambient air standard (0.25 ppm). Since the extremely low NO_x emissions achievable by lean combustion with pure hydrogen are not required, it is more practical to use small amounts of hydrogen to extend the operating range for gasoline into the ultra-lean region. It is desirable to limit the amount of hydrogen needed to minimize the hydrogen-generator size and reduce the effect of generator efficiency on overall fuel economy.

Mixtures of hydrogen and gasoline in the CFR engine showed very low NO_x emissions in the ultra-lean region. Carbon monoxide emissions were measured and found also to be below the EPA 1978 Standards, as long as adequate quantities of hydrogen were used to avoid misfire. As discussed in Section II.C., Concluding Remarks, the favorable CO results were not

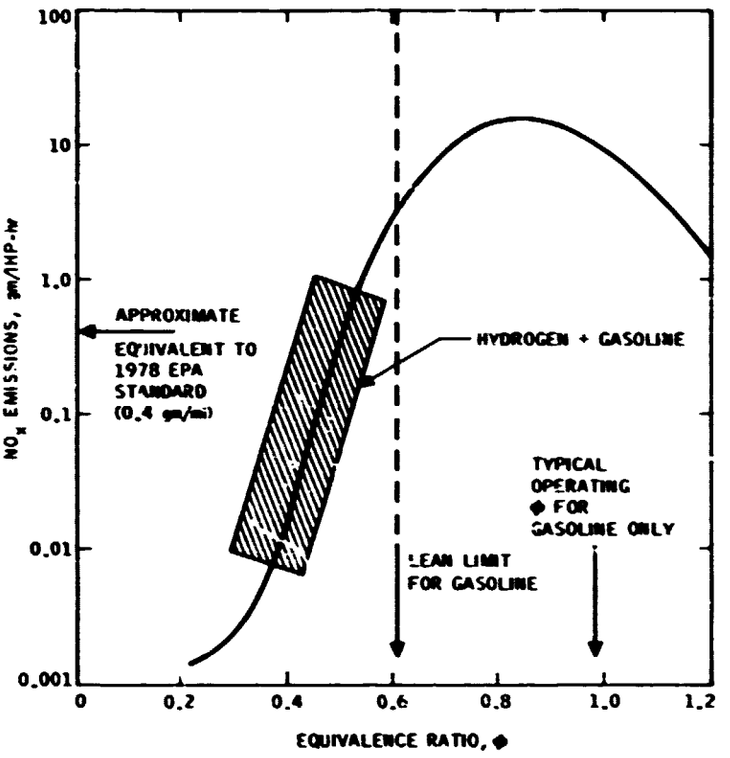

Fig. 2. CFR NO_x emissions vs equivalence ratio, ϕ

duplicated when the V-8 engine was operated with generator products. Apparently, the CO in the generator product stream is the source of the engine CO emissions. Hydrocarbon emissions were measured and found to be above the EPA 1978 Standard.

The CFR studies further indicated that engine thermal efficiency was inversely related to equivalence ratio as predicted by theory. This is illustrated in Figure 3.

Thermal efficiency increases of approximately 40% (from about 0.23 for conventional systems to about 0.33 for hydrogen and gasoline mixtures) were indicated from these studies. Increased vehicle fuel economy is directly

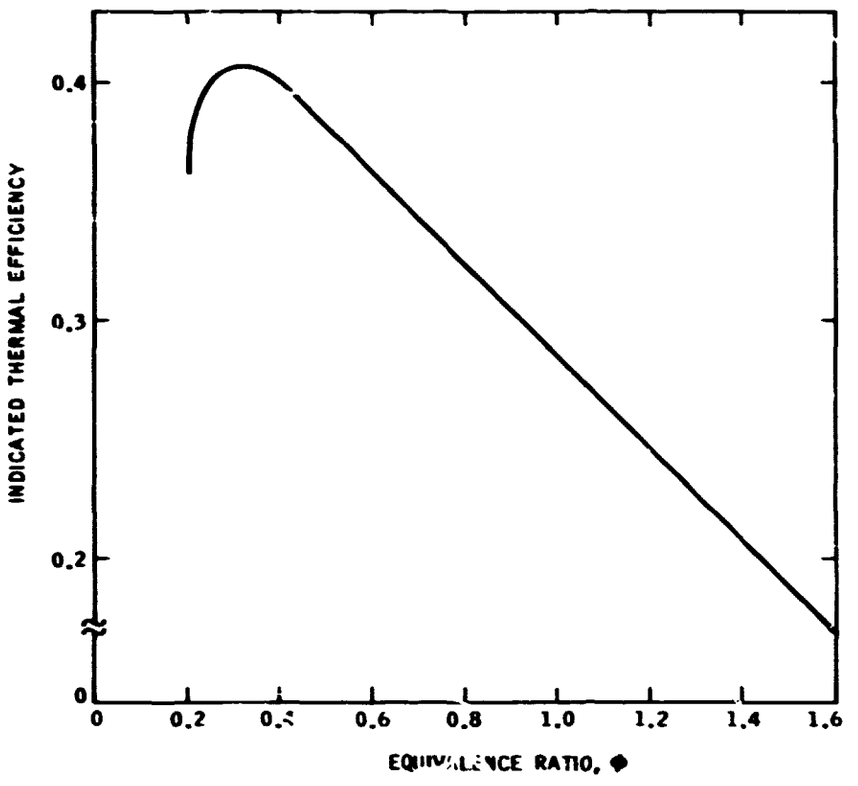

Fig. 3. CFR thermal efficiency vs equivalence ratio

proportionate to increased engine thermal efficiency and, as will be shown later, more than offsets the penalties associated with the use of the gas generator.

3. Early V-8 Engine Studies

The NO_x emission data generated by V-8 engine tests, made using bottled hydrogen, reinforced the concepts determined in the initial CFR studies. The V-8 engine NO_x vs equivalence ratio curve was similar to the CFR curve both in characteristic shape and in the values of the data. The CFR results with carbon monoxide (CO) and hydrocarbon (HC) emissions were also experienced with the V-8 engine.

The initial multi-cylinder V-8 engine thermal efficiency measurements exhibited a marked difference from the single cylinder results. The CFR results showed clear and sharp maxima. The multi-cylinder engine maxima was broad and not clearly defined. This is thought to be mainly the result of cylinder-to-cylinder variations in equivalence ratio. The phenomena is illustrated in Figure 4. The same engine was operated with two different induction systems; one was the system used for the hydrogen generator/engine tests described in Section IIC of this report and the second a laboratory system specifically designed to give uniform equivalence ratio distribution.

Work performed by JPL (after the work reported here) for the Department of Transportation, Transportation Systems Center (DOT/TSC) (Ref. 10) contributed to the knowledge of lean operating V-8 engines. The implementation

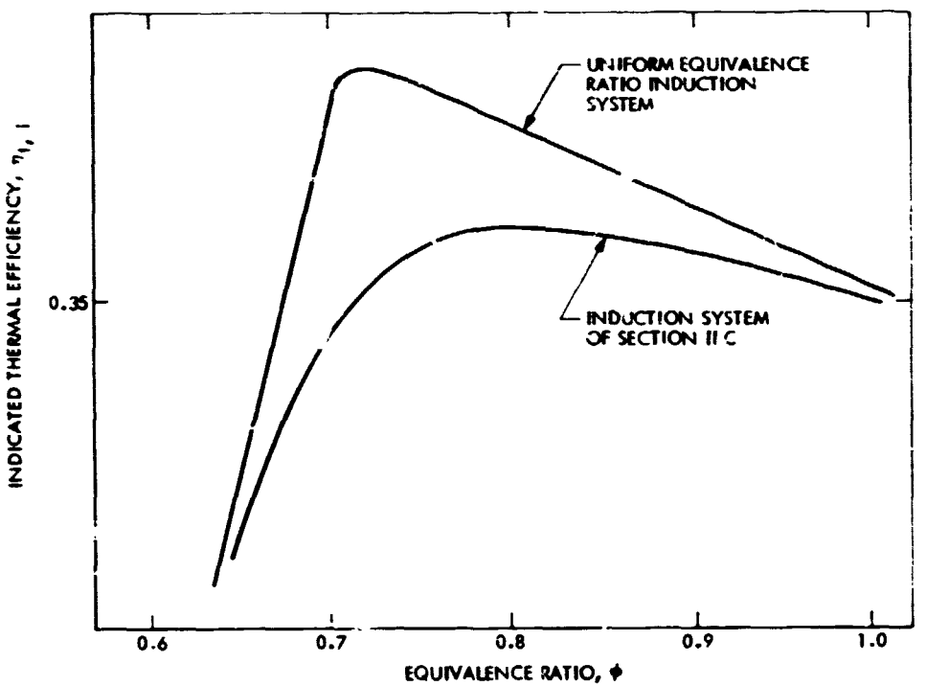

Fig. 4. (V-8) Thermal efficiency vs equivalence ratio

of several engine modifications allowed the V-8 engine, fueled by gasoline only, to operate approximately 50% leaner than a stock engine. Although no hydrogen enrichment data have been taken with this modified engine, the same trends of improved leanness are expected for ultra-lean operation. If the same improved performance is realized with hydrogen enrichment as has been observed with gasoline, then the lean limit lines of Figure 5 will result.

4. Test Vehicle

a. Description

A complete car was modified to operate on gasoline/hydrogen mixtures. This vehicle used an experimental induction system and high-pressure cylinders

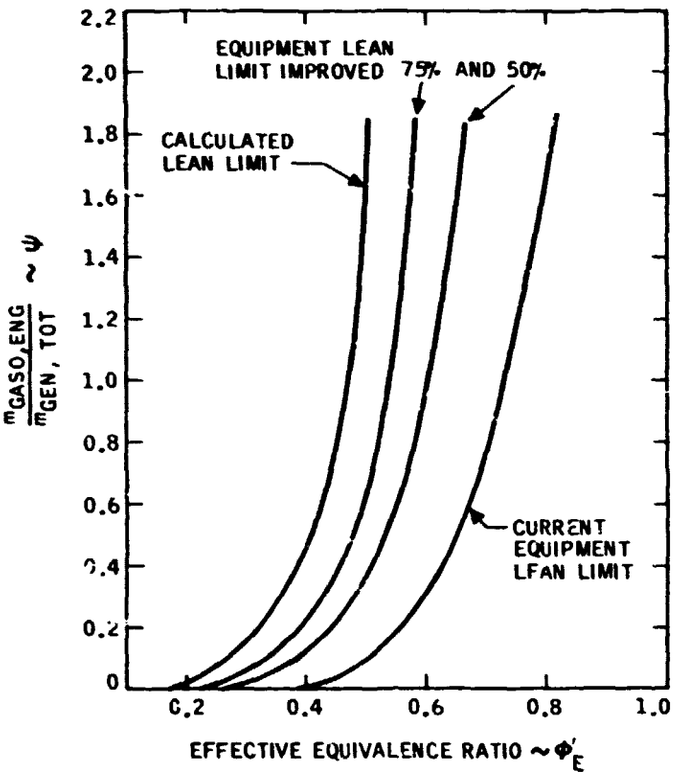

Fig. 5. Mass flow ratio vs effective equivalence ratio - ϕ'_E

of hydrogen gas mounted in the trunk. This vehicle was used initially to demonstrate to the NASA the feasibility of the concept of adding gaseous hydrogen to the fuel-air mixture to reduce emissions and increase fuel economy. The vehicle used was a 1973 Chevrolet Impala 4-door sedan equipped with a 350-cubic-inch V-8 engine.

This vehicle was tested with certain auxiliary equipment operating such as: power steering, power brakes, and an automatic transmission.

Equipment not operated because of the complications that would have resulted to a feasibility demonstration, or because it was not required, included the following:

- Evaporative controls
- Vacuum spark advance
- Exhaust gas recirculation
- Air injection reactor
- Air conditioner/heater

A bottled-gas supply system consisting of three K-size bottles was installed in the trunk and a prototype mixed fuels induction system replaced the carburetion system supplied by the car manufacturer. All engineering test instrumentation and associated power supplies were located on board the test vehicle. The test vehicle was started by means of the ignition-key with some auxiliary manual procedures. However, all start assistance equipment was on-board and all start operations were controlled from the front seat.

b. Performance Summary

Early tests indicated that the driveability, handling characteristics, and power response were very similar to a standard automobile. Initial emissions test results over the FDC were promising and are summarized as follows:

Parameters	Unmodified Vehicle	Early Bottled Gas	EPA 1978 Standard
Hydrocarbons (gm/mi)	2.3	3.1	0.41
Carbon Monoxide (gm/mi)	43.9	2.2	3.4
NO_x (gm/mi)	1.8	0.6	0.4

Tests continued with added benefit. These additional tests indicated that hydrocarbon emissions were reduced when the amount of hydrogen was increased and, for a given hydrogen flowrate, also showed a minimum as a function of equivalence ratio (see Figure 6). This work is discussed in greater detail in Section II. D, Task E.

The amount of hydrogen added to prevent misfire and the design requirements of a hydrogen generator are constraints on the amount of hydrogen that

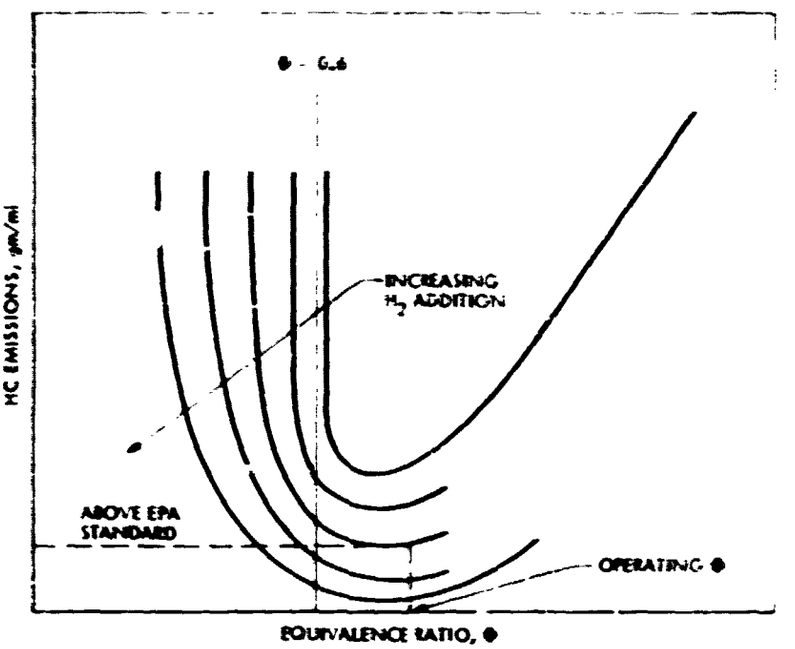

Fig. 6. HC emissions vs equivalence ratio

should be added to the gasoline-air mixture. When one considers the equivalence ratio and the amount of hydrogen required for low NO_x emission operation, the HC emission yielded by Figure 6 is substantially higher than the 1978 Federal Standard.

This information led to the consideration of using an exhaust catalyst to reduce the HC and CO emissions with the JPL hydrogen-enrichment concept used to simultaneously reduce the NO_x emissions.

Refinements to and fine tuning of the bottled-gas test vehicle enabled JPL to collect test data which reflected the lowest probable emissions that could be expected without internal engine modifications and without the use of an exhaust catalyst. Upon completion of those tests, an exhaust catalyst was added to determine the effects. Data from both sets of Federal Driving Cycle tests are summarized as follows:

Parameters	Updated Bottled-Gas Car		EPA 1978 Standard
	No Exhaust Catalyst	With Exhaust Catalyst	
Hydrocarbon (gm/mi)	2.6	0.39	0.41
Carbon Monoxide (gm/mi)	1.6	0.04	3.4
NO_x (gm/mi)	0.31	0.39	0.4

The total gasoline energy used (BTUs per mile) for the unmodified car as purchased was 12,700 for a miles/gallon equivalent of 9.5. The bottled-gas car with or without the exhaust catalyst used 8,850 BTUs per mile of hydrogen and gasoline for an equivalent 13 miles per gallon: an improvement of 37%.

5. Hydrogen Generator

A general description of the hydrogen generator was presented in Section I. B. 1., Overview. More specifically, the generation of molecular hydrogen

from a hydrocarbon source is an industrial process in wide use. The process used by JPL is described in the following paragraphs, and is similar to those employed industrially. There are, however, several major differences. A fuel rich mixture of heated air and vaporized gasoline is fed to a reaction chamber where a small portion of the gasoline feed is completely oxidized. This combustion supplies the energy necessary for the hydrogen formation. The remaining gasoline is partially oxidized according to the chemical equation:

$$C_8H_{18} + 4O_2 \longrightarrow 8CO + 9H_2$$

In addition to the CO and H_2, there are also N_2 and small amounts of CO_2 and unburned hydrocarbons (principally CH_4) in the product stream. The products exit the reactor at a temperature of approximately 1800°F and are passed through a heat exchanger where the air and gasoline feeds are heated.

This concept produced a maximum of 14.5% hydrogen by volume with a chemical energy ratio of 67% and had the disadvantages of requiring water as well as a large size. This thermal generator was approximately 40 in. long and 12 in. in diameter.

The reaction chamber may be empty (thermal reformation) or may be filled with a non-noble metal catalyst (catalytic reformation). The initial JPL experience has shown several major advantages for the use of a catalyst. The catalytic reformation has resulted in a higher hydrogen yield (although there is no theoretical advantage) and has proven much more amenable to the suppression of soot formation. The thermal reformation has required, at least at JPL, the use of water in the generator feed to prevent soot formation.

Tests were conducted to determine the sensitivity of catalysts to potential poisoning sources such as leaded-gasoline. A 100-hour test yielded no adverse

effects from the leaded test gasoline fuel on a promising hydrogen generator catalyst. A compact catalytic hydrogen generator was designed and fabricated which yields 22% hydrogen by volume. This represents an improvement of 52% over the older, thermal generator designs. In addition, the compact catalytic generator requires no water feed and is only 10 inches long, about 7 inches in diameter, and operates at a chemical energy ratio of 80% (improving the efficiency by 20% over the thermal design).

SECTION II

EXPERIMENTAL WORK

A. OVERVIEW

In this section of the report, the experimental work will be described and the results of these experiments presented. The work statement tasks which will be discussed here are Task A, Catalytic Generator Characterization Task D, V-8 Engine Tests, and Task E, CFR Engine Tests.

Three distinct experimental tasks were completed as part of the hydrogen-enrichment critical evaluation. These were characterization of a hydrogen generator for both steady-state and startup operation, single-cylinder Cooperative Fuel Research (CFR) engine tests, and multiple-cylinder engine tests with both gasoline only and gasoline/gas generator product mixtures as the fuel. Data from these three areas were used to evaluate the state of technological development of the hydrogen enrichment concept, to assist in the development of the computer simulations described in section III. C. and III. D. of this report, and to evaluate the potential of the hydrogen enrichment concept which would result from further engine-related improvements.

Prior to beginning the effort described in this document, a significant amount of engine and vehicle test experience had been acquired using mixtures of gasoline and compressed bottled hydrogen. This previous experience included operation with single-cylinder engines, multi-cylinder engines, and vehicles. All these results confirmed the hypothesis upon which the hydrogen enrichment concept is based (i. e., the use of hydrogen/gasoline mixtures allows ultra-lean operation with the attendant benefits of increased engine efficiency and decreased NO_x emissions), but left unanswered the questions concerning engine operation and performance with hydrogen-gas generator

products. Specifically, questions such as the following remained open: what is the effect of having combustibles, other than hydrogen, in the hydrogen gas enerator products? Will the hydrocarbon emissions be acceptable? What is the variation of engine thermal efficiency with equivalence ratio? What is the effect of hydrogen-gas-generator products on the engine hardware?

The primary objectives of the hydrogen-gas generator work was to characterize the input-output relationship of a gas generator and to determine the startup sequence and cold-start response of a generator. Although the statement of work required only an analytical estimate of the generator startup properties, experimental results are presented. The input-output relationships of the generator, which was subsequently used in the V-8 engine/generator tests, were completely determined and are presented below. It should be noted that there were two generator designs involved. The generator used for the engine testing represents an early state of design and was suitable only for steady-state operation. A NASA-sponsored generator development activity, which was carried on in parallel with the work described in this report, resulted in a generator design with vastly improved thermal characteristics. This latter design was the source of the start-up data presented below.

The objective of the multicylinder engine test was to determine the engine performance, in terms of fuel consumption and exhaust emissions, for a range of engine RPM, BMEP, and equivalence ratio. This was accomplished with three distinct engine configurations. Each of the configurations is described in detail. The first was the stock* engine complete with two-plane manifold, 4-barrel carburetor, exhaust gas recirculation (EGR), positive crankcase

*As explained in the detailed discussion of these tests, the air injector reactor (AIR) was not used.

ventilation (PCV), and stock ignition system/spark advance curve. An engine speed range from idle to 4000 RPM and an engine load range from zero to wide-open throttle were covered. These tests were performed, using the same test stand and instrumentation employed for all the multicylinder engine tests and thus provided a firm base for comparisons with the hydrogen-enrichment concept.

For the second engine configuration, an Autotronics induction system was employed and the EGR was disconnected. The Autotronics system replaces the intake manifold, the carburetor, and ignition system. For this configuration the spark advance was controlled manually and was, in general, set for maximum economy. This configuration was identical to the one used for the combined engine/generator tests and thus provided a measure of how much of the performance improvement resulted from the hardware changes. The engine conditions were covered as for the stock configuration.

The third configuration, as noted above, was identical to the second except for the addition of a manifold for distribution of the hydrogen gas generator products. Data were gathered at three steady-state generator flowrates corresponding to 0.5, 1.0, and 1.5 lbm/hr of hydrogen. For each generator flow, data were taken at approximately 30 combinations of RPM and BMEP. This covered an RPM range from 1000 to 3000 and a BMEP range up to 70 psi. This test matrix was selected to provide a good definition of the level-road-load performance and includes the maximum power conditions required to cover the EPA Federal driving cycle (FDC). At each operating condition the equivalence ratio and spark advance were chosen to yield maximum economy.

The single-cylinder CFR engine tests were designed to aid in understanding the "hydrocarbon problem," which appears to accompany lean combustion, and

to determine the effect of hydrogen addition on critical compression ratio. The CFR tests performed at the California Institute of Technology campus, which led to the hydrogen enrichment concept, did not include measurements of exhaust hydrocarbons. The multicylinder engine work which preceded the effort described in this document indicated that as equivalence ratio was reduced a minimum hydrocarbon level was achieved. This minimum typically occurred on the rich side of the maximum economy equivalence ratio, but the result was always clouded by the fact that in a multicylinder engine there are cylinder-to-cylinder variations in the equivalence ratio. This means that one or more cylinders reach a misfire condition well before the majority of the cylinders and hence excessive exhaust hydrocarbons may result even though the overall equivalence ratio is far removed from where misfire would be expected. Therefore, a series of CFR engine tests were performed to examine this question but without the complications of the multiple cylinders. Complete sets of exhaust emission measurements were made as well as measurements of engine thermal efficiency. The results of these tests are presented in Section II. D. 2.

It had been postulated that the use of hydrogen enrichment would increase an engine's critical compression ratio (i. e., the compression ratio at which "knock" occurs). A second series of CFR tests were performed to check this postulate. The results of these tests are also presented in Section II. D. 3.

B. CATALYTIC HYDROGEN GENERATOR CHARACTERIZATION/ STARTUP TESTS (EPA TASK A)

1. Introduction

The JPL approach to improving the efficiency of an internal combustion engine, while simultaneously reducing exhaust emissions, is based on operating the engine in an ultralean mode as a result of the addition of gaseous hydrogen to the fuel stream. The source of hydrogen chosen to meet this requirement is

one that can convert the conventional gasoline fuel, already onboard the vehicle, to hydrogen on demand. This eliminates the requirements for storage of gaseous hydrogen or other hydrogen convertible materials.

There are two basic processes which have been developed for the industrial production of hydrogen from hydrocarbons. These are steam reforming and partial oxidation. The steam reforming process consists of a reaction of a hydrocarbon, such as methane shown below, with steam to produce carbon monoxide and hydrogen:

$$CH_4 + H_2O + 280\frac{Kcal}{gm\ mole} \longrightarrow CO + 3H_2 \qquad (1)$$

The reaction is highly endothermic and requires an external source of energy.

The partial oxidation process may be visualized as a two-step reaction process in which a portion of the fuel is oxidized to provide the energy necessary for the reforming process. The first step is:

$$CH_4 + O_2 \longrightarrow CO_2 + H_2O + 1300\frac{Kcal}{gm\ mole} \qquad (2)$$

This is then followed by the process of Equation 1.

The partial oxidation process was chosen for the JPL automotive application for the following reasons:

- Partial oxidation provides a simplified system design by elimination of the external water and heat supply required for steam reforming.
- Potentially better transient response characteristics since there are no heat-transfer surfaces involved.
- There is little or no soot production dependence upon type of fuel.
- The reduced propensity for soot production allows the use of liquid fuels from naphthas to heavy fuel oils; whereas, steam reforming feedstocks are limited to naphtha or lighter hydrocarbons.

Both types of reactions may be catalyzed with either noble or non-noble metal catalysts. The use of a catalyst allows a closer approach to equilibrium hydrogen yields. The relatively high catalyst reaction temperature (1000°C) in the partial oxidation process is considered to be the source of lead and sulphur tolerance at concentration levels of 200 and 300 ppm, respectively (Refs. 1 and 2).

Initial feasibility demonstrations of the hydrogen injection concept used pure, gaseous hydrogen. Since the product resulting from the partial oxidation reforming of gasoline contains species other than hydrogen, the engine performance with generator products was somewhat unknown. Therefore, it was agreed that EPA test activities would employ a gas generator. The characterization of this gas generator is described below.

It should be noted that the gas generator used for the engine testing was the first catalytic generator attempted at JPL. The hydrogen yield was excellent: nearly equilibrium concentrations. However, as noted below, the physical size of the generator is much larger than necessary. Although no generator development was done as part of the EPA effort, a parallel, NASA-funded development has been carried out. A considerable reduction in size was accomplished, while still producing the same generator output. The transient characteristics of this significantly smaller NASA-funded generator are also described below, in lieu of the analysis called for in the statement of work.

2. General Characterization Tests

a. Test Objectives

The objective of the characterization tests of the catalytic generator was to determine the generator product composition over a range of generator fuel flowrates, reaction chamber pressures and equivalence ratios.

b. Gas Generator Hardware Description

The hydrogen generator is shown in Figure 7. A schematic of the generator is also included in Figure 8. The principal elements of the generator are a burner section, a catalytic reaction chamber, and a heat exchanger. During steady-state operation, the burner section ensures completion of the gaseous fuel-air mixing by means of a hollow cone, swirl injector. The burner section also includes a second set of fuel and air inlet fittings (see Figure 7) for generator startup with ambient temperature air and liquid gasoline. This particular mode of startup was not used during the work described in this report. As described later, generator startup was always accomplished by pre-heating the catalyst bed.

The burner is designed to permit two modes of operation, one for startup with ambient temperature air injection through the side fitting and liquid fuel atomization through the pressure atomizer. The second is the normal test mode with a mixture of vaporized-fuel and preheated air being injected via the swirl chamber. This chamber produces a short, highly-vortical-flow burning pattern between the burner and catalyst chamber.

The reaction chamber shown in Figure 7 serves as the structural and product containment vessel. It was fabricated from a 26.0-inch long section of 8-inch, schedule 5, Hastalloy-C pipe. The inlet flange, with 3-inch diameter burner aperture, is bolted to the chamber and the exit flange with 1.5-inch exit flow aperture is welded to the chamber. The operating temperature of the chamber wall is reduced to 1000°F from the catalyst bed operating temperature of 1850°F by the addition of the ceramic liner shown in Figure 7. The liner is a composite of two ceramic cylinders. The inner cylinder is high purity alumina purchased from the Coors Co. with a 5.5-inch internal diameter by 24 inch length with 1/4 inch wall thickness. The outer cylinder was cast in

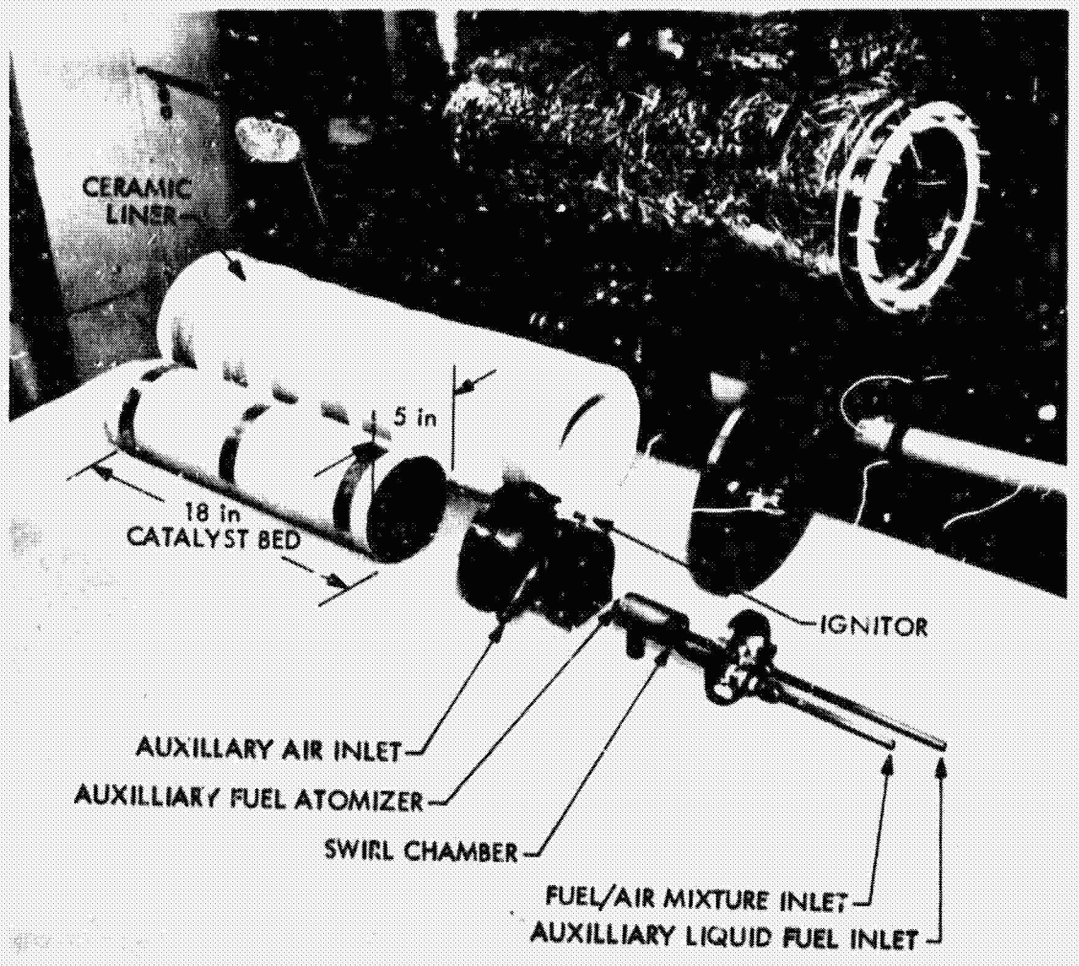

Fig. 7. The hydrogen generator

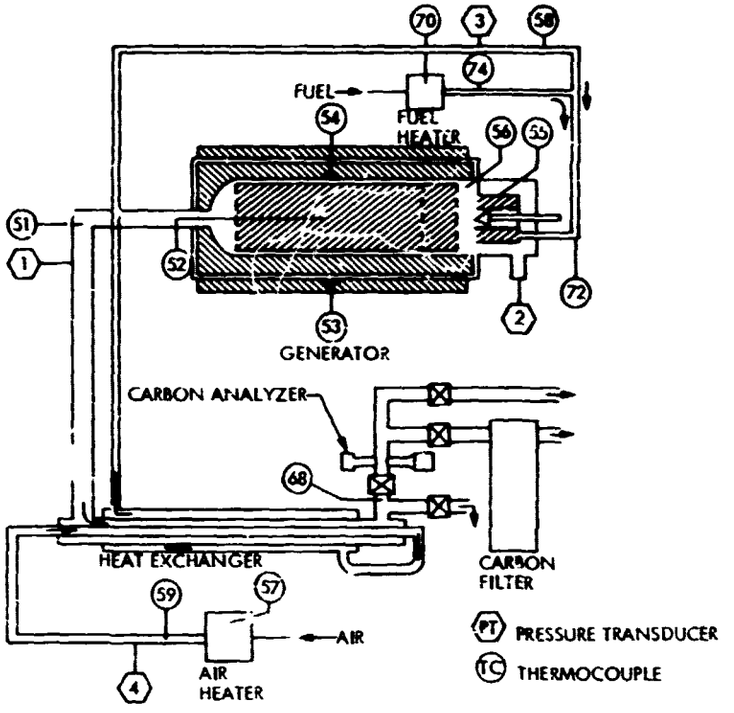

TC No. \ FUEL FLOW	MIN (0.64) gph	MID (1.96) gph	MAX (2.70) gph
	TEMPERATURE, °F		
51	1442	1614	1648
52	1712	1773	1798
53	974	1012	1019
54	1402	1415	1406
55	658	750	742
56	1358	1703	1660
57	233	202	233
58	630	86[illegible]	849
59	223	198	230
68	642	814	830
70,74	73	77	79
72	406	535	531
PT No.	PRESSURE, psig		
1	0.1	1.8	3.8
2	0.3	2.3	4.6
3	1.0	6.8	12.7
4	4.6	22.4	36.7

Fig. 8. Hydrogen-generator process schematic

place using a ceramic fiber insulation consisting of 50% each alumina and silica, and had a wall thickness of approximately 1 inch.

A total of 13.5 lbm of catalyst was used. The catalyst bed container is a welded stainless-steel unit (type 316, 0.06 inch wall thickness) with perforated end plates and is shown with a wrap of asbestos. The chamber contained 4 lbm of 15% nickel catalyst pellets (5/8 inch diameter x 3/8 inch long) and 6 lbm of 25% nickel catalyst pellets (1/8 inch diameter x 1/8 inch long). An additional 3.5 lbm of 11% nickel catalyst pellets (1/2 inch diameter x 1/2 inch long) were installed between the catalyst bed and burner, extending to within 1 inch of the burner face in a similar container not shown. The catalysts were obtained from the Chemtron Corporation and are commercial grades ($3.00 per lbm) of hydrocarbon steam reforming catalyst.

The heat exchanger is shown schematically in Figure 8. The heat exchanger was used to cool the generator products and to simultaneously preheat the air-gasoline mixture supplied to the generator. This was accomplished in a 12-foot-long triple-concentric tube. Heat exchange occurs between the generator product gas and ambient temperature combustion air being supplied to the burner. The cooling air flows through the center 1/2 inch diameter tube and returns in the outer annulus, between the 1-1/2 and 2-inch diameter tubes. The generator product is cooled in one pass through the inner annulus, between the 1/2- and 1-1/2-inch diameter tubes.

c. Test Description

Previous experience with the catalytic generator had identified two operational constraints. These were: (1) the temperature of the fuel/air mixture at the inlet of the generator should be maintained above ~400°F; direct injection of the liquid fuel into the burner section results in degraded performance of the catalyst; The degradation is presumed to be the result of carbon accumulation

on the catalyst; and (2) the maximum catalyst temperature should be maintained below ~2000°F. At a temperature of 2080°F there was a two-order-of-magnitude increase in the soot (mixture of carbon and partially oxidized hydrocarbons) production rate. This is presumed to be the result of thermal cracking of the methane in the product stream.

An electrical air heater shown schematically in Figure 8 was used during startup to meet the first constraint of air/fuel preheat (the cold-start requirements were investigated under NASA sponsorship). After startup, the heat exchanger provided the necessary air preheat and the electrical heater was de-energized. Exploratory tests with the fuel heater found that it was not needed. Injection of the liquid gasoline into the pre-heated air stream was sufficient to insure complete vaporization of the gasoline. The second constraint was met by maintaining the fuel/air equivalence ratio of the generator at 2.8 ± 0.1. For values of the ratio above 2.9, soot is formed. At equivalence ratios below 2.7, the hydrogen production rate is reduced with elevated catalyst temperatures. These effects are shown in Figure 9.

The characterization tests of the generator consisted of a series of forty operating conditions. Three values of reaction chamber pressure of 2, 8, and 12 psig at each of three fuel flowrates were included. All these tests were conducted to verify performance repeatability as well as to determine performance variation as a function of equivalence ratio. At each of the operating conditions, after steady-state operating temperatures and product composition had been established, a group of 35 operating data parameters were recorded with a digital data acquisition system on magnetic tape for post-test computer data reduction and analysis. Each data set consisted of fourteen temperature measurements, ten pressure measurements which included instrumentation of the sharp-edge orifice type air and fuel flowmeters, and four generator product

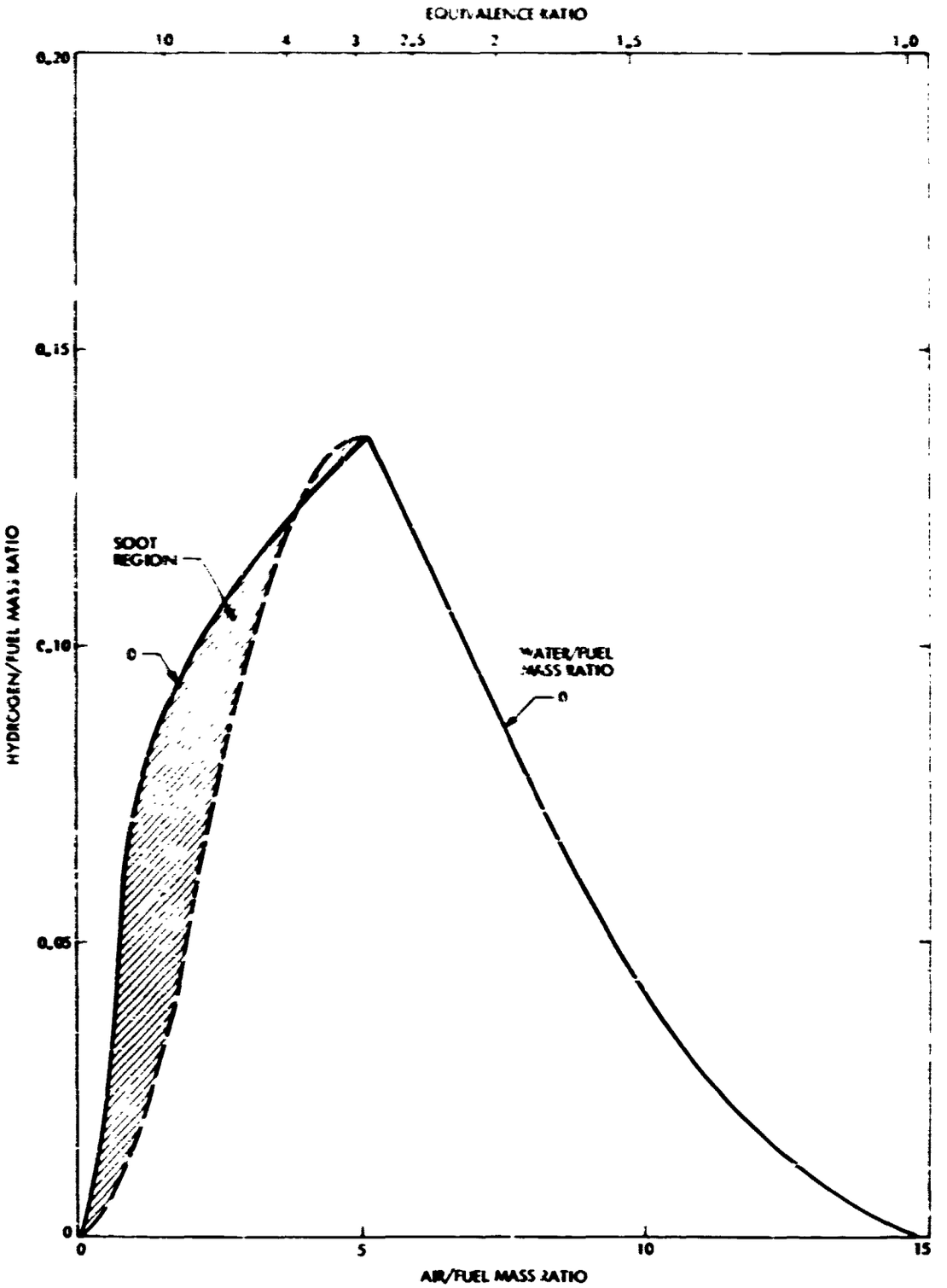

Fig. 9. Theoretical equilibrium, adiabatic combustion ($CH_{1.92}$)-water-air at 80° F, 44 psia

composition analyses for dry mole fraction of hydrogen, carbon dioxide, carbon monoxide, and unconverted hydrocarbons (CH_4 through C_6H_{14}). A gas chromotograph was used to provide backup hydrocarbon analysis as well as verification of the composition of the unconverted hydrocarbons. In general, the hydrocarbon analysis showed 90% methane, 9% ethylene and only trace amounts of heavier hydrocarbons.

One other operating characteristic was determined for the generator. This was the soot production rate over the operating range. The primary means of determining soot content of the generator product was to pass the generator product flow through a 10-micron filter for periods up to 30 minutes, using the filter-element weight increase after oven drying as a measure of the soot deposition. A second device was built and installed to provide continuous optical opacity measurements of the product stream, utilizing a variable intensity lamp and photo-multiplier. This device was used to indicate qualitative carbon content variations with the filter measurements being used to quantify these measurements.

d. Test Results

The generator was operated at an equivalence ratio of 2.8 ±0.1 over a fuel flowrate range from 3.7 to 16.2 lbm/hr with a corresponding generator product hydrogen flowrate of 0.4 to 2.1 lbm/hr. The mass yield of hydrogen was found to be relatively insensitive to reaction chamber pressures over the test range of 2 to 12 psig. At the maximum fuel flowrate, a 5% hydrogen yield increase was observed for a pressure increase from 4 to 12 psig. Figure 10 shows this variation of hydrogen volume percent in the generator product with pressure. A 10% hydrogen concentration increase from 20% to 22% is shown for the flowrate increase from 3.7 to 6.2 lbm/hr of fuel. The yield increases

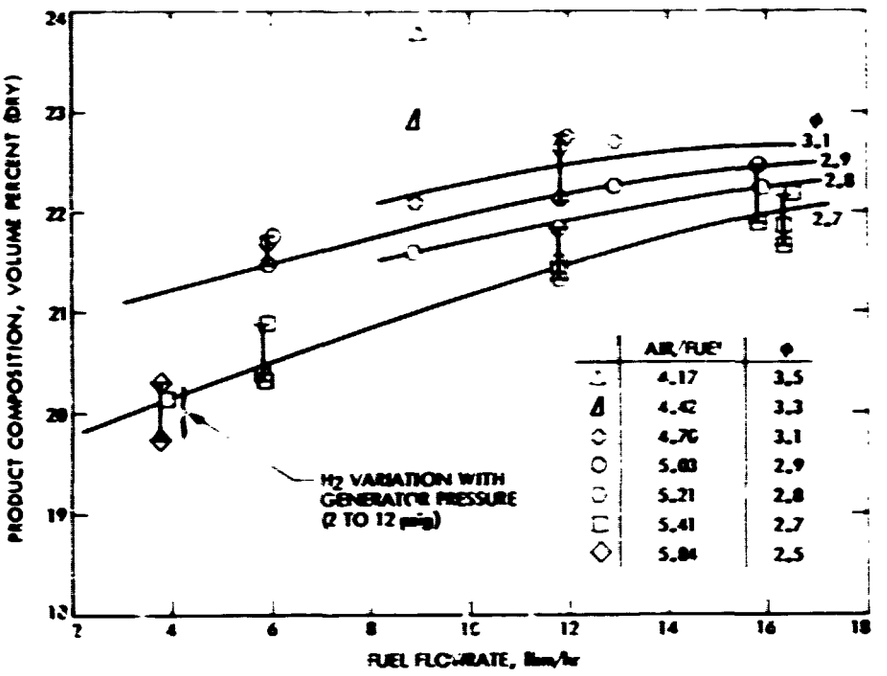

Fig. 10. Hydrogen mole fraction (dry) variation with equivalence ratio and reaction chamber pressure

with flowrate because of a catalyst temperature increase from 1700 to 1800° F. This, in turn, results in increased catalyst activity. This yield increase corresponds to a performance increase from 0.89 to 0.97 of the theoretical value of hydrogen volume percent concentrations in the generator product. The hydrogen and carbon monoxide concentration data as a function of air to fuel ratio, shown in Figure 11, agree closely with the theoretical curves.

Figure 12 shows a similar comparison for water, carbon dioxide, and methane equivalent in the generator product. The deviation between measured and theoretical methane concentration reflects the source of the sub-equilibrium

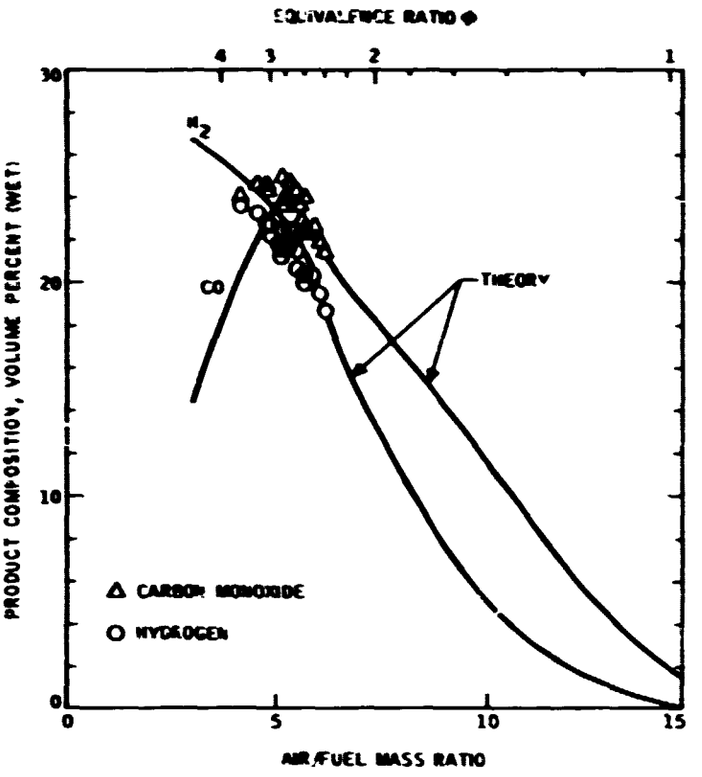

Fig. 11. Comparison of measured and theoretical mole fraction concentration for H_2 and CO

hydrogen yield. It was found in preliminary tests that the amount of unconverted hydrocarbons could be reduced to the theoretical value with an attendant increase in hydrogen yield if the catalyst was operated at a temperature of 2080° F. This operating condition has been avoided in subsequent tests since the methane conversion to hydrogen apparently takes place through a mechanism of thermal cracking as opposed to steam reforming. The thermal cracking is evidenced by a factor of 50 increase in soot in the generator product. This data is shown in Figure 13 where soot content as a fraction of fuel flow is plotted as a function of catalyst temperature.

The theoretical curves shown in Figures 11 and 12 were obtained from the computer program of Ref. 3. JP-5 ($C_8H_{15.35}$) was used as the fuel in

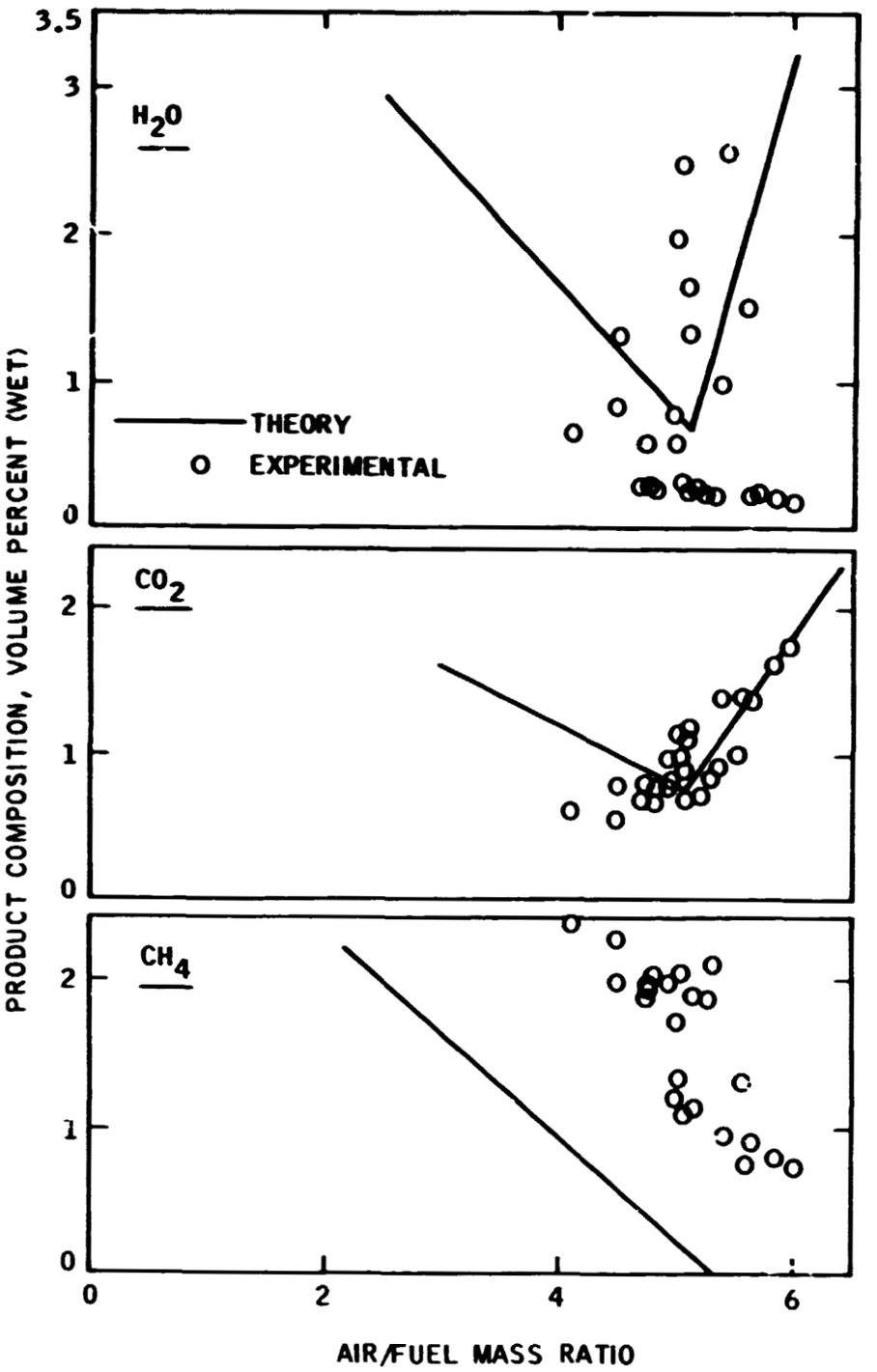

Fig. 12. Comparison of measured and theoretical mole fraction concentrations for H_2O, CO_2, and unconverted HC as methane equivalent.

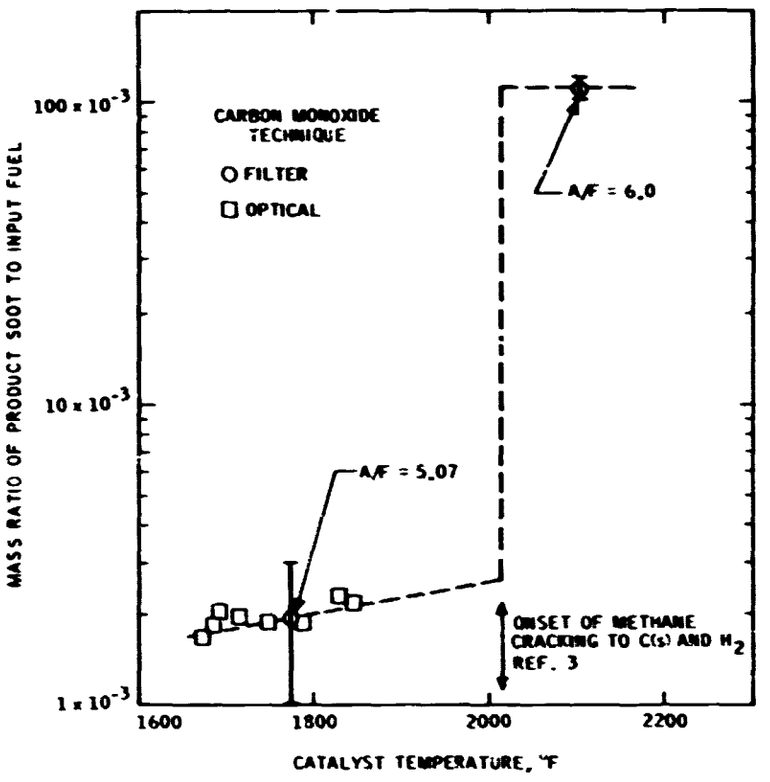

Fig. 13. Measured soot content in generator product

those calculations since the hydrogen to carbon fuel ratio is most similar to the fuel (Indolene-clear) used in the generator tests. The data presented in Figure 10 are basically raw data from the hydrogen analyzer on a dry basis since the analyzer requires sample drying with a water vapor trap. The same data are shown in Figure 11 where the hydrogen concentrations are slightly reduced as a result of including an estimate of the water vapor content in the generator product. The water vapor estimate is made in the computer data reduction program in an iterative calculation which consists of (1) picking a value of moisture content, (2) converting the measured values of mole fraction to a wet basis, (3) calculating the output mass flowrates for CO, CO_2, CH_4, H_2, N_2, and H_2O, and (4) calculating a hydrogen mass balance. This procedure

is repeated until the hydrogen balance (input minus output) is equal to zero. Carbon, oxygen, and nitrogen have shown agreement to within 1% for oxygen and nitrogen, and to about 3% for carbon. The soot production measurements, shown in Figure 13, have characterized this generator as producing 0.002 lbm of carbon per lbm of fuel. This accounts for 2/3 of the carbon balance error.

During the generator development tests, an operating condition was noted in which there was no apparent flame in the void volume upstream of the catalyst bed. This "flameless" catalytic-oxidation is a desirable condition and was employed in all subsequent generator/engine tests. The operating procedures which result in "flameless" operation also preclude catalyst temperatures above 2000° F. The conclusion that there is no flame is based on observations of the temperature of the gasoline/air mixture in the void (see Figure 8 for location of TC-56). At an equivalence ratio of 2.8 and in a chamber without a catalyst, combustion was visually observed at the TC-56 location. Under these conditions, the temperature indicated by TC-56 ranged between 1800 and 2200° F. With the addition of a catalyst and using the proper startup technique, the TC-56 temperature ranged between 400 and 1600° F. This low void temperature occurs with high yields of hydrogen and catalyst bed temperatures of ~1800° F. The temperature at TC-56 is apparently a strong function of the distance between the swirl tube and catalyst bed. This dimension has been varied from 1 to 18 inches. It is concluded that the transition from the flameless mode to the high carbon yield mode, where the catalyst temperature is 2100° F and the TC-56 temperature is 2400° F, is controlled by a combination of rich flammability limit dependence on temperature and flame instability.

The computer data analysis output for a typical run condition is shown in Figure 14. The first four groups of printout lists the operating temperatures, pressures, input flowrates, and flow densities. The next two lines of printout show the wet and dry mole fraction concentrations in the generator product. Using the water vapor estimate from the hydrogen balance calculation, the bottom line of printout shows the mass balance errors for the product flowrates shown in the line above. A set of calculation results are shown in Table I for the same test condition. For this calculation, an iterative hand calculation was made in which all four species mass-balance errors equal zero. The mole fraction and output flowrates in Figures 14 and Table I are seen to agree closely.

Figures 15 and 16 show the generator product mass composition variation as a function of input fuel flowrate. The lines represent the locus of operating conditions at an equivalence ratio of 2.8. This equivalence ratio was used for all subsequent engine/generator tests. The product variation with input fuel-flow rate is very nearly linear, over the range of fuel flowrates tested, and the variation in composition of the combustibles is small for a range of Φ from 2.4 to 3.1.

3. Startup Tests

a. Background

In parallel with the engine/generator tests described in Task D, further development of the catalytic hydrogen-gas generator occurred under NASA sponsorship. The improved generator is significantly smaller than the one described above and consequently has superior thermal transient properties. In lieu of the analysis called for in the work statement, the startup tests conducted with this generator are described below.

```
----
03/04  09110  RUN NO. / 15 47

DATA REDUCTION PROGRAM  /DATAREL036/
SPECIFIC HEATS, BTU/LBM DEG F, .2916  .2017 3.6120  .2794  .5432 1. 101 1.0616 T2=1231

                                TEMPERATURES, DEG.F
                                ---  ------  ---

EXIT PROBE (51)= 1527 CAT. PRB(52)= 1774  INLET WALL(53)=  562      WALL  (54)= 1 71   MIX CHMBR (55)=  64  BURN.PR  (56)= 147
AIR 1 HTR (57) =  10  AIR 1 EX(58)=  740     AIR EXIT(59)=  250          (60)= 2651          (61)=  15          (62)=  16
FUEL HTR   (63)=  162 STM ORF (64)=   9  FUEL 1 ORF.(65)=   74 AIR ORIFICE(66)=   74 WATER  ORF(67)=   72 H.L. MIX(68)=  810
           (69)=  032 AIR HTR(70)=  2 1  FUEL FLOW (71)=  2 6   BURN.MIX (72)=  667          (73)=  156 AIR 2 EX (74)=  200

                                PRESSURES, PSIA
                                ---------  ----

GENERATOR EXIT =   15.2 GEN. INLET    =  15.6 BURNER INLET  =  10.6 H.L.INLET   =  29.0 STM ORIFICE IN =  14.2 STM ORFC DP =   .0
FUEL 1 ORIFICE =   14.7 FUEL 1 DP     =  1.52 FUEL 2 ORIFICE=  14.0 FUEL 2 DP   =   .01 AIR ORIF OT IN = 103.  AIR ORFC DP =  5.9 6
FUEL VAPZR EX  =   14.0 REFORMER INLET=  14.2

                                FLOWRATES, LBM/HR
                                ----------  ---

STEAM =    .050   BURNER FUEL =   0.000  REFORMER FUEL =    .0    BURNER AIR =  45.564  TOTAL FUEL =    .0

                                FLOW DENSITIES, LBM/FT**3
                                ----  ---------  ---  --

STEAM =  .049  BURNER FUEL = 45.607 1.61  REFORMER FUEL = 45.607 .00 BURNER AIR =  .527 6.02 TOTAL FUEL =  45.650  0  6  9

                                GAS ANALYSIS, VOLUME %
                                --- --------  ------ -

CO =   23.025      CO2 =   1.1 5    CH4=   1.103   H2 =  21.572   N2 =  51.531   H2O =   1.654
CO =   23.242      CO2 =   1.126    CH4=   1.113   H2 =  21.776   N2 =  52.743   H2O =    .01

                                FLOW-RATE RATIOS
                                ---- ----- ------

AIR/FUEL= 5.11 WATER/FUEL=  .0 6  EQUIVALENCE= 2.05   SEC.EQUIV=  .0   H2/FUEL=  .119  MOLES CO/N2=.4 7  CO2/N2=.02   H2/N2=  .419

                                GAS ANALYSIS, WEIGHT %
                                --- -------- ------ -

CO =   28.946      CO2 =   2. 04    CH4=    .792   H2 =   1.937  N2 =  64.70  H2O =   1.347

                                GAS COMPOSITION , LBM / HR
                                --- -----------   --- -- -

CO =   15.036      CO2 =,  1.206    CH4=    .43    H2 =   1.060  N2 =  35.35 H2O =    .720 MEAN MOL.WT.=  22.27 TOTAL M  =  54.53

                                WEIGHT BALANCE, (INPUT-OUTPUT), LBM/HR
 CARBON =    .196  OXYGEN =    .092 HYDROGEN =    .030 NITROGEN =   -.370 PO FLAME TEMP= 2300, 2601  EFFICIENCY= .9603, .7055
CURRENT LOCATION OF DT36DATA FILE IS  20

                                / 15 47
```

Fig. 14. Computer data and analysis summary for a representative generator operating condition

Table 1. Results of calculation for operating conditions with exact input/output mass balances for carbon, oxygen, nitrogen, and hydrogen

INPUT CONDITIONS

AIR FLOWRATE, lbm/hr	45.6
FUEL FLOW, lbm/hr	8.9
AIR/FUEL RATIO	5.16
EQUIVALENCE RATIO	2.83
GENERATOR PRESSURE, psig	14
CATALYST TEMPERATURE, °F	1774

OUTPUT CONDITIONS

	MOLE FRACTION	MASS FRACTION	MASS OUTPUT lbm/hr
H_2	0.2160	0.0194	1.06
CO	0.2360	0.296	16.19
CH_4	0.103	0.0074	0.404
C_2H_4	0.0009	0.0011	0.062
CO_2	0.0123	0.024	1.326
H_2O	0.0120	0.0097	0.529
N_2	0.5125	0.6420	35.15
	1.0000	1.0000	54.72
MEAN MOLECULAR WEIGHT		22.33	
H_2/FUEL		0.12	
H_2/C		1.925	

EXIT PRESSURE, psig	1.0
EXIT TEMPERATURE, °F	1527.0
GENERATOR EFFICIENCY	0.785
EFFICIENCY/THEORETICAL EFFICIENCY	0.957

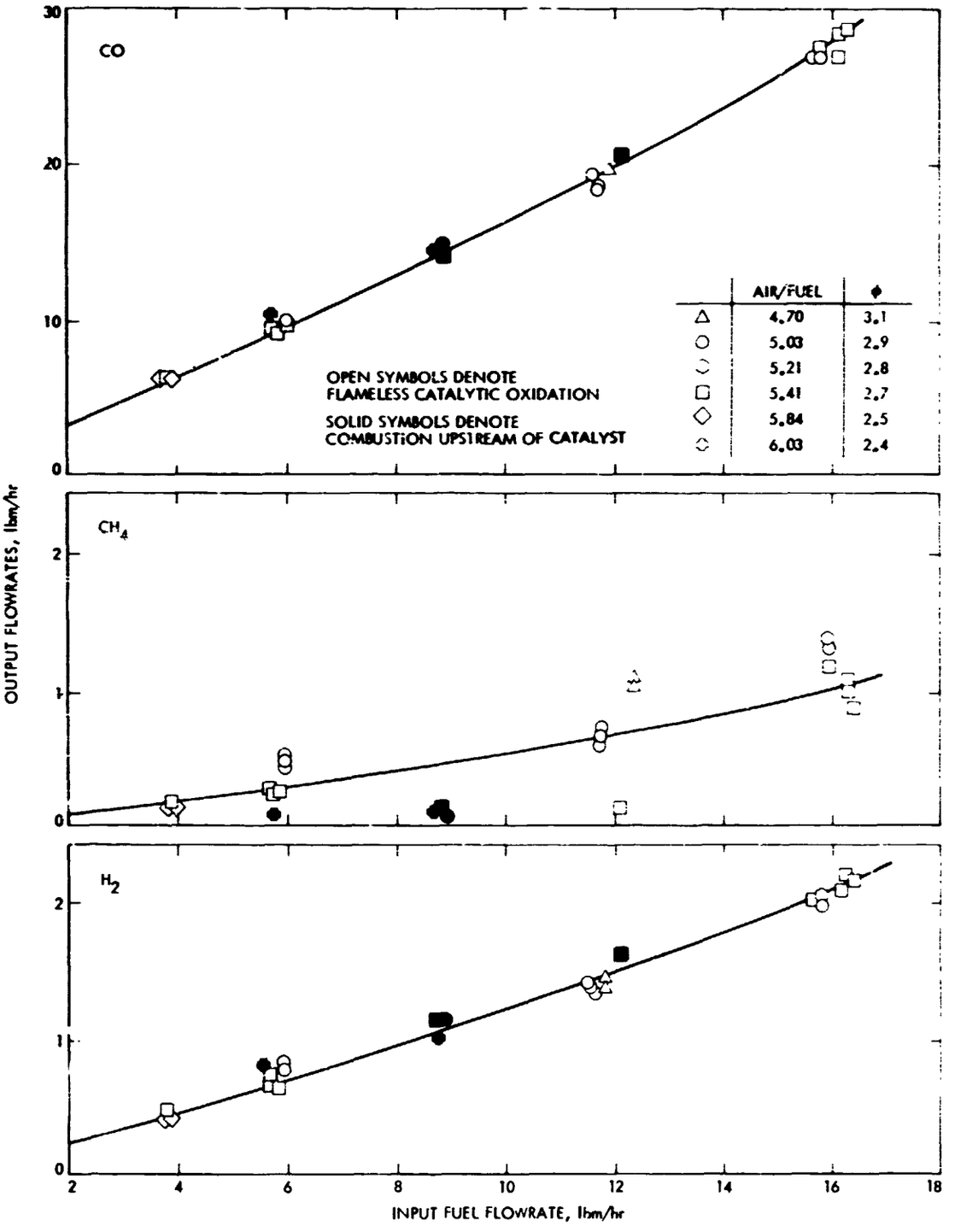

Fig. 15. Generator product combustible - component flowrates: CO, CH_4, and H_2 as a function of fuel flow

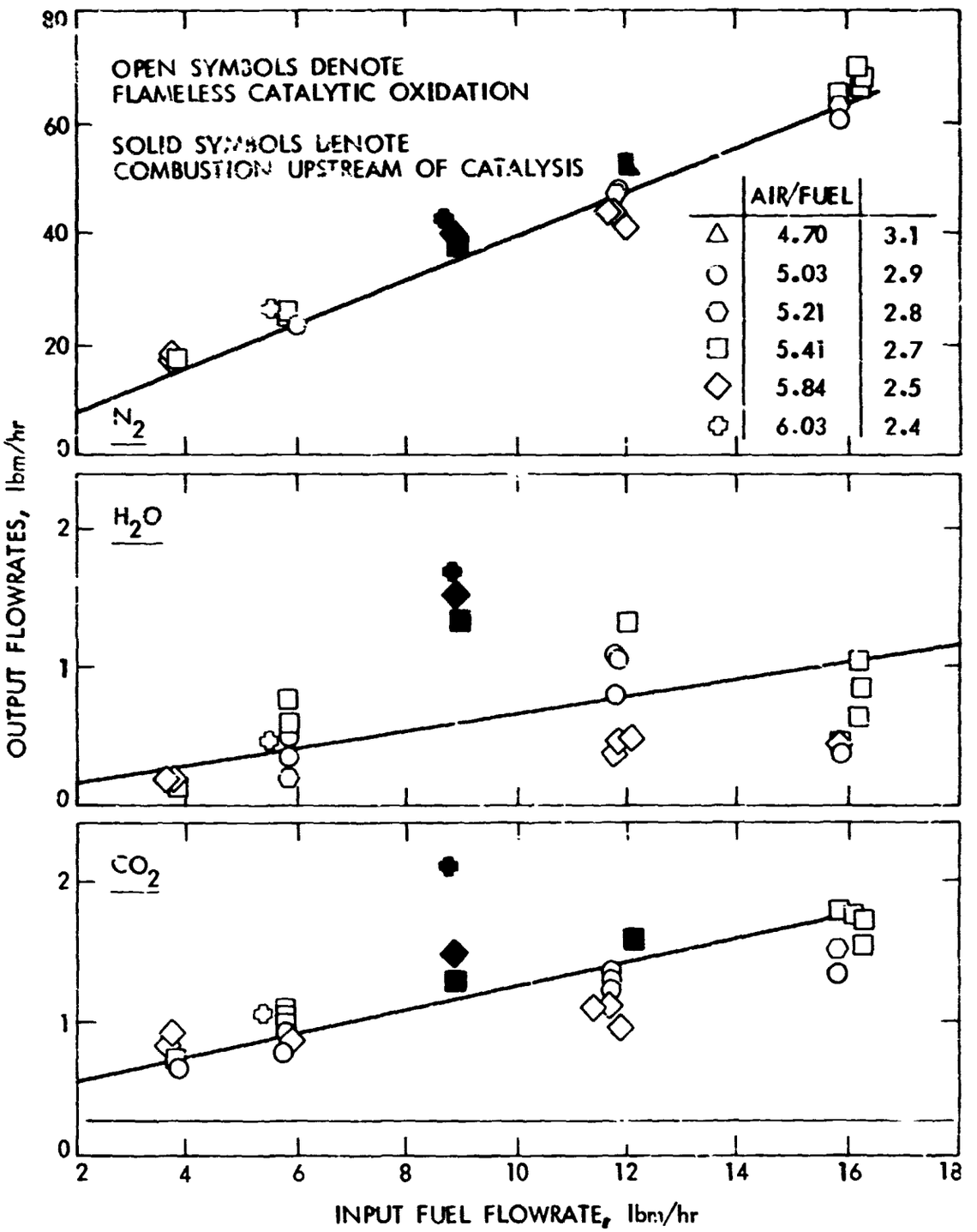

Fig. 16. Generator product diluent - component flowrates: N_2, H_2O, and CO_2 as a function of fuel flow

As noted in the description of the generator characterization above, the maximum production of hydrogen, without soot production, requires a homogeneous, single-phase mixture of fuel and air and a minimum catalyst temperature of 1400°F. A startup process was evolved which would allow a smooth, reasonably rapid transition from an ambient temperature catalyst bed and liquid fuel to the conditions necessary for maximum hydrogen yield noted above. The three-step process consists of:

1) Operation at an air/fuel ratio of 9.0 for ~30 sec. During this step, combustion occurs upstream of the catalyst bed. This step is primarily one of "activating" the catalyst bed.
2) Operation at an intermediate air/fuel ratio of 6.6 for ~30 sec. This step continues the catalyst activation, but at a reduced air/fuel ratio so as to preclude catalyst overheating which may result from prolonged operation at an air/fuel ratio of 9.
3) The final step is a richening of the air/fuel ratio to 5.2 (ϕ = 2.8). This is the desired operating condition.

Further details of this startup process are given below. This further discussion is keyed to Figure 17, which is a schematic of the generator used for the startup development.

During step one of the startup, liquid gasoline flows to the air/fuel mixer and is ignited and burned in the startup reaction chamber. The air for step 1 is directed through the startup heat exchanger. Step 1 is considered complete when the temperature of the air leaving the startup heat exchanger is ~500°F (i.e., high enough to insure vaporization of the gasoline) and the catalyst itself is at a minimum temperature of 350°F. This is hot enough to allow mixture

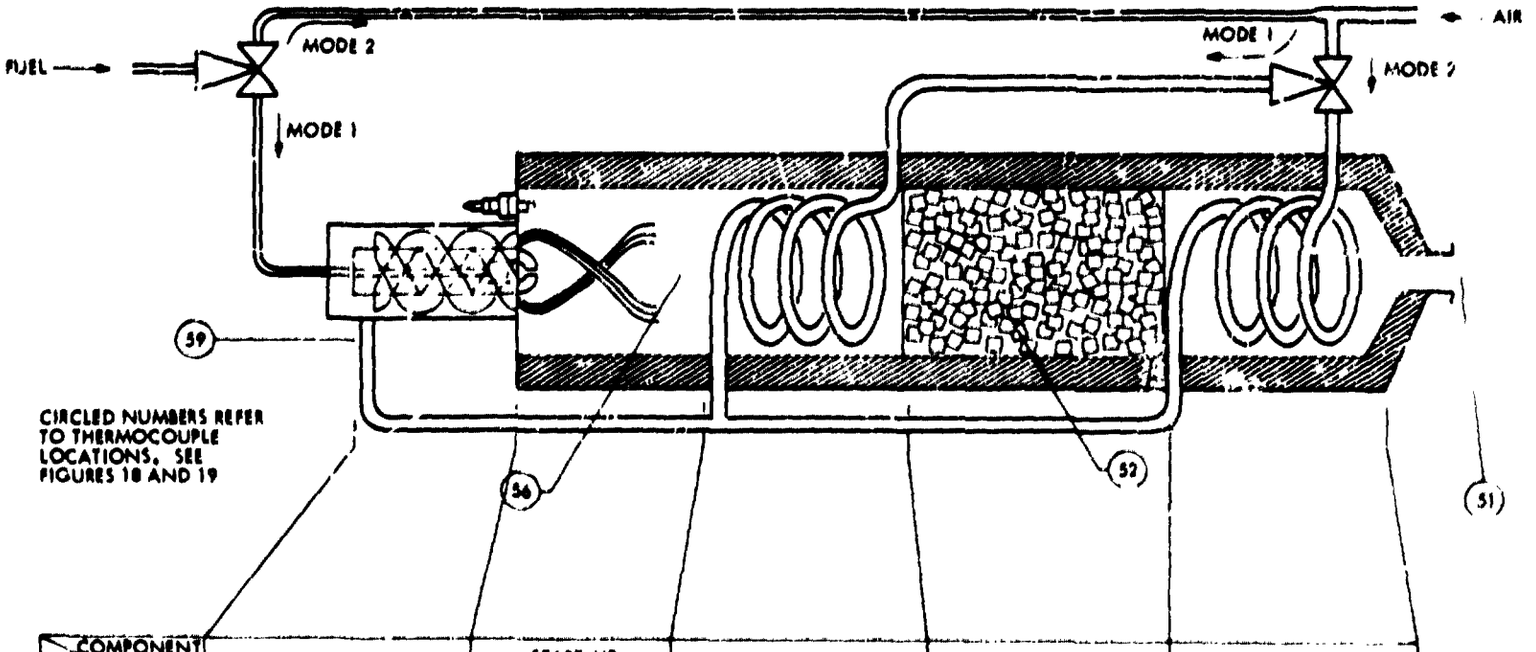

COMPONENT / FUNCTION	AIR/FUEL MIXER	START-UP REACTION CHAMBER	START-UP HEAT EXCHANGER	CATALYST BED	STEADY STATE HEAT EXCHANGER
MODE 1 START-UP	COLD FUEL ATOMIZATION COLD AIR INJECTION	FUEL/AIR MIX, FLAME REACTION TO 10% CH_4, 5% H_2	FUEL/AIR PREHEAT TO 300°C PRODUCT COOL TO 1000°C	FLAMELESS REACTION TO 8% CH_4, 7% H_2	
MODE 2 STEADY STATE	VAPORIZED FUEL/ PREHEATED AIR MIX	ADDITIONAL FUEL/AIR MIXING		FLAMELESS REACTION TO 1% CH_4, 21% H_2	FUEL/AIR PREHEAT TO 300°C PRODUCT COOL TO 600°C

Fig. 17. Integrated catalytic hydrogen-generator design concept

richening to an A/F = 6.6. Operation time at an A/F = 9 must be minimized so as to prevent overheating the catalyst.

At the end of step 1 the fuel and air are re-routed, as shown in Figure 17, through the steady-state heat exchanger and the A/F ratio is reduced to 6.6. Step two results in at least a partial shift of the reforming process from thermal to catalytic and continues until the catalyst bed reaches a temperature of ~1400°F. That temperature is high enough so that the catalyst is sufficiently activated to sustain steady-state operation at an A/F = 5.2. Mixture richening to an A/F = 5.2 completely extinguishes the flame in the startup reaction chamber, but the reactions continue, "flamelessly" on the catalyst.

b. Test Hardware Description

The generator hardware used for the startup tests is shown in Figure 18. As shown there, two coiled tube type heat exchangers were used. The tube material was 321 SS, with an OD of 0.375" and a wall thickness of 0.035". There are 30 in. of tube length in the startup heat exchanger and 57 in. of length in the steady state unit. The catalyst shown in the 3.5 in. dia. by 4.5 in. long wire mesh container is 1.5 lbm of 1/8 in. dia. x 1/8 in. long cylindrical alumina pellets containing 10% by weight molybedenum and 2.4% cobalt. This was purchased from the Harshaw Chemical Co. as catalyst type 0402T. The burner housing provided the volume necessary for the startup reaction and served as the attachment point for the fuel/air feed lines and the startup heat-exchanger lines. The chamber is 13 in. long with a 4 in. ID and is lined with a 1/4 in. layer of alumina. When assembled, the reaction chamber is 3-1/2 in. in diameter with 2-1/2 in. between the exit of the fuel/air mixer and the start-up heat exchanger. There is a 1/4 in. gap between each of the two heat exchangers and the catalyst bed. A conventional automobile spark plug is shown

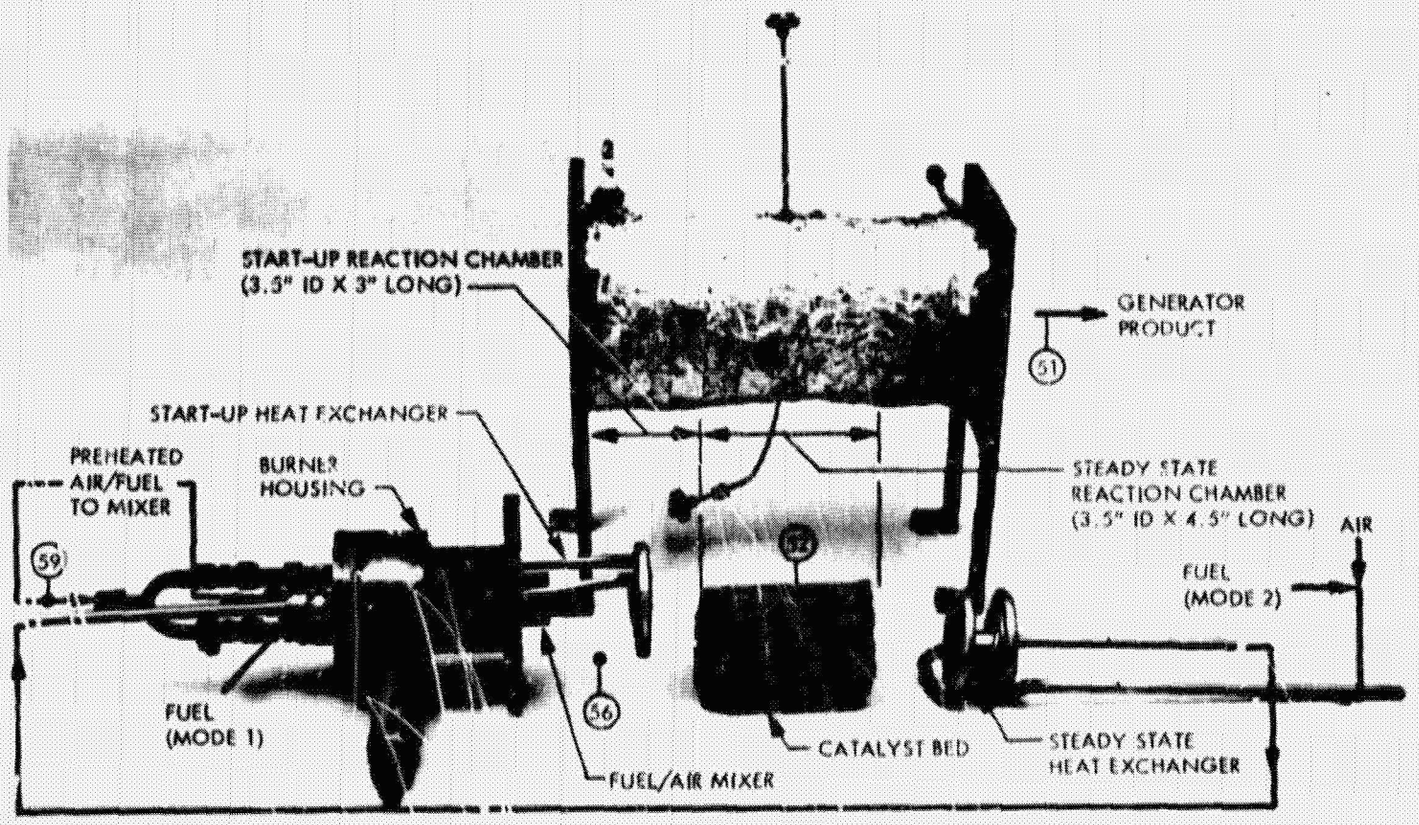

Circled numbers refer to thermocouple locations. See Figures 17 and 19.

Fig. 18. Experimental catalytic hydrogen generator with coiled tube-type heat exchanger

installed in the chamber wall. It is used to initiate combustion, and once combustion has been established the plug is no longer energized.

c. Test Results

Figure 19 summarizes the temperatures variations during the three-step startup sequence. The temperatures were measured by the thermocouples located as shown in Figures 17 and 18. The temperature in the void upstream of the catalyst bed, TC 56, indicates the presence of the flame during operation at an A/F = 9.0. During this same period, the air preheat temperature, TC 59, reaches 490° F. Immediately after the air/fuel ratio is enriched to 6.6, the void temperature (TC 56) begins a rapid decrease. During the second step operation, the catalyst bed temperature (TC 52) rises at an increasing rate. At the end of this second step, the air preheat temperature (TC 59) and void temperature (TC 56) are nearly equal, and the catalyst bed temperature is well above the catalyst activation temperature of 1400° F. The product gas temperature (TC 51) rises continuously during the startup process and reaches its equilibrium value of ~1200° F after approximately 200 seconds.

Continuous analysis of the generator products during startup was made for concentrations of four species. A thermal conductivity analyzer was used for hydrogen, nondispersive infrared analyzers for carbon dioxide and carbon monoxide, and a flame ionization analyzer was used to measure unconverted hydrocarbon concentrations. As in previous generator tests, product analyses with a gas chromatograph indicated the composition of the unconverted species was generally 90% methane, 10% ethylene and only trace quantities of higher molecular weight hydrocarbons.

The analog output from the four gas analyzers as well as all other test data (temperatures, pressures, and flowrates) are recorded on printed paper

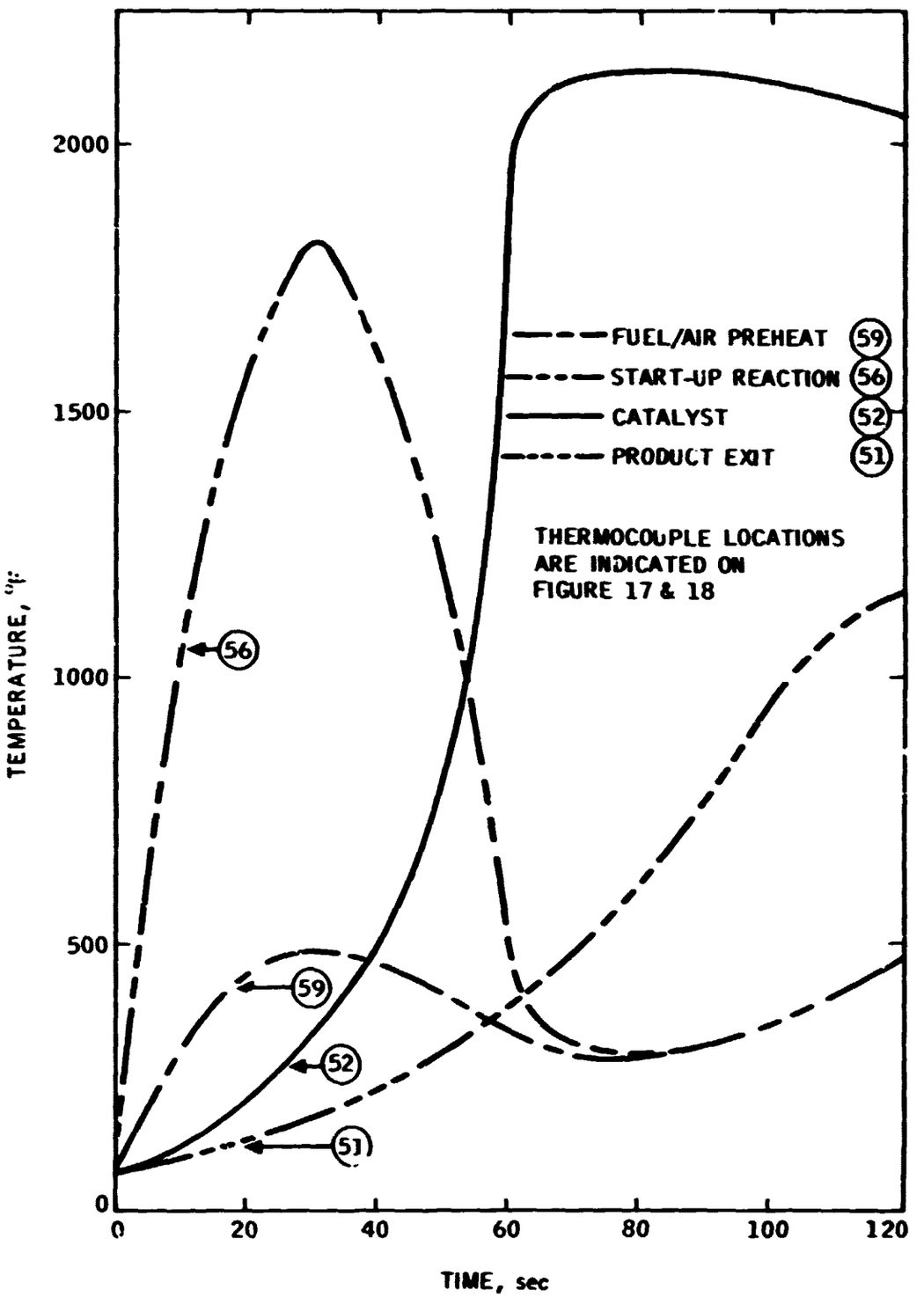

Fig. 19. Generator start-up operating temperatures

and magnetic tape. The magnetic tape is used for post-test computer data analysis. The gas analysis data, as well as key temperatures, are also recorded with continuous recording multiple-pen recorders. The response lag of the analysis system, considering both the sample transit time from generator-to-analyzer and the analyzer equilibration time, has been subtracted from the gas analysis data in Figures 20 and 21. By operating the generator at steady-state conditions and alternately sampling the generator product and injecting 100% nitrogen into the sample line, the response characteristics of the analysis system was determined. The sample transit time is 20 seconds, and the analyzer equilibration period is 35 seconds for the hydrogen and carbon monoxide.

Figures 20 and 21 show H_2, CO, CO_2 and CH_4 compositions as functions of time for the startup test shown in Figure 19. The dashed lines represent the theoretical equilibrium composition assuming instantaneous response to the step changes in air/fuel ratio. Forty-four seconds are required to reach the equilibrium level at A/F - 9.1, with an additional 20 seconds to reach the A/F - 6 level, and 10 seconds more to reach the steady-state level. This assumes the asymptotic approach to equilibrium shown is not a generator characteristic but a result of not completely subtracting the analyzer response characteristic. The dotted line shown is considered to be the actual hydrogen response. Earlier tests have shown the generator response to be instananeous for fuel flow and air-to-fuel ratio changes of 25% as long as the catalyst temperature is 1800°F or higher. Similar instantaneous response was obtained when doubling the air and fuel flowrates at a constant air/fuel ratio.

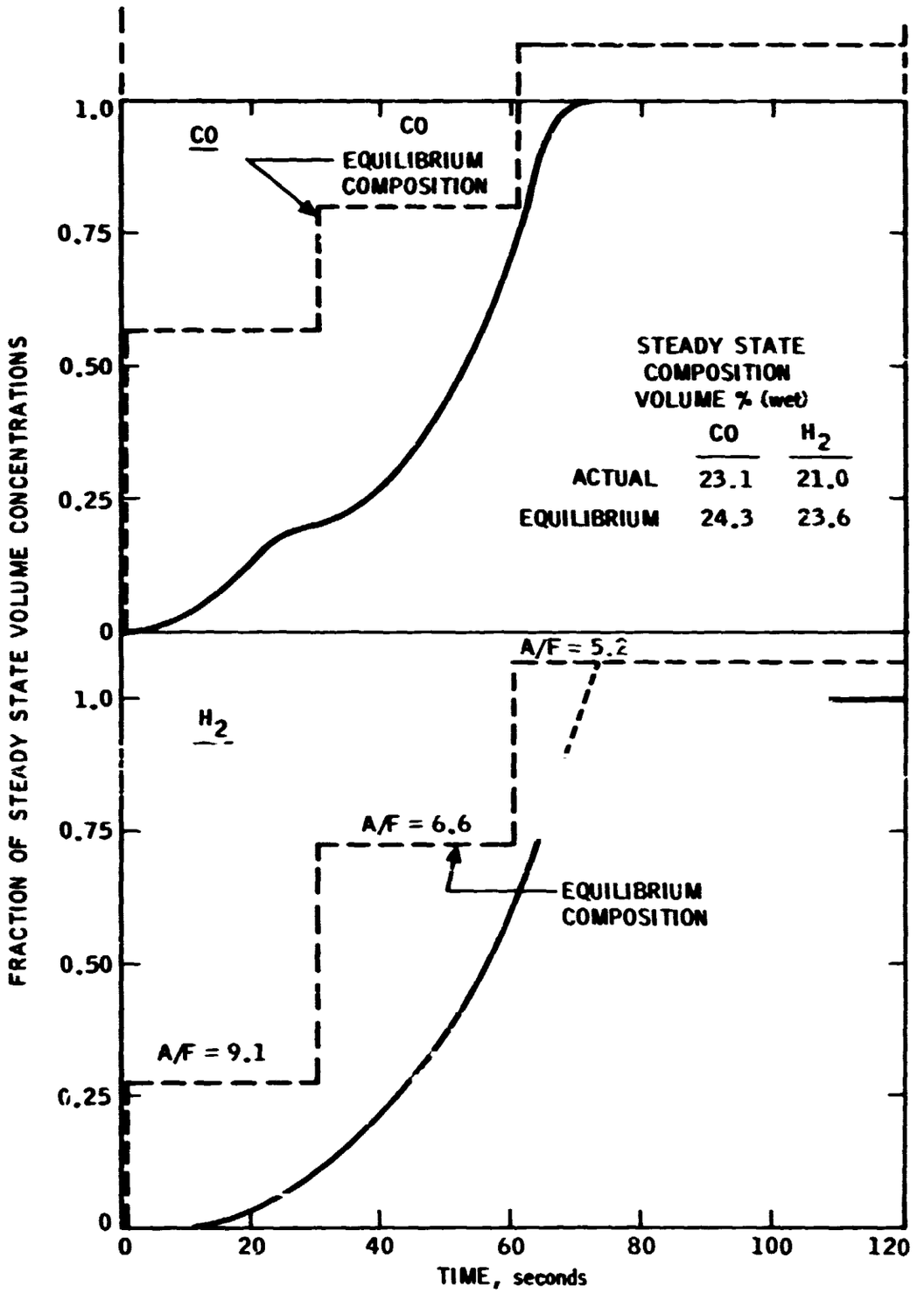

Fig. 20. Generator product H_2 and CO volume concentrations during start-up

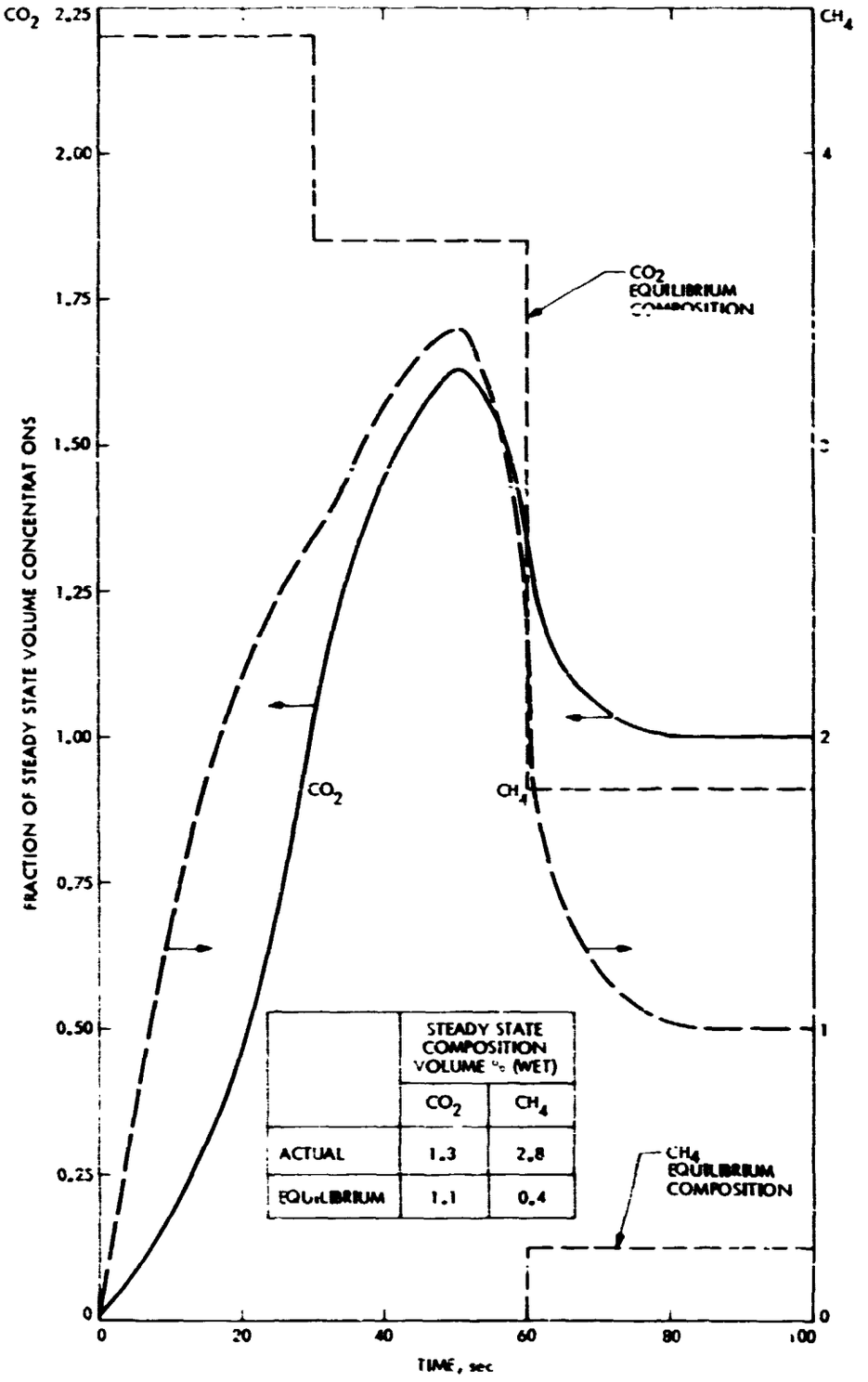

Fig. 21. Generator product: CO_2 and unconverted HC volume concentrations during start-up

Figure 21 shows the carbon dioxide and unconverted hydrocarbon (as methane equivalent) concentrations normalized by their respective steady-state concentrations. This shows the average methane concentration to be approximately 2.5 times the steady-state value during the first 50 seconds of operation. This is the result of the relative ease of thermally decomposing gasoline to methane (as compared to cracking for hydrogen) when the average reaction temperature is less than 1000°F. This is a fortituous condition which raises the heating value of the generator product to a level, after only 20 seconds, sufficient to start the engine; whereas, the heating value of the hydrogen plus carbon monoxide does not reach the same value until 55 seconds after generator startup.

Using the mole fraction composition data of Figures 20 and 21, the mass flowrates, $\dot{m}_i$, of the four species were calculated from the following equation:

$$\dot{m}_i = \frac{n_i \times mw_i \times (\dot{m}_a + \dot{m}_f)}{\overline{mw}}$$

where

n_i = mole fraction (wet) of i^{th} species (H_2, CO, CO_2, CH_4, N_2, H_2O)

mw_i = molecular weight of i^{th} species

$\dot{m}_a$ = input air flowrate

$\dot{m}_f$ = input fuel flowrate

$\overline{mw}$ = mixture molecular weight

$$\overline{mw} = \sum_{i=1}^{6} n_i \times mw_i$$

This calculation requires nitrogen and water mole fraction as input quantities. The nitrogen concentration is, of course, directly calculable from the input air flowrate. The water vapor content in the generator product is unknown.

An iterative type calculation is used to estimate the water-vapor content which balances the atomic oxygen mass balance. Carbon and hydrogen mass balance calculations for the product composition during the last 20 seconds of the startup show the compositional data to be consistent. Carbon and hydrogen mass balance differences during the first 45 seconds of generator operation indicate that the concentrations shown in Figs. 20 and 21 for hydrogen and methane underestimate the actual generator outputs. Since this will provide a conservative estimate of generator startup performance, the higher methane and hydrogen concentrations that are calculated using mass balance constraints are not shown here. Future tests will be required to verify the apparent undermeasurement of hydrogen and methane.

The mass flowrates of H_2, CO_2, CO and CH_4 calculated from Figures 20 and 21 composition data are shown in Figure 22. The mass flowrates of the combustible species (H_2, CO, and CH_4) were used to calculate the heating value of the generator product during the generator startup. These values are shown in Figure 23, normalized by the lower heating value of the gasoline (5 lbm/hr) required to idle the V-8 engine of Task D. When this parameter, termed heating value fraction (HVF) becomes unity, the engine should start on generator product alone. The engine/generator combination of Task D has already demonstrated an engine start on a steady-state flow of generator products containing 0.5 lbm/hr of hydrogen. This corresponds to an HVF = 1.33.

The calculated flowrates for carbon monoxide, carbon dioxide, methane, and hydrogen species are shown in Figure 22. The total generator exit

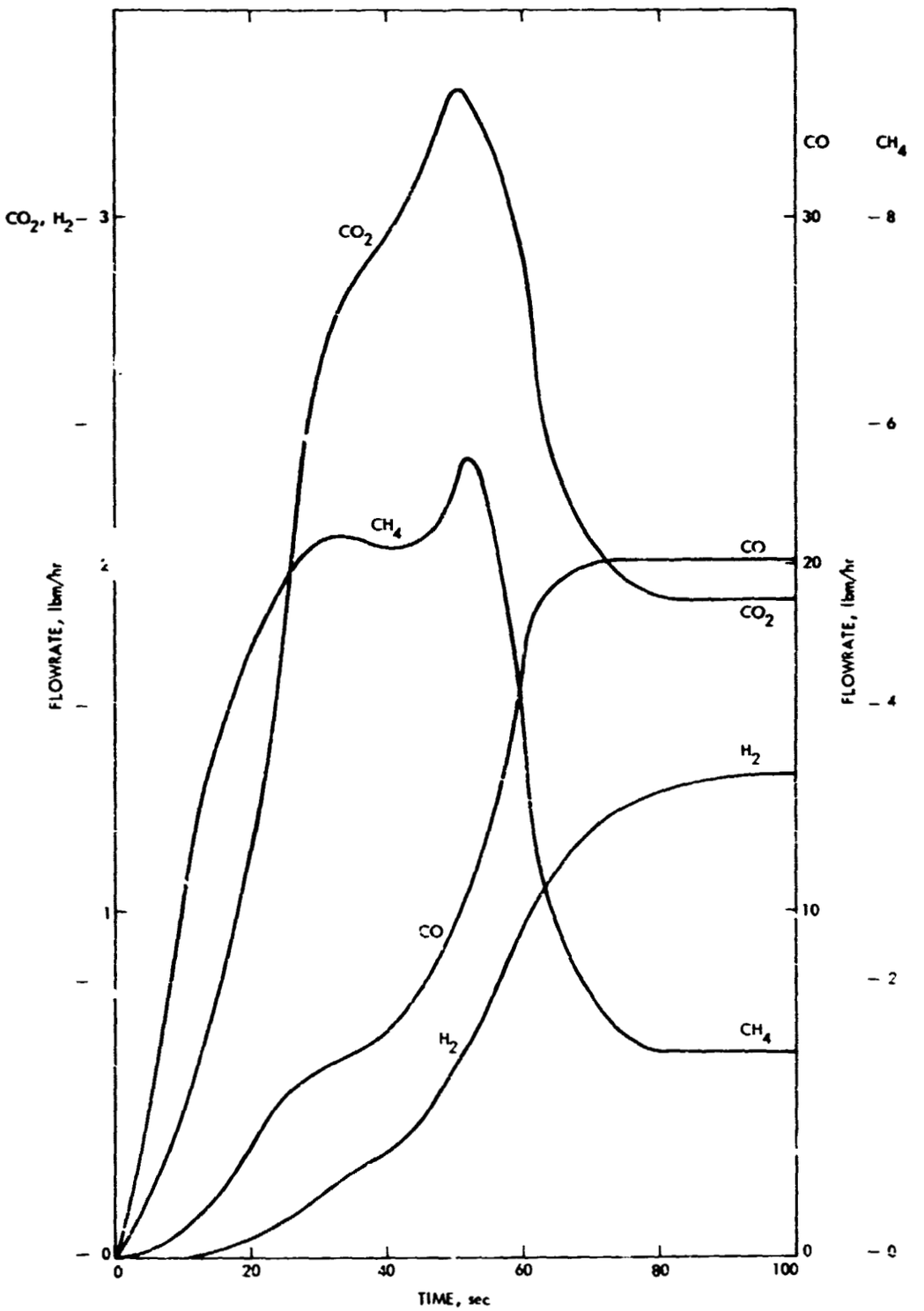

Fig. 22. Generator product flow rates of: H_2, CO, CO_2, and CH_4 during start-up

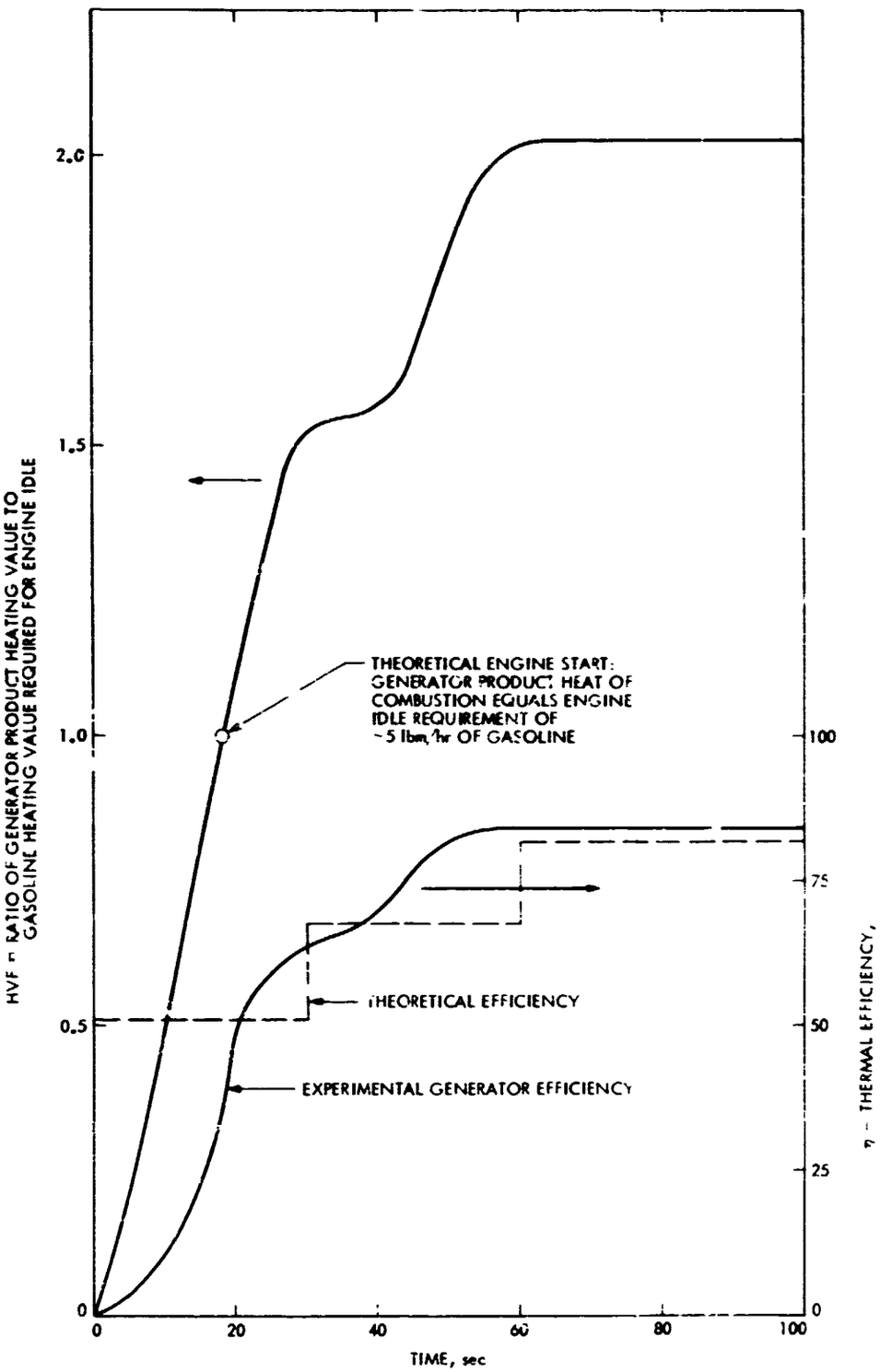

Fig. 23. Generator thermal efficiency and generator product heating value variation during start-up

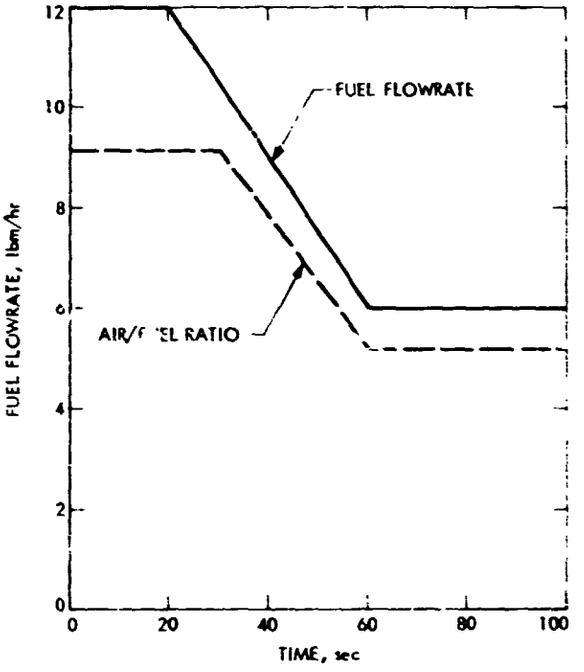

Fig. 24. Theoretical generator fuel flow and air/fuel ratio programming required for constant engine idle speed after start-up

flowrates, including nitrogen and water vapor flowrates, were found to be 12, 8, and 1% less than the air plus fuel input flowrate 30, 50, and 80 secs after startup, respectively. The error in composition is attributed to incomplete compensation for the slow response of the gas analyzers. The response characteristic consists of a 20-second sample transit period plus an additional 35 seconds for full hydrogen analyzer response and 20 seconds for the CO, CO_2, and CH_4 analyzers. A molecular species mass balance can be made to estimate the product composition from time zero at startup, but this requires the assumptions (1) that there is an equilibrium concentration of water vapor of 12% and no free oxygen, and (2) there is no mass holdup of either solid carbon or

unreacted hydrocarbons which condense on the cold catalyst or cold chamber walls during the first 20 seconds of operation. With these uncertainties, it was considered prudent to use the gas analyzer-induced-composition even though in error by approximately 20% over the startup cycle since the indicated composition is an underestimate of the actual generator output.

The variation of generator thermal efficiency during generator startup is also shown in Figure 23. The quantities HVF and η shown in Figure 23 are defined as follows:

HVF = generator product heating value fraction

η = generator thermal efficiency

$$HVF = \frac{\sum_{i=1}^{3} \dot{m}_i \times h_i}{\dot{m}_{e_o} \times h_g}$$

$$\eta = \frac{HVF \times \dot{m}_{e_o}}{\dot{m}_g} \times 100$$

where:

$\dot{m}_i$ = mass flowrate of i^{th} species (H_2, CO, CH_4)

h_i = lower heat of combustion of i^{th} species

$\dot{m}_{e_o}$ = gasoline flowrate at engine idle

h_g = gasoline lower heat of combustion

$\dot{m}_g$ = gasoline flowrate to generator

The heating value fraction is shown in Figure 23 to be 2.03 by the end of generator startup, indicating the engine speed at the end of MODE 2 would be approximately double normal engine idle speed. Figure 24 shows the air/fuel

ratio and fuel flowrate variation necessary during startup to achieve constant engine idle speed (i.e., achieve a constant value of HVF = 1.0) during generator startup.

4. Conclusions and Summary

a) A catalytic generator with 13.5 lbm of catalyst has demonstrated experimental hydrogen yield fractions of 0.89 to 0.98 of theoretical yield. Hydrogen output flowrates of 0.4 to 2.1 lbm/hr of hydrogen were obtained. No water or steam was required for these results.

b) The increase in hydrogen yield fraction with increasing fuel/air flowrate indicated the generator volume (i.e., the generator containing 13.5 lbm of catalyst) and/or the catalyst volume is larger than needed to obtain hydrogen outputs of up to 2 lbm/hr.

c) High efficiency operation was obtained over a wide range of catalyst temperature, 1500 to 1900°F, thus providing a satisfactory safety margin.

d) The relatively low reaction temperature combined with the use of ceramic liner materials produced reaction chamber temperatures of 1000°F or less, thus making the use of inexpensive structural materials possible.

e) The controllability of the flameless catalytic oxidation process in the generator was established. This process is requisite for (1) high-yield efficiency, (2) elimination of water or steam injection, and (3) low solid-carbon production rates of 0.002 lbm of carbon per pound of fuel.

f) Equilibrium hydrogen output was achieved in ~60 seconds.

g) The energy content of the generator output stream was sufficient ~20 seconds after generator startup to achieve engine start.

C. MULTI-CYLINDER ENGINE TESTS (EPA TASK D)

1. Introduction

The primary objectives of the task were to assess quantitatively the state-of-the-art of the hydrogen enrichment concept and to provide an experimental base from which to estimate the potential of the concept. The work described in the report was undertaken early in the evolution of the hydrogen enrichment. In particular, it was recognized that both the hydrogen generator and IC engines, as related to ultra-lean operation, were not maturely developed. Nevertheless, previous experience using mixtures of pure hydrogen and gasoline had shown a dramatic decrease in NO_x emissions and a significant increase in engine thermal efficiency. However, since the same experience had been acquired with bottled, compressed hydrogen and not with the products from a hydrogen gas generator, there were still unanswered questions concerning hydrogen enrichment. In particular, (1) the effect of non-hydrogen constituents, both combustible and non-combustible, in the generator gas stream; (2) the effect of the use of a gas generator on overall brake specific fuel consumption (BSFC); and (3) the effect of the use of generator products on hydrocarbon and carbon monoxide exhaust emissions, were all unknowns.

Three distinct engine configurations were used. These were: (1) a stock engine, complete with carburetor, two-plane intake manifold, inductive ignition system, exhaust gas recirculation (EGR) and operated with only gasoline as the fuel; (2) the same engine block as (1) but equipped with a single plane intake manifold, an Autotronics gasoline delivery system, and a multiple-strike, capacitive discharge ignition system and operated with only gasoline as the fuel; and (3) the same configuration as (2) but further modified to allow distribution of the hydrogen-generator products and operated with mixtures of gasoline and

generator products as the fuel. The details of these engine configurations are given below.

The rationale for testing the three engine configurations are as follows. Configuration (1) duplicated as nearly as possible the engine as used on a vehicle. Tests of this configuration represented a baseline condition from which all other test data were compared. Configurations (2) and (3) were identical except that generator products were not used in tests of the (#2) configuration. Tests of the (#2) engine were performed so that any benefits attributable only to the hardware change could be so identified. The configuration (3) then differed from (2) only in the use of hydrogen-generator product gases and was the hardware used to evaluate the hydrogen-enrichment concept. The test results of these three engine configurations are presented below.

2. Test Hardware Description

a. Engine Configuration (1)

The Chevrolet 350 CID engine (1973) was selected as representative of a production passenger car engine in wide use. A few of the pertinent characteristics are tabulated below.

Induction System

The stock engine induction system consisted of a dual-plane intake manifold and 4-barrel Quadrajet carburetor. In place of the engine fuel pump, a pressurized facility storage tank was used to feed gasoline to the carburetor float chamber.

Ignition System

The stock ignition system was the standard breaker-point type consisting of a coil, condenser, distributor, wiring and spark plugs. Factory equipped carbon-core spark plug wires were replaced with metallic conductor,

Engine Manufacturer Specifications

Engine: Chevrolet 1973

No. Cyl.: V-8

Bore: 4.00 in.

Stroke: 3.48 in.

Displacement: 349.7 cu. in.

Specified Compression Ratio: 8.5

Advertised HP: 175 @ 4000 RPM

Advertised Torque: 260 lb-ft @ 2800 RPM

silicon-insulated ignition wire. The AC R-44 resistor type spark plugs were gapped at 0.035 inches.

Emission Control Devices

The factory-installed devices for emissions control included (1) an air injection reactor (AIR) pump and distribution manifold, (2) an exhaust gas recirculation (EGR) system and (3) a positive crankcase ventilation (PCV) system. The purpose of the AIR system was to provide additional air to the exhaust gases and thus reduce unburned hydrocarbons and carbon monoxide. The EGR (used to reduce oxides of nitrogen) control valve was externally located in the intake manifold adjacent to the rocker arm cover. Internal flow passages directed the exhaust gases into the intake manifold below the carburetor throttle plates. The PCV system maintained a positive flow of crankcase blowby gases back into the engine air intake system and was used during all tests of the baseline stock engine and modified test configurations.

b. Engine Configurations (2) and (3)

The modified engine was derived from configuration (1) by removing the AIR and EGR emission devices and replacing the carburetor and intake manifold with an Autotronics induction system. The PCV system was connected for all engine tests using the Autotronics induction control system. The Autotronics equipment was selected primarily for the flexibility of the associated controls and for the potential improvements in atomization and distribution offered at lean operating conditions. The modified system is shown schematically is Figure 25. Air flow to the engine was sensed by a turbine air-flow transducer. Gasoline flow to the engine was controlled by a variable speed, positive displacement pump. The pump speed, proportional to gasoline flow, and the air flow signal were used by the processor to calculate air/fuel ratio. The computed air/fuel ratio was compared to the value selected by the user and the resulting error signal was used by the pump power-drive circuit to supply more or less electrical power to the pump, hence changing the gasoline flowrate in accordance with the user selected air/fuel ratio setting. Component parts of the Autotronics induction control system are shown in Figure 26.

Air throttling was achieved by rotation of an air butterfly valve located upstream of the plenum chamber. Primary air for the engine entered the chamber with a vortex flow pattern while a portion of the air bypasses the throttle plate and was the working fluid for a Hartman whistle atomizer. The atomizer, which was centered directly above the intake manifold, received gasoline from the positive displacement metering pump. The atomized gasoline was then mixed with the primary air stream as it flowed through the plenum chamber. The gasoline and air mixture was distributed to each cylinder with an aluminum, single-plane Tarantula (Edelbrock Co.) intake manifold.

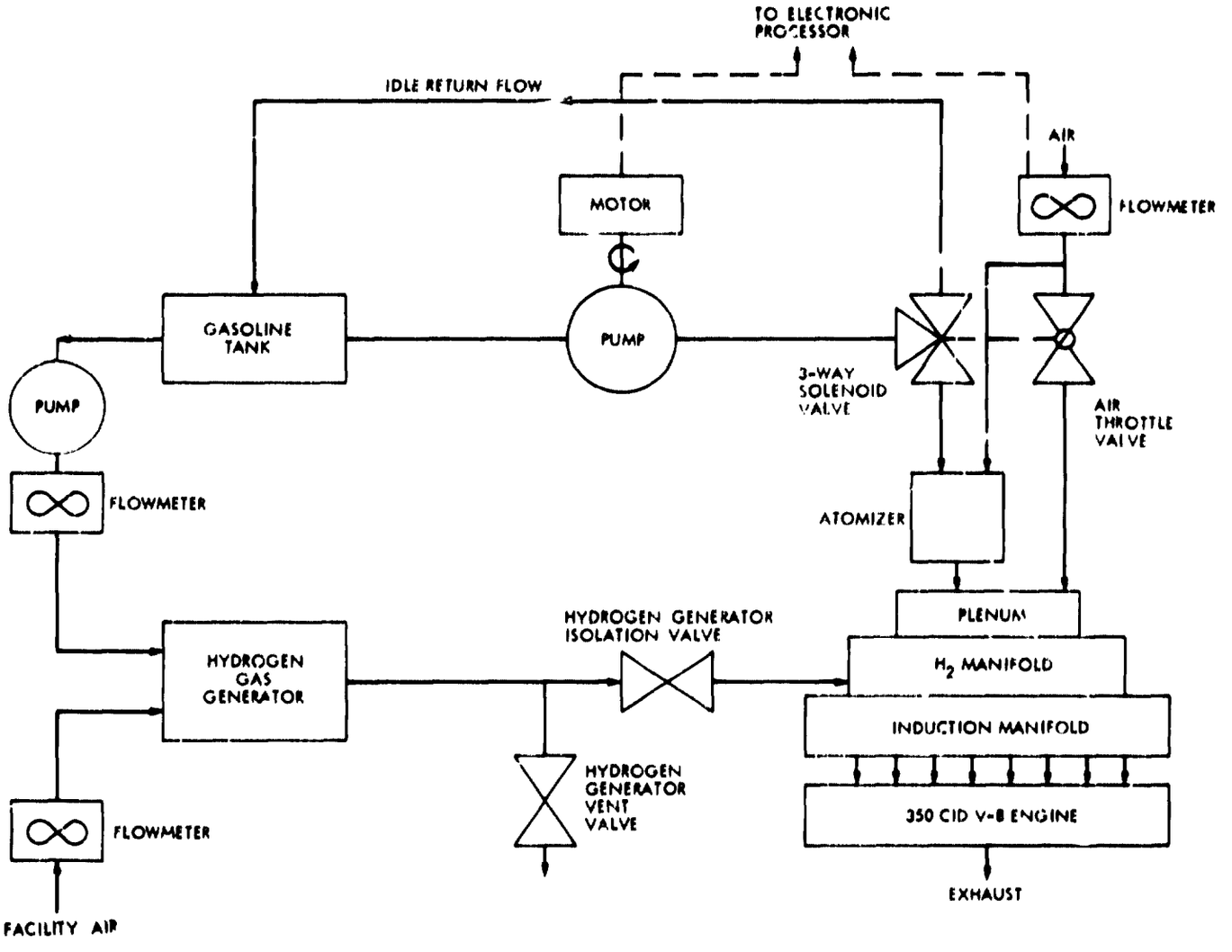

Fig. 25. System schematic for modified test engine with hydrogen-gas generator

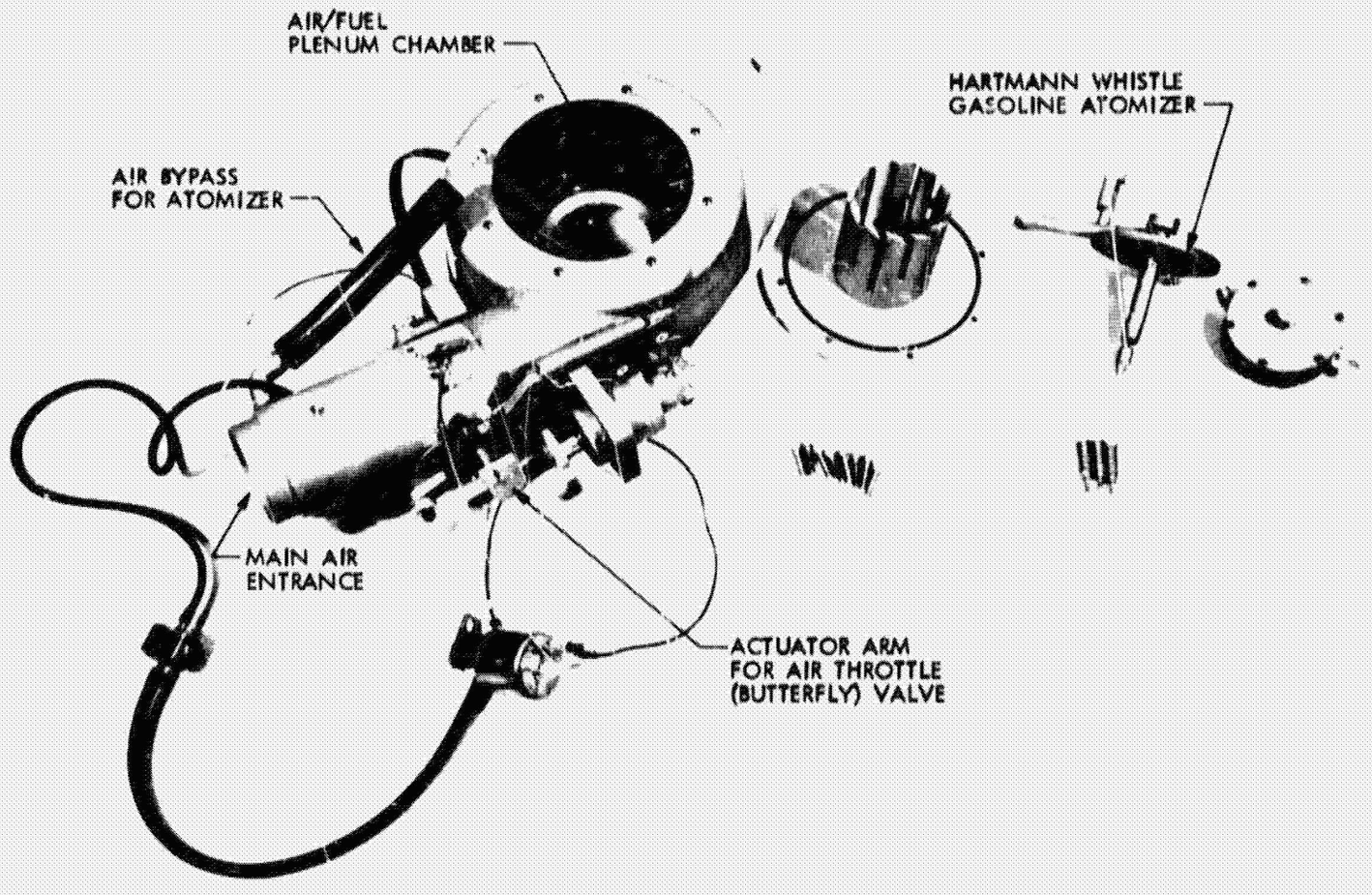

Fig. 26. Components of the Autotronics induction control system

A modified ignition system, supplied as a part of the Autotronics equipment, was used. The ignition system included a special coil with a rise time faster than the stock system, a condenser, and distribution breaker points. The high energy (60,000 volts open circuit voltage) capacitative discharge ignition system also provided multiple striking capability with external control of the number of degrees of crankshaft rotation over which multiple sparks would take place. An electronic retard capability exists but was not used for the tests described here. Champion RBL-17Y spark plugs were used with a 0.070-inch gap. The Autotronics electronics required shielding from the ignition system; therefore, special ignition wires were employed that had metal conductors with Monel wire shields. The stock dual-exhaust manifolds were replaced with special headers to permit exhaust gas sampling of the individual cylinders. Figure 27 shows the engine/gas generator test setup.

The products from the hydrogen-gas generator, described earlier in this report, were connected to a special distribution manifold. This manifold was installed between the Autotronics air plenum and single-plane intake manifold. The generator gases enter the distribution manifold through four lines, spaced 90° from each other, and into an annular space. Flow from the annulus into the intake manifold is through eight slots. Generator product gases were injected at near-atmospheric pressure into the engine-induction system. During generator warmup, the output gases were vented overboard using a facility vent valve (see Figures 25 and 27). The product gas was periodically analyzed to determine the H_2, CH_4, CO and CO_2 content prior to its introduction to the engine. No significant deviations from the data of Table 1 and Figure 15 were noted.

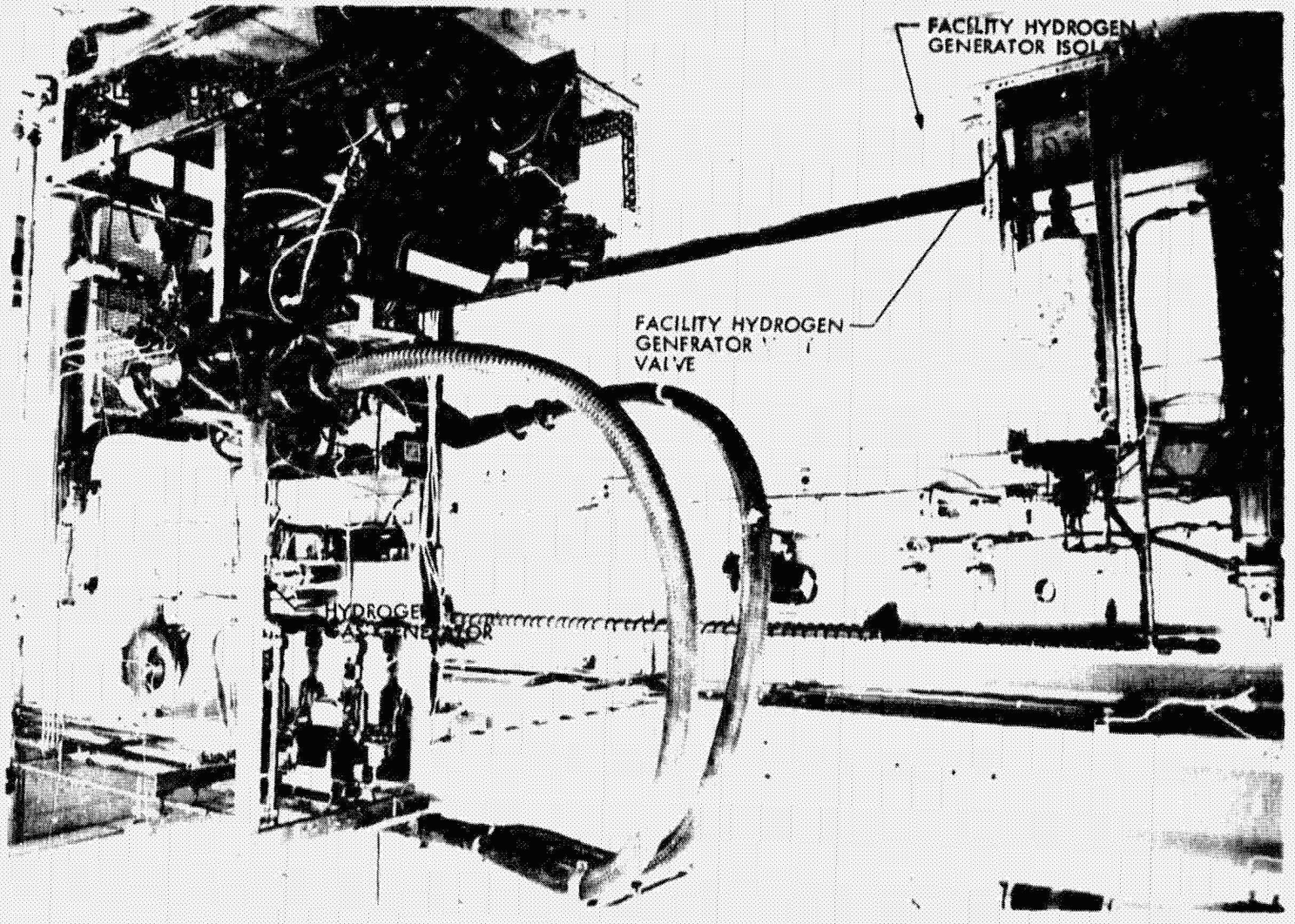

Fig. 27. The engine/gas generator setup

3. Test Instrumentation

The following paragraphs contain a general discussion of what parameters were measured, the type of transducer used for the key parameters, the recording devices, and special data techniques used.

A digital data acquisition system was used and is the heart of the instrumentation capabilities. The IDAC (Integrated Data Acquisition and Control) data system was designed at JPL in 1966 for rocket propulsion test programs and includes both real-time engineering unit output and control capabilities.

The real-time data capability is provided by a combination of printed paper tape, eight video displays, and 16 digital-to-analog converters. In addition, recording on magnetic tape is possible. The engineering units capability includes ranging and scale factors for all standard transducers, thermocouple linearization, and output with appropriate units. The system will limit-check 64 data channels in real-time. The IDAC can also accept digital inputs in addition to analog signals. The digital capability was used for gasoline flowrates (turbine flowmeters), for digital spark timing data, and to accept digital codes which automatically define the status and range of the various emission instruments.

The IDAC hardware and basic program was used for the engine tests, described here, without modification. An additional program was developed that provided the real-time calculation and display of several parameters unique to the engine test program. This program calculated these key parameters and was used to facilitate the testing. These parameters were:

1) Gasoline mass flowrate (for both engine and gas generator).

2) Air-mass flowrate (for both engine and gas generator).

3) Equivalence ratio (including the contribution of the generator products).

4) Thermal efficiency (including the effect of the generator).

5) Emission data independent of the operator selected instrument range.

Calculation errors for these parameters, independent of transducer errors, were on the order of 0.2%. Calculations for approximately 30 other parameters were also made and were available for real-time output. Data were updated at approximately 1/2-second intervals, which was more than adequate for the steady-state test conditions employed. A much-faster sampling capability is inherent in the IDAC, but was not used for the testing described in this report.

The hydrogen enrichment concept leads to engine operating conditions which result in very low flowrates of liquid gasoline to the engine. Gasoline flowrates ranging from 0.001 gpm to 0.5 gpm were encountered. JPL has successfully made use of turbine flowmeters for flows of liquids, and the IDAC was designed specifically to be compatible with this type of meter. However, turbine flowmeters typically have a dynamic flow range of 10:1. To cover the range of flowrates of interest here, three meters were required. They were arranged as shown schematically in Figure 28, and the gasoline flow was routed to the desired flowmeter by the solenoid valves.

The flowmeter frequency, gasoline temperature, gasoline pressure, and flowmeter codes (i.e., which meter was active) were input to the IDAC. The code signal was used to access the flowmeter calibration constants for the active flowmeter; a quadratic equation was used to convert the frequency to volume flow. Real-time mass flowrate data, corrected for temperature effects, was output in units of lbm/hour.

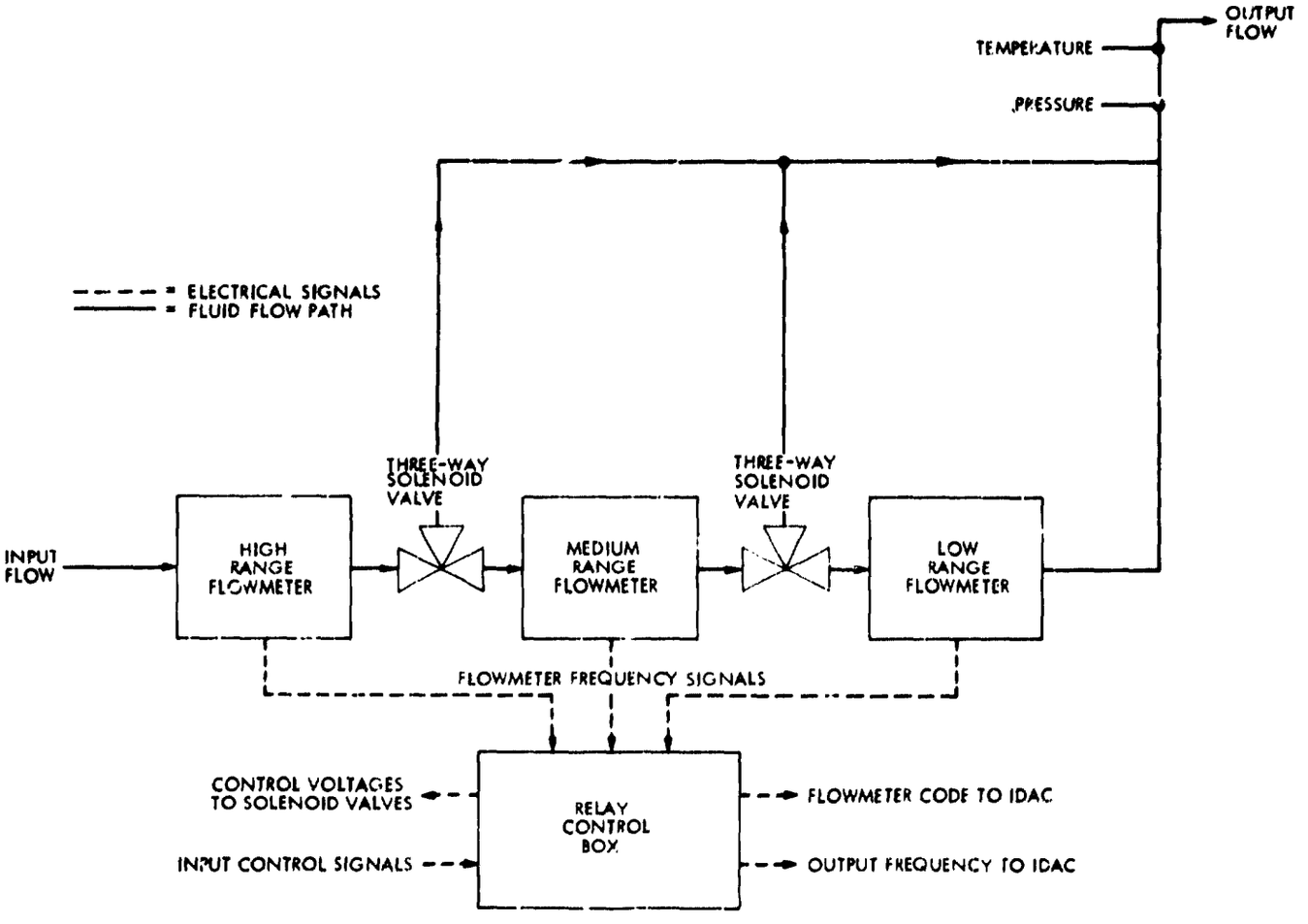

Fig. 28. Gasoline flowmeter block diagram for V-8 engine

Gaseous flows were measured by a laminar flow transducer; the differential pressure across the flowmeter is linearly proportional to the actual volume flow through the flowmeter. To provide mass flow data, absolute pressure and temperature of the flowing gas were measured and input to the IDAC.

A signal proportional to spark timing was derived from the mechanical hardware shown in Figure 29. The disc, attached directly to the engine crankshaft, contains a ring of holes (the innermost) located at 10° crankshaft intervals. A light source on one side of the disc excites a light sensitive detector whenever a disc hole passes between the light source and detector.

These pulses are input to an electronic phase locked loop circuit. This loop tracks the 10° pulses and provides an output frequency 100 times the input frequency, i.e., 0.1° degree resolution. Firing of the number 1 spark plug generates a signal that passes the 0.1° pulses to a counter. The counter is turned off at top dead center, TDC, thus providing a count equal to the spark timing with 0.1° resolution. The logic includes the capability to measure spark timing after TDC. The spark timing error is less than ±0.2 at steady-state engine speeds. The counter output is available in binary coded decimal form and is recorded by IDAC via a digital input channel.

Continuous analyses were made of the engine exhaust gas to determine the concentration of CO, CO_2, NO_x (NO_2 and NO), and unburned hydrocarbons. The CO_2 and CO analyzers operate on the principle of non-dispersive infrared adsorption. Nitric oxide (NO) and nitrogen dioxide (NO_2) were measured with a chemiluminescent instrument. Oxides of nitrogen (NO_x) are reported as the sum of NO and NO_2 contained in a gas sample as if the NO were in the form of NO_2. Hydrocarbons were measured with a flame ionization detector.

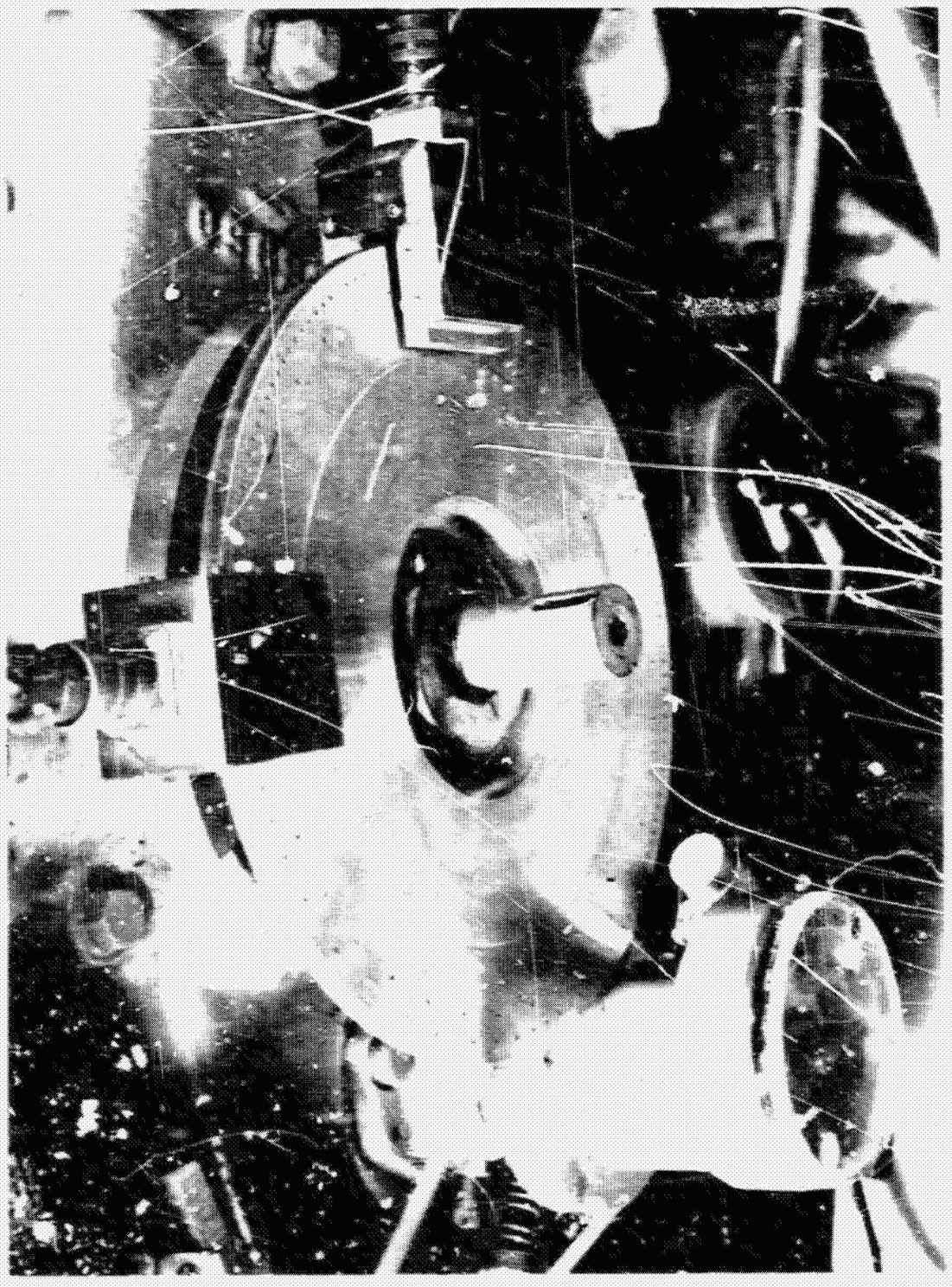

Fig. 24. Timing disc

Engine brake horsepower was measured with a water-brake dynamometer rated from 4 to 800 BHP at speeds to 10,000 RPM. A part throttle friction horsepower curve, obtained from General Motors for a similar engine, was used to calculate the corresponding indicated horsepower.

4. Test Description

As noted earlier, three distinct sets of tests were made. The first tests involved the "stock" engine, as described in preceding paragraphs, and provided the baseline data from which comparisons were made. These tests used the equivalence ratio (i.e., fuel/air ratio) built into the carburetor and the spark timing built into the distributor. Two deviations from a "stock" engine configuration were employed. First, the engine-driven fuel pump was removed, and a pressurized tank was used to supply gasoline to the carburetor float chamber. This was done to improve the quality of the fuel flowrate measurement. Secondly, the "stock" exhaust manifolds were replaced by exhaust headers (see Figure 27). These headers allowed exhaust samples to be taken from the individual cylinders, but prevented the use of the air injection reactor (AIR) device. Thus, the HC and CO emissions presented here for the "stock" engine are not truly representative of the 1973 Chevrolet 350 CID engine but are more nearly indicative of those from an uncontrolled engine.

The baseline tests covered an engine speed range from idle (~800 RPM) up to 4000 RPM. Engine output from a no-load condition up to the wide-open throttle (WOT) power was covered. Data were taken at approximately 70 discrete RPM-load combinations. Measurements of exhaust emissions and engine performance were recorded at each of these operating conditions.

The data taken during these tests were first reduced to obtain calculated values of parameters such as brake specific fuel consumption (BSFC), equivalence ratio, brake and indicated specific emissions, and brake and indicated power. The final desired form of the data was contour plots of BSFC and brake specific emissions of oxides of nitrogen, of unburned hydrocarbons, and of carbon monoxide, as functions of engine RPM and brake mean effective pressure (BMEP). (See Figures 30 through 33.) The computer program which produced the contour plots required that all data points be provided at specific RPM intervals. Thus, it was often necessary to refer a data point taken at 2010 RPM, for example, back to 2000 RPM. This was accomplished by assuming indicated specific fuel consumption, engine air flow and emissions were constant for the range of the correction. To increase the number of points for the contour plotting program, the reduced data was curve fit with a third-order polynomial. This polynomial was used only to interpolate the data. No attempt was made to extrapolate the contours beyond the region where data were taken. These same techniques were used for the data from all tests including those involving the gas generator.

The other two engine configurations tested required a somewhat different test approach since neither the equivalence ratio nor the spark timing could be specified in advance. The following approach was adopted. The use of hydrogen allows operation at ultra-lean equivalence ratios, which in turn results in greatly reduced peak combustion temperatures. As a result, a spark timing which gives best engine economy (i.e., peak thermal efficiency) is entirely feasible. All tests involving the gas generator (i.e., configuration (3)) were performed at an equivalence ratio and spark timing which gave best engine efficiency. Therefore, tests involving configuration (2) were likewise performed at maximum engine

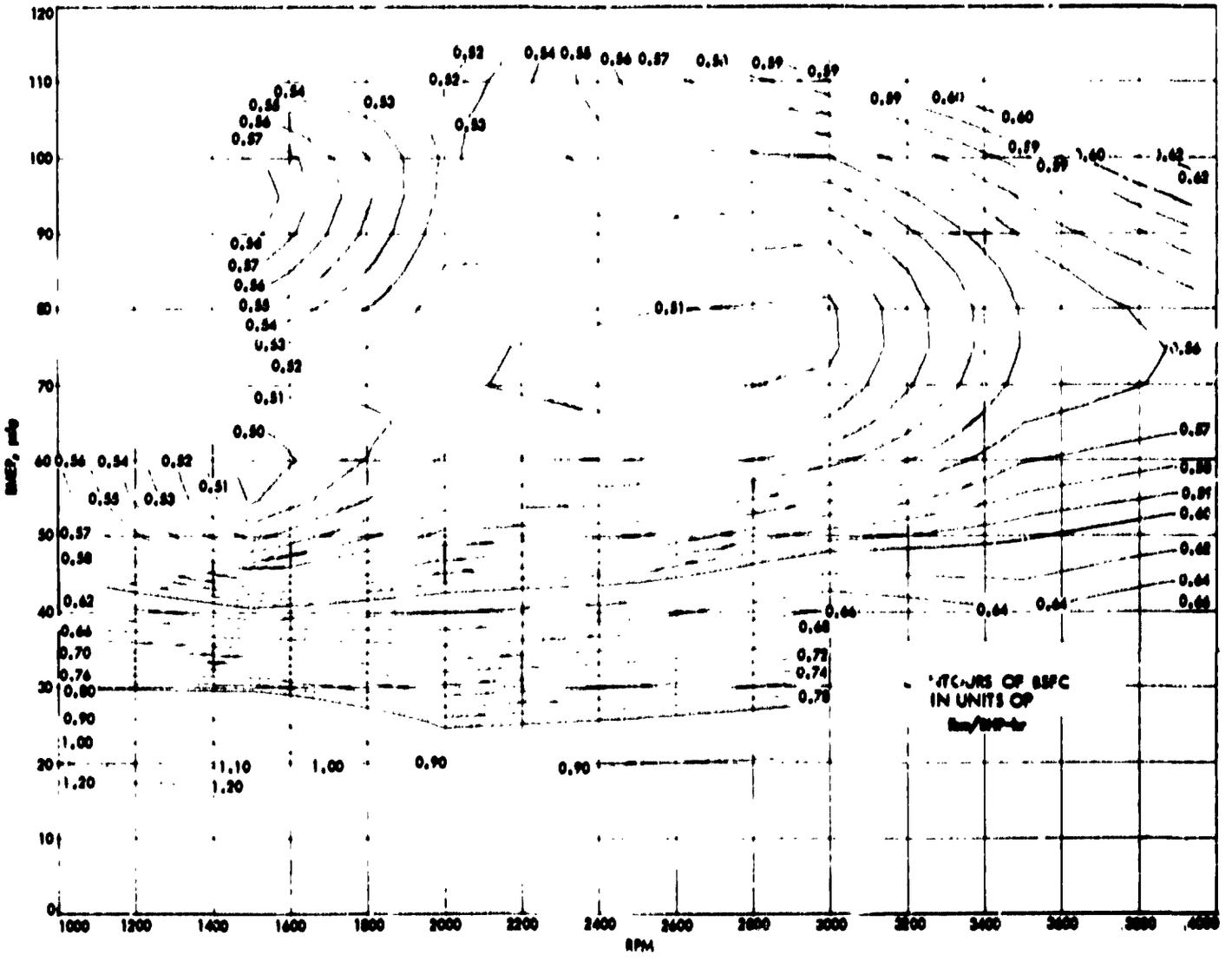

Fig. 30. BSFC contours (engine configuration 1)

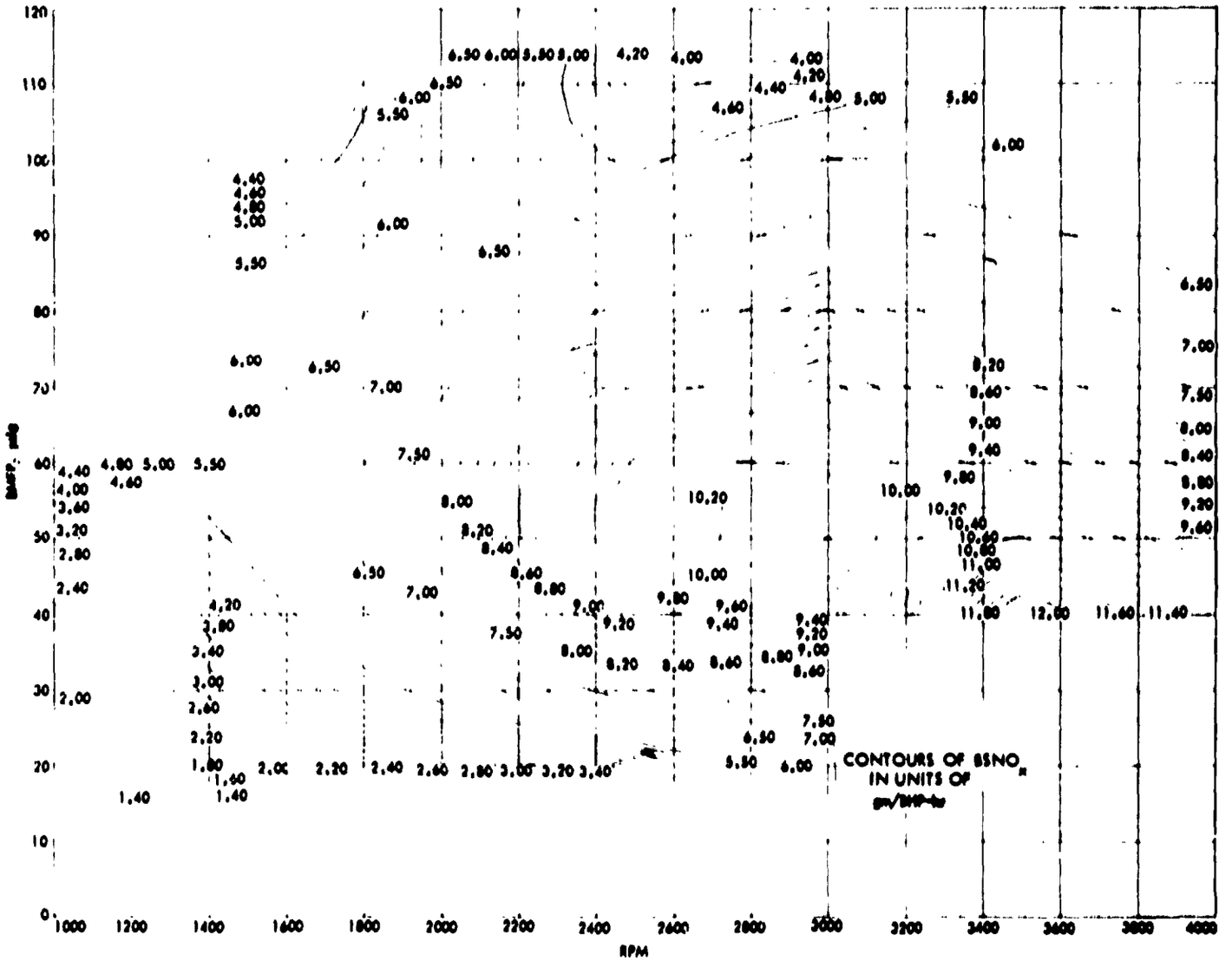

Fig. 31. BSNO$_x$ contours (engine configuration 1)

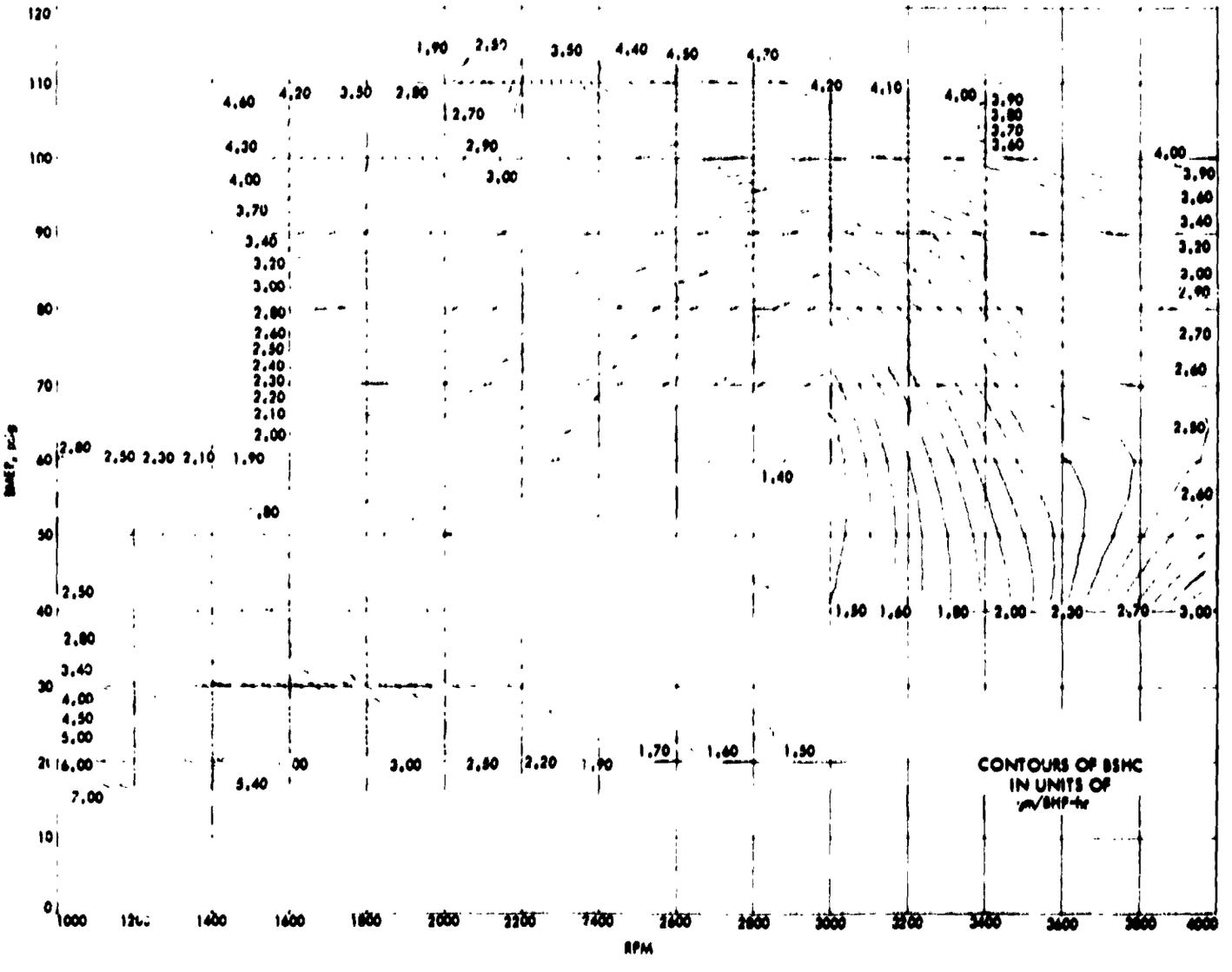

Fig. 32. BSHC contours (engine configuration 1)

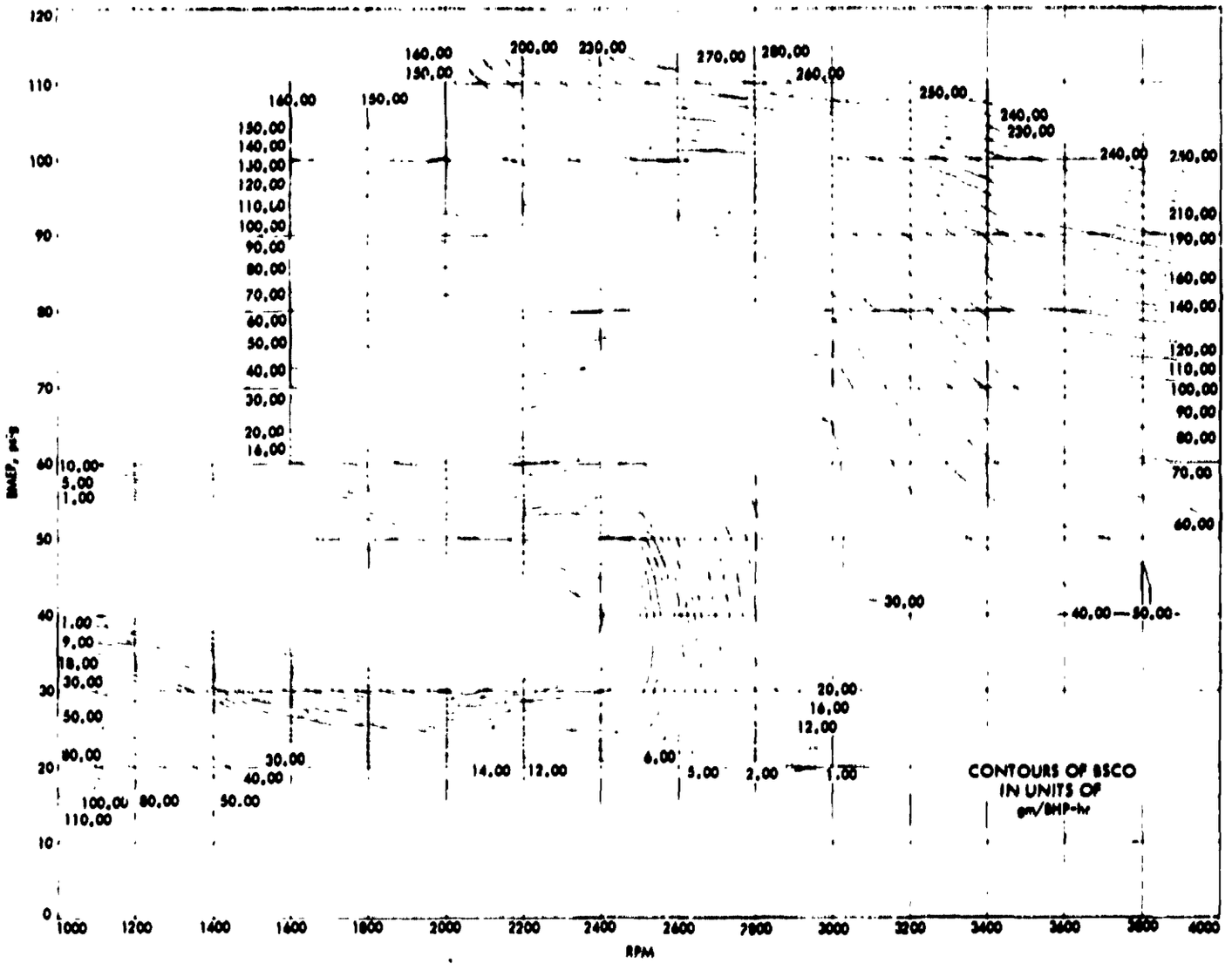

Fig. 33. BSCO contours (engine configuration 1)

efficiency conditions. This allowed a direct assessment of how much of the gain associated with the use of the generator products could be assigned to the other hardware differences.

To determine the best operating condition for a given RPM-load condition, a series of "sensitivity" tests were performed. These sensitivity tests consisted of (1) determining in real time the "best" operating condition by maximizing the engine thermal efficiency,* and (2) making small perturbations in equivalence ratio and spark timing, as shown in the Sketch A below. Data were recorded at the conditions indicated by the darkened circles.

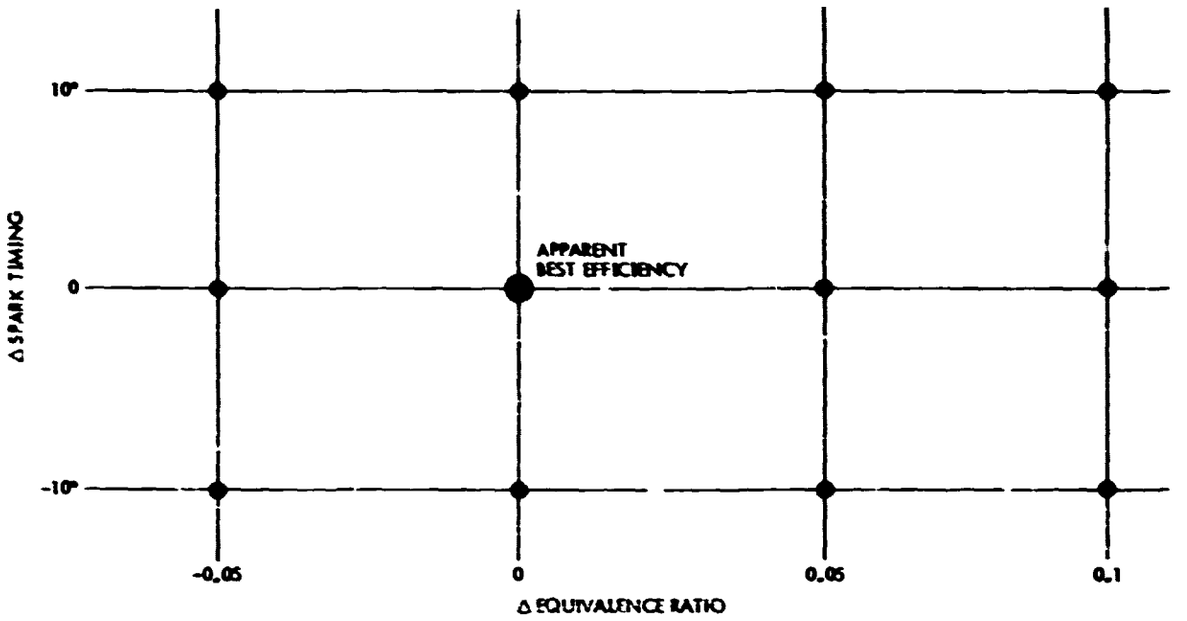

Sketch A

*When the hydrogen-gas generator was used, the system thermal efficiency, which includes the gasoline flowing to the gas generator, was used. This particular technique was feasible only because the IDAC system provided a real-time calculation and display of the thermal efficiency.

A typical result of the sensitivity tests is shown in Figure 34. From these plots, an equivalence ratio and spark timing were then selected for use in the mapping tests. The RPM-load conditions for which sensitivity tests were performed for engine configuration (2) are listed in Table 2. It was found that best efficiency for configuration (2) was achieved at an equivalence ratio of ~0.85 and a spark timing of ~50° BTDC and was almost independent of RPM and load. These values were used for the mapping tests which resulted in the contour plots of Figures 35 through 38.

Similar sensitivity tests were conducted using the engine configuration (3) in conjunction with the hydrogen-gas generator. These tests occurred shortly after completion of the model development described in Task C. The models

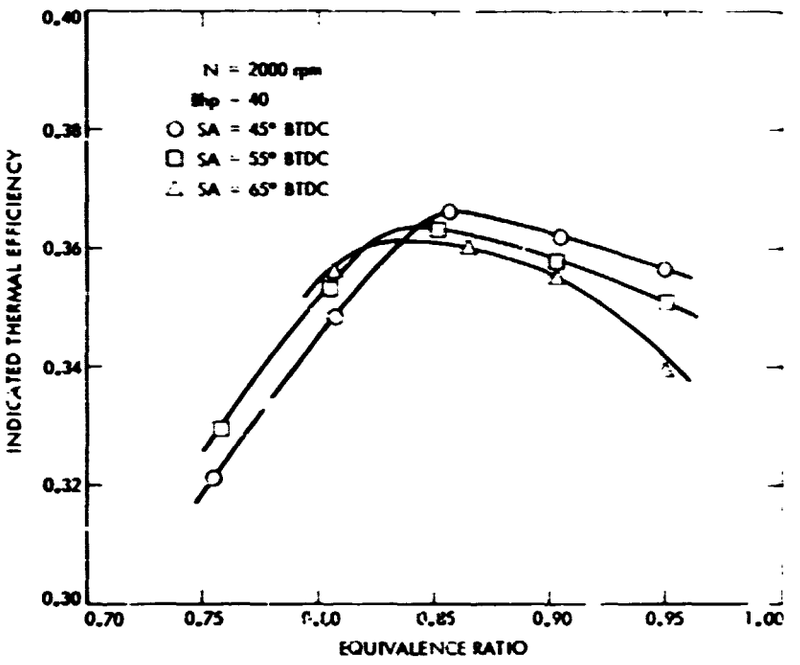

Fig. 34. Sensitivity test results for engine configuration 2

Table 2. Sensitivity engine/generator test matrix

RPM	BMEP
800	0
1500	0
2000	0
1000	10
1000	40
1000	70
1500	15
1500	30
1500	50
1500	65
2000	20
2000	45
2000	64
2000	Max
2500	30
2500	55
2500	68
3000	64

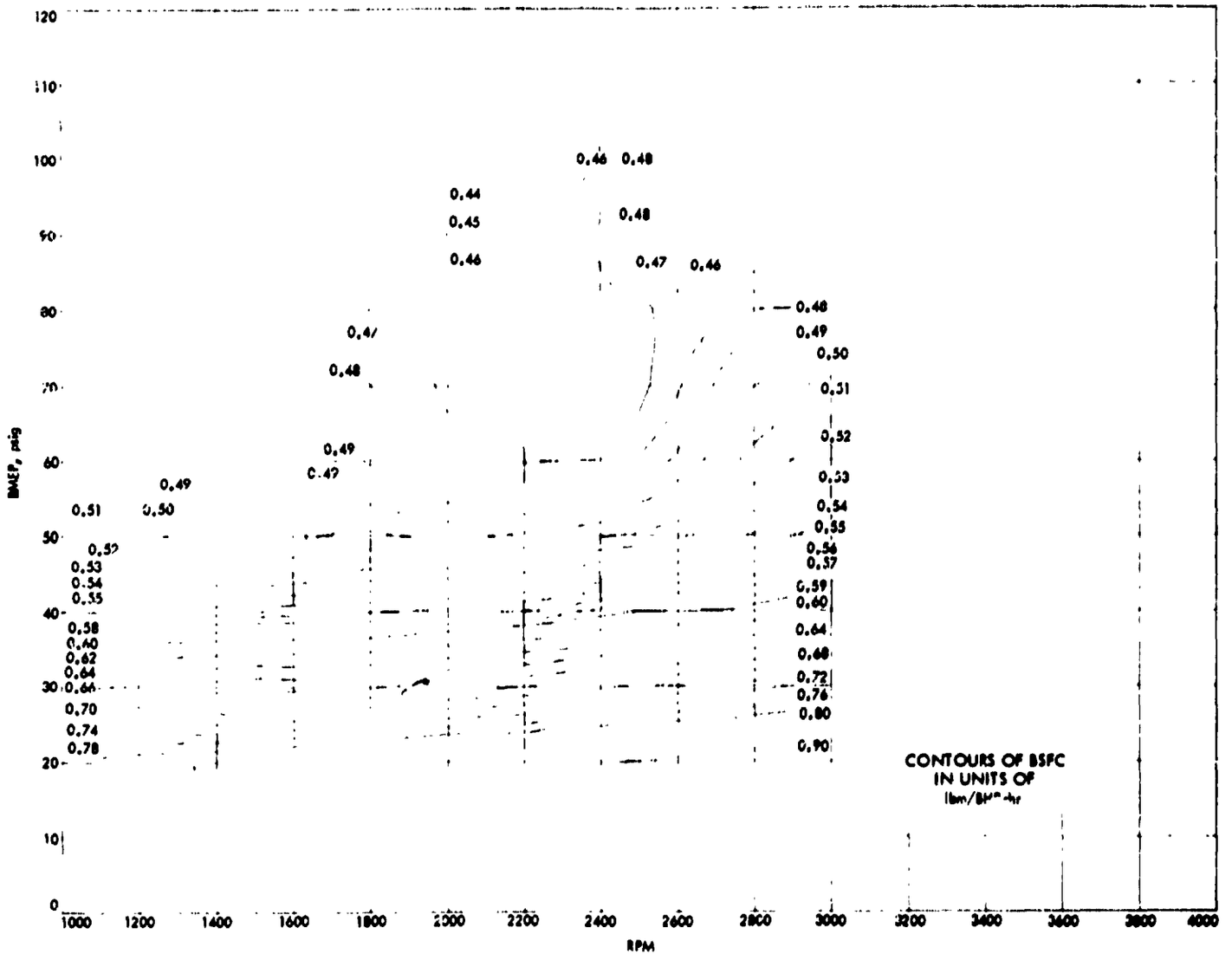

Fig. 35. BSFC contours (engine configuration 2)

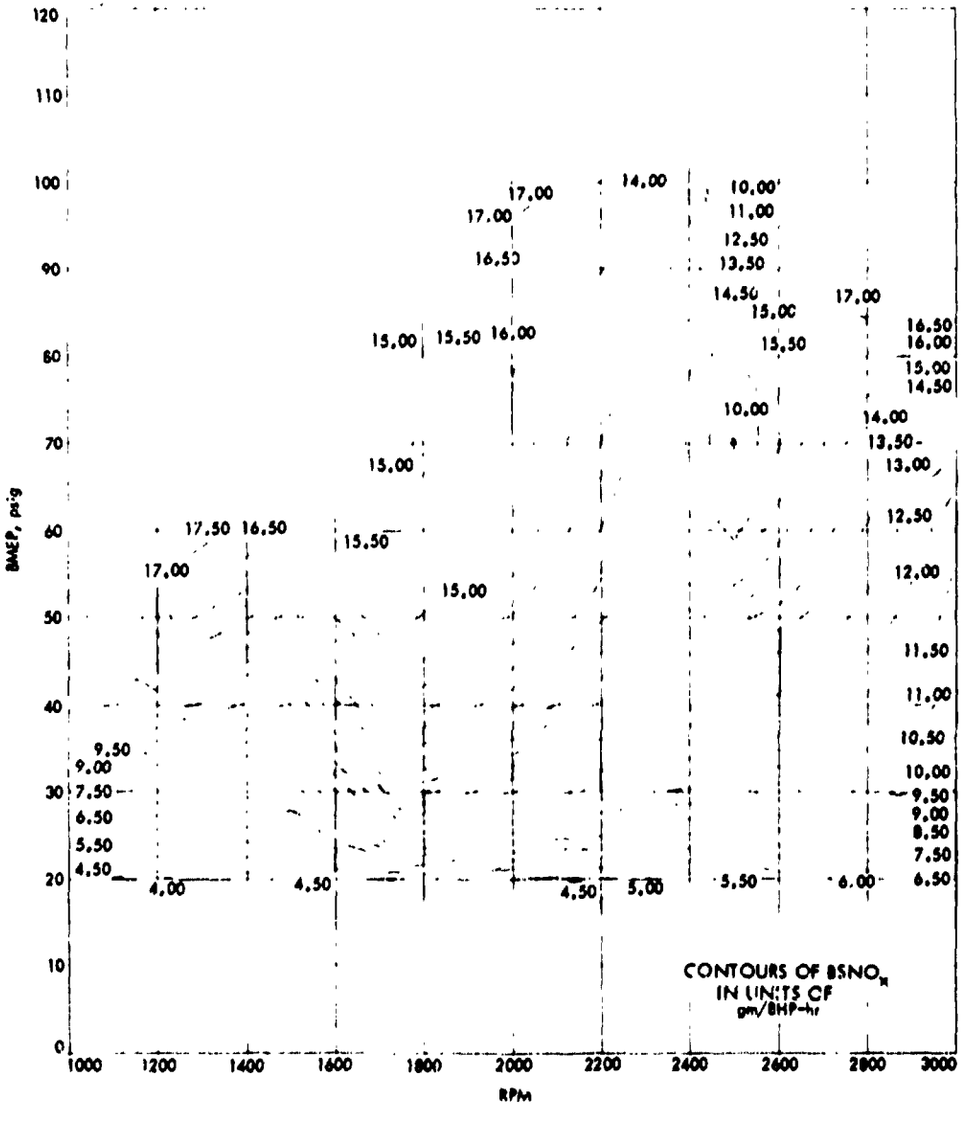

Fig. 36. BSNO$_x$ contours (engine configuration 2)

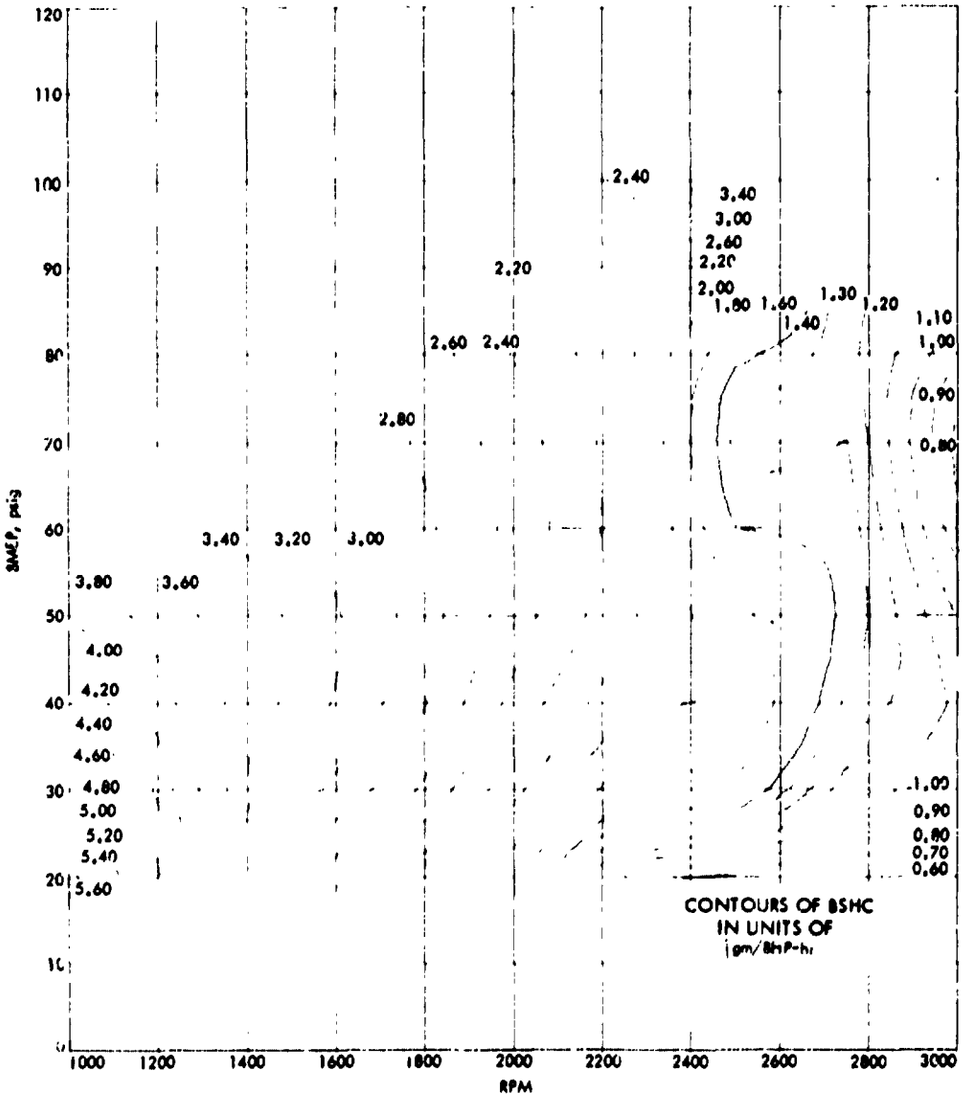

Fig. 37. BSHC contours (engine configuration 2)

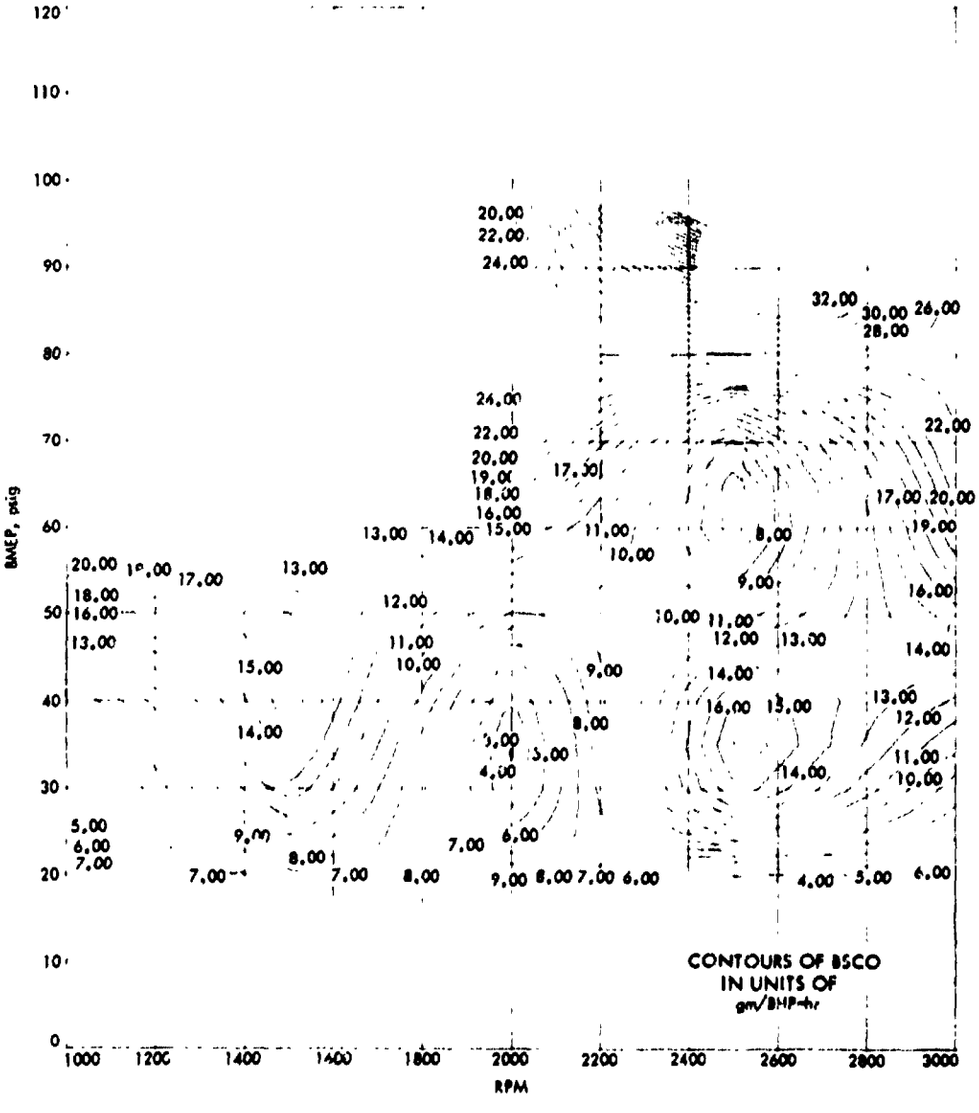

Fig. 38. BSCO contours (engine configuration 2)

were most helpful in the testing by predicting the best engine operating conditions. At the same time the sensitivity data showed areas where the models needed improvement. Because of the synergistic effect between model and data, more sensitivity testing was performed than originally planned.

5. Test Results

A typical set of results from the engine/generator sensitivity tests are shown in Figure 39. The apparent best efficiency point, as determined by the test crew, was at an equivalence ratio (Φ) of 0.74 and a spark timing of 40° BTDC. The sensitivity data were then taken at spark timings of 30°, 40°, and 50° BTDC and at Φ's of 0.70, 0.75, 0.80, 0.85, and 0.90. No data were taken at 30° BTDC and Φ = 0.70, because the engine was misfiring badly at this condition. As can be seen from Fig. 39 the best efficiency actually was at a spark timing of 50° BTDC and Φ = 0.73. However, the efficiency at 40° BTDC is the same, within the experimental error, but occurs at a slightly richer Φ of 0.75. Therefore, for the purposes of the mapping tests, data for this same engine condition were taken at Φ = 0.74 and 50° BTDC. The sensitivity tests turned out to be a convenient method for deciding on an engine operating condition.

The engine/generator combination was mapped for three values of generator throughput. These throughputs, 26 lbm/hr, 52 lbm/hr, and 79 lbm/hr corresponded to 0.5 lbm/hr, 1.0 lbm/hr, and 1.5 lbm/hr, respectively, of hydrogen in the product gas stream. The contour maps, Figures 40 through 51, are the results of these tests. Only a portion of the RPM-BMEP plane was covered in the engine/generator tests. Low values of BMEP were precluded by the chemical energy content of the generator gases. Thus, for a generator hydrogen flowrate of 1.5 lbm/hr, BMEP's less than ~45 psi could not be achieved. BMEP's above ~70 psi were precluded by the operating equivalence

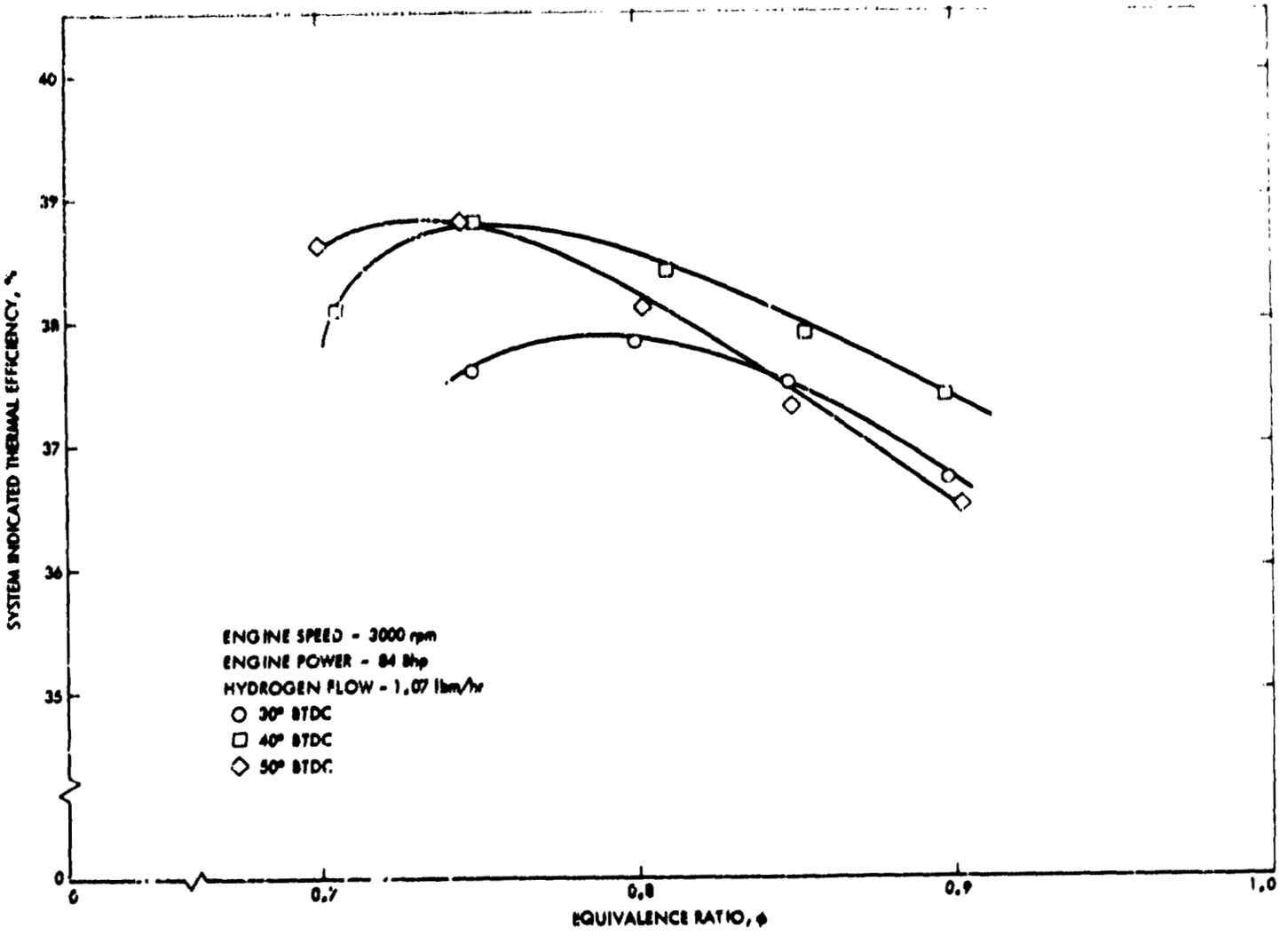

Fig. 39. Sensitivity test results for engine/generator

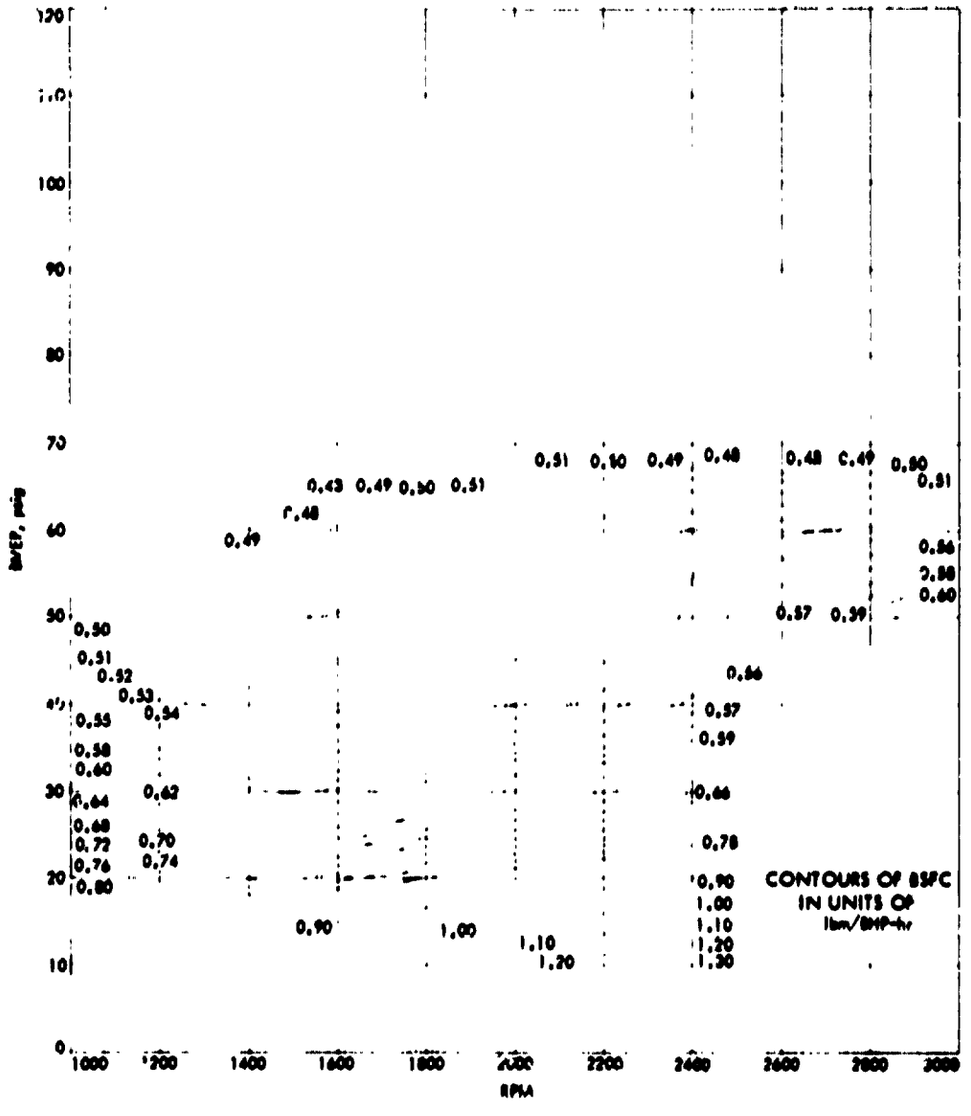

Fig. 40. Hydrogen flow 0.5 lbm/hr BSFC contours (engine configuration 3)

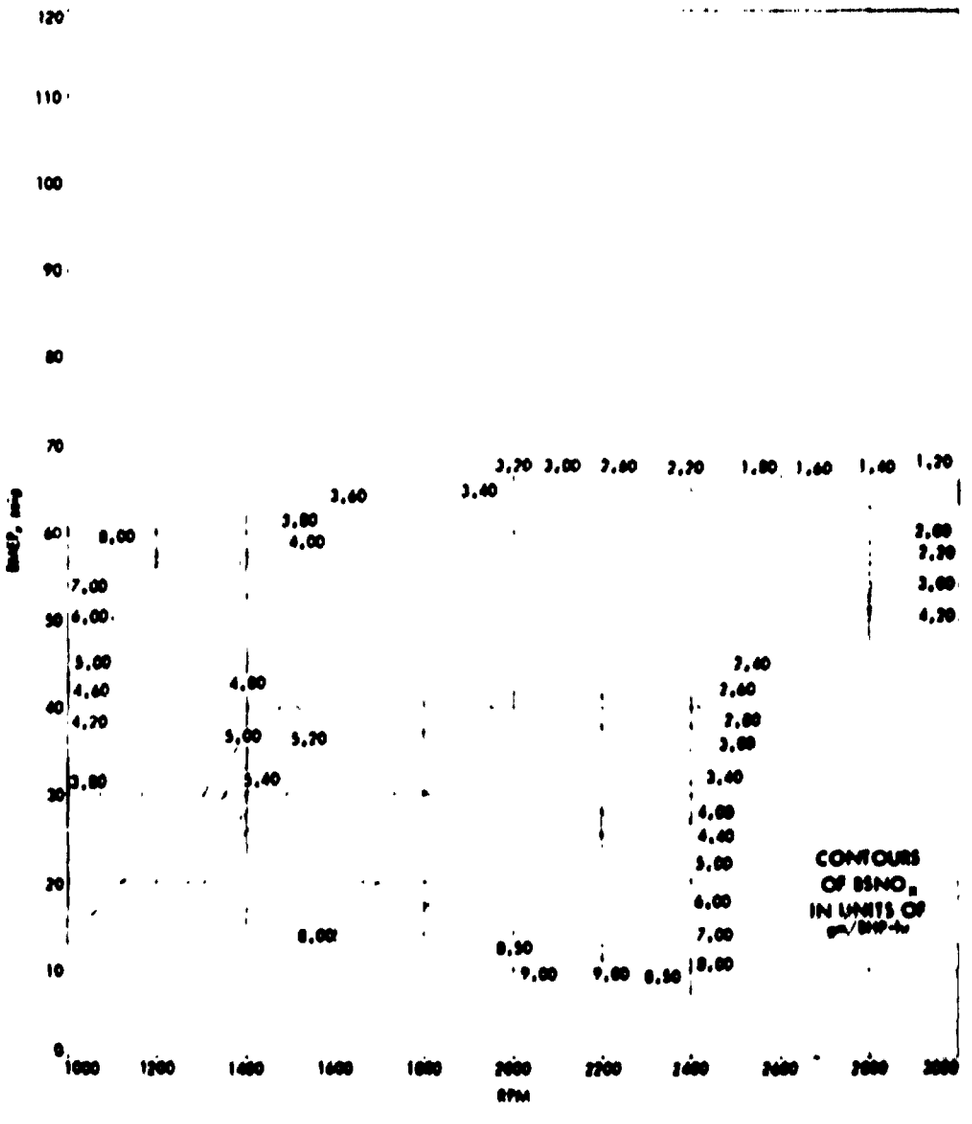

Fig. 41. Hydrogen flow 0.5 lbm/hr BSNO$_x$ contours (engine configuration 3)

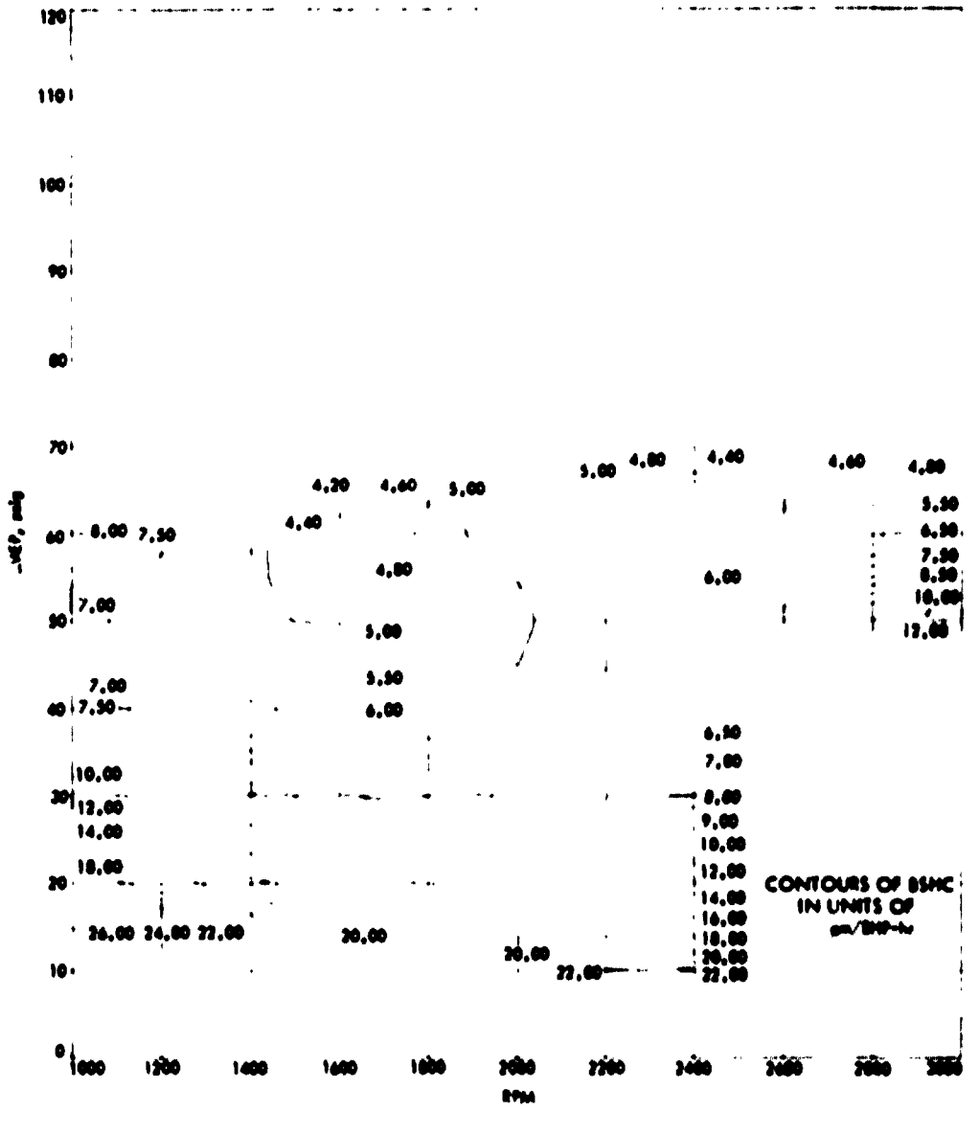

Fig. 42. Hydrogen flow 0.5 lbm/hr BSHC contours (engine configuration 3)

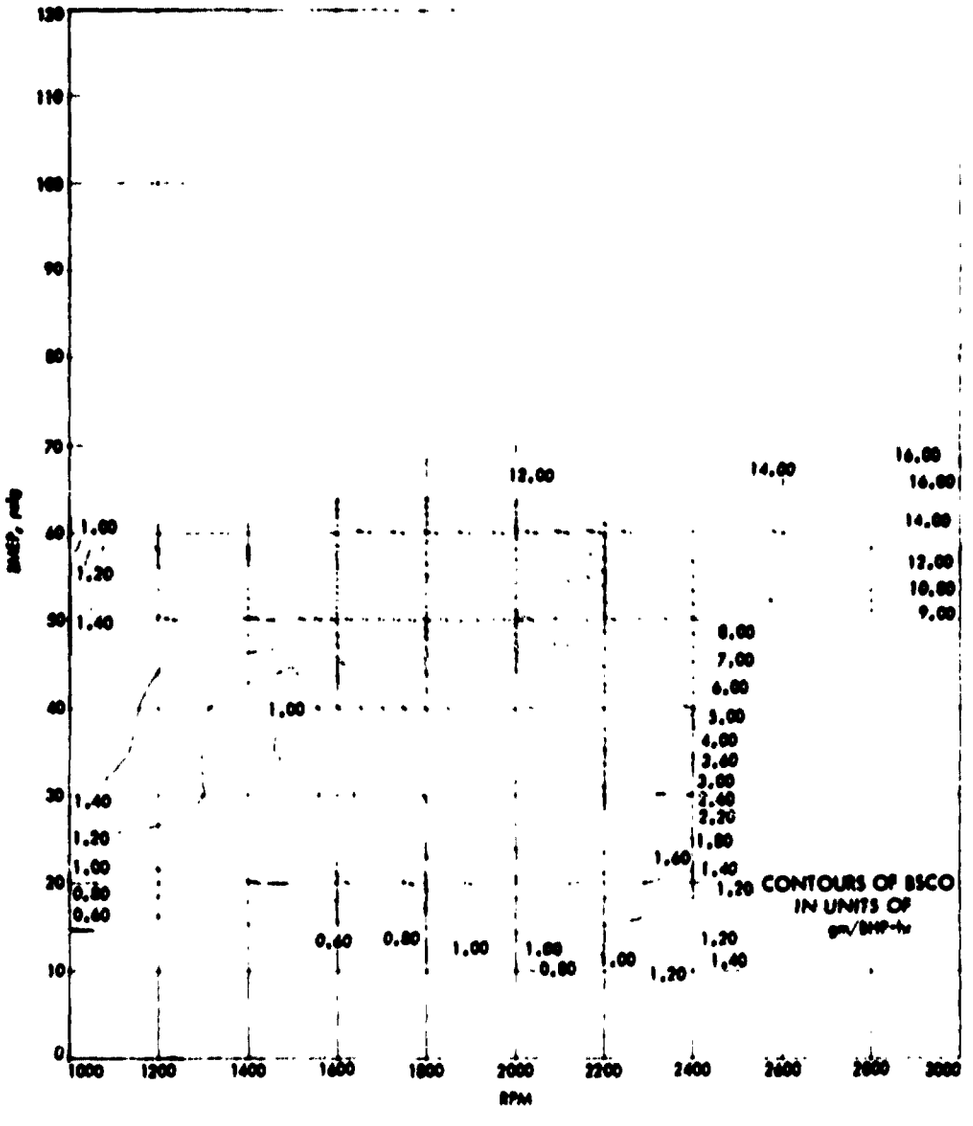

Fig. 43. Hydrogen flow 0.5 lbm/hr BSCO contours (engine configuration 3)

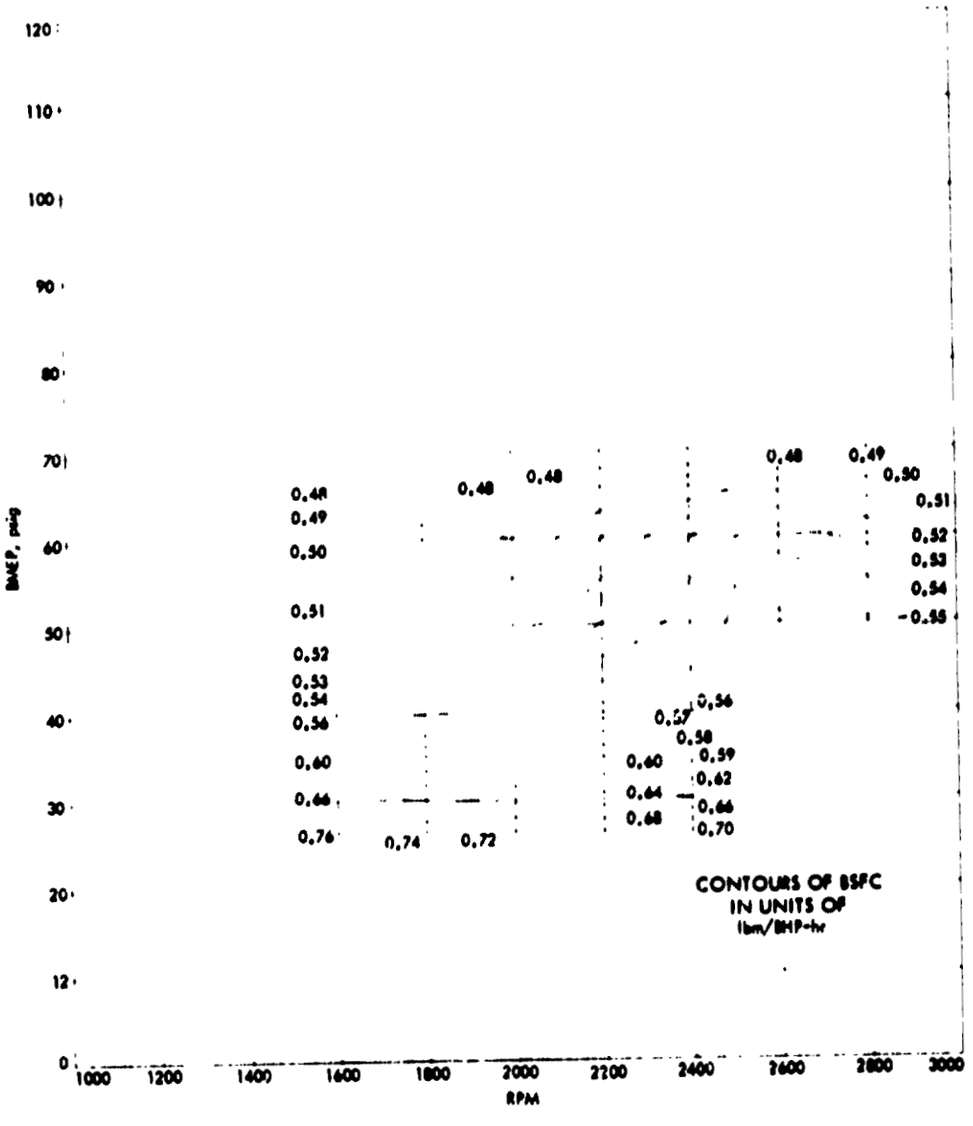

Fig. 44. Hydrogen flow 1.0 lbm/hr BSFC contours (engine configuration 3)

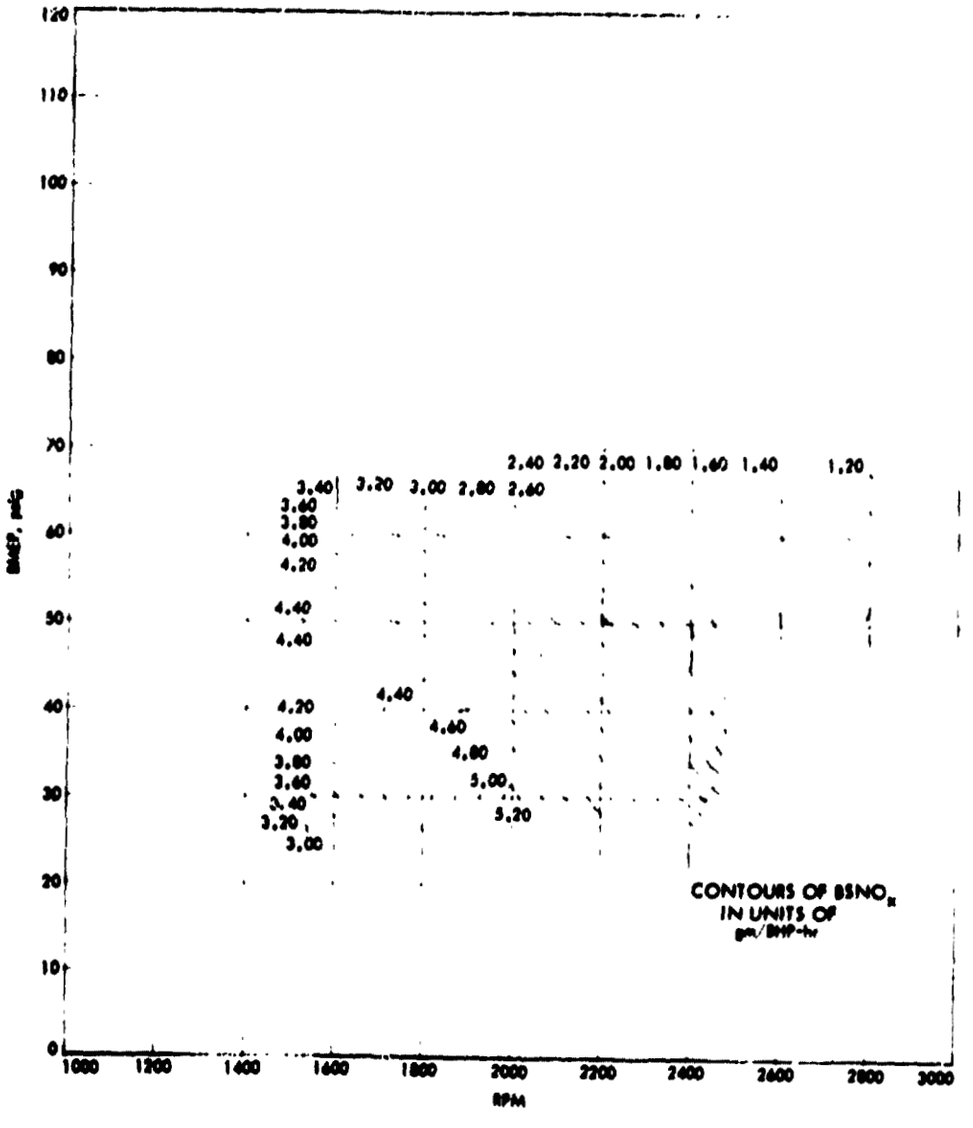

Fig. 45. Hydrogen flow 1.0 lbm/hr BSNO$_x$ contours (engine configuration 3)

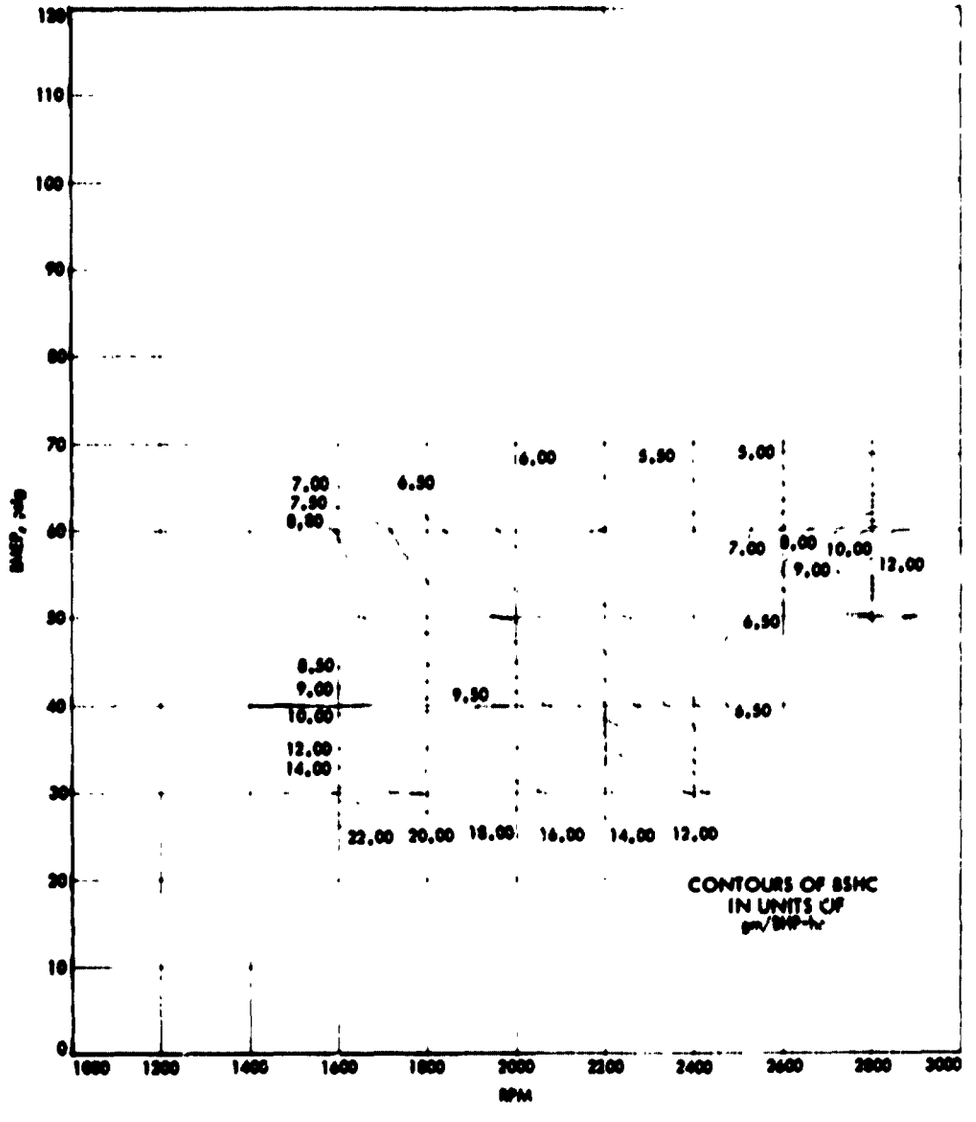

Fig. 46. Hydrogen flow 1.0 lbm/hr BSHC contours (engine configuration 3)

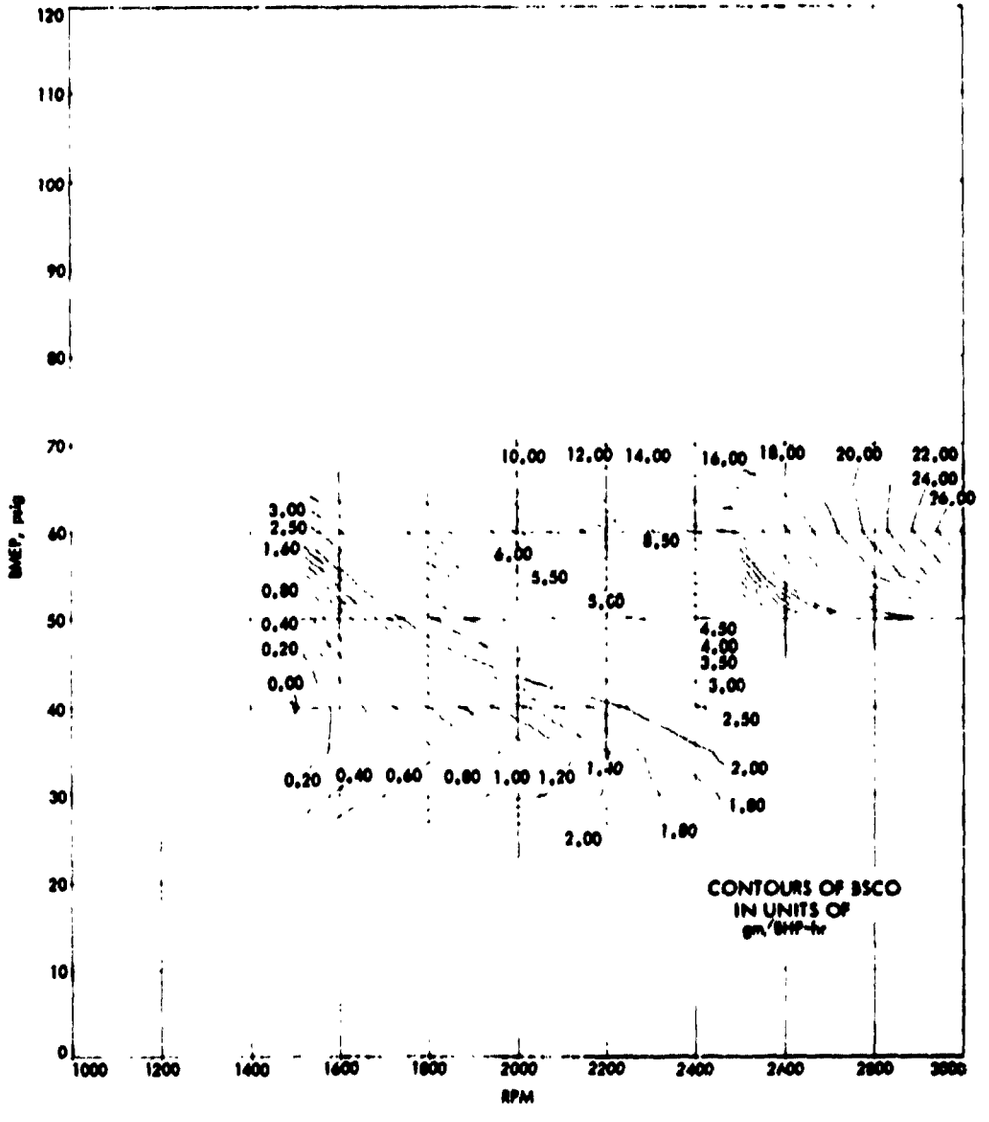

Fig. 47. Hydrogen flow 1.0 lbm/hr BSCO contours (engine configuration 3)

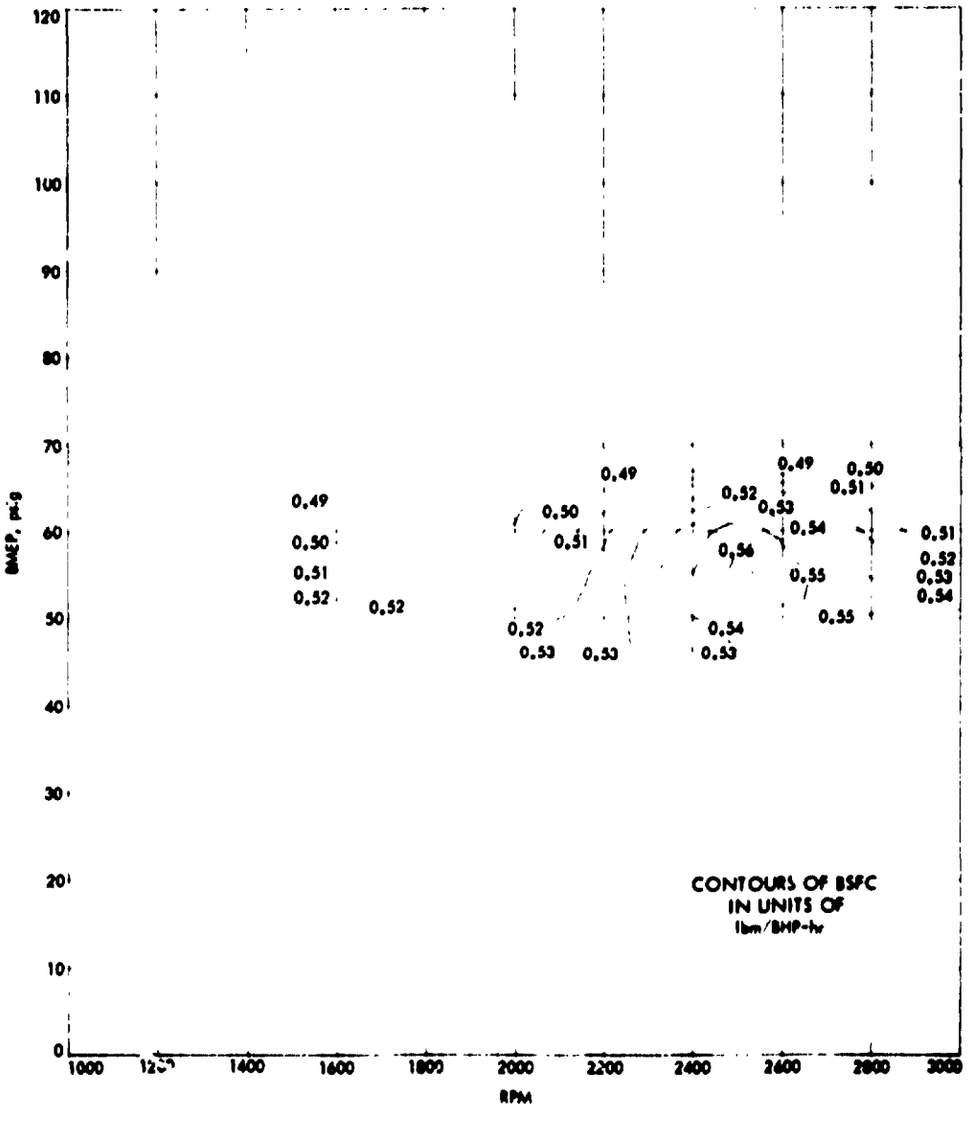

Fig. 48. Hydrogen flow 1.5 lbm/hr BSFC contours (engine configuration 3)

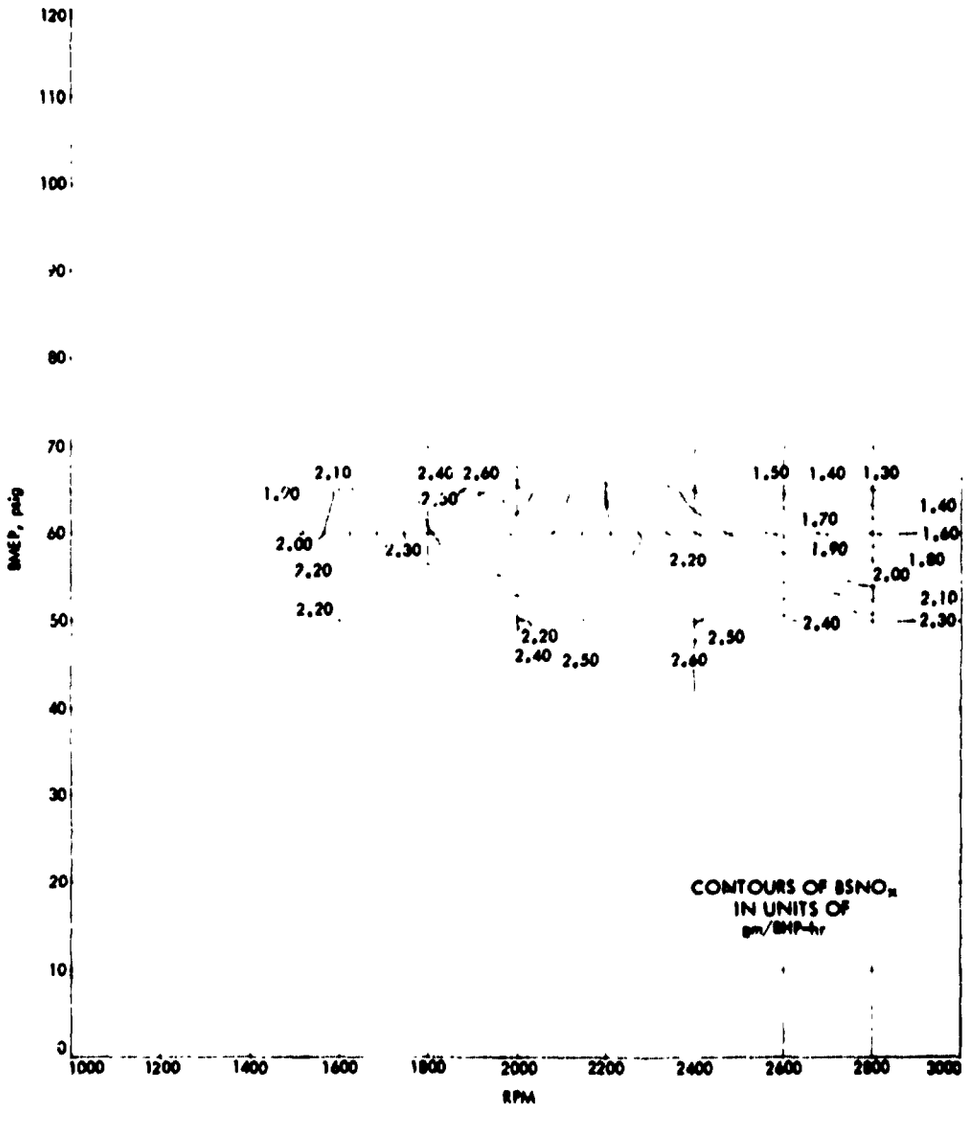

Fig. 49. Hydrogen flow 1.5 lbm/hr BSNO$_x$ contours (engine configuration 3)

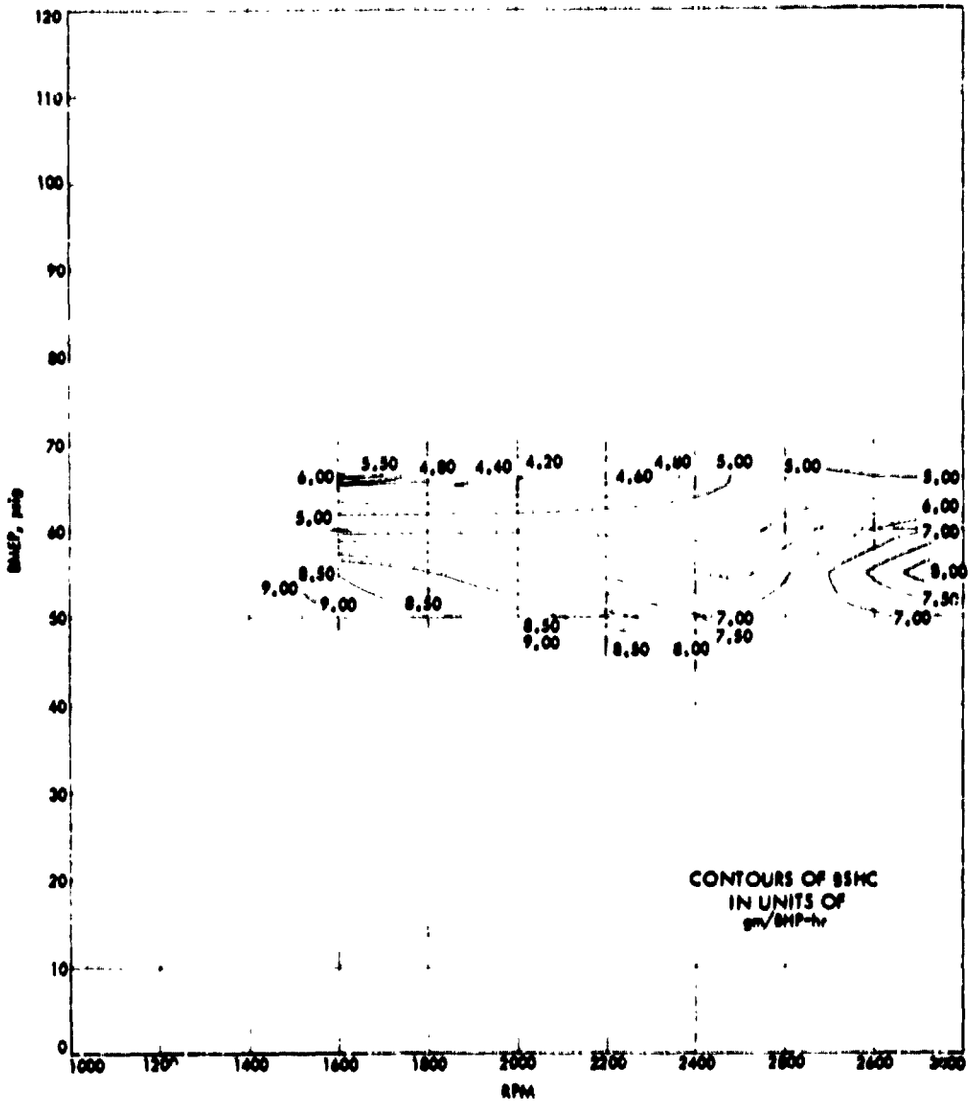

Fig. 50. Hydrogen flow 1.5 lbm/hr BSHC contours (engine configuration 3)

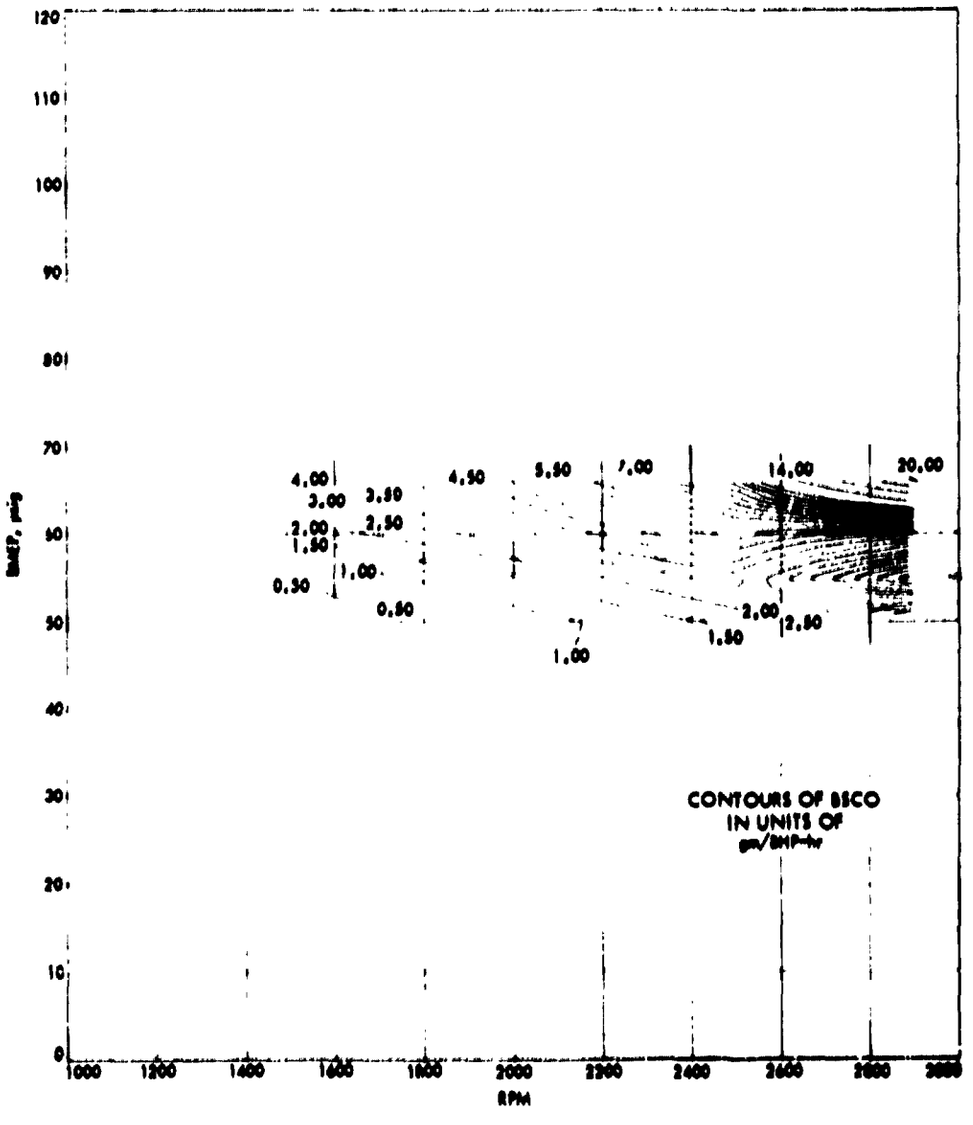

Fig. 51. Hydrogen flow 1.5 lbm/hr BSCO contours (engine configuration 3)

ratio. This is another way of stating that the engine was air-limited. For any given equivalence ratio and RPM, the maximum amount of fuel (and hence the maximum torque which can be produced by the engine) is fixed by the maximum air flow possible. Higher BMEP s could be achieved simply by increasing the the equivalence ratio.* Since the results of operating at increased equivalence ratio are not expected to be greatly different from that achieved with engine configuration (1), no attempt was made to operate the engine/generator combination at any equivalence ratio other than best efficiency. Note that the engine configuration (2) results, Figures 35 through 38, exhibit the same limitation to a smaller degree. No data were taken for RPMs in excess of 3600. The particular vehicle/engine/generator combination of concern does not require an engine speed above 2700 RPM to run the driving cycle.

In addition to the equivalence ratio limitations imposed on the engine, there was a limitation associated with the test hardware. In particular, the water supply to the water brake dynamometer was not adequate to allow large loads at low engine RPMs. This is reflected in all the contour plots.

The contour plots (Figures 40 through 51) contain a wealth of information. However, making comparisons between engine configurations with only those plots is very difficult. Complete comparisons can best be done using a computer simulation of the driving cycle and these are included in the Task F results. However, several interesting observations are readily apparent when the test results are presented in a different manner. Figures 52 through 57 show the performance of the three engine configurations at an engine speed of 2,000 RPM.

---

*This option of increasing the equivalence ratio would most likely be included in the controls of any vehicle employing the hydrogen-enrichment concept. For rapid accelerations, such as passing or entering a high-speed highway, the driver would be allowed to enrichen the mixture, but at the expense of both fuel economy and increased emissions.

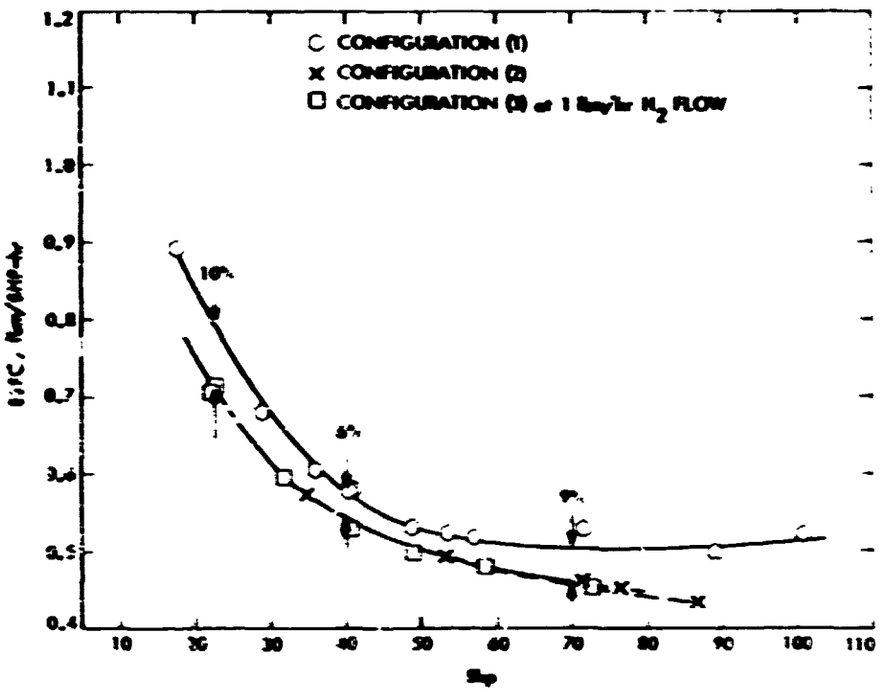

Fig. 52. BSFC vs BHP at 2,000 RPM

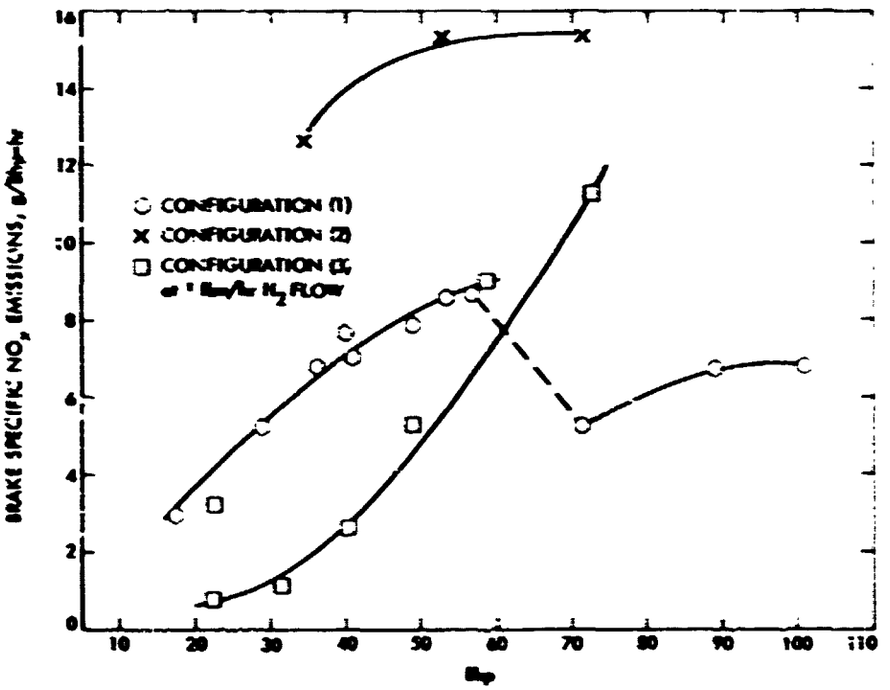

Fig. 53. $BSNO_x$ vs BHP at 2,000 RPM

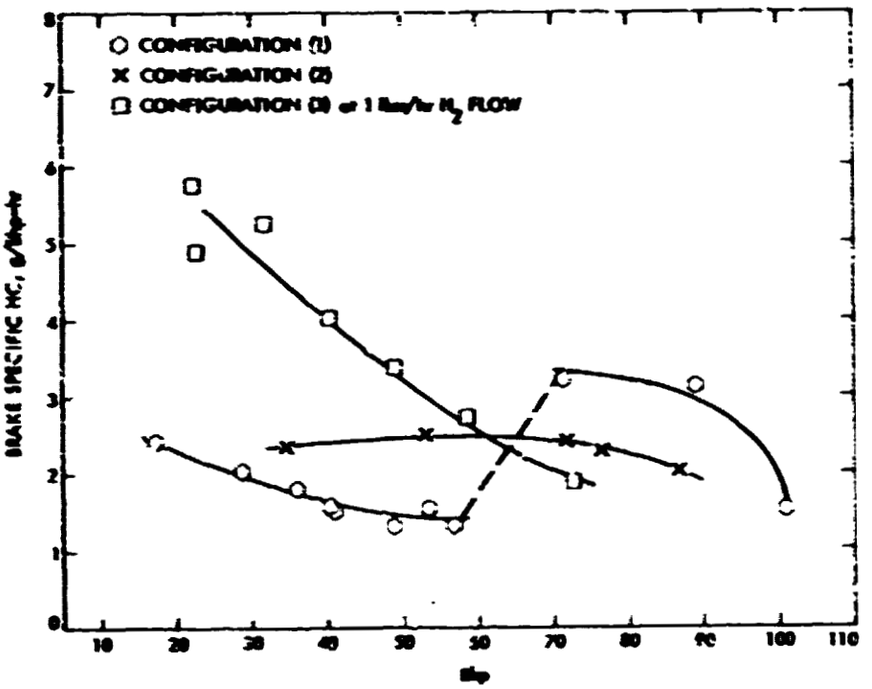

Fig. 54. BSHC vs BHP at 2, 000 RPM

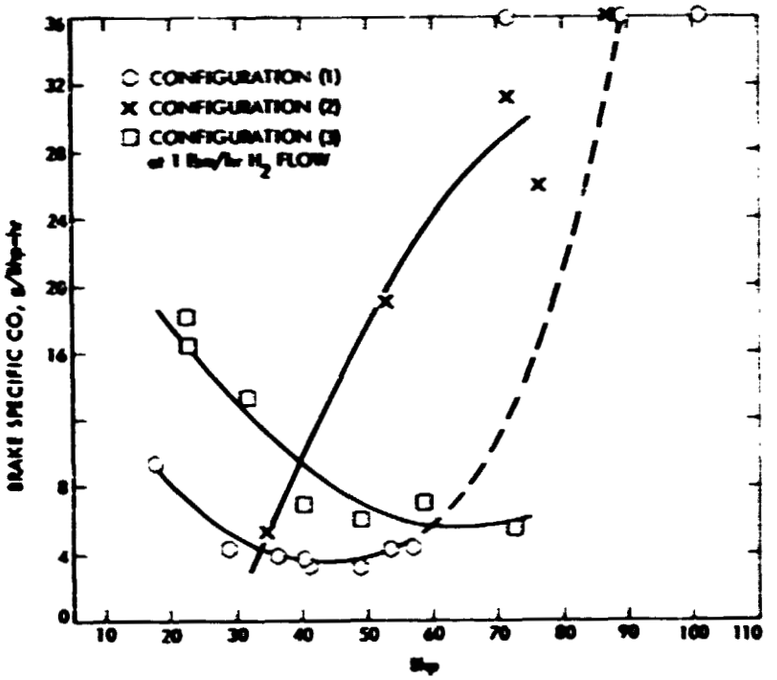

Fig. 55. BSCO vs BHP at 2, 000 RPM

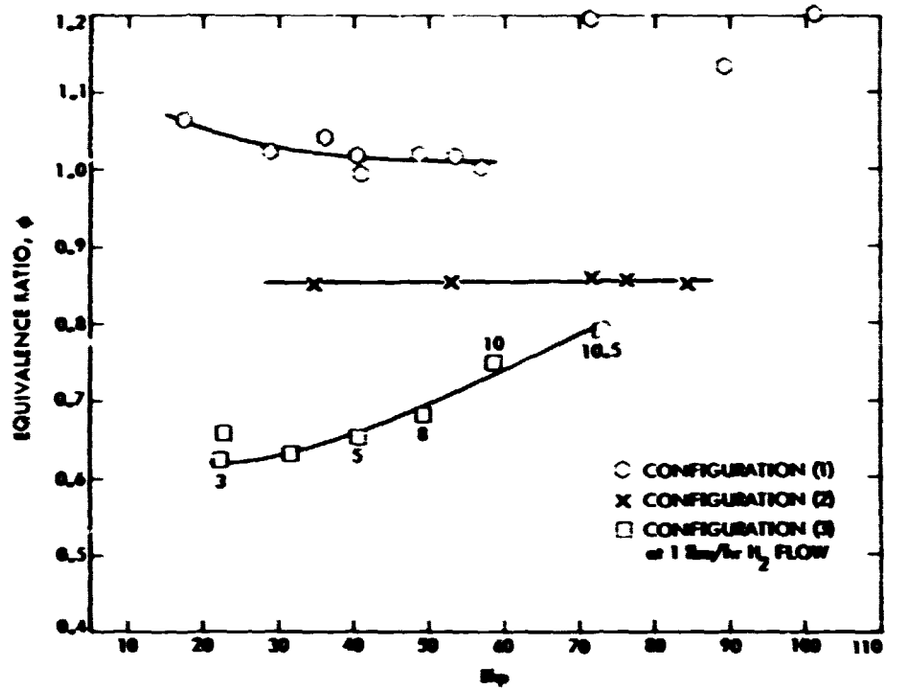

Fig. 56. Φ vs BHP at 2, 000 RPM

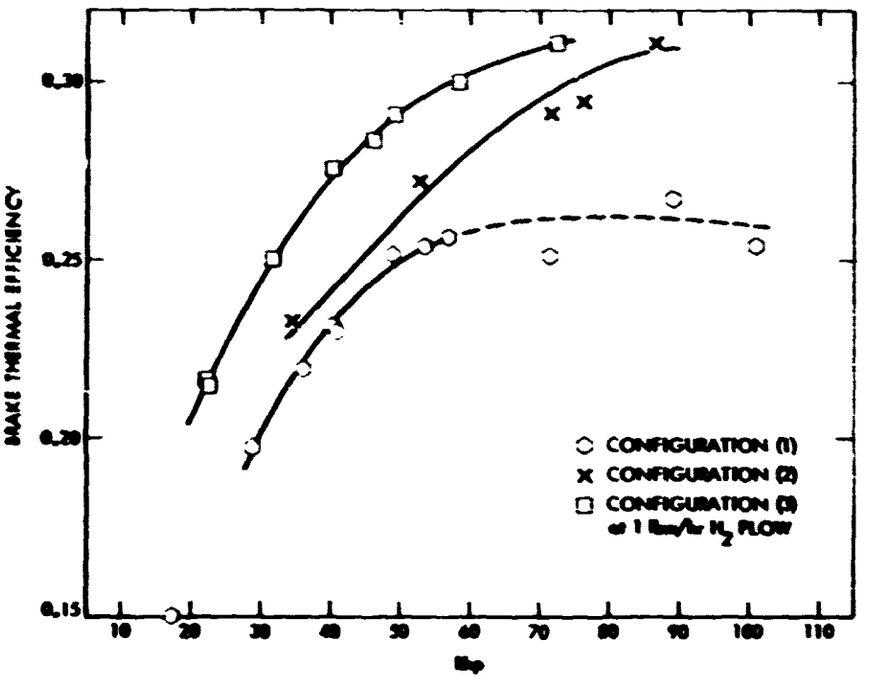

Fig. 57. Brake thermal efficiency vs BHP at 2, 000 RPM

Figures 58 through 62 compare the BSFC and NO_x emissions for the three configurations at level-road load conditions. Figures 63, 64, and 65 illustrate the relationship between BSFC, $BSNO_x$, and hydrogen flowrate at three different engine speeds. These 14 figures are discussed in more detail in the following paragraphs.

Figures 52 through 57 show BSFC, $BSNO_x$, BSHC, BSCO, engine thermal efficiency, and equivalence ratio, respectively, as functions of BHP at an engine speed of 2000 RPM. Data for each of the three engine configurations are shown there; however, only the 1.0 lbm/hr of hydrogen results are included for configuration (3).

Figures 52 and 53 illustrate the two primary benefits associated with the hydrogen enrichment concept, and at the same time Figure 52 illustrates one of the negative aspects as well. The BSFC associated with hydrogen enrichment is ~10% improved over the stock configuration (1) at 20 and 70 BHP. At 40 BHP, the condition is equivalent to 55 mph level-road load, the improvement is 6%. The configuration (2) BSFC results are virtually identical to those of configuration (3) even though the operating equivalence ratios are very different (see Figure 56). This is clearly the result of including (as it properly should be) the effect of the hydrogen-gas generator on fuel consumption. Reference to Figures 56 and 57 shows that configuration (3) was operated at a lower equivalence ratio, and as a result the engine thermal efficiency was ~10% higher. However, since there is about a 20% loss in chemical energy for that portion of the gasoline which goes to the generator, all of the improvement in thermal efficiency is not translated into improvements in BSFC. For the particular operating conditions shown, the net effect is that configuration (2) and (3) achieve the same BSFC.

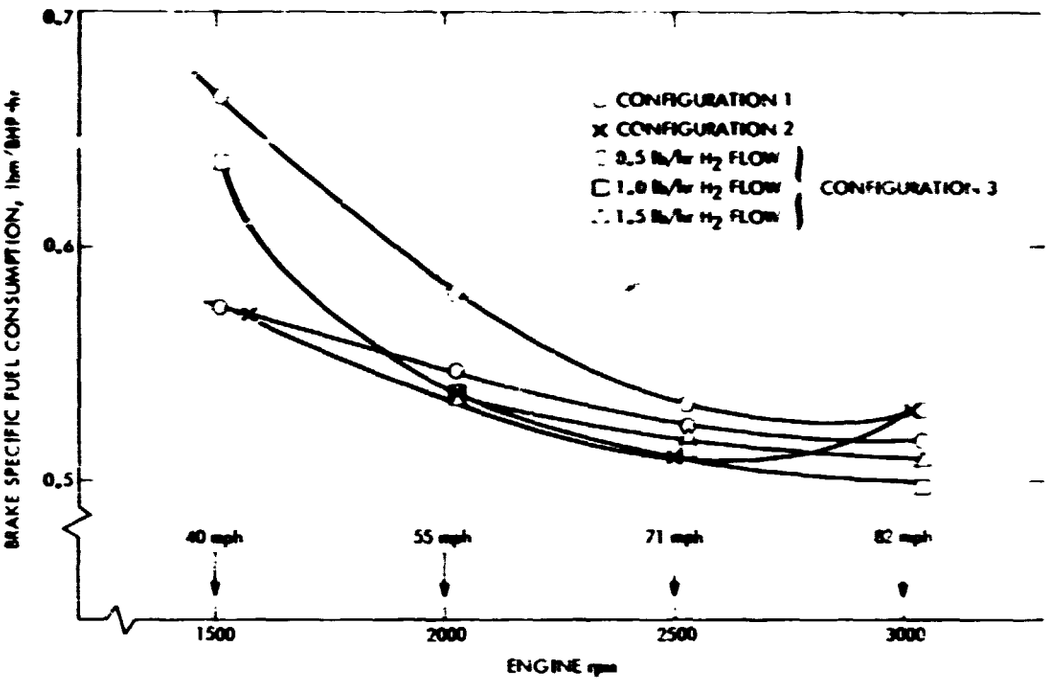

Fig. 58. BSFC vs engine speed at level road load

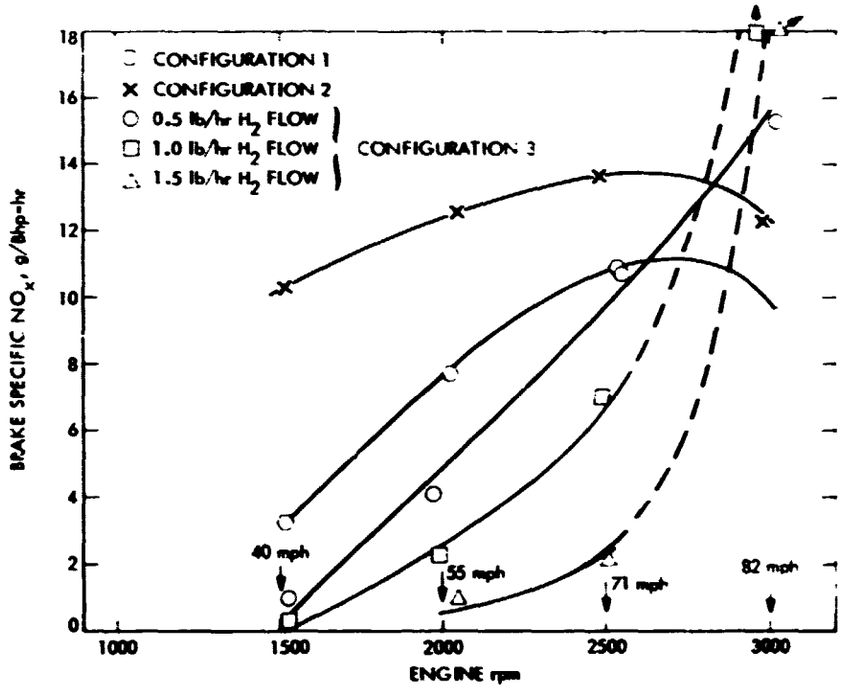

Fig. 59. $BSNO_x$ vs engine speed at level road load

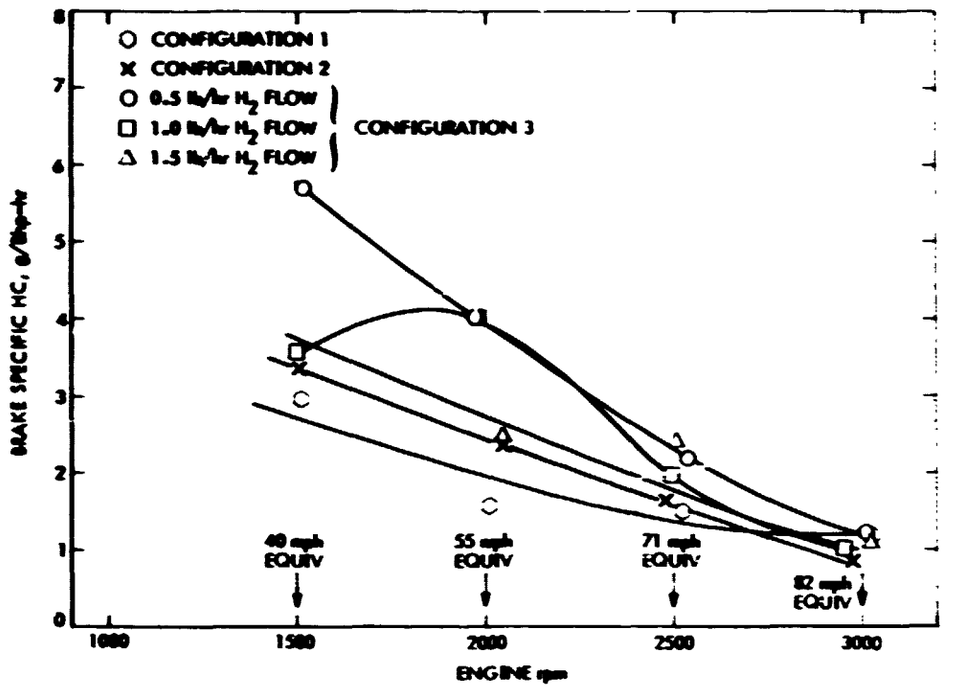

Fig. 60. BSHC vs engine speed at level road load

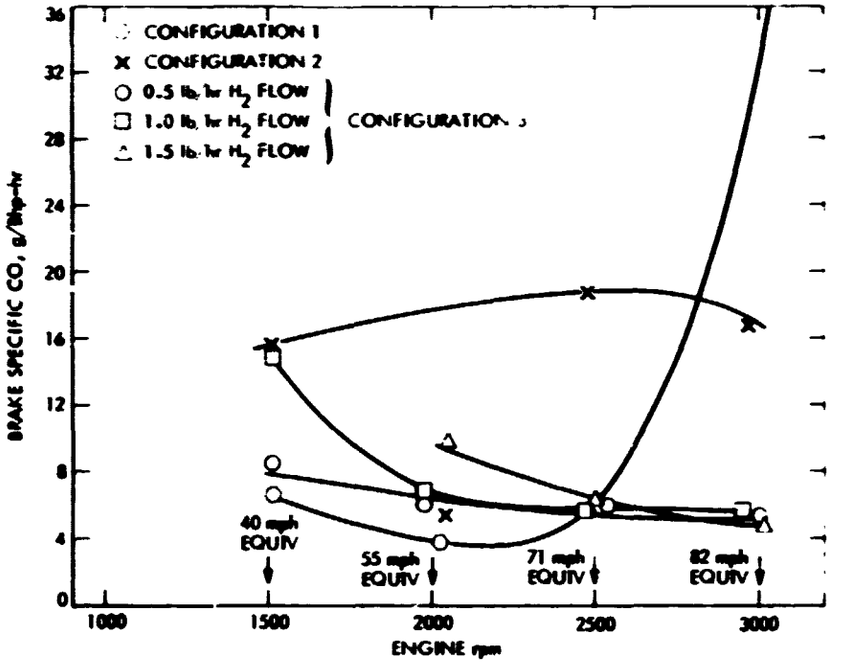

Fig. 61. BSCO vs engine speed at level road load

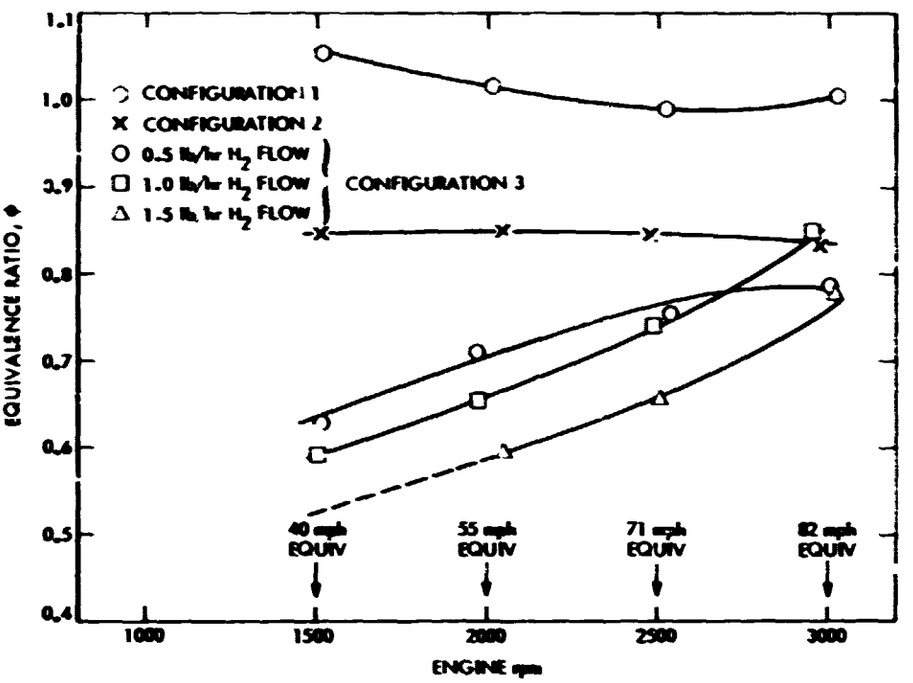

Fig. 62. Level road load data comparison 4

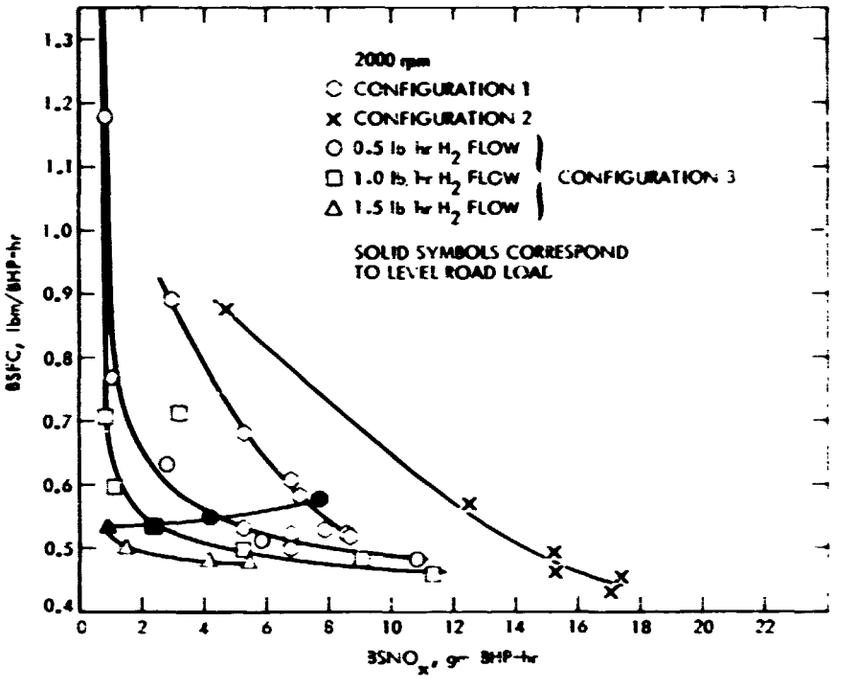

Fig. 63. BSFC vs $BSNO_x$

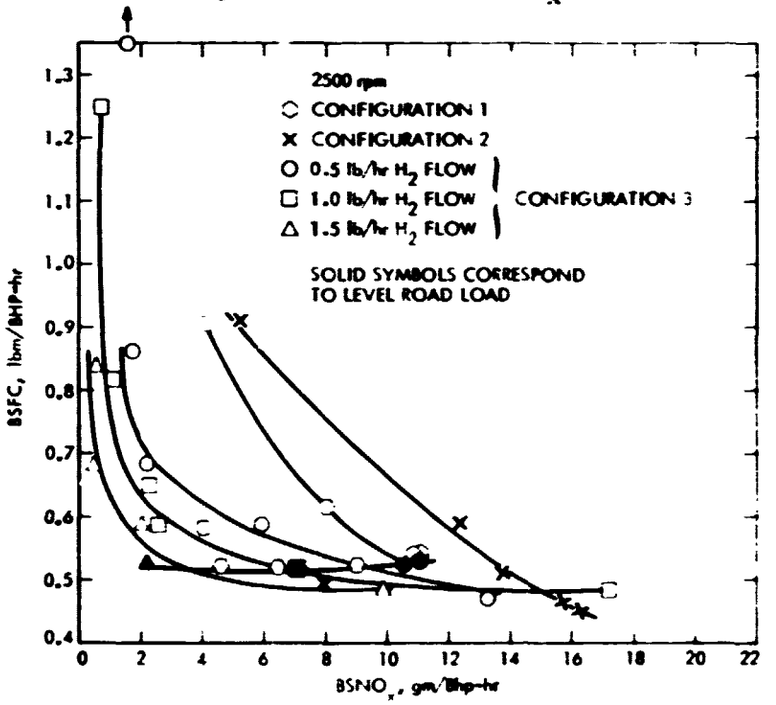

Fig. 64. BSFC vs $BSNO_x$

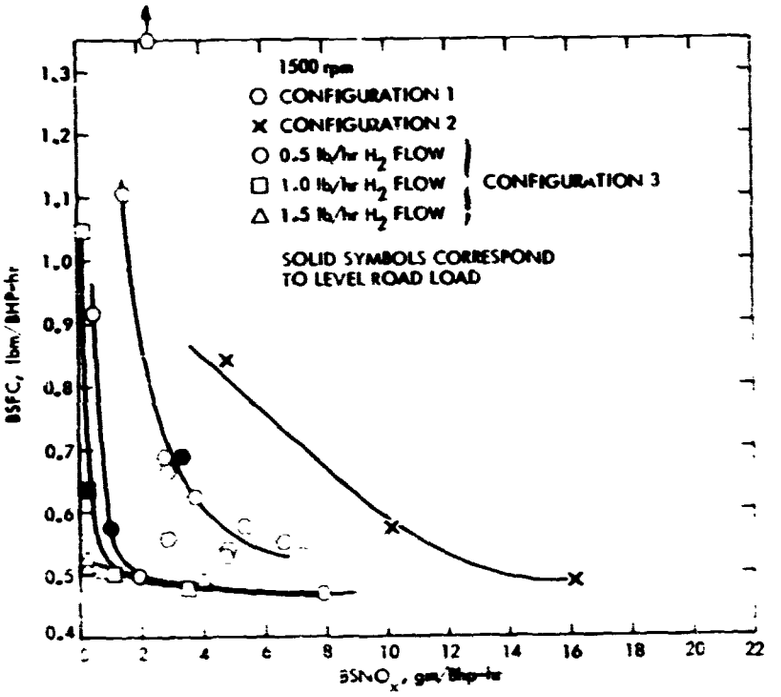

Fig. 65. BSFC vs $BSNO_x$

The use of the Autotronics hardware does not in and of itself lead to improvements in BSFC. The BSFC improvements shown in Figure 52 are the direct result of leaner operation and the use of MBT ignition timings. Presumably, if the configuration (1) engine were operated at the same equivalence as the configuration (2), the BSFC's would be the same. The same comments may be made with regard to hydrogen. The use of hydrogen in and of itself offers no particular advantage in terms of engine efficiency, and the CFR engine results of page 108 of this report verify this. However, the use of hydrogen does allow ultra-lean operation and this is what results in reduced fuel consumption.

Figure 53 clearly shows the advantage of they hydrogen-enrichment concept in terms of NO_x emissions. Use of the generator products permits operation at ultralean equivalence ratios (see Figure 56) and results in the significant reduction in NO_x emissions shown in Figure 53. Recall also that configurations (2) and (3) include no devices such as EGR, for NO_x control. Thus, the advantage shown by configuration (3) is due almost entirely* to the low equivalence ratio.

Figures 54 and 55 are plots of hydrocarbon (BSHC) and carbon monoxide (BSCO) exhaust emissions against BHP. Most lean-burn engines, including the hydrogen-enrichment concept, do not exhibit good hydrocarbon emissions. Under conditions of low equivalence ratio, the hydrogen-enriched fuel results are a factor of ~ 3 greater than either the configurations (1) and (2). Recall that neither of the latter engines included any air injection into the exhaust manifold and, thus, the hydrocarbon emissions for those two engines are probably larger than in a roadable vehicle. However, note that at ~70 BHP, where the configuration (3) engine equivalence ratio is about the same as configuration (2), the hydrocarbons are slightly lower for configuration (3). This is quire likely the result of having a significant part of the fuel in a totally gaseous condition.

The carbon monoxide results are similar in that at low BHPs the hydrogen enriched fuels prodice higher CO emissions than the other two engine configurations tested. At higher BHPs the BSCO from configurations (1) and (3) are comparable. Again note that at higher BHPs where the operating equivalence ratios of configurations (2) and (3) were about the same (see Figure 57), BSCO

*The generator products contain large quantities of the diluents N_2 and CO_2. They play no role in the combustion process but do affect NO_x emissions in much the same way as EGR.

levels from engine (3) were much lower. The source of the CO for the hydrogen enriched engine is unquestionably the generator products. Operating the same engine at the same equivalence ratio, but with pure hydrogen, the amount of CO emitted is about 2 orders of magnitude less than shown on Figure 55.

Figure 58 through 62 also compare the three engine configurations, but at level-road load conditions. The abscissa of Figures 58-62 are engine rotational speed. For each value of engine speed, there is a unique engine load that corresponds to a vehicle speed. The vehicle speeds indicated are for a 4500-lbm Chevrolet Impala as driven in third gear. Three hydrogen-generator flowrates, equivalent to 0.5, 1.0, and 1.5 lbm/hr of hydrogen, are shown in Figures 58-62.

The level-road-load data exhibits many of the same features as the constant engine speed results of Figures 52-57. The hydrogen enriched fuels give fuel consumptions which are superior to the stock engine over the entire range of engine speeds tested, but are no better than configuration (2). The interplay equivalence ratio and hydrogen flowrate can be seen in Figures 58 and 62. Increasing amounts of hydrogen allow lower engine equivalence ratio (see Figure 62) and hence a higher engine thermal efficiency, but the benefit is offset by the losses in the generator to the extent that minimum system BSFC occurs not at minimum equivalence ratio but at ~1.0 lbm/hr hydrogen flowrate. On the other hand, increasing amounts of hydrogen, and hence lower equivalence ratios, leads directly to lower NO_x emissions as shown in Figure 59.

The hydrocarbon and carbon monoxide emitted are again higher for the hydrogen enriched fuels, as they were for the constant engine speed results, but the differences are not nearly as large.

The interactions and effects of equivalence ratio and generator flowrate are illustrated in Figures 63, 64, and 65. In Figure 63 BSFC is plotted against $BSNO_x$ for an engine speed of 2000 RPM. Each of the data points correspond to a different engine load. The level-road load points are shown as the solid symbols. At both 2000 and 2500 RPM, additional hydrogen has beneficial effects on both NO_x and fuel consumption, although at both engine speeds the BSFCs associated with 1.0 and 1.5 lbm/hr of hydrogen are the same. At 1500 RPM, however, this is not the case. Increasing the hydrogen flowrate from 0.5 lbm/hr to 1.0 lbm/hr* decreases the NO_x emitted but results in a poorer BSFC. However, note that the BSFC associated with 1.0 lbm/hr hydrogen flowrate is still superior to that achieved with stock engine.

6. Conclusions

1) The initial tests in which a hydrogen gas generator was mated to a multi-cylinder IC engine went very smoothly. There was no evidence of any deleterious effects on the engine hardware, and there were no incidents to suggest any significant safety problems associated with the use of hydrogen.

2) The trends of increased engine efficiency and decreased NO_x emissions in the ultra-lean regime, which were observed with bottled hydrogen, were also observed with hydrogen gas generator products.

3) The trend of increasing hydrocarbon emissions with ultra-lean combustion, reported by several investigators, were observed with the hydrogen-enriched fuels. Increasing amounts of hydrogen

*At 1.5 lbm/hr of hydrogen, the chemical energy content of the generator products is too large to operate at the level-road load condition of 22 BHP.

has a beneficial result on the problem, but under no operating conditions were the HC emissions below the equivalent EPA 1978 standard.

4) Quantities of carbon monoxide emissions approximating the 1978 CO allowable level of 3.4 gm/mi were observed in conjunction with use of the hydrogen generator products. Carbon monoxide emissions were extremely low when pure hydrogen was used, and hence the conclusion is that the CO contained in the generator products is not completely oxidized in the engine combustion chamber.

5) Brake specific fuel consumption decreases (including the generator losses) of 10-15% from the stock engine were observed over most of the engine BMEP-RPM operating regime. These are the result of lean operation and the use of MBT ignition timing.

6) Oxides of nitrogen emissions were significantly reduced when the hydrogen enriched fuels were used. The specific amount of the reduction varies directly with the engine equivalence ratio, which in turn is directly affected by the power required from the engine.

D. CFR ENGINE TESTS (EPA TASK E)

1. Introduction

A single-cylinder, Cooperative Fuels Research (CFR) engine was used to investigate two aspects of the hydrogen enrichment concept. The first of these was the general relationship between engine performance, in terms of thermal efficiency and emissions, and equivalence ratio and fuel composition. The second was the dependence of critical compression ratio on equivalence ratio and fuel composition.

The two groups of tests differed not only in objective, but also in physical location of the engine, in several of the test procedures, and in the details of

the hardware installation. Where significant to the test results, these are noted below.

The investigation of the relationship between engine inputs and outputs is very nearly a duplicate of the multi-cylinder engine mapping tests. That is to say, the inlet conditions were varied in a systematic way and the engine efficiency and exhaust gas composition determined. The use of the CFR engine, however, has the advantage of allowing a more distinct separation of concept phenomena from hardware phenomena. In particular, the use of the CFR engine eliminates cylinder-to-cylinder distribution and engine speed as experimental variables. The data from the CFR engine tests is believed to give a good representation of what may be expected from the hydrogen enrichment concept. It is then reasonable to expect that significant differences between V-8 and CFR data are results of hardware limitations and not fundamental limitations.

The critical compression tests are easily accomplished with the CFR engine since that is closely related to the purpose for which the CFR engine was originally developed. That is, the "octane" rating of fuels. The techniques used to detect "knock" in the experiments described here is different from that used in the octane testing. The detection method is discussed in detail below.

The remainder of this task description is divided into two parts. The first is a description of the performance tests and the second deals with the critical compression ratio tests.

2. Performance/Emission Tests

a. CFR Engine Description

The CFR engine in use at JPL for this test series was acquired on loan from the Union Oil Co. The CFR is a single-cylinder engine of continuously variable compression ratio up to a maximum of ~13.5:1. The

engine is connected by pulleys and belts to a synchronous electrical motor capable of starting the engine and of either absorbing the excess power developed by the engine or supplying power so as to maintain a constant speed of 1200 RPM.* Detailed dimensions and component descriptions are given in Ref. 4.

No changes were made to the basic CFR engine except in the induction area. The CFR carburetor was replaced by a pneumatic atomizer (Spraying Systems Atomizer with a #64 Air Nozzle and a #1650 fuel nozzle). The modified induction system is shown in Figure 66. The pneumatic atomizer provides superior atomization of the liquid gasoline and is also a convenient means of mixing the gasoline and gaseous hydrogen. (The hydrogen is introduced through the pneumatic half of the atomizer.) The atomizer is connected to the CFR engine intake port by means of a 28" long x 1-1/4" I.D. flexible tube. The connecting tube provides a large mixing/vaporization volume and helps to insure a uniform, largely gaseous charge to the engine.

b. Instrumentation

The parameters measured during the test series, included cylinder chamber pressure, engine inlet manifold pressure and temperature, exhaust gas pressure and temperature, indicated horsepower and the pressure, temperature, and volumetric flowrates of the air, liquid fuel, and gaseous hydrogen.

The flowrates (air, gasoline, and hydrogen) were measured by Rotameters (Brooks and Fischer & Porter); the pressures were measured by both electronic strain-gage transducers (Statham and Kistler) and direct reading dial gages; and temperatures were measured by both thermocouples (Cr.-Const. and Cr.-Al) and direct reading dial gages (Weston). The parameters measured are specified in Table 3 with the instrument locations coded to the Figure 67 schematic.

*Other preset speeds are possible by using different pulley combinations.

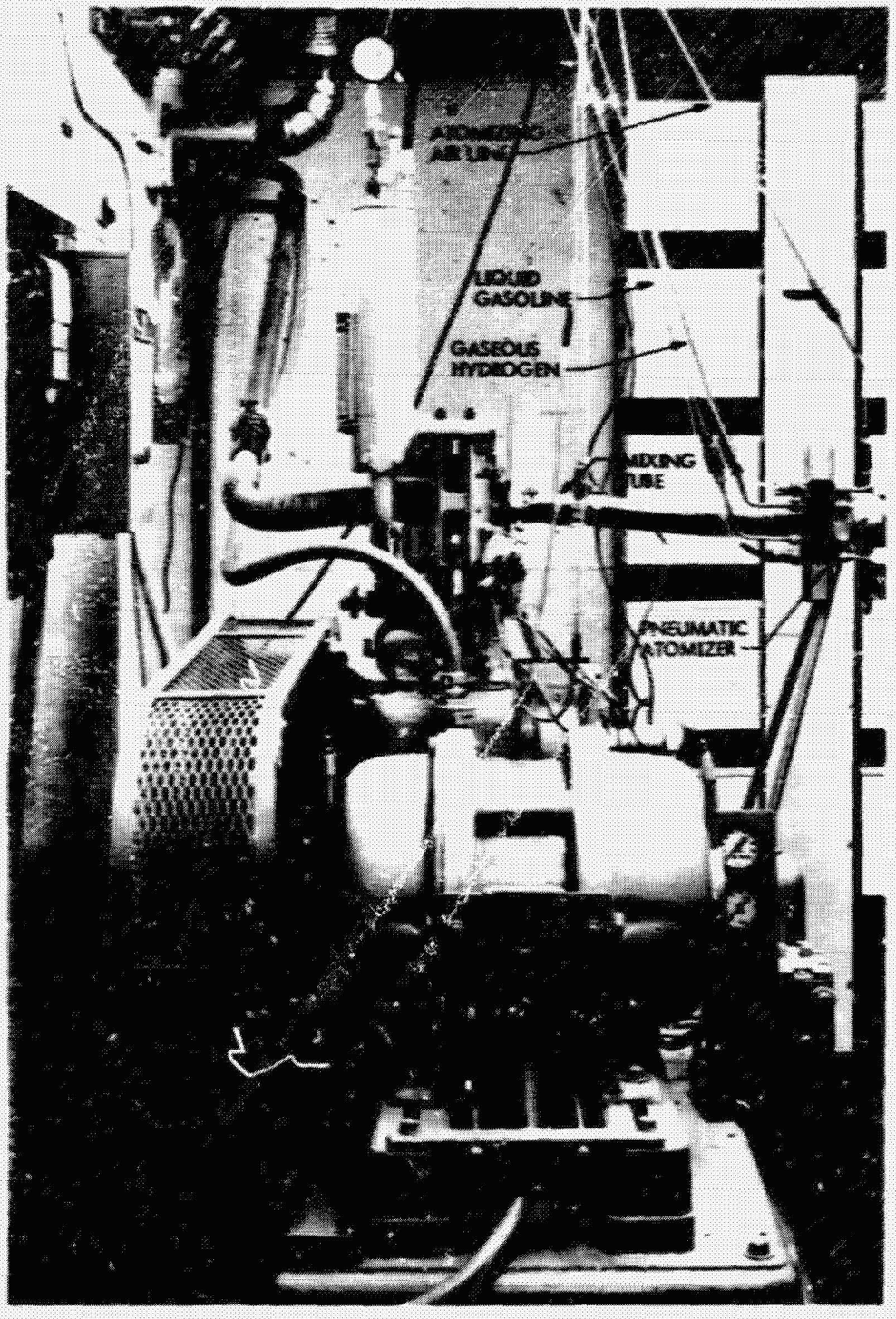

Fig. 66. Modified induction system

Table 3. Instrumentation (Reference Fig. 67)

I. D.	TYPE	SOURCE	MFG/MODEL	RANGE
FLOW				
F_1	Rotameter	Induction Air Feed	Brooks/Md. 9-1110-15	0-55 #/HR
F_2	Rotameter	Atomizer Air Feed	F & P/FP-1/4 -20-G-5/26	0-5 #/HR
F_3	Rotameter	Gasoline Feed	F & P/MD. 10A3565A	0-5 #/HR
F_4	Rotameter	Hydrogen Feed	F & P/MD. 10A3565S	0-1.2 #/HR
PRESSURE				
P_1	Gage	Hydrogen Bottle Manifold	Victor	0-4000 PSIG
P_2	Gage	Hydrogen Feed U/S	U.S. Gauge	0-200 PSIG
P_3	Gage	Hydrogen Feed D/S	Heise	0-100 PSIG
P_4	Gage	Gasoline Feed	U.S. Gauge	0-30-PSIG
P_5	Gage	Atomizer Air Feed	U.S. Gauge	0-30 PSIG
P_6	Gage	Main Engine Air	Ashcroft	0-60 PSIG
P_7	Gage	Atomizer	U.S. Gauge	0-60 PSIG
P_8	Gage	Coolant Water	U.S. Gauge	0-100 PSIG

Table 3. Instrumentation (Reference Fig. 67) (Contd)

I.D.	TYPE	SOURCE	MFG/MODEL	RANGE
P_9	Gage	Oil	G. W. Corp.	0-100 PSIG
P_{10}	Monometer	Inlet Air	-	-
P_{11}	Transducer	Cylinder	Kistler/ MD. 601	0-100 PSIG
P_{12}	Transducer	Inlet	Statham/ M. D. PM280	2 1/2 PSID
P_{13}	Transducer	Exhaust	Statham/ M. D. PM131	12 1/2 PSID
TEMPERATURE				
T_1	Gage	Main Air	Weston	-40—120° F
T_2	Gage	Atomizer Air	Weston	-40—120° F
T_3	Gage	Gasoline	Weston	0—200° F
T_4	Gage	Hydrogen	Weston	-40—120° F
T_5	Gage	Oil	J. P. Marsh	
T_6	Thermocouple	Inlet	Cr.-Al.-Const.	-450 —1222° F
T_7	Thermocouple	Exhaust	Cr.-Al	ΔT

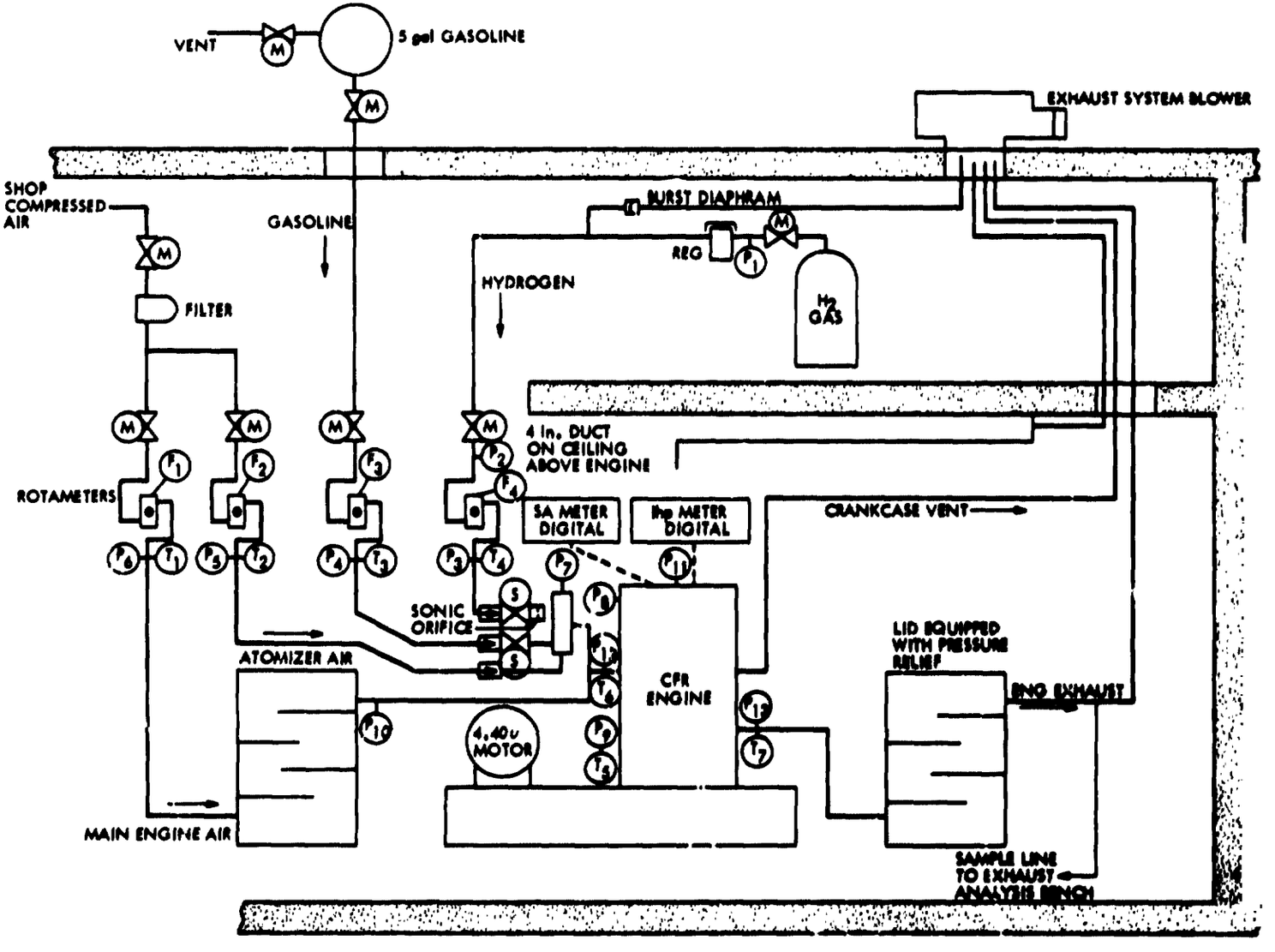

Fig. 67. JPL CFR schematic (instrument locations)

One of the key measurements, indicated horsepower, will be described here since it is somewhat different from the usual measurement of engine power. Indicated horsepower (IHP) is derived from a direct measure of combustion cylinder pressure and a signal proportional to the chamber volume. The cylinder pressure is measured by a high-response transducer. The chamber volume signal is derived in the same manner as the spark timing signal for the V-8 tests. (See Section II. C. -3.) The chamber volume signal is taken from the same disc (see Figure 29) as spark timing in the case of the CFR engine. The disc used for the spark timing circuit includes a second set of holes that provide pulses at equal combustion chamber volume increments. Fifty holes for each 180° of crankshaft rotation were drilled at locations calculated from the piston stroke and connecting rod length to provide equal volume increments between the holes. The equal volume pulse is sent to the control logic; an analog switch is closed causing the cylinder pressure to be sampled for a period of 145 microseconds. Signals from the spark timing circuitry control the switches that define positive (power stroke) or negative (compression stroke) IHP. The resulting voltage-time pulse is stored in a capacitor, providing an electrical charge proportional to the average cylinder pressure for the volume increment. The sum of the charge generated by the 50 pressure-time samples for each cycle is, thus, proportional to the integral of pressure and incremental volume (i. e., $\int pdv$). With the proper scaling, this signal is directly IHP.

The charge stored on the capacitor is amplified and scaled to provide an analog voltage that reads directly in IHP. The time constant of the analog circuitry is approximately 2 seconds, so that the analog output voltage represents IHP averaged over several cycles.

An emissions sample was taken from the exhaust products through a line connected from the exhaust pipe to the emissions analyzer bench. The same emissions analysis instrumentation used for the V-8 tests was utilized, and hence will not be further described here.

Because the CFR engine was in a temporary location for this first group of tests, only the emissions bench was connected to the IDAC. Consequently, all data were hand-recorded and later reduced to engineering units. Further manipulation of the data was by digital computer. The parameters of interest here, equivalence ratio, indicated thermal efficiency, and indicated specific emissions were results of the computer treatment.

c. Test Description

The single-cylinder engine was operated at local ambient inlet conditions, at full throttle, at a constant engine speed of 1200 RPM, and with a compression ratio setting of 8.0 to 1.

Approximately 120 discrete combinations of equivalence ratio and hydrogen fraction were tested. These tests were grouped and are identified as Series I through IX. Each series corresponds to a constant value of the ratio of air flowrate to hydrogen flowrate. Series I and II were conducted with pure Indolene-30 and pure hydrogen, respectively. The mixed-fuels tests were conducted by fixing the hydrogen flowrate and varying the gasoline flowrate. This procedure was chosen for its experimental convenience. However, it does result in the simultaneous variation of both equivalence ratio and the hydrogen fraction. The specific values of air-to-hydrogen ratio tested are noted on Figure 68. Additional mixed-fuel tests were made in which the shrouded valve was replaced by a plain (i.e., non-shrouded) valve. All test points represent a condition of maximum power spark advance (MPSA), and data were recorded only after a period of stabilized operation.

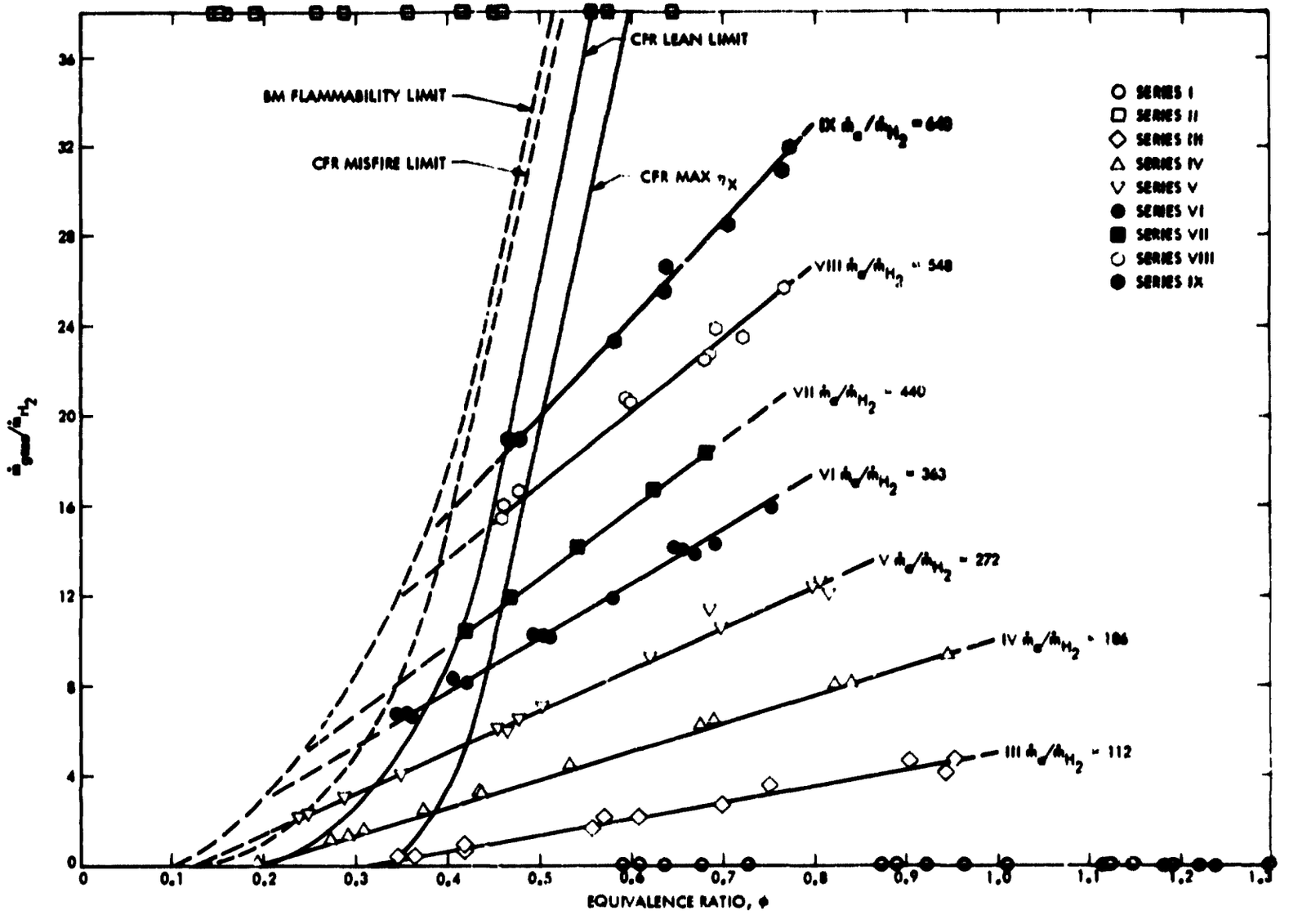

Fig. 68. $\dot{m}_{gasoline}/\dot{m}_{H_2}$ vs equivalence ratio, ϕ

d. Test Results

The data from the individual test series were plotted versus equivalence ratio and curves hand-fitted to the data points. Indicated thermal efficiency (η_t), indicated horsepower (IHP), volumetric efficiency (η_v), spark advance (SA), and indicated specific emissions (NO_x, CO, and HC) were each plotted. Typical plots of η_t, η_v, and SA for four fuel compositions are shown in Figures 69 and 70. The derived curves of η_t and SA for all the tests are shown on the single plot, Figure 71. Figure 72 is a plot of IHP as a function of equivalence ratio and shows the magnitude of the power loss associated with ultra-lean combustion.

The individual plots of η_t vs Φ were used to locate the two lines labeled CFR lean limit and CFR maximum η_t, of Figures 68 and 73. The maximum η_t line is simply the loci of the maxima as typified by Figures 69 and 70. The lean limit is the loci points which are 5% lower than the maximum and to the lean side (i.e., lower Φ) of the maximum. The CFR misfire curve of Figures 69 and 72 represents the minimum Φ at which the engine could be operated without significant misfire. The curve labeled BM flammability limit is calculated according to Le Chatlier's Rule from Bureau of the Mines data. This curve was first presented in Reference 5. Plots of specific emissions for all tests are shown in Figures 74, 75, and 76.

The data, when plotted with air/hydrogen ratio as a parameter, are of limited value since one of the key parameters, $\%H_2$ (or synonomously hydrogen to gasoline mass ratio) does not appear explicitly. By choosing data points which fell within a selected band of hydrogen percentage, the plot of Figure 77 was constructed. The emissions curves of Figures 78 and 79 labeled 5% H_2 and 10%H_2 were derived in a similar way, although the scatter of the emissions data made that task more difficult.

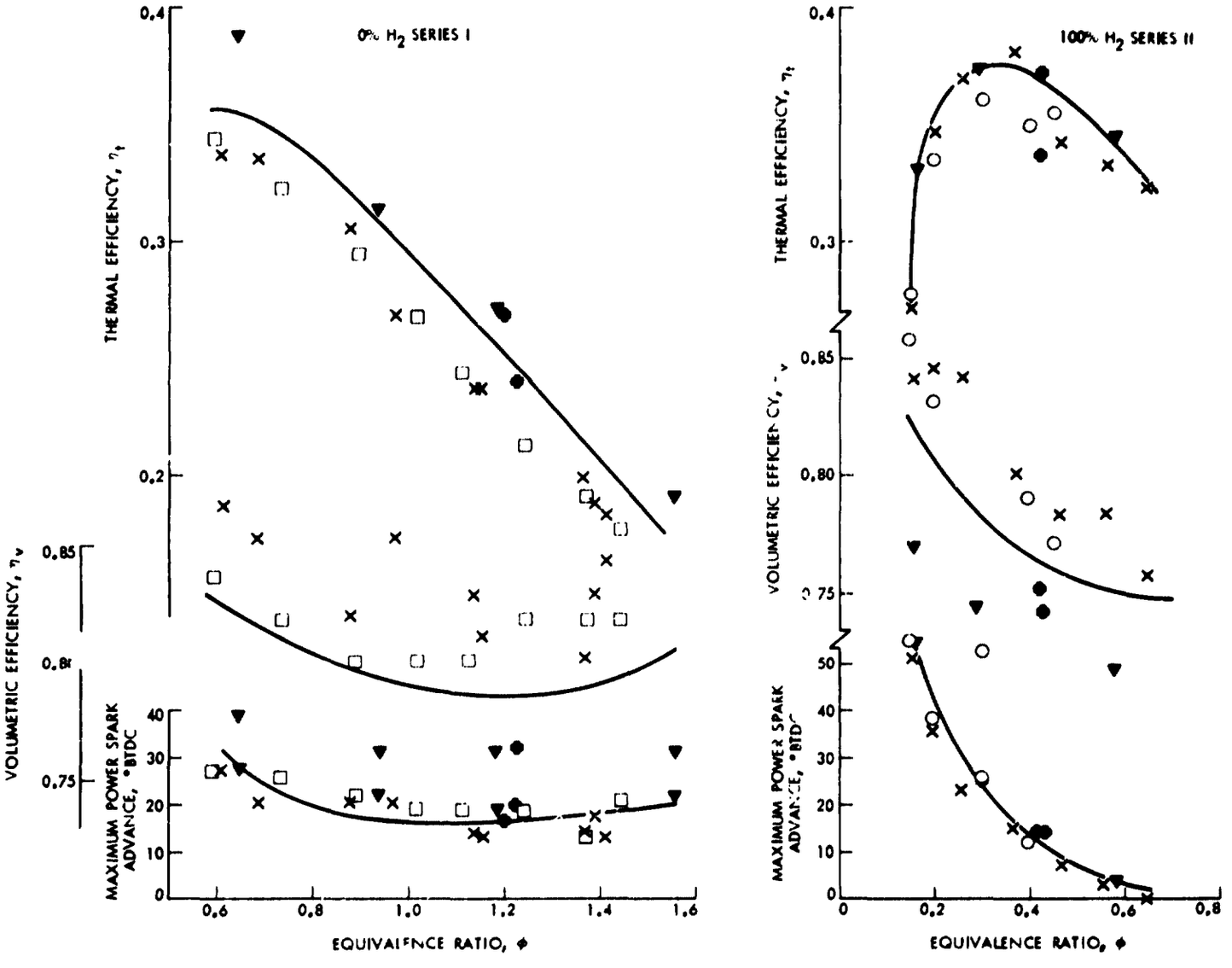

Fig. 69. Thermal efficiency, volumetric efficiency, and maximum power spark advance vs equivalence ratio (plot 1)

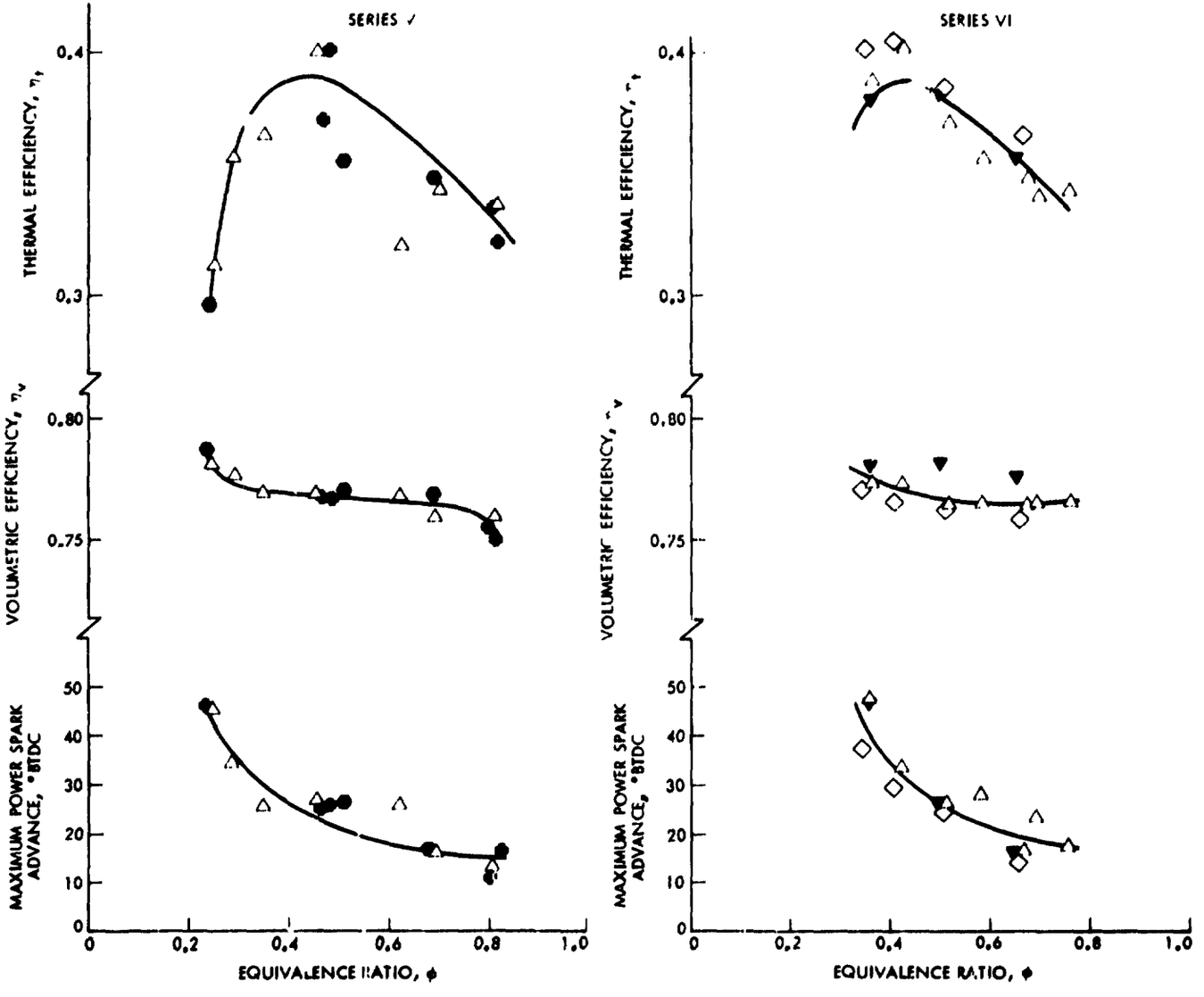

Fig. 70. Thermal efficiency, volumetric efficiency, and maximum power spark advance vs equivalence ratio (plot 2)

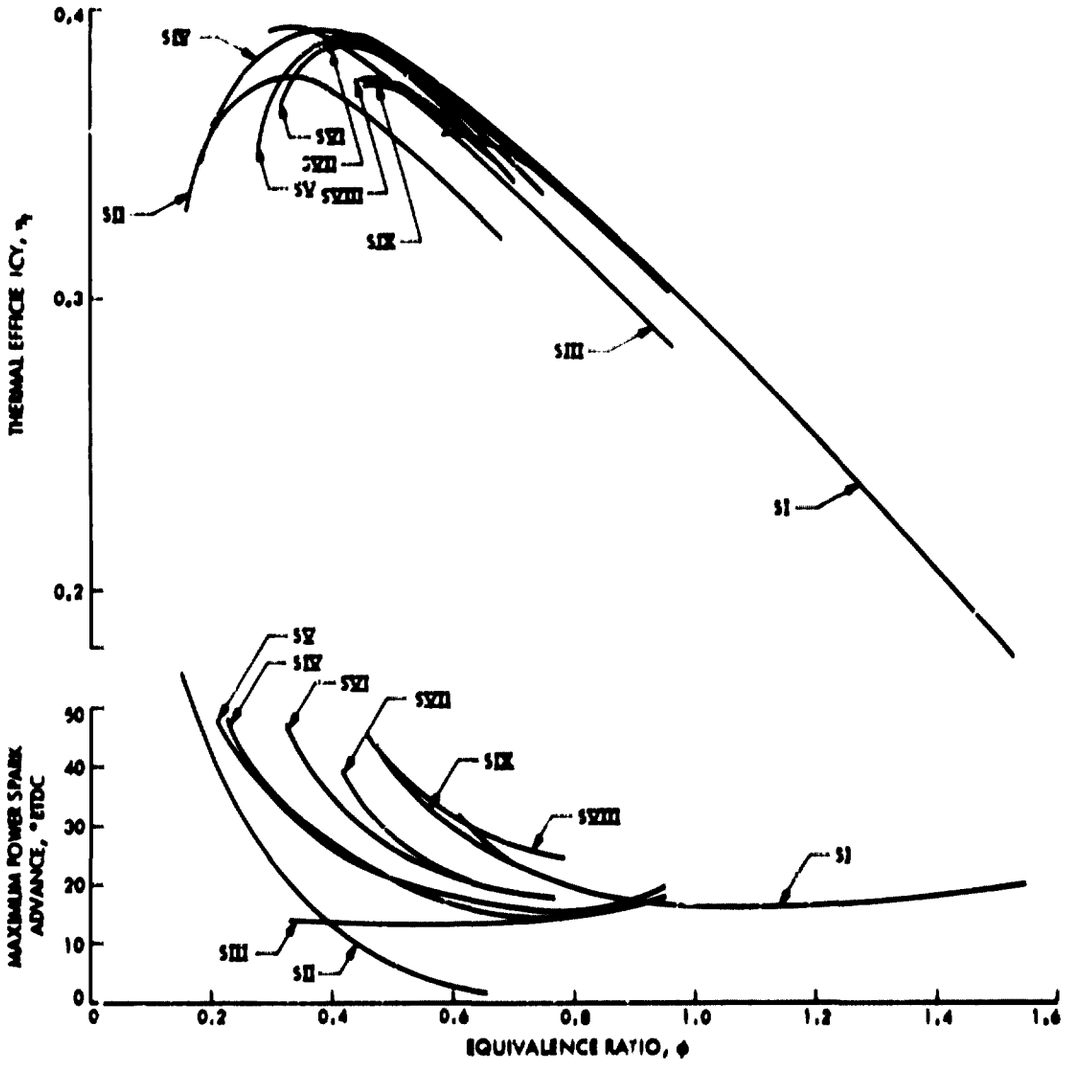

Fig. 71. Derived curves of η_t and SA for all tests

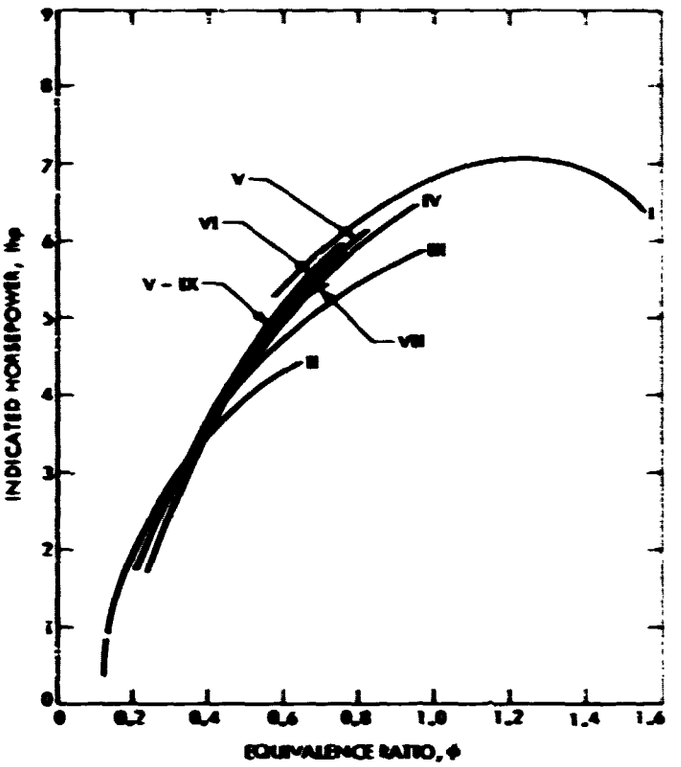

Fig. 72. Equivalence ratio vs indicated HP

Several observations may be made from Figures 75 through 77. These are:

1) The inverse relationship of η_t with ϕ has been clearly verified.

2) The addition of hydrogen allows the combustion of gasoline at conditions which are well below the flammability limit of gasoline alone.

3) There is a clear dependence of η_t, CO, and HC on the fuel composition.

4) More data at low percentage of hydrogen should be gathered since that is the region of interest for the multi-cylinder engine.

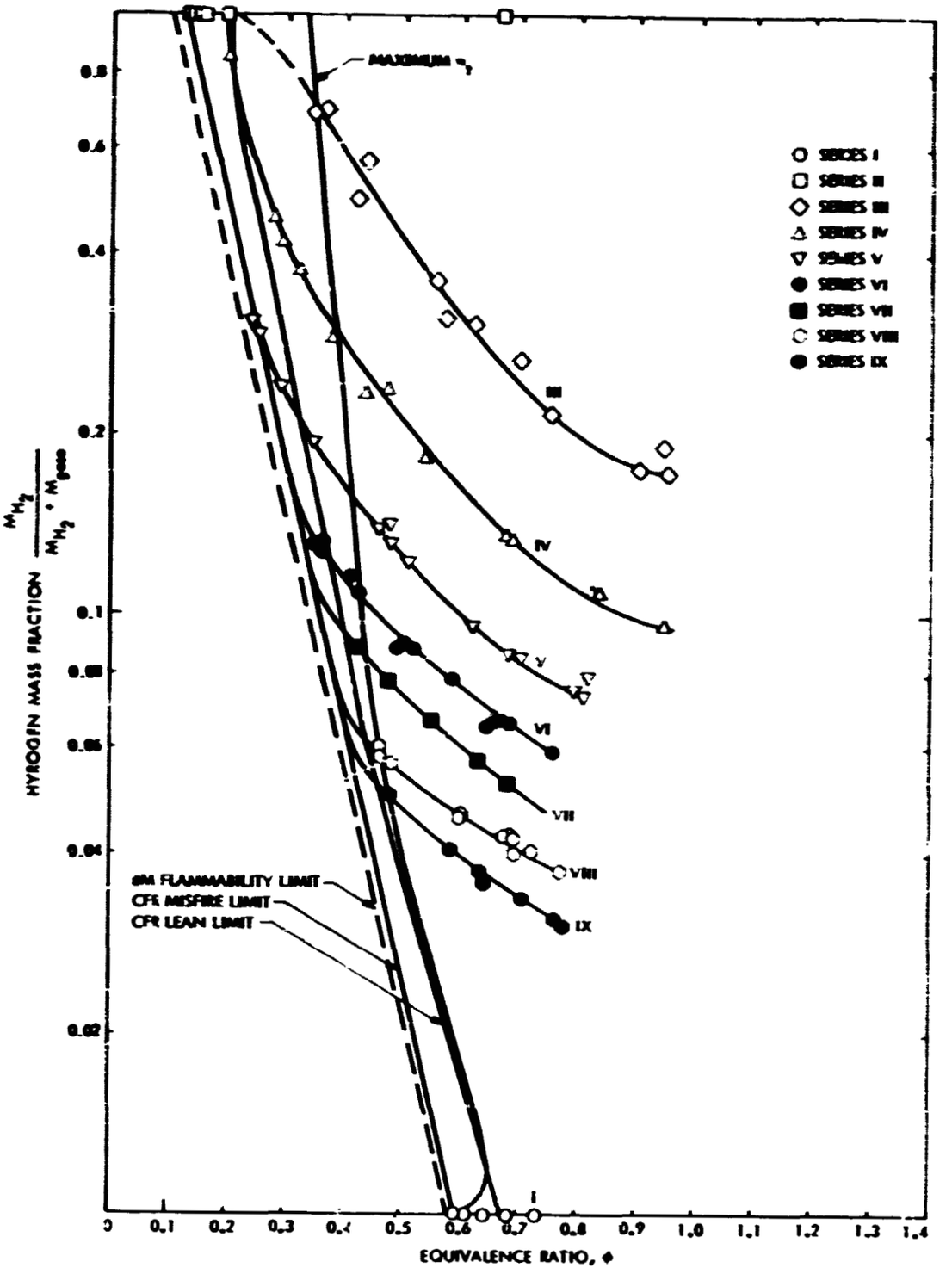

Fig. 73. Equivalence ratio vs hydrogen mass fraction

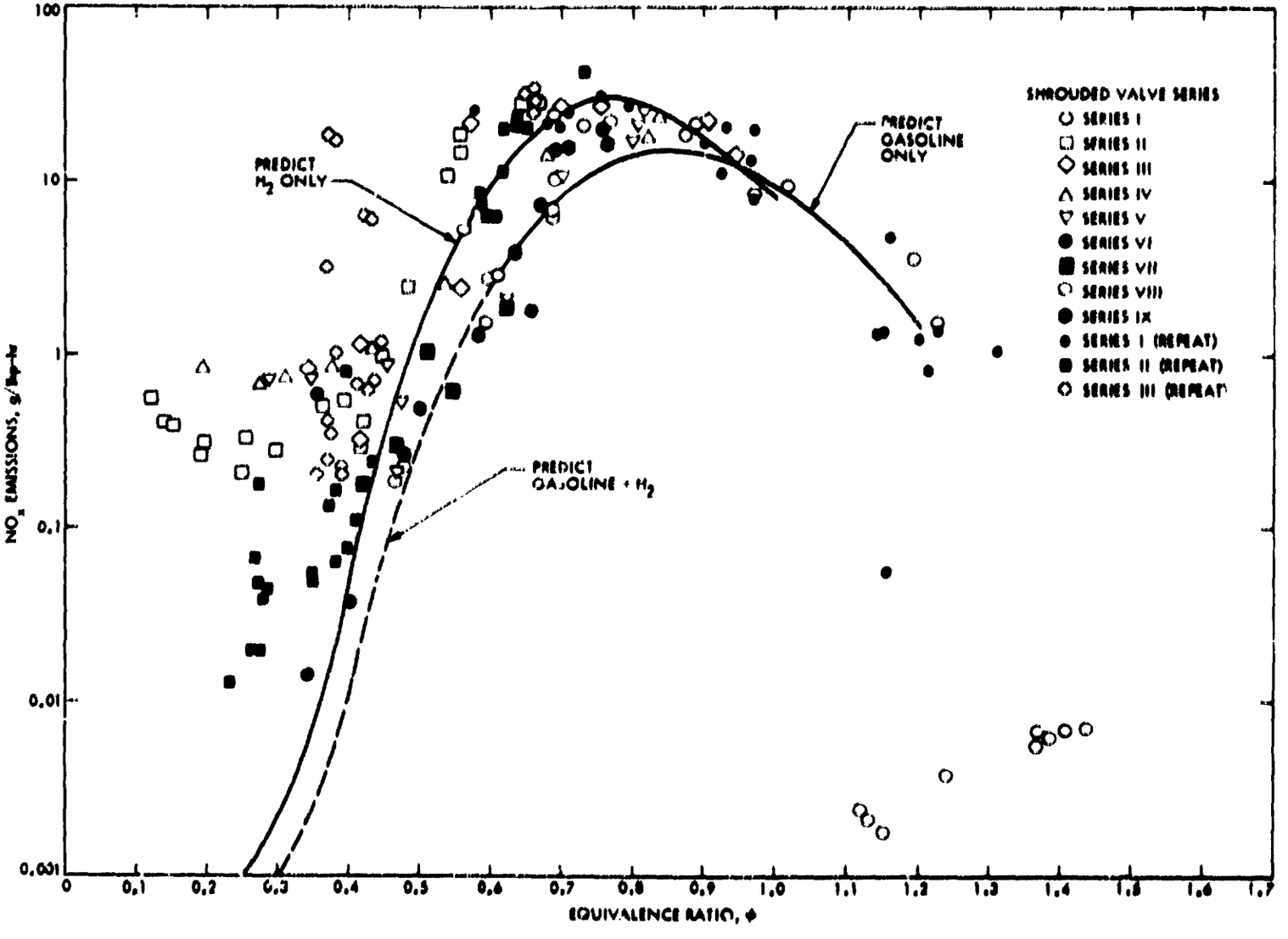

Fig. 74. NO_x vs equivalence ratio

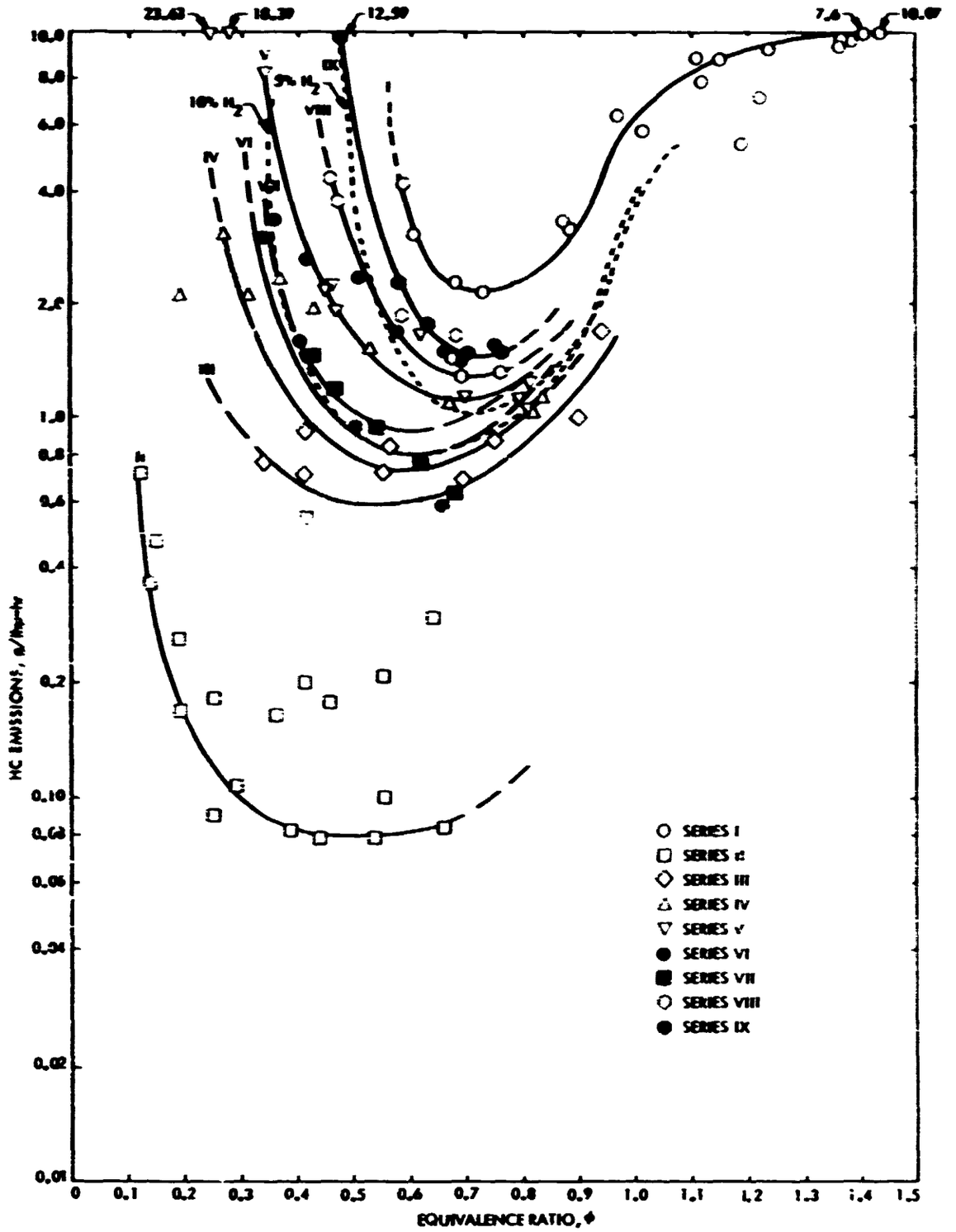

Fig. 75. HC emissions vs equivalence ratio

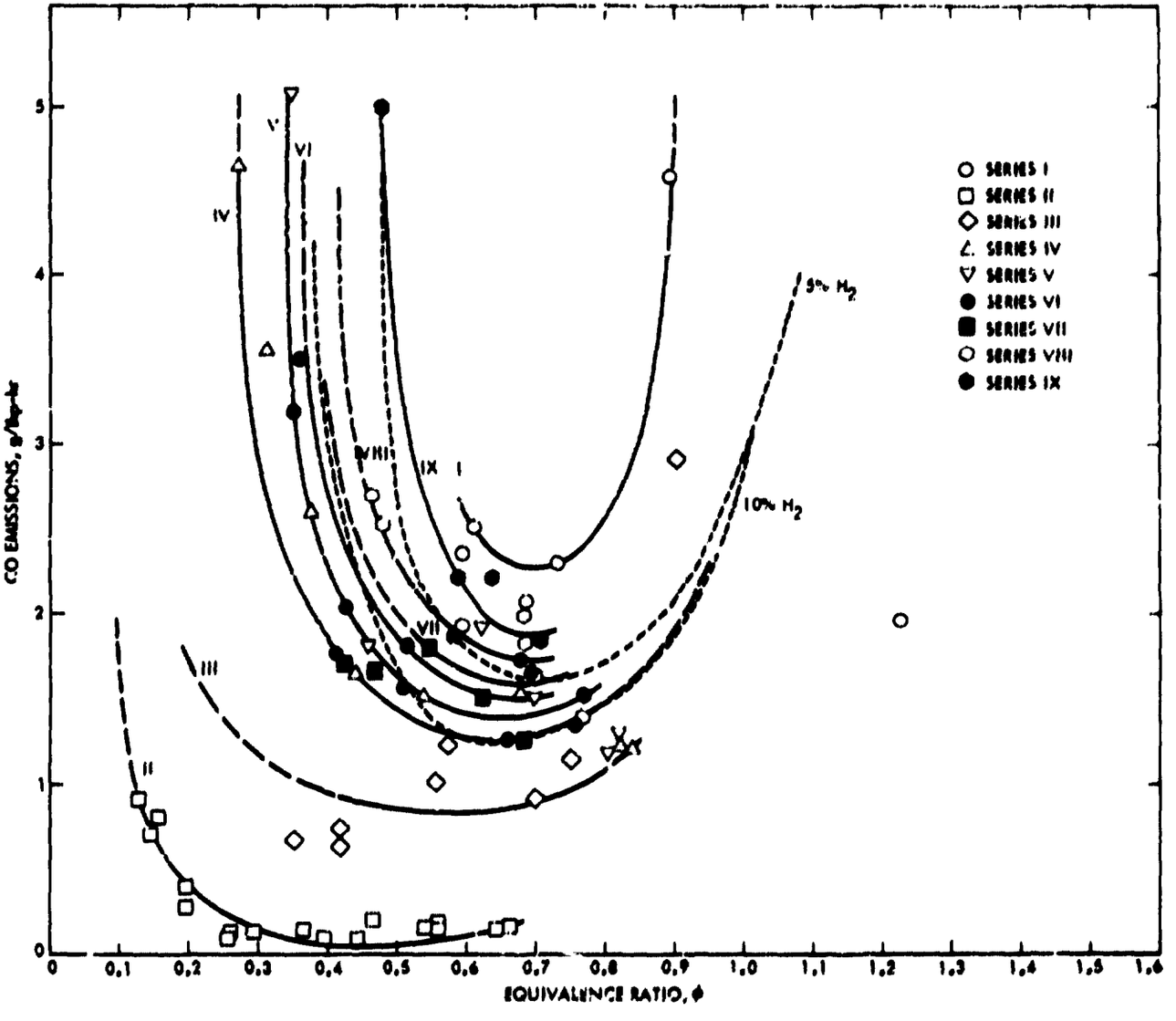

Fig. 76. CO emissions vs equivalence ratio

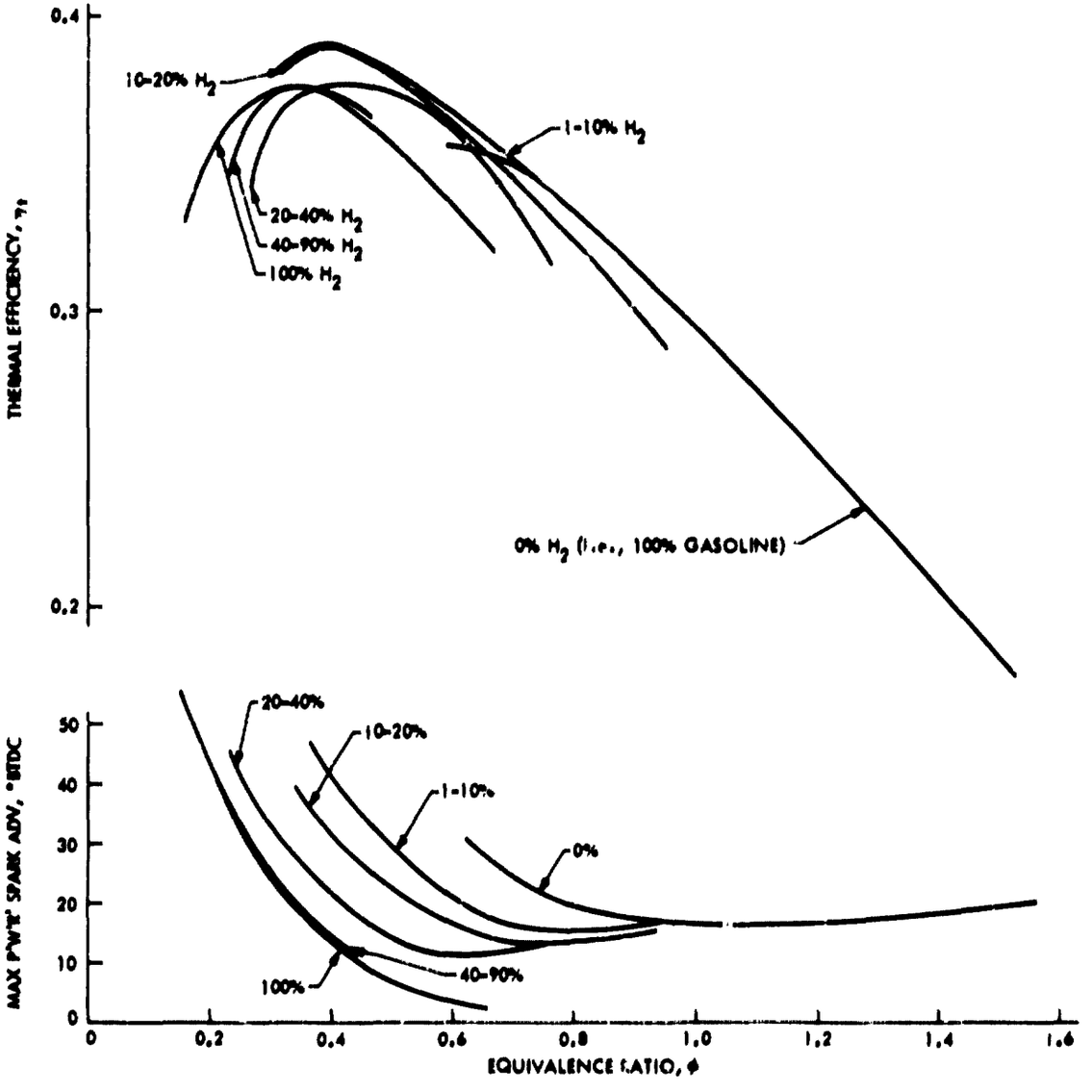

Fig. 77. Thermal efficiency vs equivalence ratio

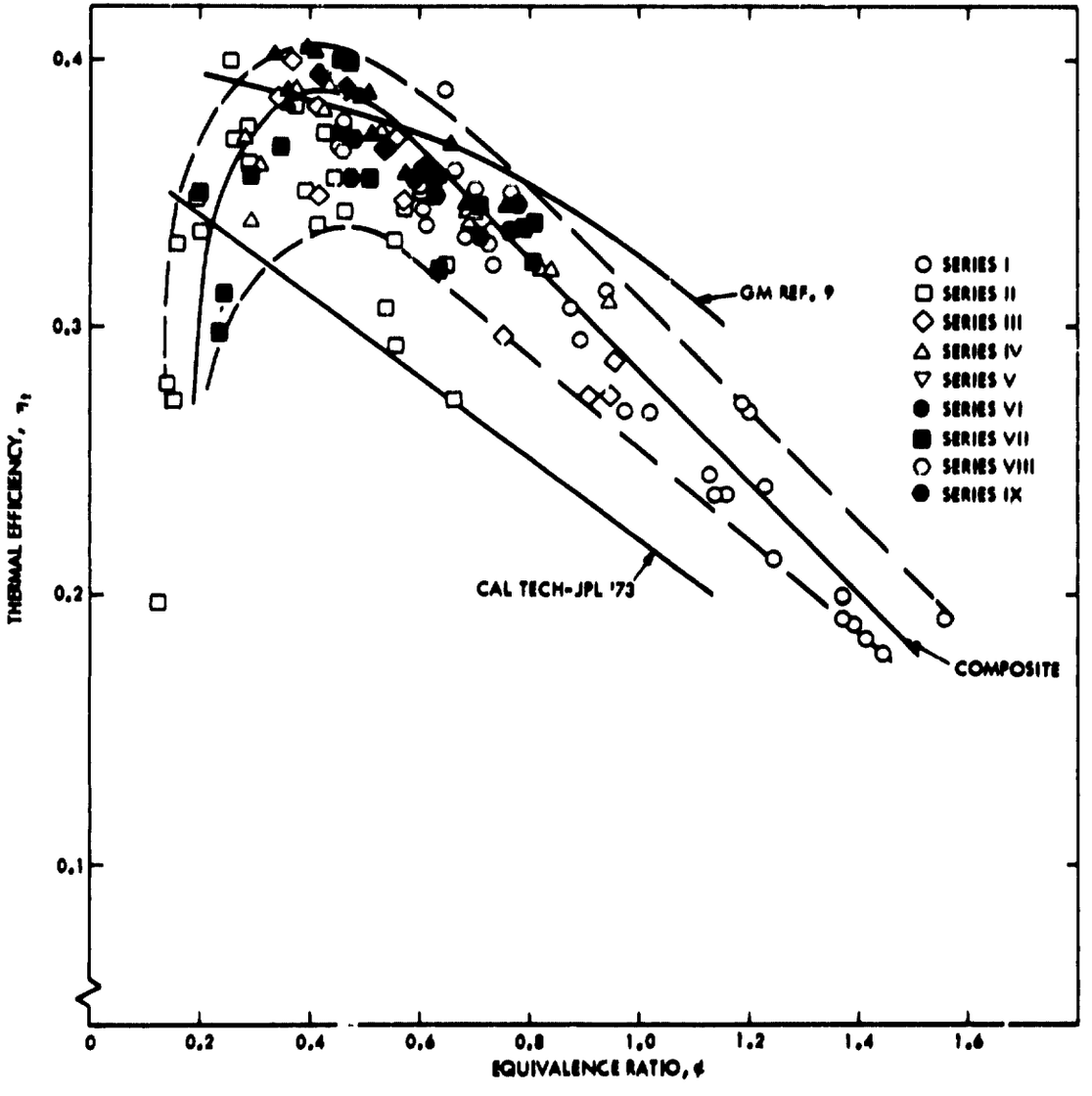

Fig. 78. Thermal efficiency vs equivalence ratio

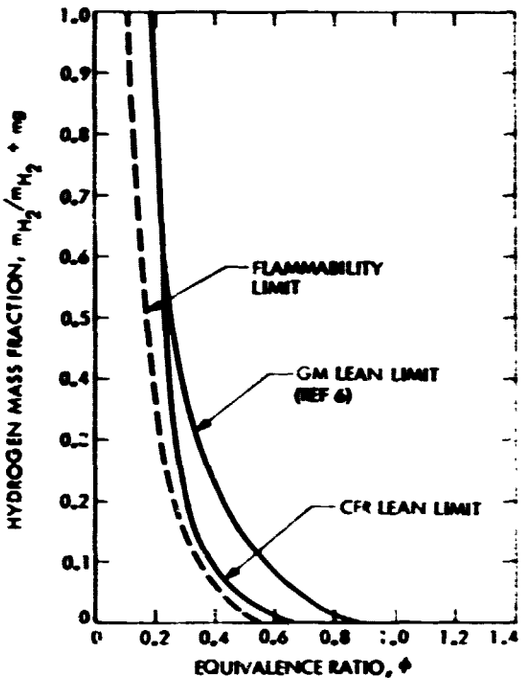

Fig. 79. Hydrogen fraction vs equivalence ratio

5) The strong dependence of NO_x emissions on equivalence ratio is apparent, thus confirming that control of NO_x by ultra-lean combustion is possible.

6) The HC difficulties observed with the V-8 engine are also apparent in the CFR engine data.

A comparison was desired between the data reported here and both the unpublished data of Rupe, Lee, Houseman, and Shair (which led directly to the hydrogen enrichment concept) and the data of Stebar and Parks (Ref. 6). This comparison is shown in Figure 78. Indicated thermal efficiency data from all the test series were plotted as a function of equivalence ratio and a composite curve drawn. Although the data within the envelope appears to exhibit excessive

scatter, as shown previously (Figures 72 and 73), the data actually represents a "family of curves." The three sets of data exhibit the same inverse relationship of equivalence ratio and thermal efficiency. However, the GM data does not show a maximum in thermal efficiency. The absolute values of η_t differ considerably among the three curves, but this may reflect in part the three different experimental setups and differences in instrumentation techniques.

For comparative purposes, the lines identified as the flammability limit and the lean limit (Figures 68 and 73) were replotted in Figure 79, along with the line identified as the GM lean limit. (This line is defined in the GM report of Reference 6.) This comparison shows that the GM and JPL lean limits start to diverge at an equivalence ratio of approximately 0.25, and the divergence increases at higher equivalence ratios. The JPL data indicate lean limit operation for 100% gasoline at a much lower equivalence ratio than the GM data. This is most likely the result of the good gasoline atomization and long mixing length in the JPL experimental setup.

It had been speculated at the beginning of this work that the use of shrouded intake valves would improve the engine thermal efficiency and simultaneously reduce the unburned hydrocarbons. It was presumed that low efficiency and high hydrocarbons resulted from incomplete combustion in the main charge. Consequently, it was planned to do a comparative set of tests using shrouded and unshrouded intake valves in the CFR engine. A small number of tests with the unshrouded valves were conducted, but were not definitive because the range of equivalence ratio covered was not large enough. These tests were not repeated because during the relocation of the CFR engine, similar multi-cylinder engine tests were performed.

Comparative tests of shrouded and unshrouded intake valve, using a V-8 engine, have shown that the original speculation was false. In these tests the use of shrouded valves did significantly increase the engine thermal efficiency, but the unburned hydrocarbons emitted increased by a factor of ~3. It is clear that the use of shrouded valves increases the turbulence level of the charge, and hence increases the apparent flame speed. The increase in efficiency then arises from the fact that combustion occurs over a much shorter time interval and thus more closely approximates the ideal cycle. However, at the same time, the increased turbulence changes the heat-transfer rates to the "cold" chamber walls, increasing the amount of hydrocarbons trapped in the quench layer. Therefore, it is no longer believed that the use of shrouded valves will decrease the hydrocarbons; however, it is clear that combustion turbulence is a key parameter in achieving ultralean, high-efficiency operation.

3. Critical Compression Ratio Tests

a. Discussion

The objectives of this group of tests were to investigate and to quantify the "knock" characteristics of hydrogen-enriched gasoline. It was expected that for a fixed hydrogen-to-hydrocarbon ratio, the critical compression ratio (the compression ratio at which knock is first observed) would vary inversely with equivalence ratio, Φ, and in fact this trend was observed. All "knock" tests were done using Indolene-clear as the liquid fuel. Indolene-clear is lead-free and has a research octane number of 97. Since all previous CFR testing at JPL was performed with Indolene-30, research octane number of 104, a set of tests using the Indolene-clear as the fuel were first conducted. Two other fuel compositions, 5% and 10% by mass hydrogen, were tested.

Knock is generally presumed to result from the detonation of the "end gas." (Ref. 7.) The end gas is the last fuel consumed during ary given cycle, and as a result of the high cylinder pressures and temperature existing at that time, the end gas may be detonable. The passage of the detonation wave results in the audible sound (termed knock). Since the strength of the detonation wave is variable, different magnitudes of knock are observed.

One of the characteristics associated with knock is a high-frequency pressure oscillation superimposed on the normal cylinder pressure waveform. The characteristic frequency of these pressure oscillations is determined by the combustion chamber geometry and volume, and the physical properties of the gas through which the detonation wave passes. Since these do not vary appreciably for a given engine, this characteristic may be used to detect knock and to quantify its strength. The signal from the high response pressure transducer, also used for the IHP measurement, was filtered and conditioned. Two knock measurements were derived. These were the fraction of cycles (KP) for which knock was detected and the relative measurement of magnitude (KM). The magnitude is a combination of the superimposed pressure amplitude and the KP measurement. For KP = 100% and "large" (i.e., clearly audible knock) amplitude pressure fluctuation, KM = 100%. Either KP = 50% and large pressure amplitudes or KP = 100% and moderate pressure amplitude will result in KM $\cong$ 50%. This technique for quantifying knock magnitude is not an accepted one and presents some obvious difficulties in interpreting the results. In addition, the entire technique is a very sensitive one and detects "knock" when there is no audible indication. This presents difficulties in defining the onset of knock.

Comments concerning the experimental technique employed may be summarized as follows. The technique is a sensitive one, perhaps too sensitive. The correlation between it and industry-accepted techniques is not clear at this time and further effort is required to achieve that understanding. In spite of the difficulties noted, the method employed is felt to give valid relative results, although the absolute values are open to question.

b. Test Description

The CFR engine was installed in its permanent location and was setup as depicted schematically in Figure 80. This installation differed from that used for the performance/emissions tests in that the inlet air heater was added, the inlet and exhaust surge tanks were replaced by newly designed tanks, and other minor modifications were made to accommodate the new location installation.

Instrumentation utilized in the new location (Figure 80) was similar to that used in the Series I, but included additional transducers and the special electronic equipment to characterize "knock" of the mixed fuels. The same high response pressure transducer, which supplies a portion of the signal for the IHP meter, also served as the source for the "knock" measurements.

Initial operation of the CFR engine showed a characteristic (Ref. 6) low-amplitude oscillation super-imposed on the normal cylinder pressure signal during conditions when audible knock was apparent (See Figure 93). This characteristic frequency of approximately 6.3 kHz was used to provide a comparative indication of knock at different engine operating conditions.

The cylinder pressure signal is sent to a bandpass filter that passes only the characteristic knock frequency. This 6th-order filter has selectable low and high pass sections; the cutoff frequency controls were experimentally varied to optimize the filter output ratio between the knocking and normal operation

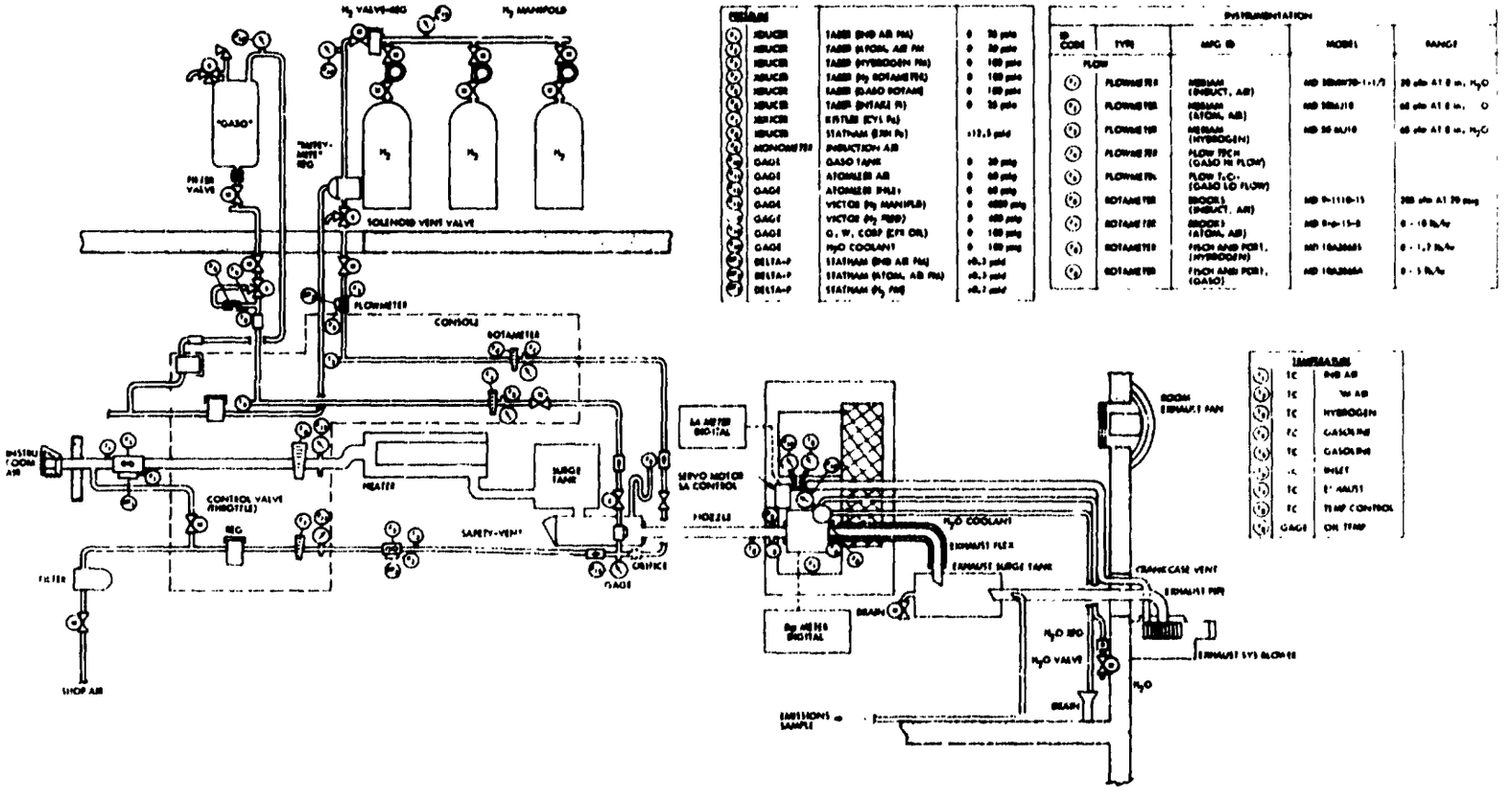

Fig. 80. Instrumentation schematic — CFR laboratory

modes. Two output meters were used to provide indications of the frequency (i.e., the fraction of engine cycles exhibiting knock) and the magnitude of the knock signal. The frequency meter defines the percent of cycles when knock occurred. This signal is developed by a constant width, constant amplitude pulse whenever the characteristic knock frequency exceeds a minimum threshold. The circuit is calibrated to provide full-scale meter deflection when the knock frequency is presented on every firing cycle. The magnitude meter indicates a relative combination of the knock amplitude and its frequency. Maximum meter deflection is obtained with 100% frequency and high amplitude; either a 50% frequency and high amplitude or 100% frequency and half the amplitude will give 50% meter deflection.

As was the case for the performance/emission tests, the CFR engine was operated at a constant speed of 1200 rpm and at wide open throttle. "Knock" is a function of the incoming charge temperature, and so this temperature was eliminated as an experimental variable. This was accomplished by heating the main air. The energy added was controlled, through a feedback loop, so that the temperature of the charge (i.e., gasoline, hydrogen and air) was maintained at -80° F.

Three fuel compositions were tested. These were 0%, 5%, and 10% hydrogen by mass. The gasoline used for all "knock" tests was Indolene-clear (i.e., contains no lead). Equivalence ratios from 0.4 to 1.15 were tested, although not all combinations of fuel composition and equivalence ratio were covered. The combinations covered are shown in Table 4.

The test procedure used was as follows. Steady-state engine operation was established for the desired fuel composition and equivalence ratio at a compression ratio of 8.0. The spark advance was set for maximum power, and

Table 4. Fuel composition and equivalence ratio for knock tests

Fuel Composition, % H_2	Equivalence Ratio
0	1.15
	0.8
	0.6
5	0.7
	0.55
	0.47
10	0.8
	0.6
	0.4
Note: All tests run at maximum power spark advance. All tests run with Indolene-clear.	

the data were recorded. The compression ratio was then increased to a higher value (the increment generally employed was $\Delta CR = 0.5$), the spark advance was re-adjusted for maximum power, and the data were recorded. This procedure was continued until a strong, audible knock was observed or until a compression ratio equal to ~11.5 was reached.

c. Test Results

The test data were reduced to engineering units, plotted, and curves hand fitted to the data. Figures 81 through 89 are plots of knock magnitude (KM) knock frequency (KP), indicated thermal efficiency (η_t), and maximum power power spark advance (MPSA) versus compression ratio. Several observations can be readily drawn from these figures. Thermal efficiency varies directly

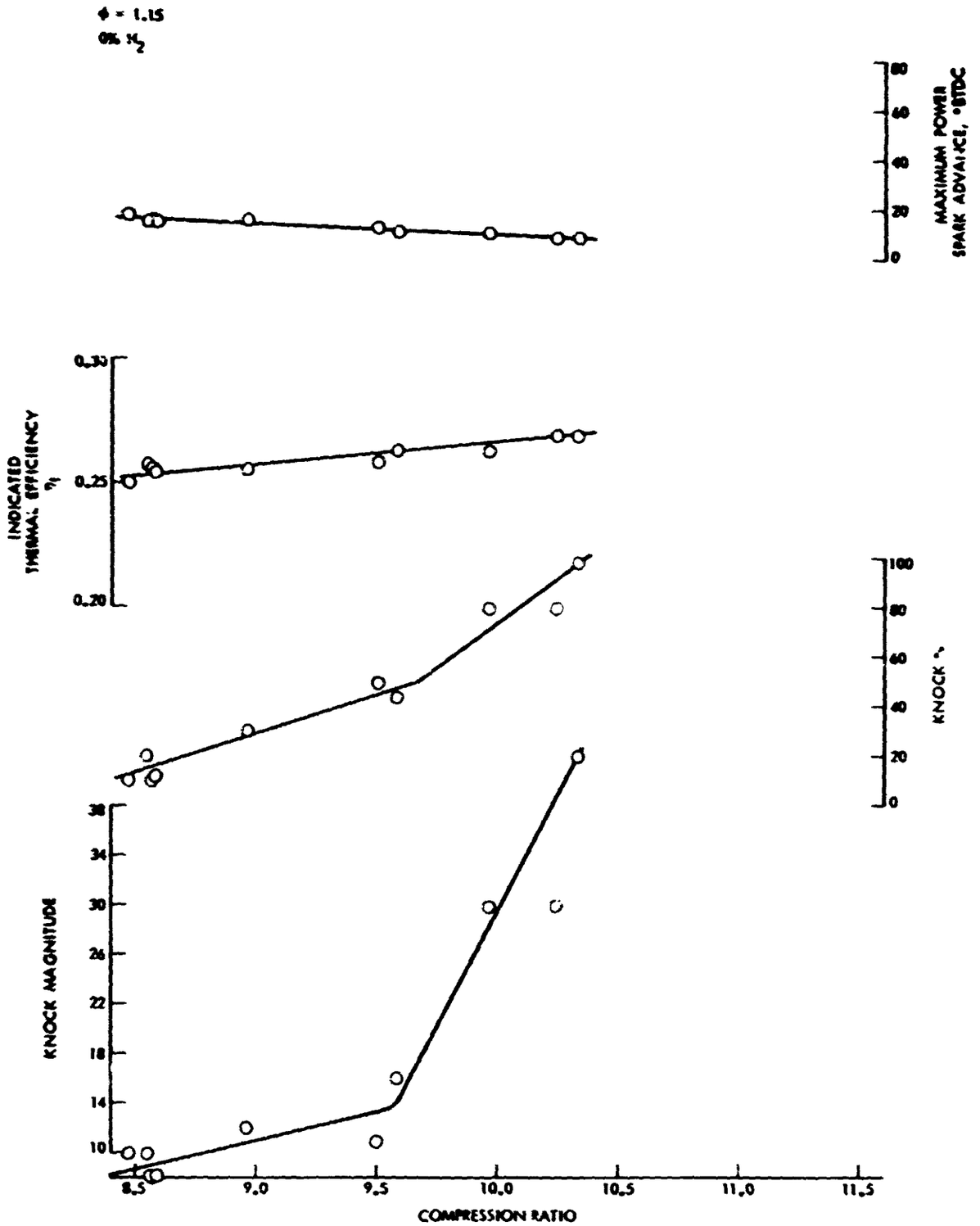

Fig. 81. Knock magnitude, knock %, η_t, and MPSA vs compression ratio (plot 1)

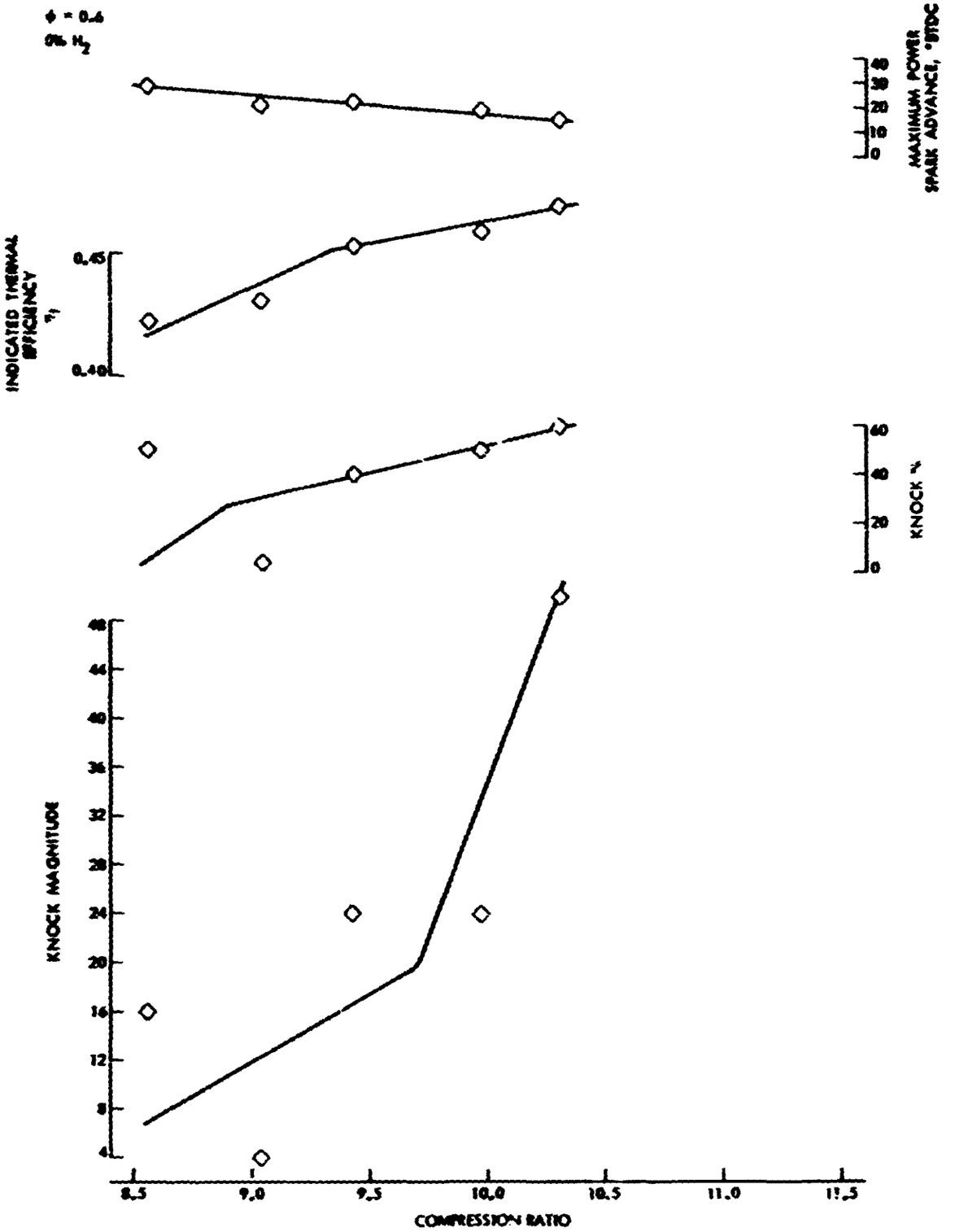

Fig. 82. Knock magnitude, knock %, η_t, and MPSA vs compression ratio (plot 2)

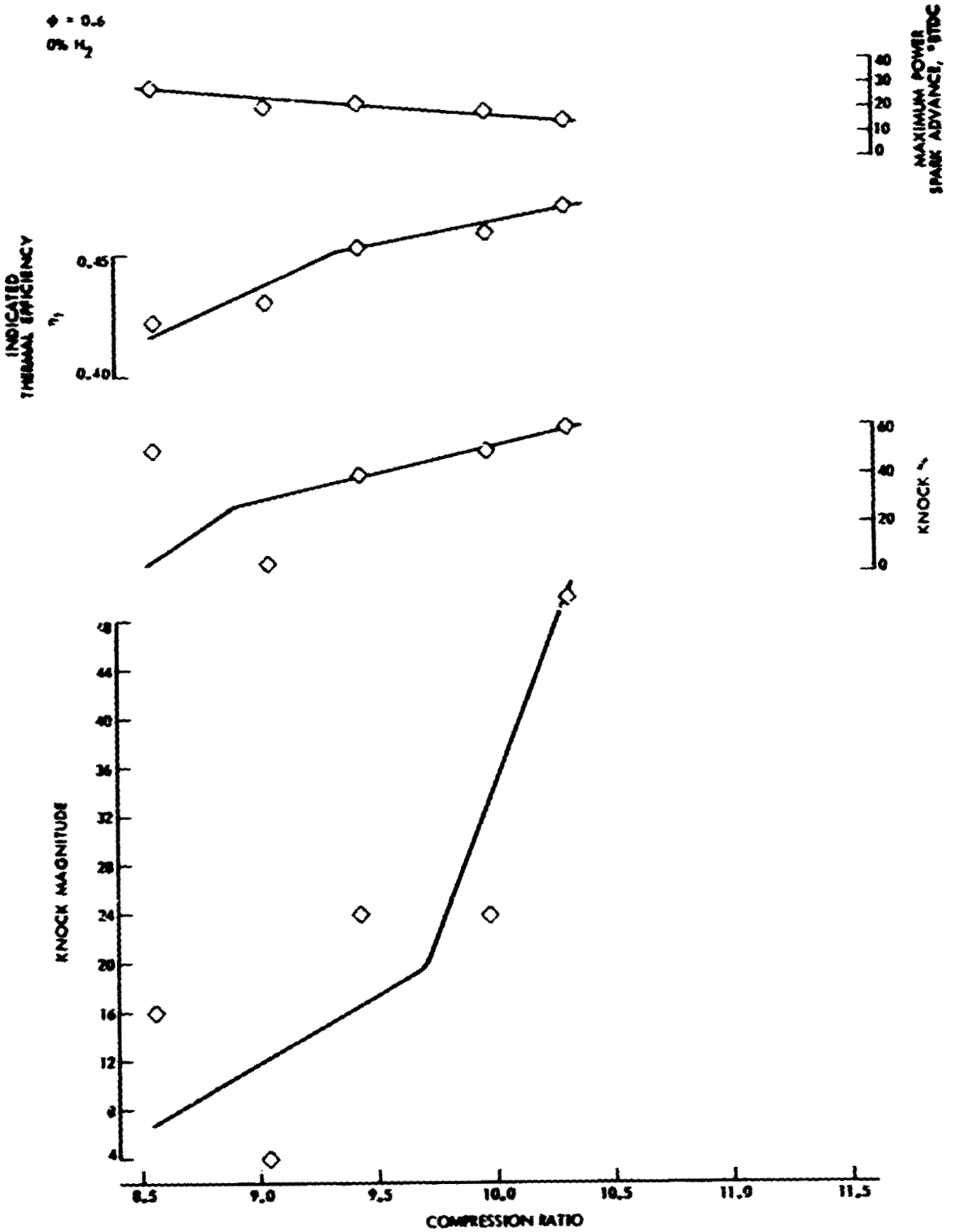

Fig. 83. Knock magnitude, knock %, η_t, and MPSA vs compression ratio (plot 3)

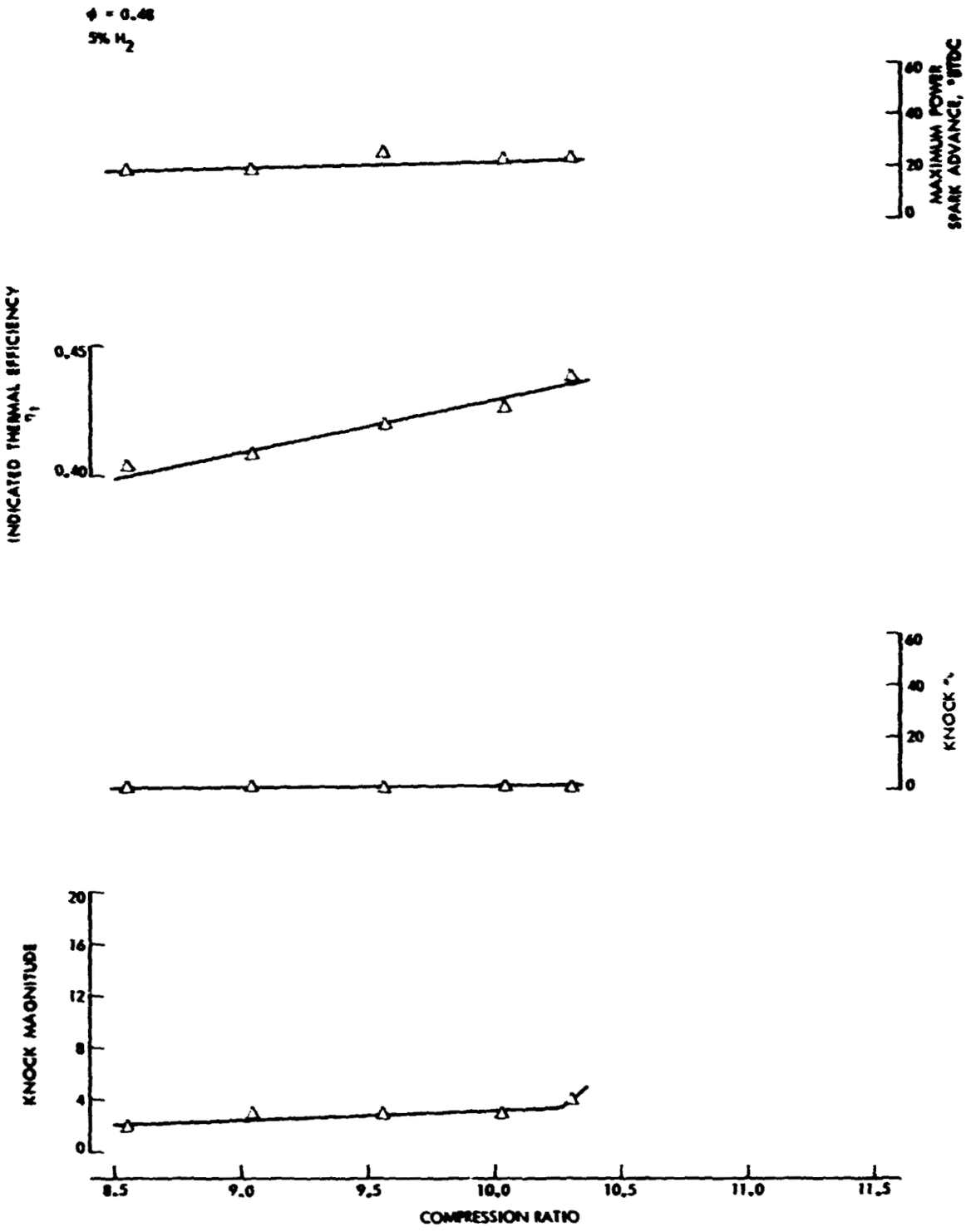

Fig. 84. Knock magnitude, knock %, η_t, and MPSA vs compression ratio (plot 4)

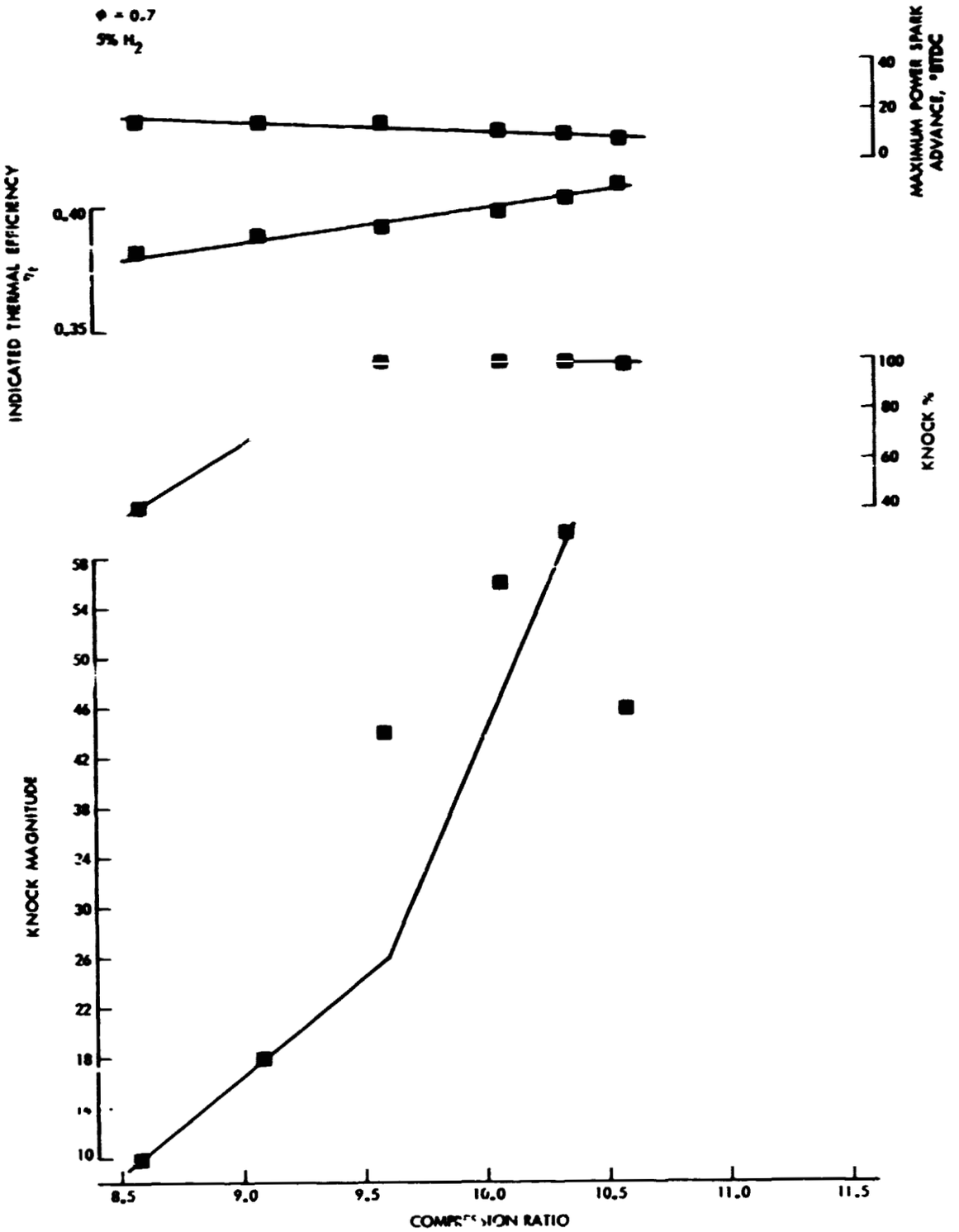

Fig. 85. Knock magnitude, knock %, η_t, and MPSA vs compression ratio (plot 5)

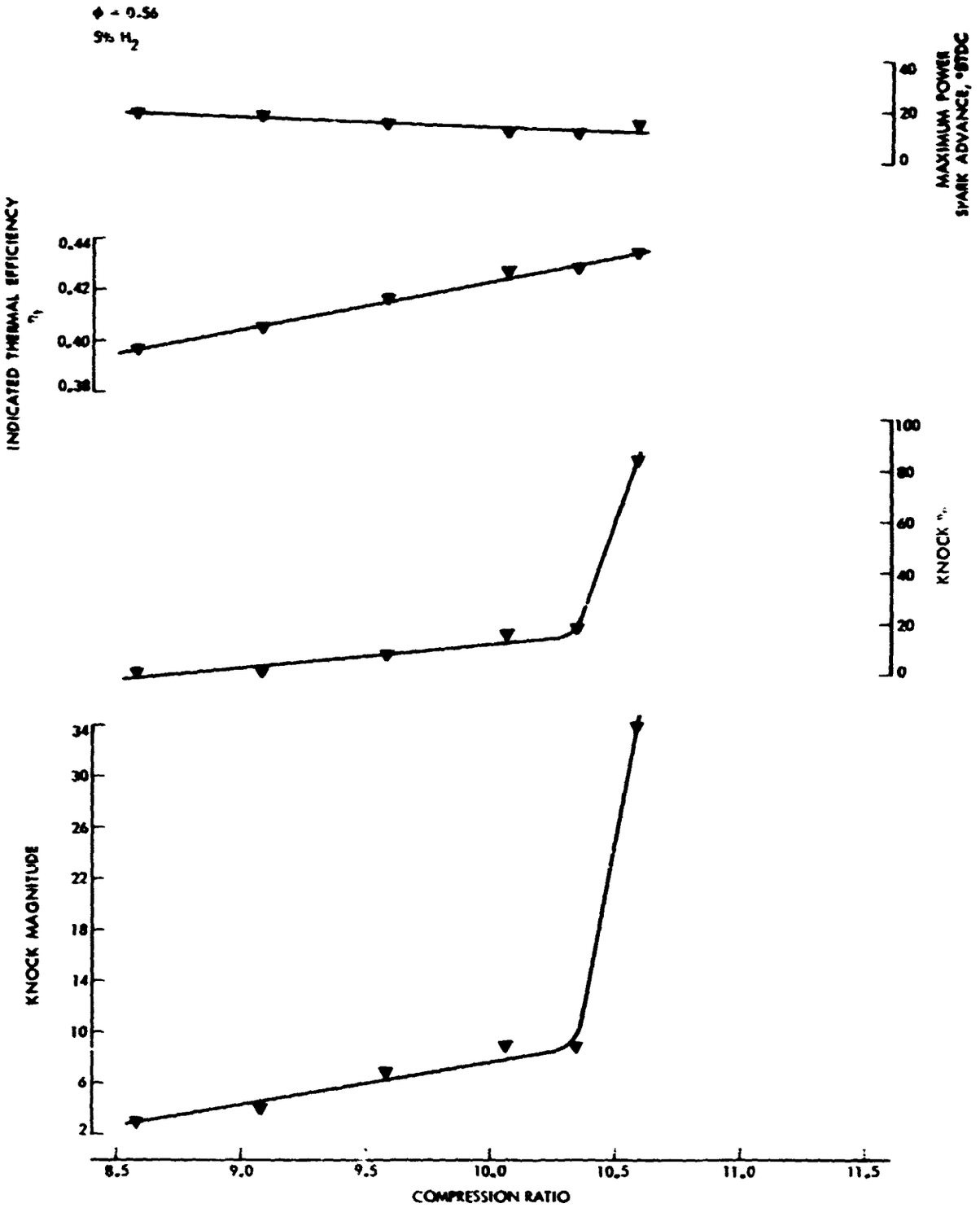

Fig. 86. Knock magnitude, knock %, η_t, and MPSA vs compression ratio (plot 6)

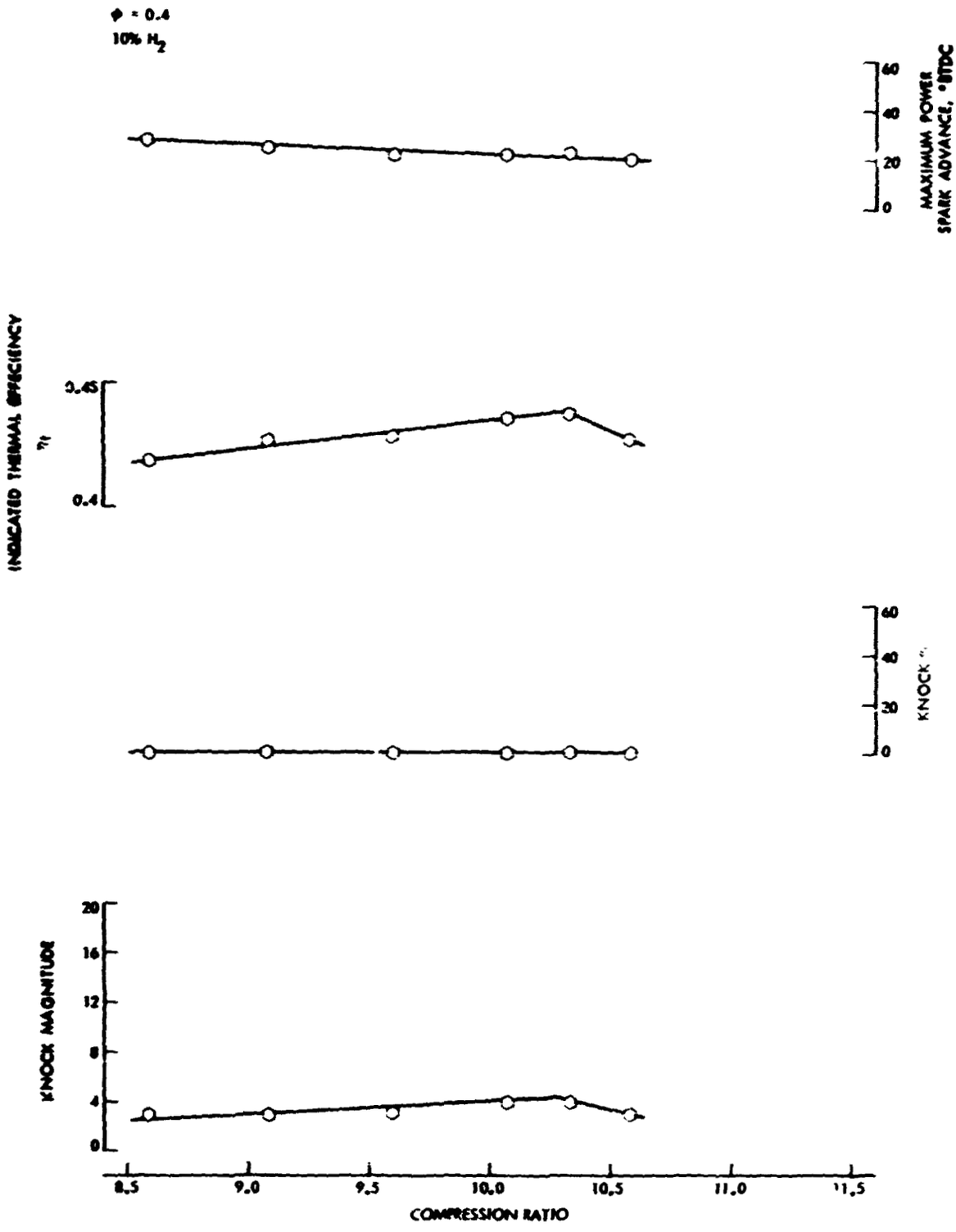

Fig. 87. Knock magnitude, knock %, η_t, and MPSA vs compression ratio (plot 7)

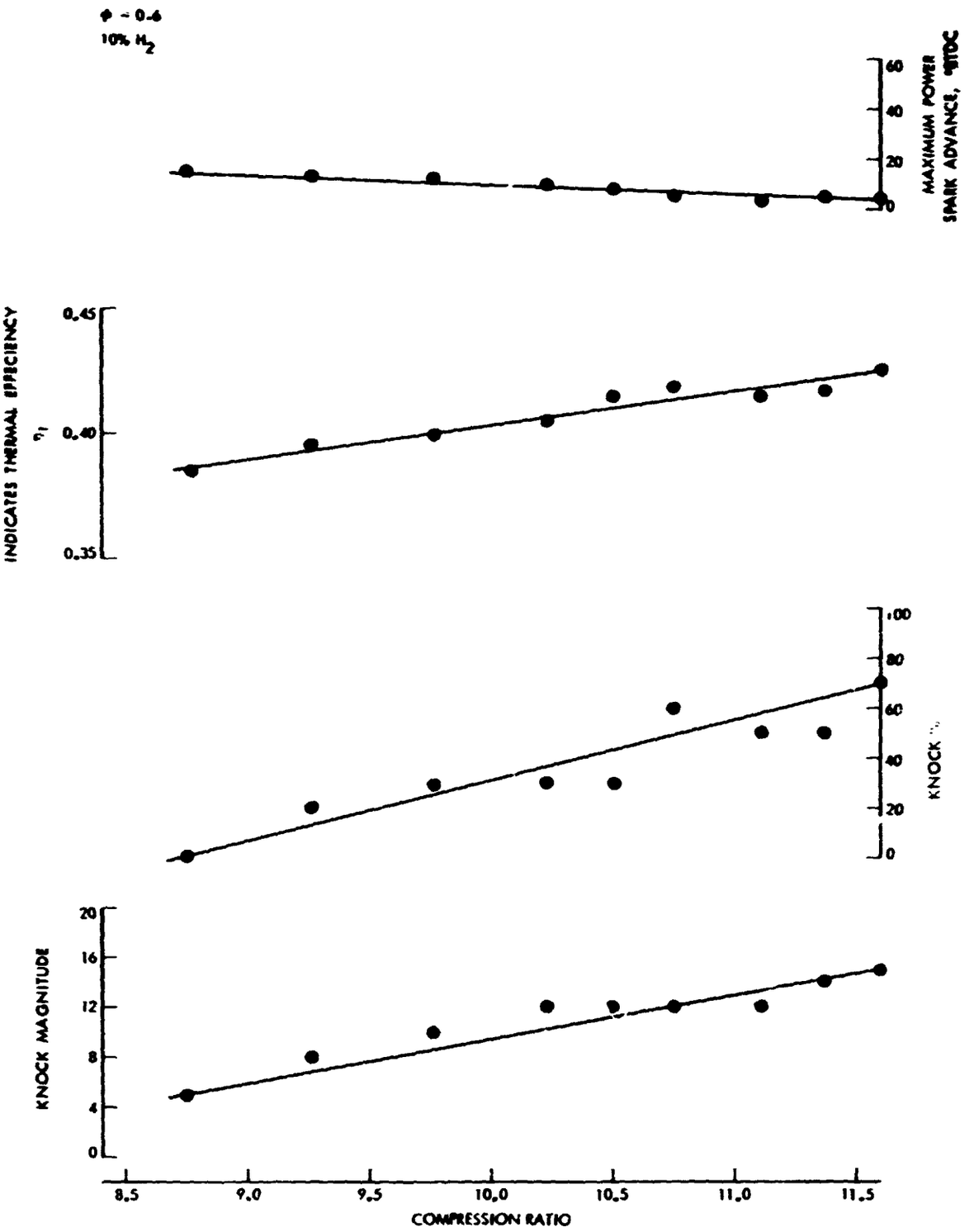

Fig. 88. Knock magnitude, knock %, η_t, and MPSA vs compression ratio (plot 8)

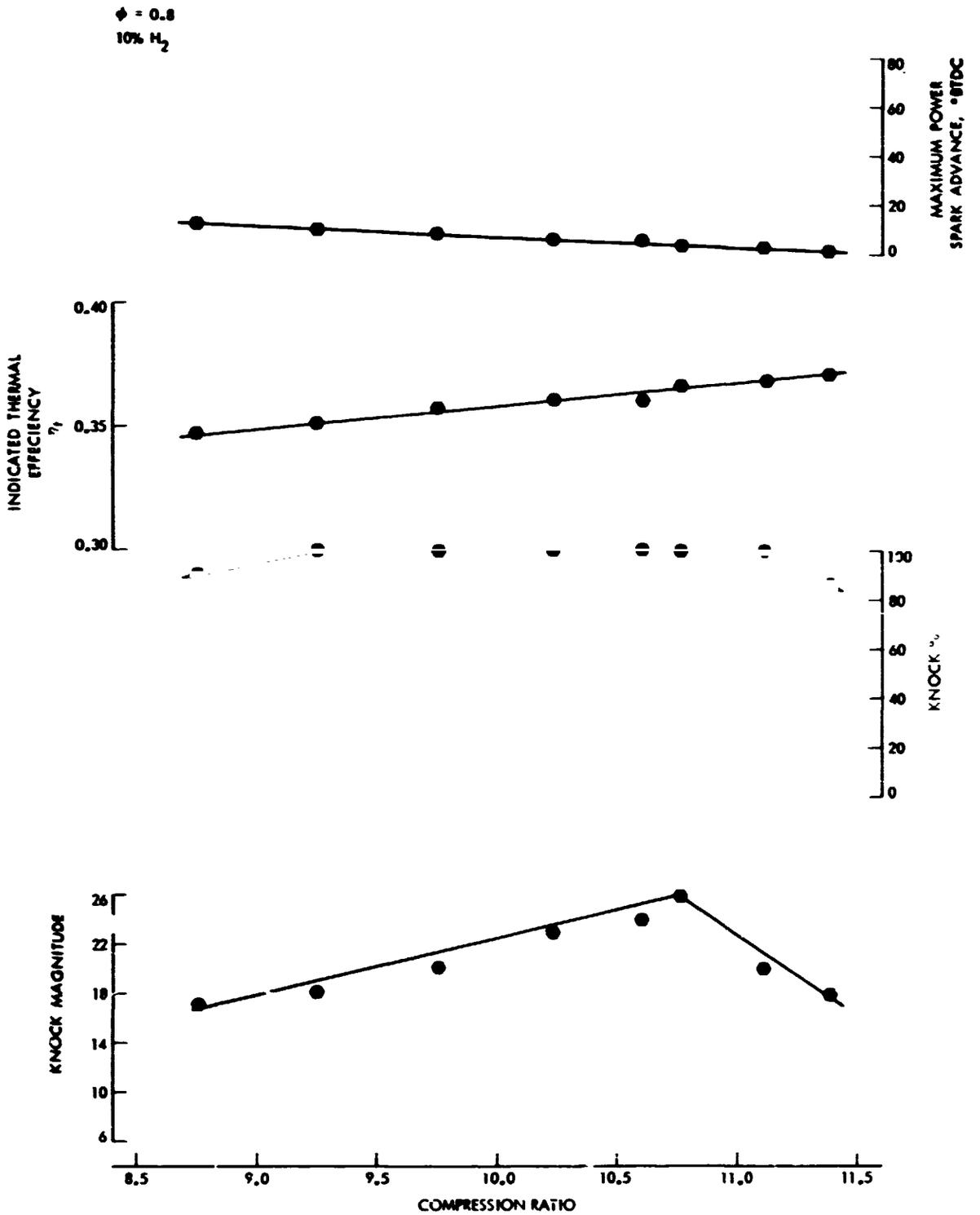

Fig. 89. Knock magnitude, knock %, η_{i_t}, and MPSA vs compression ratio (plot 9)

as compression ratio. This is predicted by theory; Ref. 7 shows that the first-order efficiency is related to compression ratio by

$$\eta_t = 1 - \frac{1}{(CR)^{\gamma-1}}$$

(where γ is the ratio of the specific heats for the combustion gases)

Therefore,

$$\frac{d\eta_t}{d\,CR} = \frac{\gamma-1}{(CR)^{\gamma}}$$

This equation predicts values of the derivative -0.015, for $\gamma = 1.3$ and $CR = 10$. The measured slopes of Figures 75 through 89 fall between 0.0097 and 0.027. The maximum power spark advance decreased with increasing compression ratio indicating that the combustion interval also decreases with increasing compression ratio.

Figure 90 is a collection of all the knock magnitude curves from Figures 81 through 89. Two trends are apparent. For a given compression ratio, lower equivalence ratio yields less knock, or at least knock of lower magnitude. For a given equivalence ratio, the fuel richer in hydrogen yields less knock. For the two test series run at Φ's of 0.48 and 0.4, there was very little change in the knock magnitude over the entire range of compression ratios tested. If an arbitrary value of KM=10 were chosen to represent the onset of knock, then a compression ratio of 10.2 could be used if $\Phi < 0.56$ and if the % $H_2 > 5$.

The results of the tests with 10% H_2 are somewhat anomalous. The shape of the curve for $\Phi = 0.8$ is different than for all other conditions in that the slope becomes negative instead of becoming more positive. The data for $\Phi = 0.4$ and $\Phi = 0.6$ do not show a slope reversal, but on the other hand they do

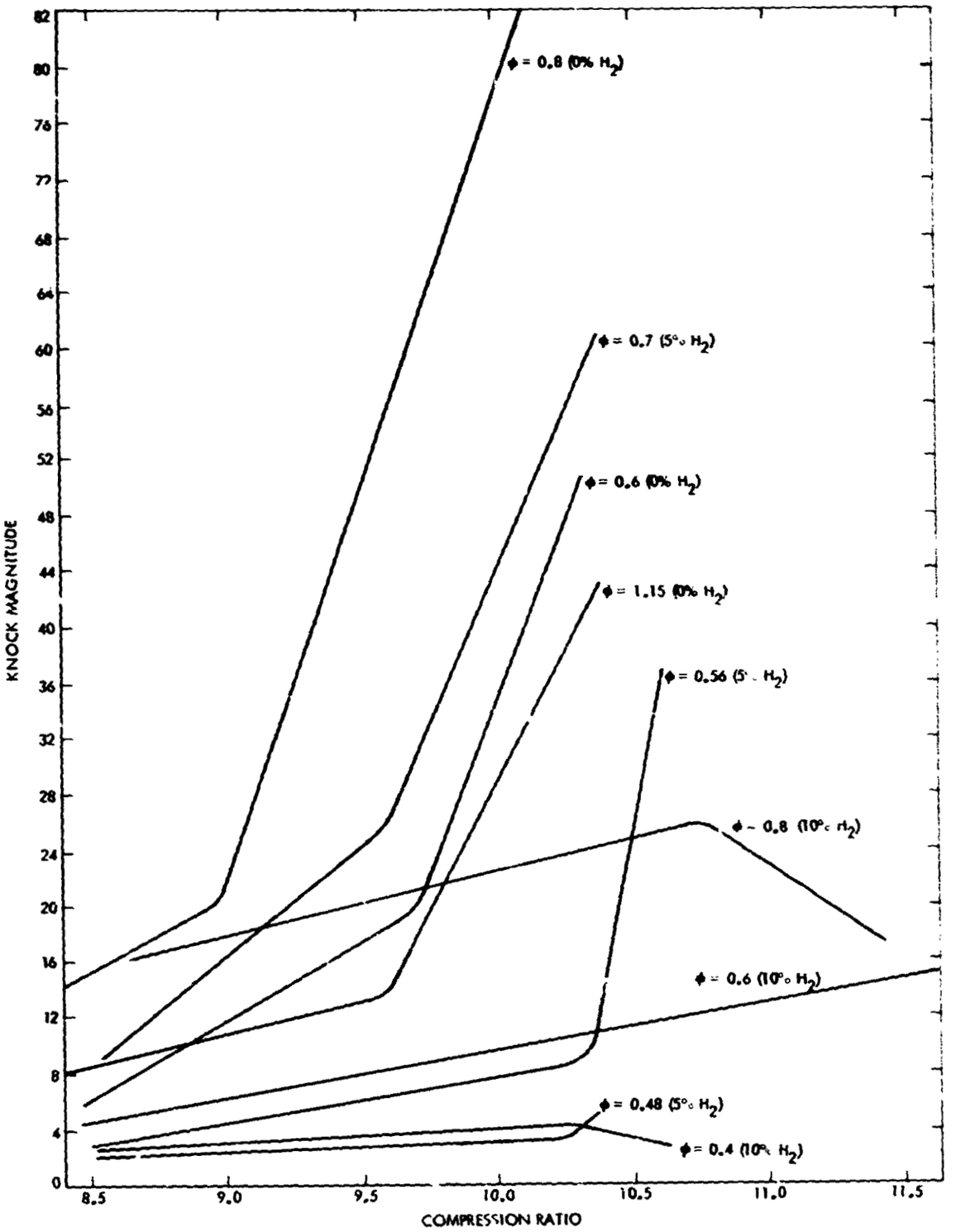

Fig. 90. Composite of knock magnitude curves from Figs. 81 thru 89

not show the sharp increase in slope exhibited by the other conditions. There is nothing in either the thermal efficiency or spark advance data to indicate some change in the character of the combustion process.

One of the potential disadvantages of increasing the compression ratio is the possibility of increasing the quantity of NO_x produced for a fixed equivalence ratio. This was not the case for the experiments described here. Figure 91 is a plot of NO_x, in units of gm/IHP-hr, versus compression ratio. As seen there is no significant change in NO_x with increasing compression ratio. The shapes of the curves of Figure 91 may be explained as follows: the compression ratio is increased, two competing processes occur. Increasing compression ratio results in increased peak combustion pressure and temperature and this tends to increase the amount of NO_x produced. On the other hand the combustion interval is shortened (at least for this engine) as indicated by the smaller spark advances required for maximum efficiency. Decreased spark advance means the combustion gases are at peak temperature for a shorter time, and hence there is less time for the NO_x to form. Apparently, the two phenomena cancel each other and there was virtually no dependence of NO_x emissions on compression ratio.

Figure 92 is a plot of the unburned hydrocarbon emissions versus compression ratio. Again, HC is apparently not strongly influenced by compression ratio. The amount of HC observed agrees with the values shown on Figure 75.

The preceding discussion of test results has been somewhat non-definitive with regard to what compression ratios are feasible for the mixed fuels. The trends noted seem clear, but this is not the case for absolute values. The problem lies in defining, from the experimental data, the critical compression

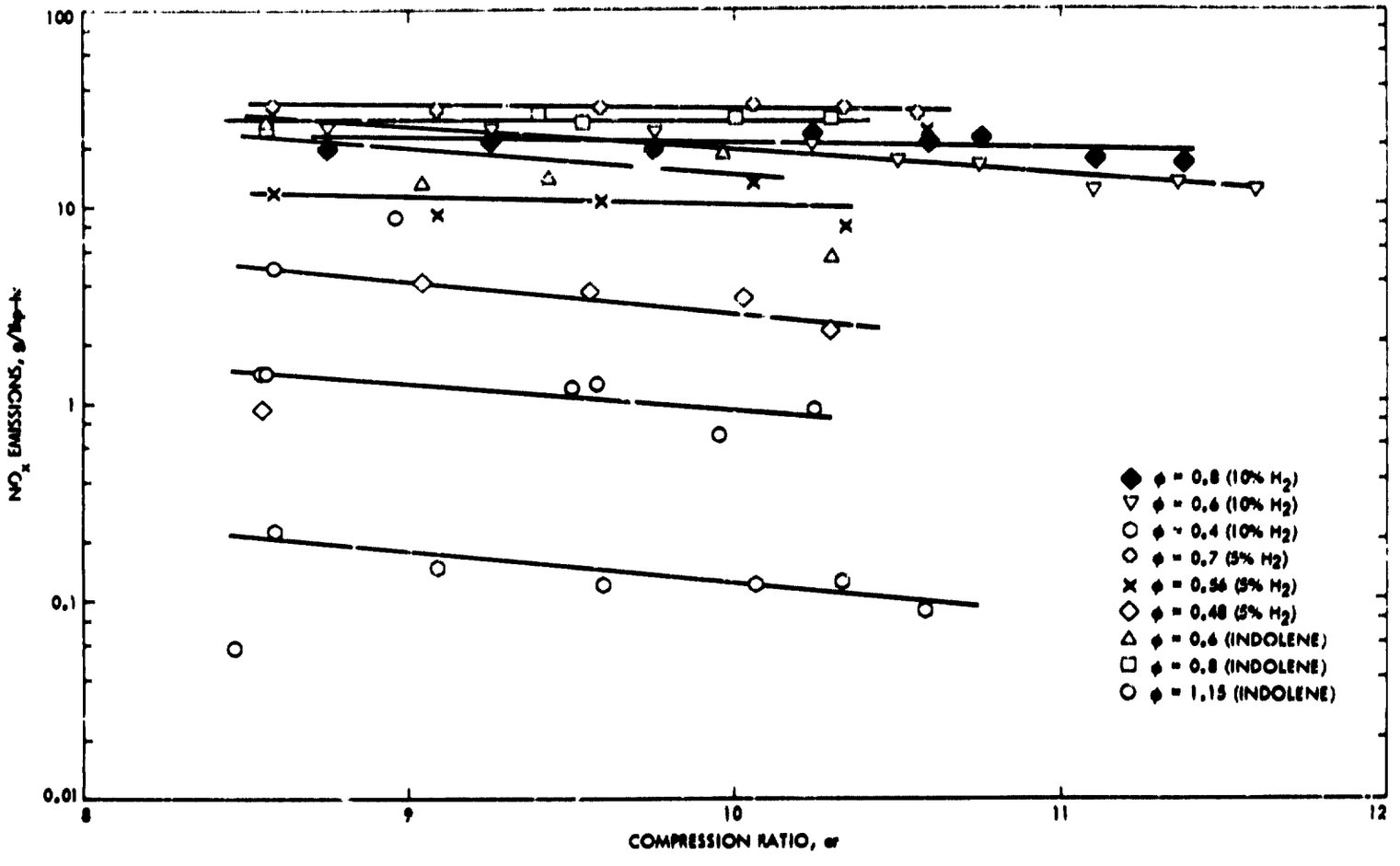

Fig. 91. NO_x vs compression ratio

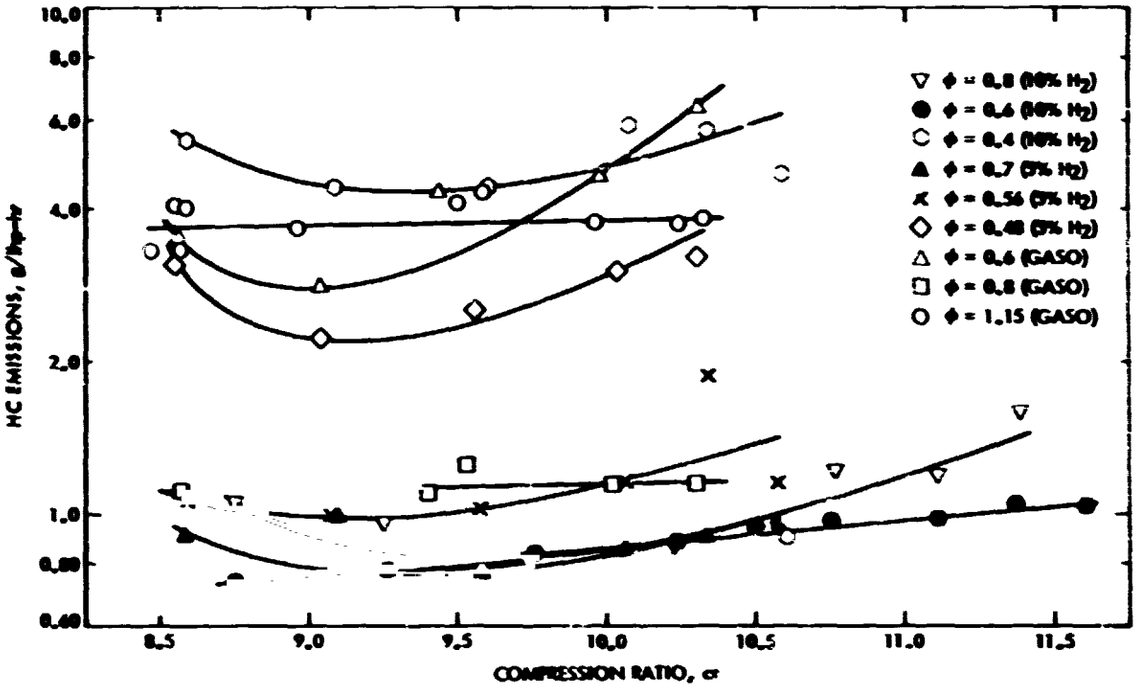

Fig. 92. HC vs compression ratio

ratio. This difficulty is illustrated in Figure 93. The three photos comprising Figure 93 are the combustion pressure, (upper trace) as a function of time, for three different compression ratios, and are taken from an oscilloscope. The lower trace is derived from the basic pressure signal and is used for the knock measurements.

Since the knock tests were conducted with a gasoline having a research octane number of 97, it was expected that operation at a compression ratio of 8.6 would exhibit no knock. However, associated with the upper photo was a KM value of 8 and a KP of 12 (i.e., during 12% of the engine cycles, some indication of knock was detected). The lower photo, compression ratio of 10.3, shows clear evidence of knock. The center photo is apparently exhibiting knock.

KM 8
KP 12

GASOLINE ONLY
ϕ = 1.16
cr = 8.6
MPSA = 15.4°
VERTICAL SCALE = 100 psi/cm
HORIZONTAL SCALE = 2 ms/cm

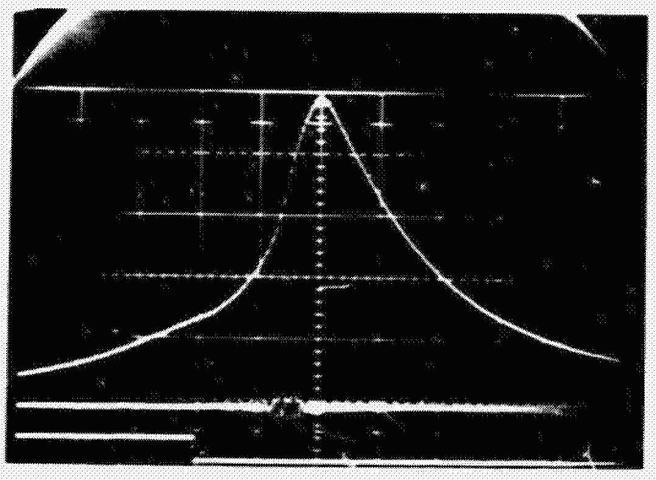

KM 16
KP 44

GASOLINE ONLY
ϕ = 1.16
cr = 9.6
MPSA = 11.3
VERTICAL SCALE = 100 psi/cm
HORIZONTAL SCALE = 2 ms/cm

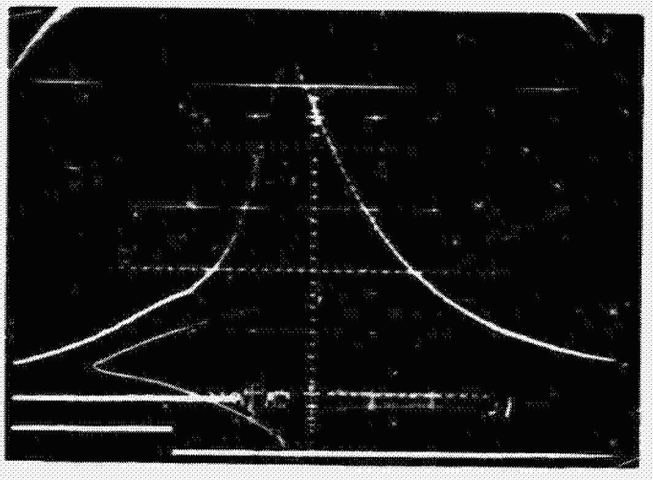

KM 42
KP 98

GASOLINE ONLY
ϕ = 1.16
cr = 10.3
MPSA = 9.4
VERTICAL SCALE = 200 psi/cm
HORIZONTAL SCALE = 2 ms/cm

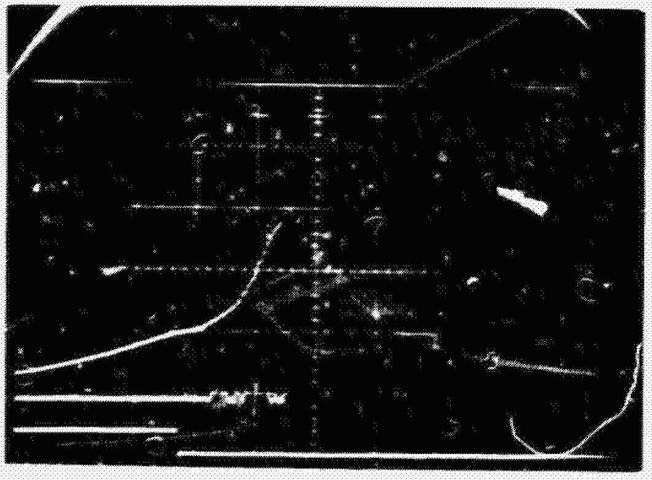

Fig. 93. Cylinder pressure-time traces showing different degrees of knocking

The pressure trace appears to show a knock that is stronger than for compression ratio of 8.6 and this is borne out by the KM value of 16. Note that the center photo corresponds to the knee of the curve in Figures 82 and 90, and it might be argued that the knee is an indication of the onset of knock. The question, which is unanswered, is what causes the acoustic excitation shown in the upper photo? Did this result from a detonation or was it triggered by some other source?

d. Conclusions

1) Increases in compression ratio are possible for ultra-lean combustion. Raising the compression ratio to ~10 should be feasible.

2) Thermal efficiency increases with increasing compression ratio, as expected.

3) NO_x was not adversely affected by increased compression ratio, but neither was it helped.

4) There was no significant effect of compression ratio on unburned hydrocarbons.

5) For a given compression ratio, a knock magnitude is inversely proportional to the amount of hydrogen in the fuel mixture.

BLANK PAGE

SECTION III

ANALYTICAL WORK

A. OVERVIEW

In this section of the report, the analytical work performed will be described and the results of these analyses presented. The work statement tasks which will be discussed in this section are Task B, Definition of System and Operational Characteristics, Task C, Thermodynamic Cycle Analysis, and Task F, Estimation of Performance Potential and System Capability.

To perform these tasks, three interrelated analytical models were developed and will be described. The first was a model of what is termed the Hydrogen-Generator Subsystem. It aggregated the operating characteristics of each of the auxiliary components necessary to the hydrogen generator (for example, the air compressor and air compressor drive train) and provided an estimate of the additional loads the subsystem would impose on the engine. In addition to making these estimates for a set of performance assumptions corresponding to a nominal case, bounding cases of minimum and maximum loads were estimated.

Next these estimates of hydrogen-generator subsystem auxiliary loads as a function of hydrogen generator flow rate were combined into the second model. This system model provided an estimate of engine/hydrogen generator output and NO_x production rate as a function of three primary variables:

- Gasoline flowrate to the engine.
- Gasoline flowrate to the hydrogen generator.
- Air flowrate.

The output of this model was a prediction of brake specific fuel consumption and brake specific NO_x emissions as functions of brake mean effective pressure (BMEP) and engine speed (RPM). The effect of changes in the performance of elements of the system on fuel consumption and NO_x emissions could then be predicted using this model.

The third model was a simulation of the Federal Urban Driving Cycle (FDC). It used the output of the system model or measurements made on an engine dynamometer to estimate vehicle performance over the driving cycle and to predict fuel consumed and NO_x produced.

The portion of this section, discussing the work performed under Task C of the statement of work, will describe these models in more detail and will compare their output with measured data. The description of the work performed under Task F will discuss the predictions of these models made for assumed improvements in system performance.

B. DEFINITION OF SYSTEM AND OPERATIONAL CHARACTERISTICS (EPA TASK B)

1. Introduction

The objective of the work performed under this task was to define a vehicle system using the hydrogen-enriched fuels concept and to estimate the performance of elements of that system. In this section of the report, the system and subsystem will be described. The elements of the hydrogen generator subsystem will be identified, their operation described, and their assumed performance parameters discussed. A model of the hydrogen generator subsystem was developed to integrate these elements of the hydrogen generator subsystem. The output of this model was an estimate of the loads the subsystem imposed on the engine as a function of hydrogen generator flow rate. A description of this model and its output is presented in this section.

2. System Description

The block diagram of the hydrogen generator/engine system is shown in Figure 94. This system is made up of an engine and a hydrogen generator subsystem. This generator subsystem provides the engine with a hydrogen rich product gas to promote lean operation and taxes the engine for the power needed to drive the air compressor and fuel pump supplying fluids to the hydrogen generator. Also included in the hydrogen generator subsystem are the sensors and control elements necessary to control the hydrogen generator flow rate.

Examination of the elements of the system will be accomplished by following the individual fluid flow paths.

a. Fluid Flow Paths

(1) Engine Fuel Flow Path. Fuel flow to the engine is provided by a variable speed, positive displacement, electric motor-driven fuel pump. This electric pump replaces the stock mechanical pump to provide precise knowledge and control of fuel flow to the engine.

(2) Generator Fuel Flow Path. Hydrogen generator fuel flow control is obtained from a pump similar to the engine fuel pump and sized for the much smaller generator subsystem fuel flow rates. Generator fuel is pumped through a start/run valve to either the generator burner pressure-atomizer or the fuel vaporizing heat exchanger. The pressure-atomizer flow path is used during initial engine start-up only. Switchover to heat exchanger operation occurs when hydrogen generator product gas temperatures are high enough to permit fuel vaporization.

(3) Generator Air Flow Path. Generator subsystem air flow is provided by a variable speed air compressor powered by an engine

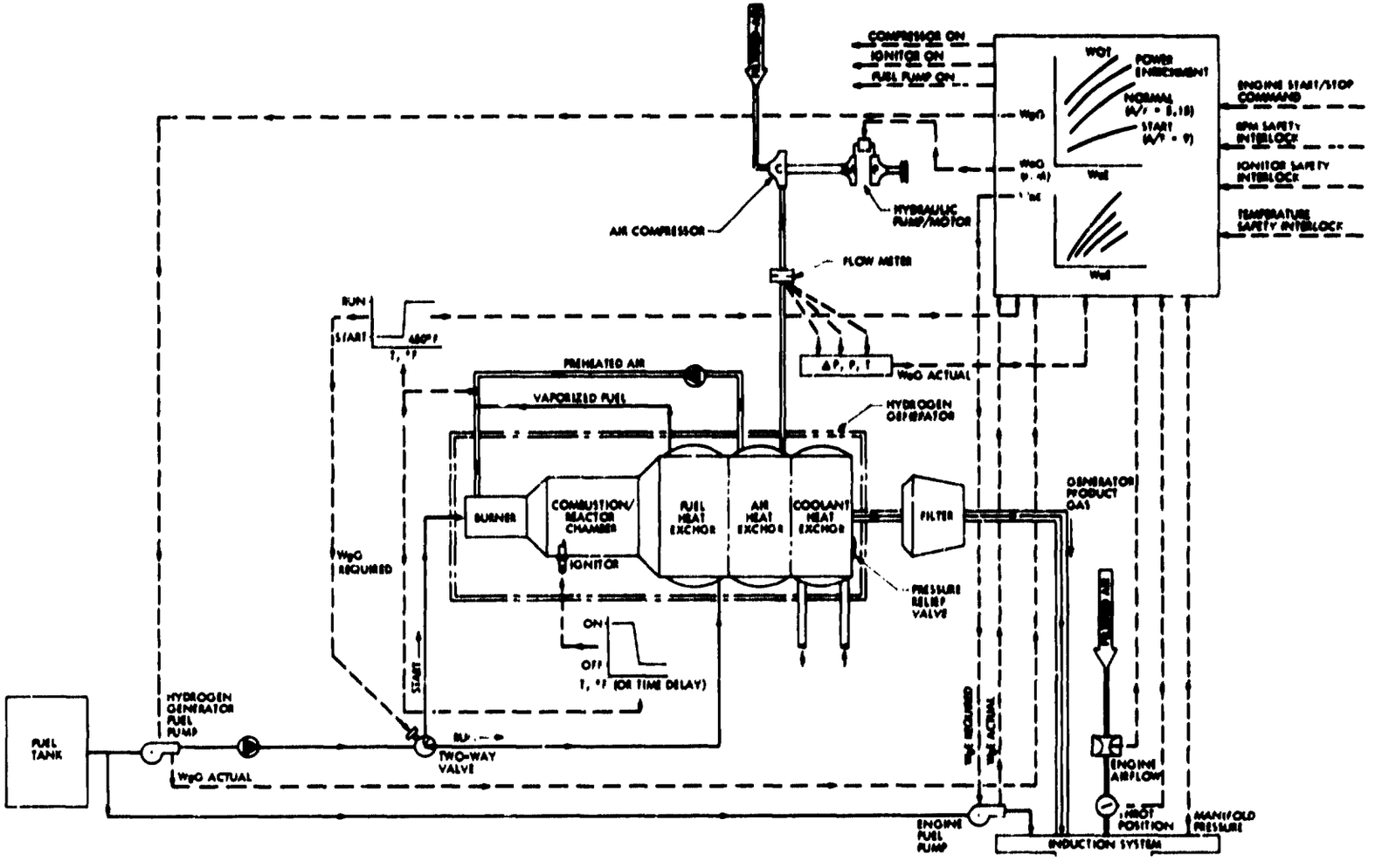

Fig. 94. Engine/generator system sche. c

V-belt driven hydraulic pump/motor assembly. The hydraulic motor is directly shaft-coupled to the compressor. Compressor discharge airflow rate modulation is achieved by varying hydraulic motor speed by controlling the hydraulic pump by-pass valve.

Airflow discharging from the compressor is measured with an orifice-type flow meter to provide a feedback signal for system controls. Compressor discharge flow then continues to the air heat exchanger where the air is pre-heated to 500°F by heat exchange with generator product gas.

Preheated air is directed through the check valve into a transition section where mixing with vaporized fuel occurs. This mixture discharges to the generator burner section, and subsequently to the combustion/reaction chamber. The reacted, high temperature hydrogen-rich product gas then flows through the fuel, air, and coolant heat exchangers, decreasing the product gas temperature to approximately 500°F at the generator discharge port. Cooled product gas is ducted through a filter and subsequently discharged to the engine induction system mixing manifold.

(4) Engine Air Flow Path. Engine airflow is controlled by a driver actuated throttle position. Both throttle position and engine airflow are measured to provide input command signals for system controls.

(5) Generator Coolant Flow Path. A generator coolant flow loop is required to reduce product gas temperature to an acceptable level so that:

- Engine volumetric efficiency penalties are minimized.
- Exposure of downstream components to excessive temperatures is precluded.
- Auto-ignition of the engine fuel is prevented.

Although other methods of reducing product gas temperature may be feasible, the cooling heat exchanger is considered one practical approach because it permits low-cost, near-term implementation.

Generator coolant flows from the high pressure, low temperature side of the engine cooling system, through a thermostatic flow control valve (which regulates coolant temperature to 220°F at the coolant heat exchanger discharge port), and then is returned to the high temperature, low pressure side of the engine cooling system.

b. Estimates of Component Performance

To estimate the effect of the accessory loads on system operation, typical performance properties for these major components were aggregated in an analytical representation of the hydrogen generator subsystem. The output of these analyses was an estimate of total accessory loads imposed on the engine as a function of hydrogen-generator flowrate (Figure 95).

In this section, the performance properties used for each of the major components will be individually described.

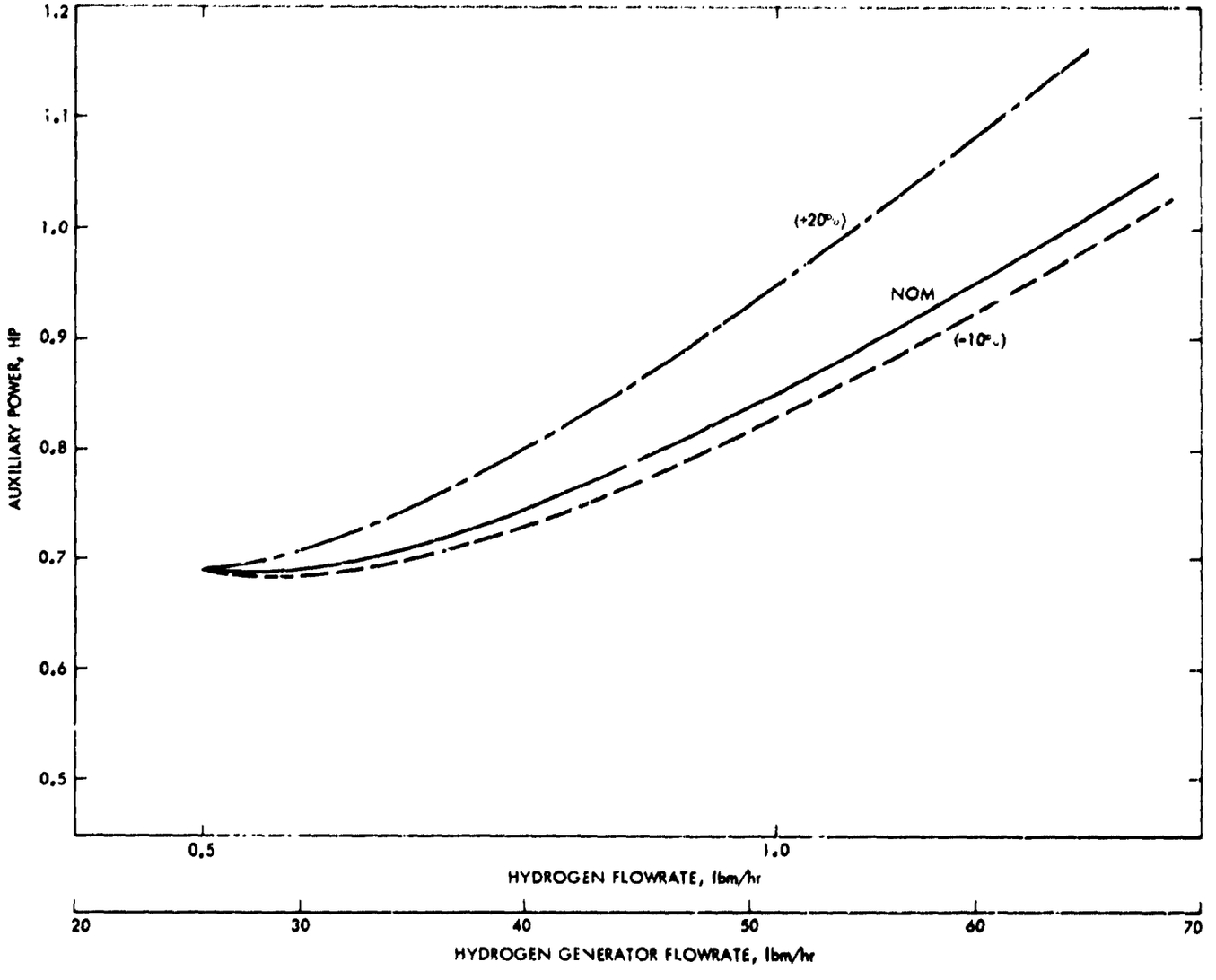

Fig. 95. Auxiliary power requirements

c. Component Hardware Description

(1) Hydrogen Generator. The basic components of the hydrogen generator consist of the burner section, reactor, combustion chamber, and three integral, compact heat exchangers.

During steady-state operation, the generator provided (by the catalytic partial oxidation of gasoline in air) hydrogen yields in the product-gas stream controllable between 0.5 and 1.5 lbm/hr.

Extensive development and testing of hydrogen generator units at JPL, under NASA sponsorship, has provided a broad data base upon which the performance characteristics of the proposed unit can be estimated. Section II.B. described the generator performance parameters, gas composition, temperature, and pressure over the complete steady-state operational envelope.

It has been demonstrated, experimentally, that optimum yield, sootless production of hydrogen gas is achieved when operating at an air/fuel ratio of 7.27 (equivalence ratio, ϕ_G, equal to 2.75).

Table 5 compares the theoretical hydrogen-generator product-gas composition with the actual gas composition obtained at a typical operating point. Averaged product gas composition obtained over the range of flowrates was used for the purpose of system performance predictions and analysis.

(2) Compressor. Variation of the speed of a centrifugal or vaned type air compressor was used to provide the necessary variation in hydrogen-generator subsystem air flowrate and pressure. Representative compressor performance characteristics were constructed from dimensionless data presented in Ref. 8. Figure 96 shows the resultant compressor performance map from which overall compressor efficiency was predicted for the range of anticipated system operating pressure ratios and flow-rate functions.

Table 5. Catalytic hydrogen-generator output composition

Component	Volume, %	
	Theoretical	Actual
H_2	22.8	21.60
CH_4	0.1	1.03
C_2H_4	—	0.09
CO	24.3	23.6
CO_2	0.8	1.23
H_2O	0.8	1.20
N_2	51.2	51.25
	100.00	100.00
Operating Equivalent Ratio = 2.75		

The compressor was oversized slightly to obtain improved design efficiencies when operating at maximum hydrogen demand flow (1.5 lbm/hr). This improvement results from the typical increase in compressor efficiency experienced as design flowrate is decreased from maximum to nominal at constant pressure ratio.

Maximum predicted compressor efficiencies range from 67% to 78%, which is considered conservative for devices of this kind. Table 6 presents compressor predicted performance for the anticipated operational envelope.

(3) Hydraulic Pump and Motor. The hydraulic motor was assumed driven by a hydraulic pump, driven in turn by V-belt power from the engine. Characteristic hydraulic pump performance is shown on Figure 97. This curve was conservatively scaled down by approximately 10% from pump performance data presented in Ref. 9.

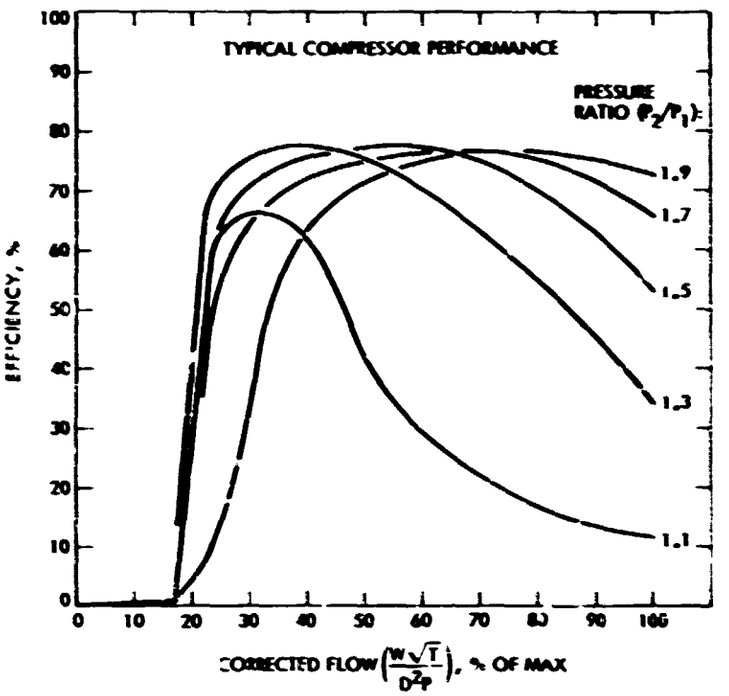

Fig. 96. Typical compressor performance

Table 6. Required compressor performance for operational envelope

Hydrogen flowrate (lb/hr)	Compressor efficiency (η_c) required for various ambient temps.		
	120°F	60°F	-25°F
0.5	0.61	0.59	0.45
1.0	0.74	0.72	0.70
1.5	0.74	0.75	0.75

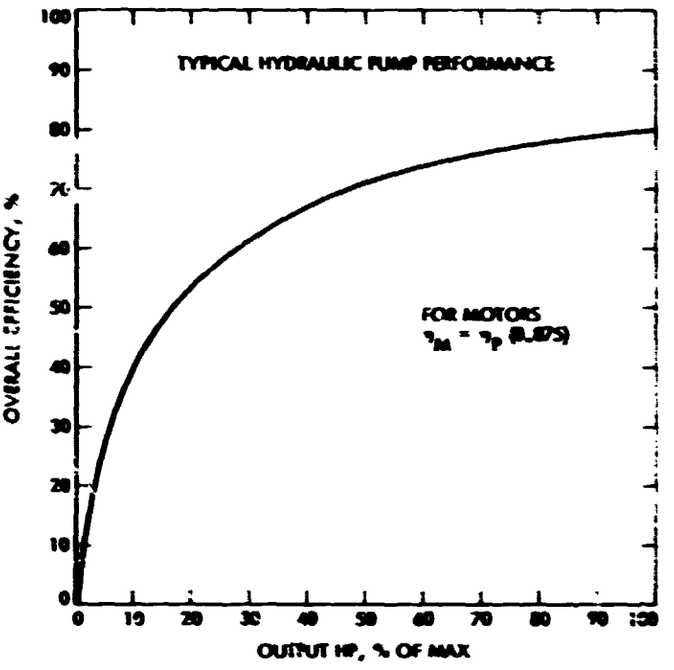

Fig. 97. Typical hydraulic pump performance

Figure 97 performance data were also assumed to be valid for the hydraulic motor, except that maximum efficiency was estimated at 70% instead of 80%. The values shown were, therefore, multiplied by 0.875 to obtain hydraulic motor efficiency.

(4) Heat Exchangers. Product gas temperature at the reactor chamber exit plane is dependent on inlet plane air/fuel ratio, mixture temperature, and flowrate. Based on test results, steady state product gas temperatures for the range of required hydrogen-yield flowrates and A/F mixture inlet temperatures are presented in Table 7.

Table 7. Estimated steady-state hydrogen-generator reactor chamber discharge temperatures

Hydrogen flowrate (lb/hr)	Reactor chamber discharge temperature	
	Fuel/air mixture temp., °F	
	@ 450	@ 550
0.5	1570	1630
1.5	1770	1830

As can be seen, the product-gas exit temperature was in the range of 1500° F to 1850°F. As described above, this temperature is reduced by using product gas heat to preheat the combustion air and to vaporize and preheat the combustion gasoline. These operations do not require enough heat to reduce the product gas temperature below 500°F. Such a reduction was desirable from the standpoints of improving volumetric efficiency, of reducing the problems associated with component exposure to high temperatures, and of eliminating any safety hazard that might exist. In these analyses, this was accomplished by assuming that this excess heat was rejected to the engine cooling system.

Heat-exchanger performance is expressed in terms of effectiveness, ϵ, which is defined as the ratio of the actual rate of heat transfer to the maximum possible rate of heat exchange. Maximum heat exchange would be obtained in a perfectly insulated counterflow heat exchanger of infinite heat-transfer area. Heat-exchanger effectiveness relations are:

$$\epsilon = \frac{C_H}{C_{MIN}} \frac{T_{H\,in} - T_{H\,out}}{T_{H\,in} - T_{C\,in}} = \frac{C_c}{C_{MIN}} \frac{T_{C\,out} - T_{C\,in}}{T_{H\,in} - T_{C\,in}}$$

where:

$C_H = m_H \cdot cp$ Hot-side heat capacity

$C_c = m_c \cdot cp$ Cold-side heat capacity

C_{MIN} = smaller of C_H and C_c

T_C = temperature of cold side

T_H = temperature of hot side

The effectiveness method allows definition of heat-exchanger performance with a minimum of required test data and calculation steps since logarithmic or mean temperature differences are not involved. Definition or calculation of overall heat-transfer coefficients can be avoided when effectiveness is expressed as a function of the hot and cold side fluid flow rates.

A typical compact heat exchanger effectiveness map obtained from Ref. 8 is shown on Figure 98. Some of the curves shown are steeply sloped with maximum effectiveness obtained at low values of hot-side flow. The shape of such a curve is representative of a heat exchanger where high performance is desired and achieved with large heat-transfer areas combined with a high Reynolds Number and fully developed turbulent flow. High performance, however, is usually compromised by the weight and pumping loss penalties associated with these large areas and high Reynolds Numbers.

The effectiveness curve obtained from tests of a preliminary version of the air heat exchanger is presented in Figure 99. The shape of this curve and the low maximum required effectiveness (only 47%) indicates that a high performance heat exchanger is not required for this application.

Figure 99 also presents predicted effectiveness curves required for the fuel, air, and coolant production heat exchangers. The predicted curves similarly show that relatively high performance is not required. The

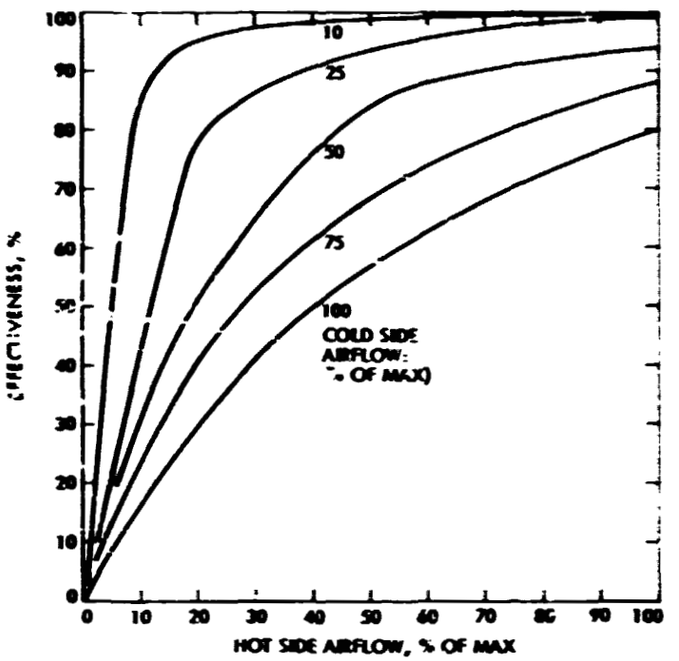

Fig. 98. Compact heat-exchanger typical performance

production heat exchangers are, therefore, expected to be low cost, light weight, and easily fabricated compact units.

The predicted heat-exchanger performance of Figure 99 was obtained by constructing faired curves through the effectiveness required at design-point flow and temperature conditions.

Heat-exchanger design goals include fuel vaporization, air preheat, and product gas cooling while simultaneously limiting the reactor chamber temperature to a region where optimum hydrogen yields are obtained. Figure 100 shows the resulting steady-state heat exchanger discharge temperatures when the effectiveness curves of Figure 99 are used over the system-design.

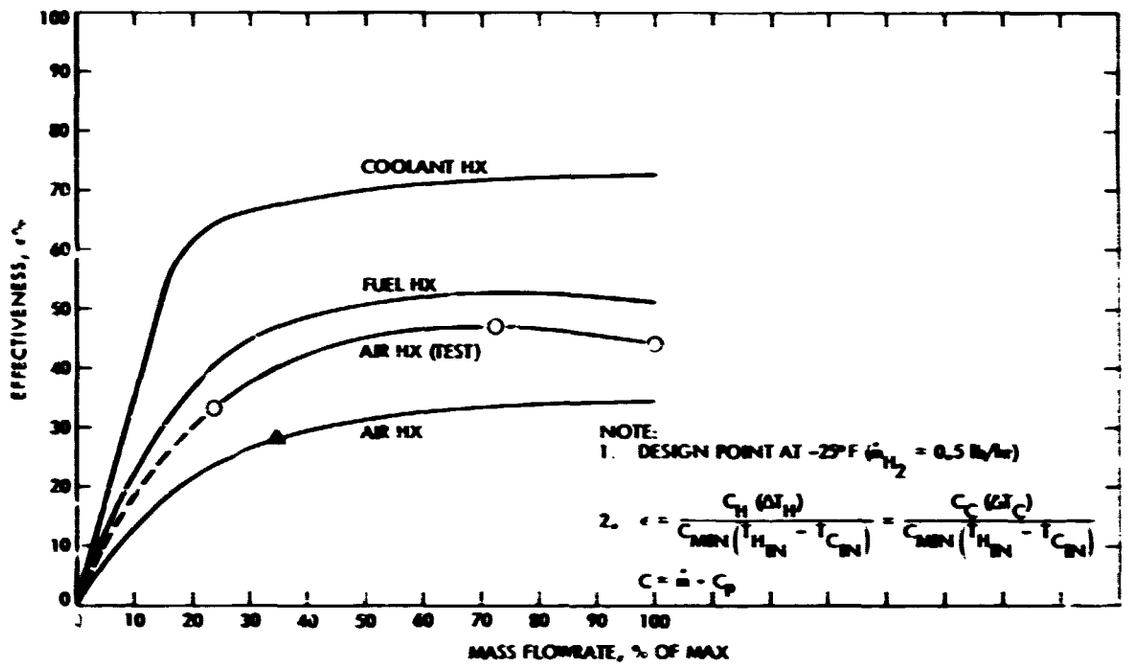

Fig. 99. Hydrogen-generator heat-exchanger required performance

envelope. These temperatures show close agreement with design requirements, demonstrating that an active temperature control system is not required.

3. System Pressure Losses

Table 8 presents the predicted pressure loss factors for the hydrogen-generator air-flow circuit. These loss factors represent the dissipation of total pressure head due to friction and to the losses associated with sudden enlargements, contractions, and turns of the air flow stream. The tabulated factors, K, can be used to calculate system pressure drop with either the compressible flow dynamic head approach or by using Fanno Line relations. The dynamic head approach was used for all the calculations in this study.

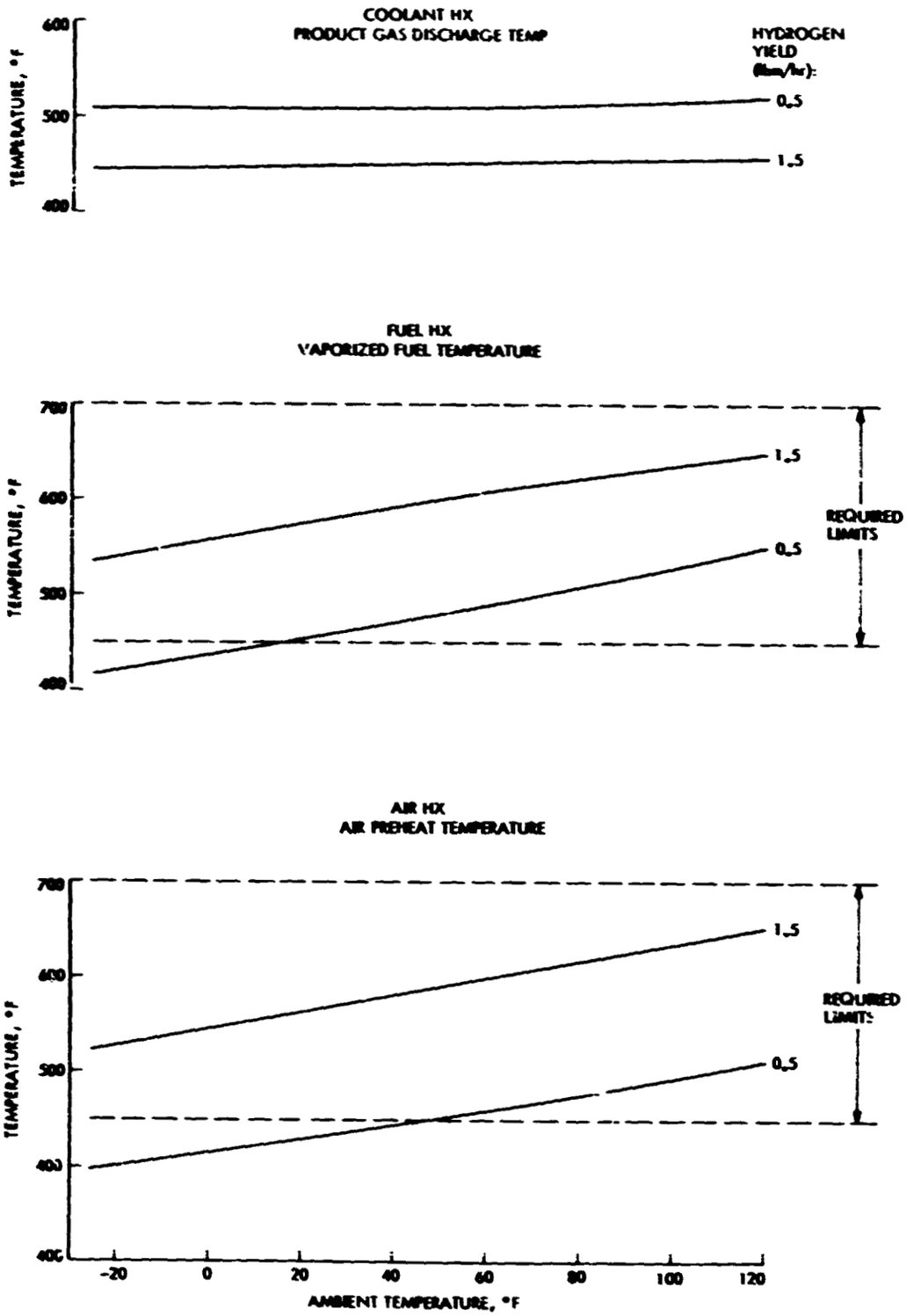

Fig. 100. Hydrogen-generator heat-exchanger estimated discharge temperatures

Table 8. Estimated pressure loss factors for hydrogen-generator air-flow path

Description	Item	$K = \frac{\Delta P_T}{q_c}$	5% K + Safety Factor
Compressor Discharge to Air HX Inlet	Six 90° Bends at K = 0.3	1.8	1.89
	2 ft. of Sched. 80 Tubing	0.96	1.01
	Flowmeter	1.0	1.05
Air HX Inlet to Generator Discharge	Hydrogen Generator	K_{TOT} = 3.95 = 4.0 at Area = 0.196 sq. in. K = 32.4 at Area = 0.196 sq. in.	
Generator Discharge to Carburetor	Eight 90° Bends at k = 0.3	2.4	2.52
	2.5 ft. of 1" I.D. Tubing	0.6	0.63
	Filter	6.0	6.30
		K_{TOT} = 9.45 9.5 at Area = 0.785 sq. in.	

4. Gas Filtration Provisions

The system design includes provision for the filtration of product gas. Such a filter may not be necessary, however, if the production generator itself demonstrates acceptable containment of contaminants that might be introduced to the discharge gas stream in the event of an upstream failure. This filter could be either a flow reversing type or a simple, wire mesh, low-pressure drop screen System analytical performance predictions include a conservatively large filter loss factor of 6 dynamic velocity heads to provide for the selection of a high-pressure drop device.

5. Subsystem Model

These component performance properties were combined in a model of the hydrogen-generator subsystem which produced an estimate of the accessory loads imposed on the engine as a function of hydrogen-generator flowrate. This estimate was shown earlier in Figure 95.

To assess the influence of changes in these performance properties, bounding cases in which these properties were modified as indicated in Table 9 were calculated. The results of these calculations are included in Table 9 and are labeled "maximum" and "minimum".

6. Conclusions

Based on these calculations, it is concluded that the accessory loads imposed on the engine will be in the range of 0.5 Hp to 2.3 Hp.

The effect of these accessory loads on system performance will be presented as part of the description of Tasks C and F, which follow.

C THERMODYNAMIC CYCLE ANALYSIS (EPA TASK C)

1. Calculation Scheme

The introduction of a hydrogen generator requires some modification to the ordinary methods of calculating the performance and emissions characteristics of a spark ignition engine. This section will describe the method used in this work to analyze the hydrogen generator/engine system. Some comparisons of the analysis results with test data will be given to provide confidence in the analysis method.

The operating characteristics of the hydrogen generator which was used in the hydrogen generator/engine analysis were based on the data from the catalytic generator characterization tests reported in Catalytic Hydrogen Generator Characterization/Start Up Tests, Section II-B of this report. For

Table 9. Range of component parametric variation

Parameters	Performance Penalty Factors*			For Nominal Values Refer to
	Minimum	Nominal	Maximum	
Air Compressor Efficiency (η_c)	1.10	1.0	0.8	Fig. 96
Hydraulic Motor Efficiency (η_m)	1.10	1.0	0.9	Fig. 97
Hydraulic Pump Efficiency (η_p)	1.10	1.0	0.9	Fig. 97
Pressure Loss Factors $K = \frac{\Delta p}{q_c}$	0.9	1.0	1.20	Sect. III-B-3
Ducting Flow Sensor, Generator, Filter	—	—	—	—
Generator Heat Exchanger (HX) Effectiveness (ϵ)	1.0	1.0	1.0	Fig. 99
Generator ϕ and Product Gas Composition	1.0	1.0	1.0	Table 5

*Multiplication factor to penalize system:

η_c, min = η_c, nom · factor = "Best" System Performance

η_c, max = η_c, nom · factor = "Worst" System Performance

the hydrogen flowrates considered (0.5 lbm/hr to 1.5 lbm/hr), the average product composition from the generator is tabulated below for a generator equivalence ratio, Φ_G, of 2.75.

Hydrogen-Generator Average Output Composition	
Component	Volume Percent
H_2	21.22
CH_4	1.11
CO	23.24
CO_2	1.05
H_2O	1.33
N_2	52.05

Over the range of hydrogen flow rates, the generator requires an average of 8.42 lbm of gasoline for every 1 lbm of hydrogen in the product gas. These average quantities were used in all the analyses since only minor deviations from these values were observed in the generator component tests.

In engines operating on gasoline, the equivalence ratio is used as the measure of leaness and provides a reasonably good correlation of NO_x emissions. The equivalence ratio is not as useful in engines running on generator products or mixtures of generator products and gasoline since it fails to properly account for the effect of the diluents in the product gas from the generator. Better correlation of thermal efficiency and NO_x emissions data from engine dynamometer tests of the generator/engine system was obtained, using an effective equivalence ratio, Φ'_E, which accounts for the dilution effect in an approximate way, as follows:

$$\Phi'_E = \frac{\left(\frac{\dot{m}_{gE}}{\zeta_g}\right) + \sum_C \left(\frac{\dot{m}_{G_i}}{\zeta_{G_i}}\right)}{(\dot{m}_{aE}) + \sum_{NC} \left(\dot{m}_{G_i}\right)} \qquad (1)$$

where:

ζ_g = stoichiometric fuel/air for gasoline

ζ_{G_i} = stoichiometric fuel/air for i^{th} component of the generator product gas.

$\dot{m}_{aE}$ = air flow rate to engine

$\dot{m}_{gE}$ = gasoline flow rate to engine

$\dot{m}_{G_i}$ = flow rate of i^{th} component of the generator product gas to engine

C = combustibles

NC = non-combustibles

Combustion of a fuel is possible only over the range of fuel/air for which the fuel is flammable. The generator product gas has a much lower lean flammability limit than gasoline because of the hydrogen concentration in the product gas. This permits the generator product gas to be burned at a lower equivalence ratio than gasoline to help in controlling NO_x emissions. The lean flammability limit of mixtures of generator gases and gasoline places an operating constraint on the generator/engine system. Using Bureau of Mines flammability data and LeChatlier's Rule for computing the flammability limit of mixtures, the lean flammability limit for mixtures of generator gases and gasoline was calculated and is shown plotted in Figure 101.

2. Constraints

It is rarely possible in practice to operate an engine at this calculated lean flammability limit. Theoretically, as the equivalence ratio is decreased,

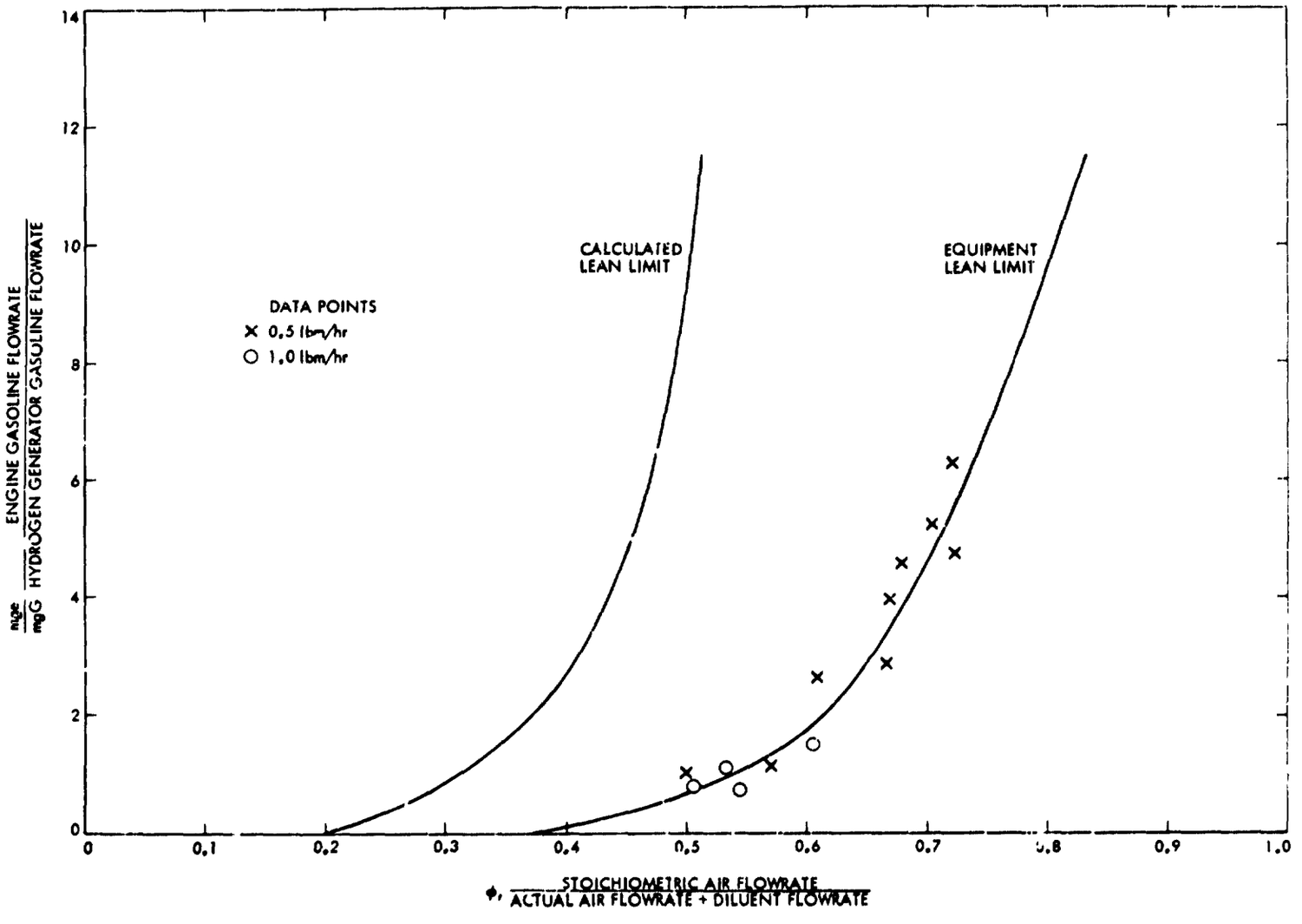

Fig. 101. The V-8 lean limit

the thermal efficiency of the engine should increase, approaching the air cycle efficiency. In a practical engine, the combustion time increases and the cycle-to-cycle pressure variations increase as the lean-flammability limit of the fuel is approached. These factors combined with cylinder-to-cylinder equivalence ratio variations result in a decrease in thermal efficiency, as the lean limit is approached. Since it is not desirable to operate leaner than the point where peak thermal efficiency is obtained, peak thermal efficiency data from engine dynamometer tests were used to establish an equipment lean flammability limit for the 350-CID Chevrolet engine used in this study. This equipment lean limit is also shown in Figure 101 along with the data corresponding to peak efficiency.

Another engine operating constraint is the maximum volume flow rate of charge through the engine. This is imposed by the engine displacement and the wide-open-throttle (WOT) volumetric efficiency, e_v, of the engine at any given engine speed. The WOT volumetric efficiency was assumed to be constant at a value of 0.7 for all the analyses. For a given effective equivalence ratio, this constraint places an upper bound on the allowable gasoline flowrate to the engine.

3. Operating Regime

These two engine operating constraints help define an available operating regime for the engine as shown in Figure 102. The engine cannot operate to the left of the lean limit constraint without a loss in thermal efficiency. The engine breathing constraint is shown for an engine speed of 2500 RPM and the minimum hydrogen flow rate of 0.5 lbm/hr. Increasing the hydrogen flowrate decreases the available operating regime on this plot by shifting the engine breathing constraint down. For a given engine speed and hydrogen flowrate, any operating point in the available operating regime can be obtained by changing the engine effective equivalence ratio and/or air throttling ratio, τ. It is

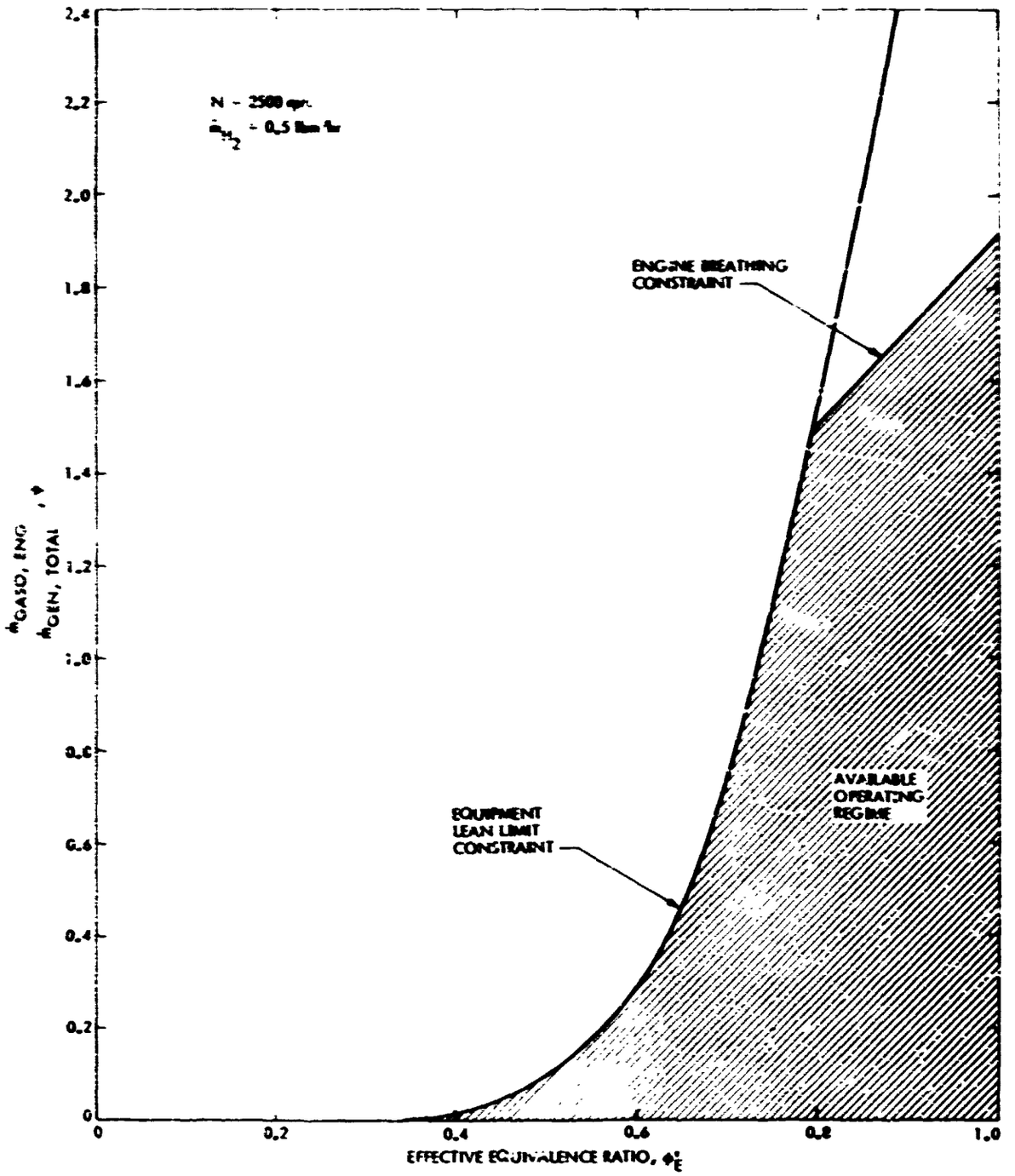

Fig. 102. Operating regime for generator/engine system

desirable to operate near the equipment lean limit since this leads to peak thermal efficiency and helps minimize NO_x emissions.

4. Prediction Model

The relationships and assumptions used to predict the brake specific fuel consumption and brake specific NO_x emissions of the hydrogen generator/engine system will now be described.

The product gas from the hydrogen generator subsystem will, in general, be at a higher temperature than the ambient air being inducted into the engine. For a given generator flowrate, a model of the hydrogen-generator subsystem, described in Task B, Section III. B., was used to calculate the product gas temperature entering the engine. The product gas is assumed to thoroughly mix with the gasoline-air charge in the intake manifold. An expression for the mixture temperature, T_M, was obtained by assuming steady flow, adiabatic mixing of the two streams.

$$T_M = \frac{(\dot{m}_{aE})(C_{Pa})(T_a) + \sum_P \left(\dot{m}_{G_i}\right)\left(C_{P_{Gi}}\right)(T_G)}{(\dot{m}_{aE})(C_{Pa}) + \sum_P \left(\dot{m}_{G_i}\right)\left(C_{P_{Gi}}\right)} \qquad (2)$$

where:

C_{Pa} = constant pressure specific heat for air

$C_{P_{Gi}}$ = constant pressure specific heat for i^{th} component of the generator product gas

T_a = air temperature

T_G = temperature of generator product gas

P = product gas from generator

The gasoline was assumed to have a negligible effect on the mixture temperature.

An expression for engine air-flow rate, $\dot{m}_{aE}$, was obtained by equating the engine pumping capacity to the flow of mixture to the engine.

$$\dot{m}_{aE} = \left(\frac{\tau e_v \frac{N}{2} V_D P_{amb} \bar{M}a}{\bar{R} T_M}\right)\left(\frac{\bar{M}_a}{\bar{M}_G}\right)(\dot{m}_G) \qquad (3)$$

where:

τ = air throttling ratio

e_v = WOT volumetric efficiency

N = engine RPM

V_D = engine displacement

$\bar{R}$ = universal gas constant

P_{amb} = ambient pressure

$\bar{M}_G$ = molecular weight of product gas

$\bar{M}_a$ = molecular weight of air

$\dot{m}_G$ = generator flow rate

This equation includes the effects of mass flow rate and temperature of the generator product gas on the air breathing capacity of the engine. The gasoline is assumed to remain in an atomized state during the induction process and to have a negligible effect on engine breathing.

For a given air throttling ratio, engine speed, and hydrogen flow rate, Equations (2) and (3) can be solved simultaneously for mixture temperature and engine air flow rate. Once engine air flow rate is known, Equation (1) can be used to calculate gasoline flow rate to the engine for any given engine effective

equivalence ratio which falls within the allowable operating regime described in Figure 102.

The equipment lean flammability limit line can be represented by the following equation.

$$\phi'_{E_{ELL}} = f\left(\frac{\dot{m}_{gE}}{\dot{m}_{gG}}\right) \tag{4}$$

where:

ELL = equipment lean limit

m_{gG} = gasoline flow rate to generator

m_{gE} = gasoline flow rate to engine

For system operation at the equipment lean flammability limit, it is necessary to solve Equations (1) and (4) simultaneously to obtain the engine gasoline flow rate and engine effective equivalence ratio.

In the analysis, it was assumed that the engine indicated thermal efficiency, η_{IE}, could be adequately represented by a linear function of the engine effective equivalence ratio.

$$\eta_{IE} = 0.50 - 0.17\phi'_E \tag{5}$$

This kind of relationship is predicted theoretically if the combustion time can be maintained constant while decreasing the equivalence ratio. Hydrogen generator/engine data from engine dynamometer tests is shown along with this equation in Figure 103. The assumed equation passes through the data at the higher equivalence ratios and begins to deviate from the data as the thermal efficiency begins to decrease at the leaner equivalence ratios. It is felt that the assumed equation is adequate to represent the thermal efficiency in the

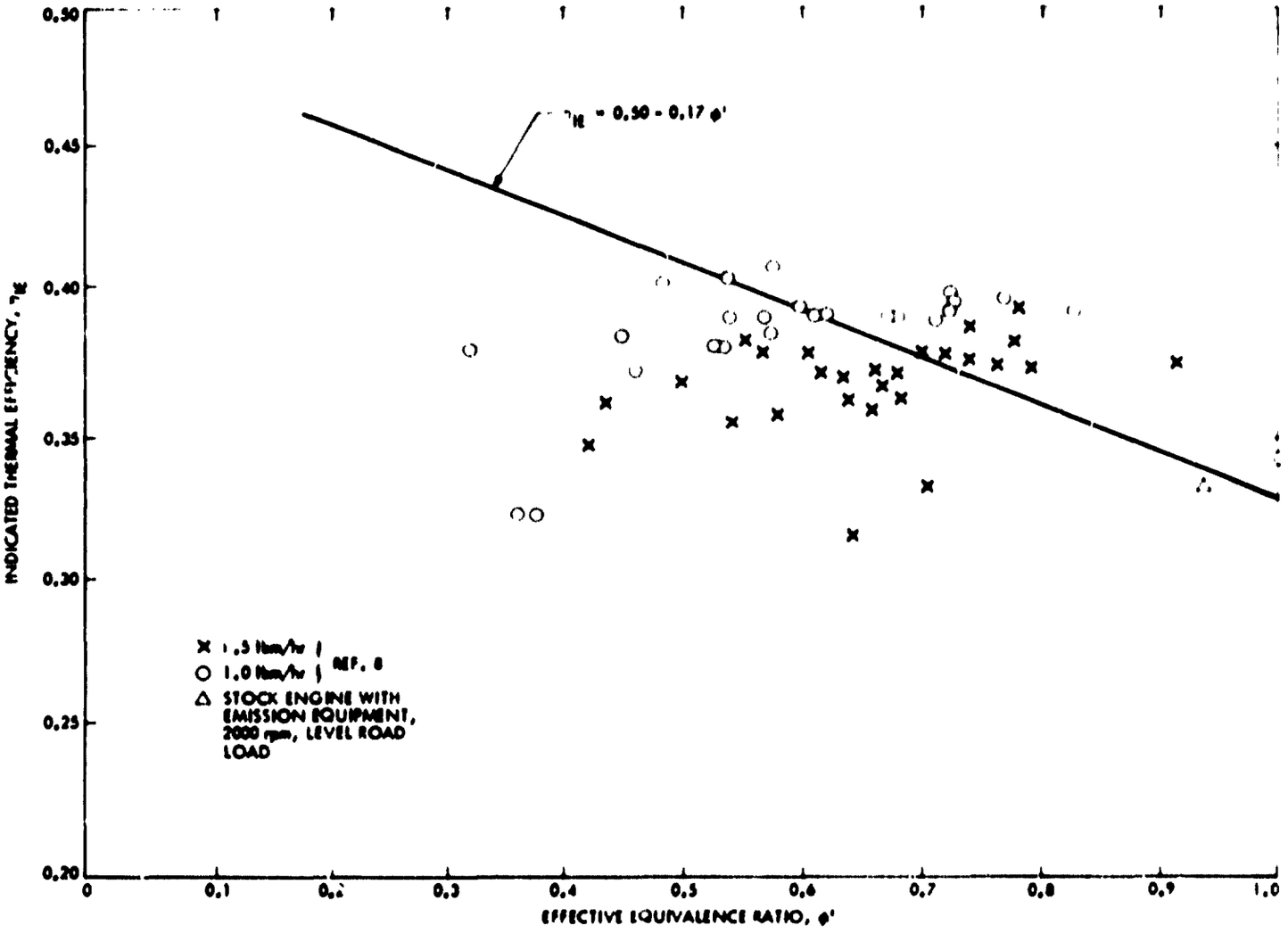

Fig. 103. The V-8 indicated thermal efficiency

available operating regime for the engine and which is identified in Figure 102. It also provides a means for evaluating the effect of engine changes which permit efficient operation at leaner equivalence ratios.

Once engine gasoline flowrate and engine indicated thermal efficiency are known, the following equation was used to calculate engine brake horsepower, P_B.

$$P_B = \eta_{IE}\left[\dot{m}_{gE} Q_g - \sum_c \dot{m}_{G_i} Q_{G_i}\right] - P_F \qquad (6)$$

where:

Q_g - lower heating value of gasoline

Q_{g_i} - lower heating value for i^{th} combustible component of generator product gas

C - combustibles

P_F - engine friction and pumping loss horsepower pluse horsepower required to operate hydrogen generator subsystem.

Pumping and engine friction losses were based on data supplied by GM for the 350-CID V-8 as shown in Figure 104. An average loss characteristic, midway between the WOT and closed throttle data, was used in the hydrogen generator/engine model. The horsepower required to operate the hydrogen generator includes the power input to the hydraulic pump/motor assembly in the generator subsystem and the additional power required by the engine water pump to provide the necessary cooling of the product gas from the generator. A model of the hydrogen generator subsystem was used to calculate the power loss for any operating condition.

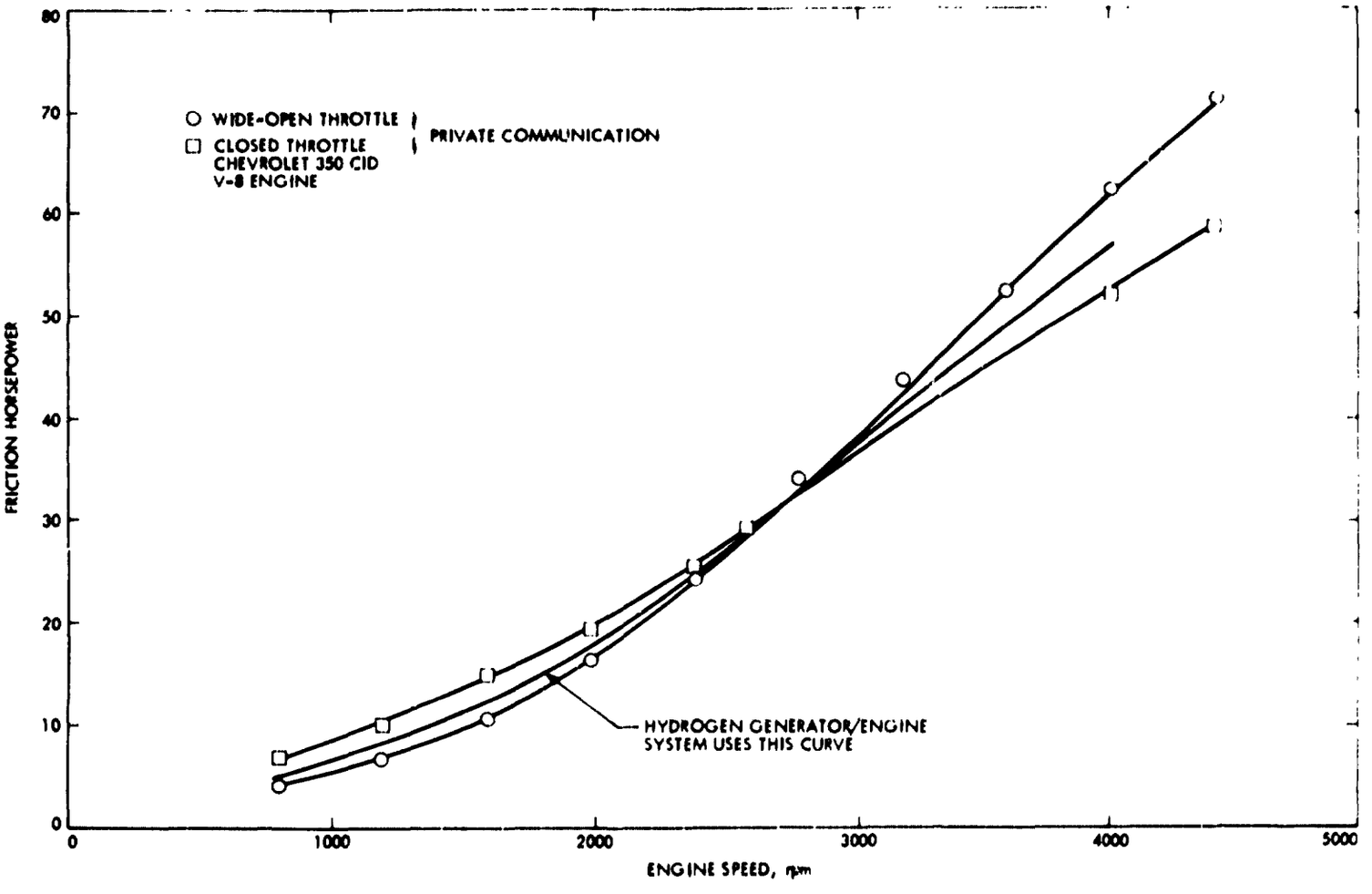

Fig. 104. Engine friction and pumping loss characteristics

The brake mean effective pressure, BMEP, was calculated using the following equation.

$$BMEP = \frac{2P_B}{NV_D} \tag{7}$$

Using the results of the above calculations, the brake specific fuel consumption, BSFC, of the hydrogen generator/engine system can be calculated for a given engine speed, air throttling ratio, hydrogen flowrate, and engine effective equivalence ratio.

$$BSFC = \frac{\dot{m}_{gE} + \dot{m}_{gG}}{P_B} \tag{8}$$

where:

$\dot{m}_{gE}$ = gasoline flowrate to engine

$\dot{m}_{gG}$ = gasoline flowrate to hydrogen generator

P_B = engine brake horsepower

Given the hydrogen requirement, the gasoline flowrate to the generator is known being an average of 8.43 lbm/gasoline/lbm hydrogen.

Hydrogen generator/engine data from engine dynamometer tests were used to obtain the NO_x emissions correlations used in the system anaiyses. For a hydrogen flow rate of 0.5 lbm/hr, the indicated specific NO_x emissions, $ISNO_x$, are shown plotted versus engine effective equivalence ratio in Figure 105. Similar correlations were also available for hydrogen flow rates of 1.0 lbm/hr and 1.5 lbm/hr. The NO_x correlation assumes that $ISNO_x$ is a function of the effective equivalence ratio and the hydrogen flow rate. There is a need for a more comprehensive analysis of the NO_x data to evaluate the effects of other

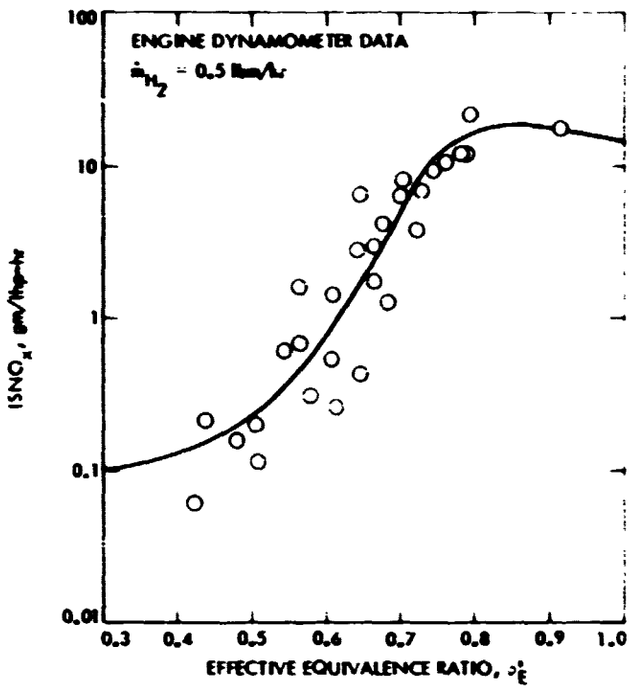

Fig. 105. NO_x emissions characteristics for generator/engine system

factors such as engine RPM and throttle setting. This would help identify better NO_x correlation parameters. Although some of the data deviates significantly from the present correlation curve, the correlation does an adequate job of estimating the total NO_x emissions over the urban driving cycle, which covers a wide range of engine RPM and load conditions. Once indicated emissions were obtained from the data correlations, the brake specific NO_x emissions, $BSNO_x$, were calculated using the following equation.

$$BSNO_x = \frac{ISNO_x \times P_B + P_F}{P_B} \tag{9}$$

where:

P = power

B = brake

F = friction

5. Prediction and Test Comparison

This semiempirical model of the hydrogen generator/engine system was used to compile tables of brake specific fuel consumption and brake specific NO_x emissions as a function of brake mean effective pressure for engine speeds from 1000 to 4000 RPM. The results of these calculations are compared with engine dynamometer data for a hydrogen flowrate of 0.5 lbm/hr in Table 10.

It is necessary to evaluate the agreement between analytical, estimate, and experiment. The analysis provides a reasonably good, slightly optimistic estimate of BSFC and a somewhat poorer, conservative estimate of $BSNO_x$ based on the following rationale.

If the differences between the test and predicted columns in Table 10 are averaged over all the listed RPM-BMEP combinations, the following results are obtained. The average BSFC difference is -2.2% (analysis yields smaller values) and the average $BSNO_x$ difference is +50% (analysis yields larger values). The agreement for individual points may vary significantly from the average, but on the average the analysis yields slightly smaller BSFC's and much larger $BSNO_x$'s than were measured experimentally. The results for the other two generator flowrates tested (1.0 and 1.5 lbm/hr of H_2) were similar. For the 1.0 lbm/hr data, the average BSFC difference was -3.0% and the average $BSNO_x$ difference was 0%. For the 1.5 lbm/hr data, the average BSFC difference was -1.1% and the average $BSNO_x$ difference +290%. Averaged over all the test points, the difference in BSFC was -2.1% and the difference in $BSNO_x$ was 105%.

Table 10. Comparison of test and predicted results for baseline engine (0.5 lb_m/hr Constant Hydrogen Flowrate

RPM	BMEP	BSFC		$BSNO_x$	
		Test	Predicted	Test	Predicted
1000	14.90	0.8876	0.7773	0.42	0.06
	41.46	0.5279	0.5036	1.59	0.53
	59.87	0.5054	0.4578	0.77	0.98
1500	13.80	0.9031	0.8477	0.45	0.52
	32.35	0.5736	0.5611	1.00	1.16
	50.06	0.4990	0.4897	1.88	2.46
	65.47	0.4698	0.4612	7.89	4.64
2000	10.48	1.1927	--	0.89	1.24
	19.92	0.7697	0.7317	1.08	1.78
	30.59	0.6291	0.6018	2.81	3.02
	46.16	0.5494	0.5234	4.16	6.53
	55.07	0.5119	0.4991	5.87	8.17
	64.70	0.4804	0.4811	10.85	9.80
	82.60	0.4580	0.4640	27.40	16.26
2500	9.33	1.4042	--	1.53	3.52
	20.08	0.8556	0.8055	1.67	5.41
	30.73	0.6800	0.6538	2.26	8.97
	40.52	0.5826	0.5857	5.92	11.01
	55.44	0.5235	0.5312	10.56	13.73
	68.18	0.4785	0.5049	13.14	16.64
3000	50.26	0.6365	0.5784	8.45	19.51
	64.33	0.5212	0.5388	15.28	24.37
	69.39	0.4978	0.5290	17.37	26.39
	83.23	0.4824	0.5122	22.98	27.05

$BSNO_x$ prediction average error for above comparison = 50%

BSFC prediction average error for above comparison = -2.2%

These results indicate that the analytical work is adequate for the purpose of predicting performance potential. The fuel economy predictions should be optimistic by several percent while the NO_x emissions should be conservative by a factor of two. However, it should be noted that simply averaging differences over all test conditions gives equal weight to each BMEP-RPM combination. These averaged differences would not be appropriate for the FDC since the engine obviously does not spend equal time at all points in the BMEP-RPM plane.

A more meaningful estimation of the validity of the analytical techniques over the driving cycle is given in Table 11. Driving cycle calculations of fuel economy and NO_x emissions based on steady-state engine dynamometer data are compared with actual vehicle data from chassis dynamometer tests. These comparisons between experiment and calculation lead to slightly different conclusions than those reached in the preceding paragraph. The fuel economy values of Figure 107 show that the agreement between experiment and analysis

Table 11. Urban driving cycle results

Parameters	Fuel Economy (MPG)	NO_x Emissions (GM/MI)
Stock measured (vehicle-chassis dyno)	10.6	2.05
calculated (steady-state engine dyno)	12.11	2.16
Autotronics*-measured (vehicle-chassis dyno)	12.8	5.12
calculated (steady-state engine dyno)	13.82	5.54

*All emission equipment except PCV disconnected.

is on the order 8-14%, but still optimistic. The agreement for the NO_x emissions is much closer, 5-8%, and still conservative. Of more significance are the incremental changes between two different engine configurations, engine configurations (1) and (2). An increase in fuel economy of ~21% was measured and an increase of ~14% was predicted. The change in NO_x emissions was predicted to be 156% and the measured change was 150%. Thus, the following conclusions concerning the analysis methods used to predict performance potential of the hydrogen enrichment concept are offered.

1) The absolute values of fuel economy are optimistic, but the relative change from the baseline engine is valid within 10%.
2) The absolute values of NO_x emissions are conservative, but again the relative change is valid.

A computer program was written to simulate the EPA urban driving cycle which is the standard test cycle for evaluating automobile emissions. The program divides the driving cycle into 1-second increments and uses the velocity profile, vehicle inertia, rolling resistance and drive train losses to determine the required engine brake mean effective pressure and RPM. Tables of brake specific fuel consumption and brake specific NO_x emissions as functions of brake mean effective pressure and engine RPM were used to establish the fuel consumed and NO_x emissions produced in each increment of the cycle. The results for each increment were then summed to obtain the miles per gallon and emissions for the cycle. The tables of brake specific fuel consumption and brake specific emissions needed in the model can be based either on steady-state engine dynanometer data or on results of the hydrogen generator/engine system model.

A third model used in this study was the Blumberg-Kummer cycle analysis program. The program incorporates the modified Zeldovitch kinetics mechanism for NO_x production into a general thermodynamic analysis of a spark-ignited internal combustion engine cycle. It is possible to predict quantitatively the NO_x emissions, mean effective pressure, horsepower, specific fuel consumption, and thermal efficiency as a function of fuel type, equivalent ratio, percent exhaust gas recirculation (EGR), compression ratio, intake manifold temperature and pressure, RPM, combustion interval, and spark advance.

The Blumberg-Kummer model was used to provide a theoretical basis for the thermal efficiency relationship used in the hydrogen generator/engine analysis. The effects of compression ratio changes on fuel consumption and NO_x emissions were also estimated using this model.

D. PERFORMANCE POTENTIAL AND SYSTEM CAPABILITY (EPA TASK F)

1. Introduction

Using the engine dynamometer data from the hydrogen generator/engine tests reported in Section II C, and the analysis techniques described in Section III C, the potential of the hydrogen generator/engine system was evaluated based on the lean performance of the 350-CID Chevrolet V-8 used in this study. Four control strategies were considered: three constant hydrogen flow rate cases, and one variable hydrogen flow-rate strategy. The sensitivity of fuel consumption and NO_x emissions to the parasitic loads imposed by the hydrogen generator subsystem were studied. The effects of increased compression ratio and improved lean limit operation of the V-8 on the hydrogen generator/engine system performance were also evaluated.

2. Control Strategies

The control strategies considered can be explained using Figure 106, which shows the engine breathing constraint and equipment lean limit constraint. The most desirable operating points for the hydrogen generator/engine system lie on the left boundary of the operating regime since this leads to the highest thermal efficiency and helps control NO_x emissions. For the constant hydrogen flow-rate strategy, the system operates along path ABC with one hydrogen flowrate. For maximum engine power, the engine operating point corresponds to an equivalence ratio of 1.0 and wide-open-throttle (WOT) represented by point A. Power output is reduced by equivalence ratio throttling along line AB, the WOT engine constraint. Further reductions in power are obtained by air

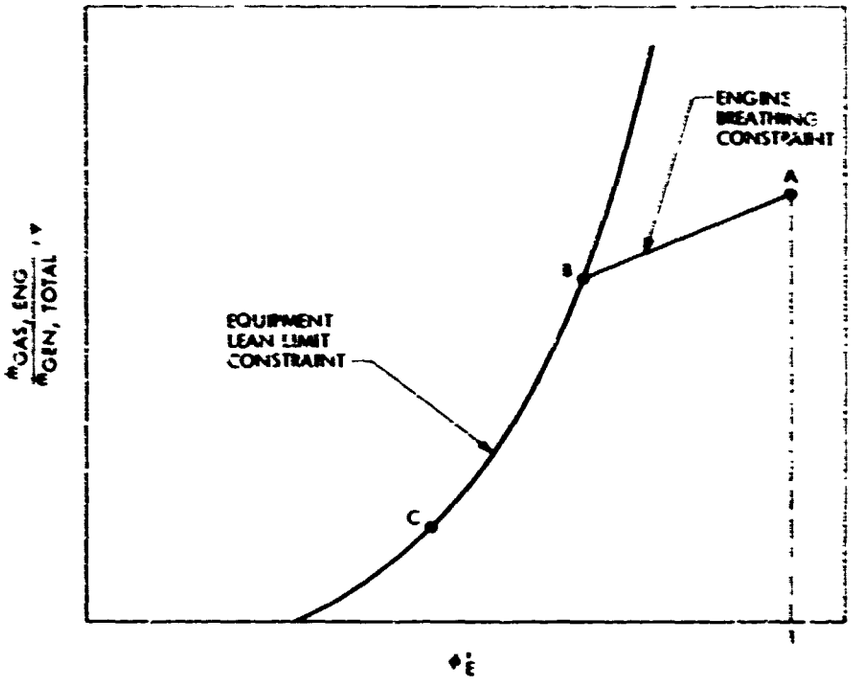

Fig. 106. Generator/engine system control strategy

and equivalence ratio throttling along line BC, which is also the equipment lean-limit constraint.

For the variable hydrogen flowrate strategy, the hydrogen generator flowrate is assumed to vary over the range necessary to supply from 0.5 to 1.5 lbm/hr of hydrogen to the engine. Again this control strategy can be represented by the path ABC in Figure 106. For maximum power, the engine operating point corresponds to an equivalence ratio of 1.0 and WOT with the minimum hydrogen-generator flowrate. Power is reduced by equivalence ratio throttling along line AB while maintaining WOT and minimum generator flowrate. When the equipment lean limit is reached at point B, further power reductions are obtained by moving along line BC by increasing hydrogen generator flowrate and decreasing engine gasoline flow rate while maintaining WOT. This operating mode continues until the maximum hydrogen generator flowrate is reached at point C. Further power reductions are obtained by air throttling while simultaneously reducing hydrogen generator flowrate and engine gasoline flowrate to maintain operation at point C. For the variable flow-rate strategy, the generator is assumed to respond instantaneously to changing hydrogen demands.

3. Nominal FDC Performance Prediction

Using a constant hydrogen flow-rate control strategy and fuel consumption and emissions data from engine dynamometer tests, the performance of the hydrogen generator/engine system over the urban driving cycle was estimated, using the driving cycle computer simulation program. The results of these calculations are given in Table 12 along with similar results for the stock engine and the Autotronics-modified engine running on gasoline only.

Table 12. Predicted urban driving cycle performance

Parameters	Fuel Economy		NO_x Emissions
	MPG	Percent Improvement	GM/MI
Stock engine	12.11	0	2.16
Autotronics-modified engine	13.82	14.1	5.54
Hydrogen generator/engine 0.5 lbm/hr hydrogen	14.14	16.8	1.29

NOTE: Predictions used engine dynamometer data.

The results for hydrogen flowrates of 1.0 and 1.5 lbm/hr are not given since the BMEP/RPM range needed on the federal driving cycle (FDC) cannot be met satisfactorily with these flowrates because of the high heating value of the generator products. The case using 0.5 lbm/hr of hydrogen shows a 16.8 percent improvement in fuel economy and reduced NO_x emissions when compared with the baseline stock engine.

4. FDC Performance Predictions with System Losses

Several components in the hydrogen generator subsystem require power inputs from the engine for their operation. Calculations were made to assess the effect of these parasitic losses on generator/engine performance. The nominal hydrogen generator parasitic loads were defined in Task B, Section III. B., as a function of generator flowrate. A range of load requirements for each generator component was considered to determine the sensitivity of system performance to variations in these parasitic loads. The load variations

considered were given in Table 9. Because system performance is insensitive to heat exchanger effectiveness, no variation in this parameter was considered.

Using the fuel consumption and NO_x emissions calculated with the hydrogen generator/engine system model, the system performance over the urban driving cycle was calculated with the driving cycle computer simulation program. Results for the current engine are shown in Table 13 for 0.5 and 1.0 lbm/hr hydrogen flowrates and for the variable hydrogen flow-rate control strategy.

Results are given for no parasitic loads, minimum, nominal, and maximum parasitic loads. For the range of parasitic loads considered, there is no significant effect on fuel consumption and NO_x emissions of the system.

The case corresponding to a hydrogen flowrate of 1.5 lbm/hr is not presented since the BMEP/RPM range needed for the driving cycle cannot be

Table 13. Effect of hydrogen generator parasitic loads on urban driving cycle performance

Configuration			Fuel Economy		NO_x Emissions
Engine	Generator System	Hydrogen Flow (lbm/hr)	MPG	Percent Improvement	(GM/MI)
Baseline	No Penalty	0.5	14.69	21.3	1.30
		1.0	14.99	23.8	0.86
		Variable	14.43	19.2	0.43
Baseline	Min Penalty	0.5	14.47	19.5	1.38
		1.0	14.60	20.6	0.97
		Variable	14.06	16.1	0.50
Baseline	Nom Penalty	0.5	14.41	19.0	1.38
		1.0	14.58	20.4	0.98
		Variable	14.04	15.9	0.50
Baseline	Max Penalty	0.5	14.25	17.7	1.38
		1.0	14.52	19.9	1.00
		Variable	13.99	15.5	0.51

provided by this generator flowrate. The variable hydrogen flow-rate strategy used the entire hydrogen generator flow rate range from 0.5 to 1.5 lbm/hr of hydrogen.

5. FDC Performance Predictions with System Improvements

To further assess the potential of the hydrogen generator/engine system, the effects of increased compression ratio and improved equipment lean limit on system performance over the urban driving cycle were evaluated. The two lean-limit improvement cases considered are shown in Figure 107. For a given fuel mixture, these cases represent a movement of the equipment lean limit 50 percent and 75 percent of the distance (in ϕ) from its current value toward the calculated lean limit for the mixture. The driving cycle results for these cases are given in Table 14 considering nominal parasitic loads.

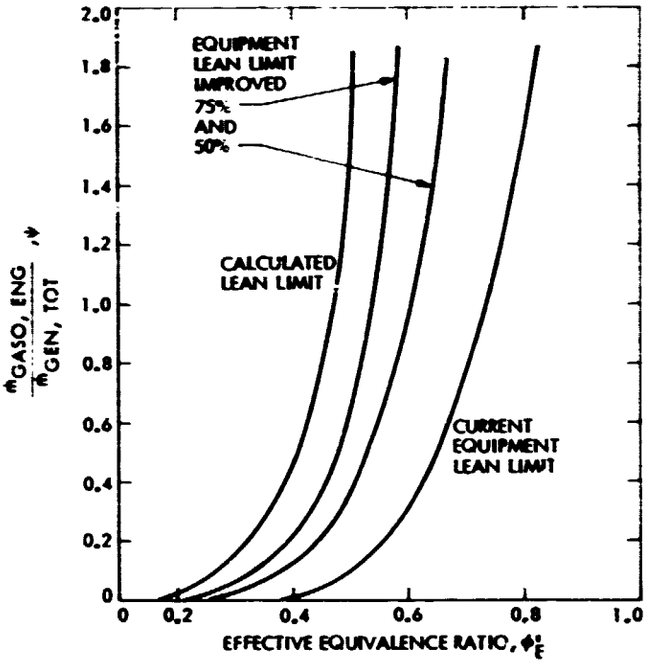

Fig. 107. Two lean-limit improvement cases considered

Table 14. Effect of engine improvements on urban driving cycle performance

Configuration			Fuel Economy		NO_x Emissions
Engine	Generator System	Hydrogen Flow (lbm/hr)	MPG	Percent* Improvement	GM/MI
Lean Limit Improved 50%	Nom Penalty	0.5	14.91	23.1	0.27
		1.0	14.85	22.6	0.85
		Controlled	14.56	20.2	0.27
Lean Limit Improved 75%	Nom Penalty	0.5	15.07	24.4	0.29
		1.0	14.93	23.3	0.86
		Controlled	14.84	22.5	0.29
Compr. Ratio = 10.0:1 Lean Limit Improved 75%	No Penalty	0.5	15.77	30.2	0.17
		1.0	15.83	30.7	0.71
		Controlled	15.56	28.5	0.17
Compr. Ratio = 10:0:1 Lean Limit Improved 75%	Nom Penalty	0.5	15.47	27.7	0.20
		1.0	15.41	27.3	0.70
		Controlled	15.20	25.5	0.20

*Relative to the stock 1973 vehicle which was used for this program.

Improvements in the equipment lean limit of the Autotronics-modified engine have been demonstrated in work sponsored by the Department of Transportation Systems Center, Ref. 10, using gasoline as the fuel. Modifications were made to reduce combustion duration by increasing combustion chamber turbulence and improving the ignition system for lean mixtures. The peak thermal efficiency for the improved engine operating on gasoline occurred at an equivalence ratio of 0.75 compared with the 0.85 equivalence ratio for the Autotronics-modified engine which was used for the hydrogen generator/engine data previously discussed. Performance improvements similar to those

demonstrated with gasoline should be realized in the hydrogen generator/engine system utilizing the improved engine. It is expected that this improved system will yield lean limit data close to the 50 percent improved lean limit curve in Figure 107.

The effect of increasing compression ratio from 8.5 to 10.0 was evaluated for the no parasitic load and nominal parasitic load cases, assuming the 75 percent improved lean limit operating constraint. The results of these calculations are given in Table 14. With the engine improvements specified, the ultimate hydrogen generator/engine system is predicted to yield a 28 percent increase (relative to the stock 1973 vehicle) while controlling the NO_x emissions to 0.2 gm/mi over the urban driving cycle. The performance improvements of Table 14 are in addition to those gains resulting from other vehicle modification, such as weight reduction, rear axle ratio changes, radial tires, etc.

It should be noted that while the increased compression ratio is for lean operation, it is possible that it would result in knock-limited performance at higher equivalence ratios and thus lead to a reduction in the maximum power output of the engine. There is some indication from CFR tests that the presence of hydrogen in the generator products increases the knock-limited compression ratio for all equivalence ratios. Further work is required to determine the compression-ratio limitations of the hydrogen generator/engine system.

6. Calculated Contour Plots

For each calculation of mileage and emissions over the FDC, contour plots of BSFC and $BSNO_x$ as functions of Brake Mean Effective Pressure (BMEP) and RPM were calculated. Typical examples are shown as Figures 108 and 109.

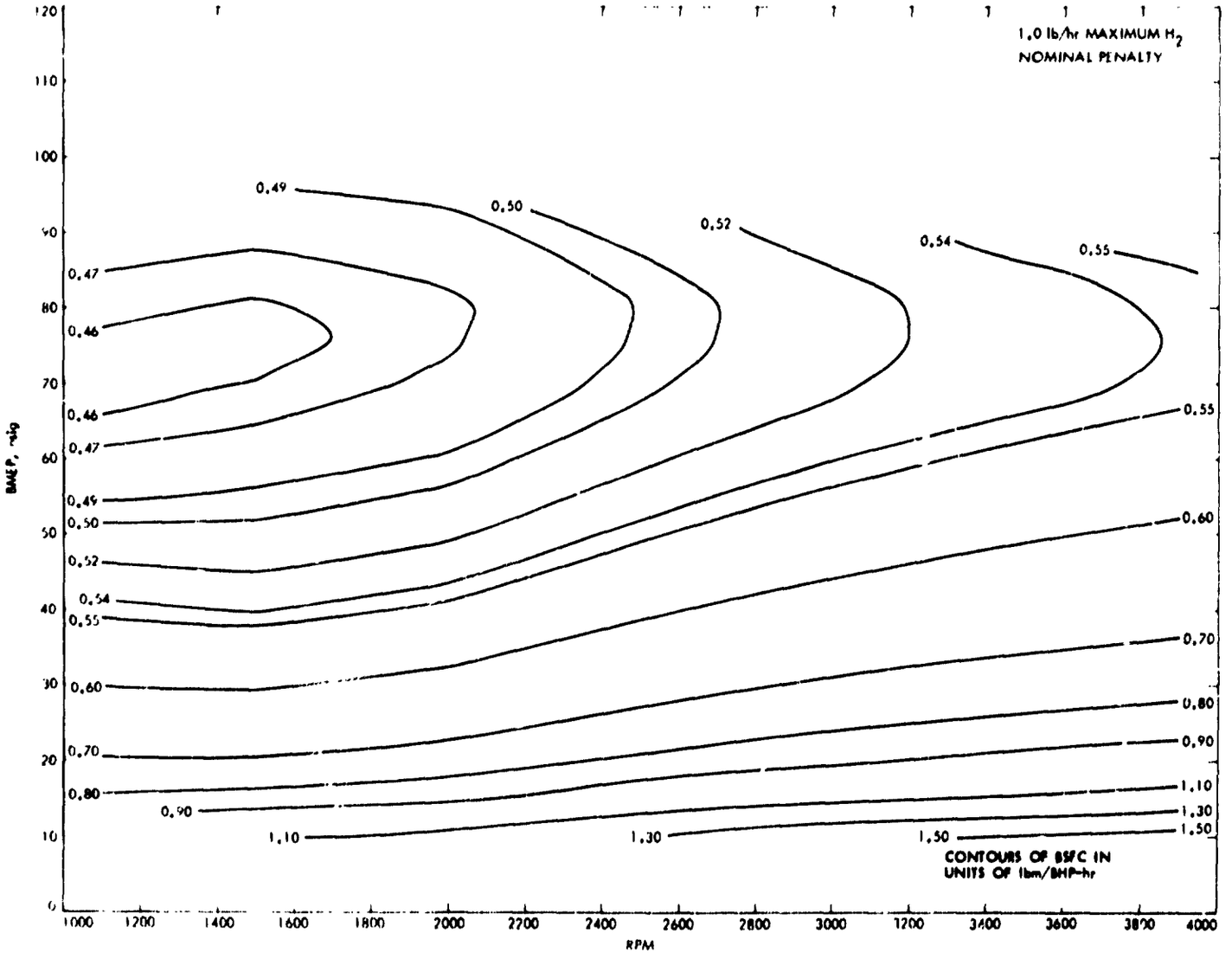

Fig. 108. BSFC contours

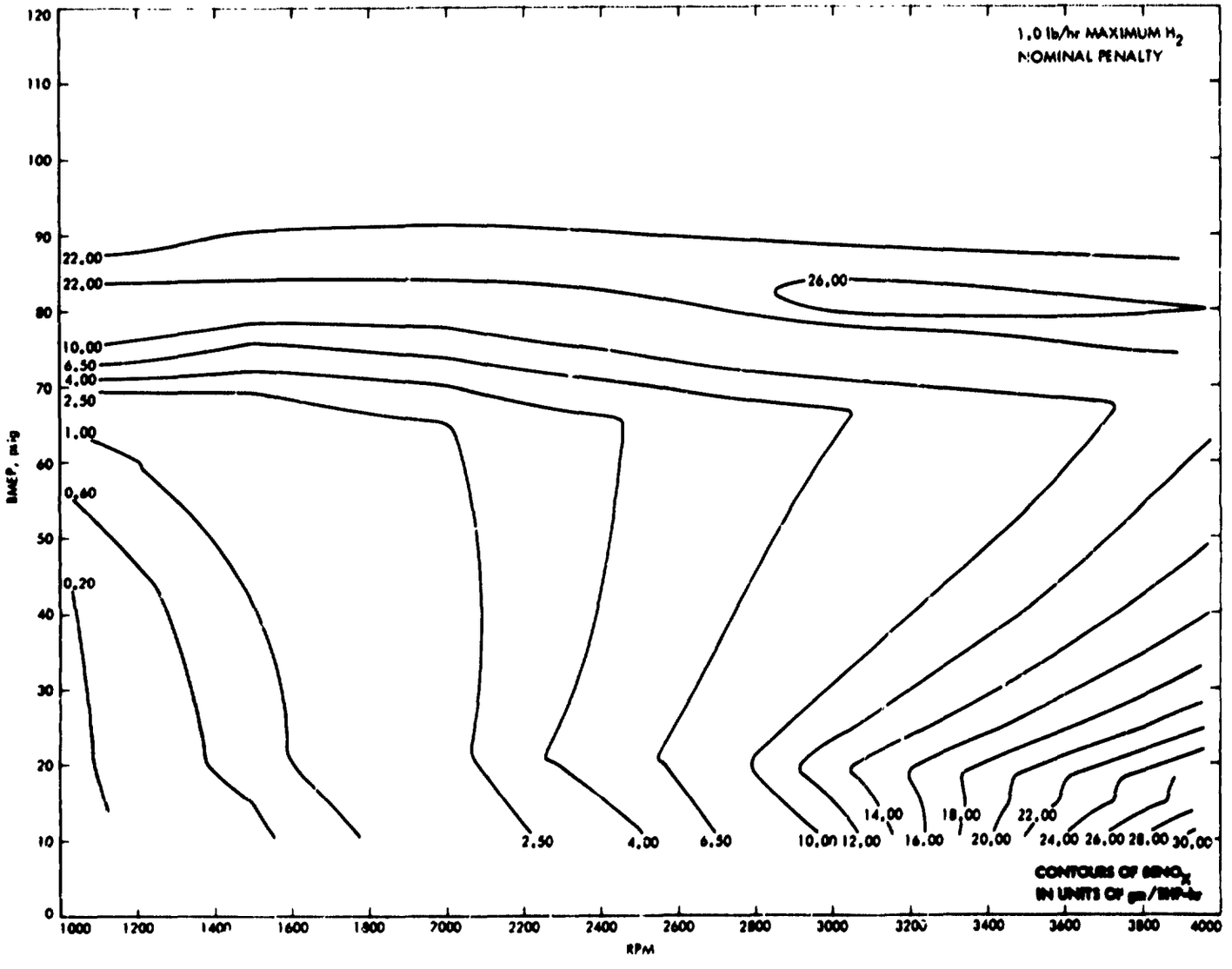

Fig. 109. $BSNO_x$ contours

7. Conclusions

Based on these analyses, two major conclusions may be drawn:

1) Integration of a hydrogen generator with an unmodified 1973 Chevrolet 350 CID V-8 engine is predicted to provide a 15% improvement in the mileage of a 1973 Chevrolet Impala and a reduction in NO_x emissions to 0.5 gm/mile. The mileage improvement may be as high as 20% and the NO_x emissions may be as great as 1.5 gm/mi. Mileage and NO_x emissions predictions were for operation over the Urban Federal Driving Cycle.

2) If the equipment lean limit of this engine were improved significantly and if its compression ratio were increased to 10:1 from 8.5:1, mileage was predicted to improve 25% to 27% and NO_x emissions were predicted to be in the range of 0.2 to 0.7 gm/mi.

E. ESTIMATED UNDERHOOD TEMPERATURES (EPA TASK A)

1. Introduction

The hydrogen generator, because it contains a high temperature reaction, has the potential of increasing the already high vehicle underhood temperatures. To estimate the magnitude of this temperature increase, a brief analysis was performed. At the minimum hydrogen-generator flowrate, this temperature increase is estimated to be less than 4°F, and at the maximum flowrate to be less than 10°F.

Figure 110 shows the predicted steady-state engine compartment maximum temperatures for a vehicle powered with the 350 CID Chevrolet V-8 engine. The figure shows that a baseline compartment temperature of 110°F was assumed for the stock engine powered vehicle at all engine speed conditions and 60°F ambient temperature.

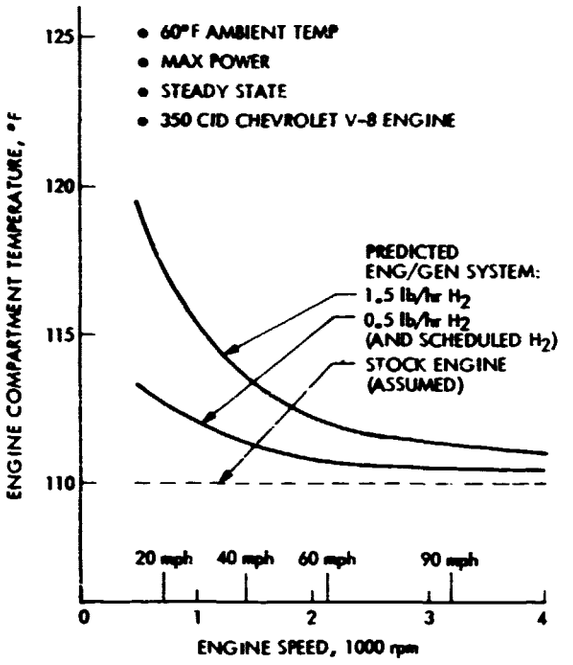

Fig. 110. Maximum engine compartment temperatures

2. Calculation Scheme

Baseline heat rejection rates at maximum power for the stock engine were obtained from stock test data assuming 52% of the consumed fuel energy content was rejected to the engine coolant. If the heat rejected to the engine coolant were considered proportional to the temperature increase of the air flowing into the underhood area, the following relation can be used:

$$\dot{Q}_R = K(110-60) \text{ Btu/hr}$$

where:

Q_R = Engine heat rejection rate (Btu/hr)

K = Overall heat-transfer coefficient (Btu/hr - °F)

110 = Engine compartment air perature (°F)

60 = Ambient air temperature (°F)

Engine compartment temperatures for a vehicle equipped with the hydrogen-enriched fuels system were predicted by using the above relation, modified to account for the heat loads imposed by the hydrogen generator and its auxiliary components. The pump/motor and air compressor heat loads were assumed to consist of component mechanical or thermal inefficiencies which amount to 0.7 HP at 0.5 lb/hr H_2 delivery and 1.15 HP at 1.0 lb/hr H_2. The generator heat load consisted of the heat transfer required to cool the product gas from reactor chamber temperature to generator discharge temperature. Generator heat balance calculations (which included allowance for generator air preheat) predicted engine compartment heat loads of 6,244 Btu/hr at 0.5 lb/hr H_2 and 19,811 Btu/hr at 1.5 lb/hr H_2. The following equations were used to combine engine heat rejection rates with generator system heat-rejection rates for calculation of engine compartment steady-state temperature.

$$\dot{Q}_R + \dot{Q}_{Mech} + \dot{Q}_{Gen} = K(T_{ec} - 60)$$

or

$$T_{ec} = \frac{(\dot{Q}_R + \dot{Q}_{Mech} + \dot{Q}_{Gen})}{K} + 60$$

where:

T_{ec} = Engine compartment temperature (°F)

Q_R = Engine heat rejection rate (Btu/hr)

Q_{Mech} = Heat rejection rate due to H_2 generator system inefficiency (Btu/hr)

Q_{Gen} = Generator product gas heat load (Btu/hr)

$K = \frac{\dot{Q}_R}{(110-60)}$ = Overall heat-transfer coefficient (Btu/hr-°F)

60 = Ambient temperature (°F)

3. Results

The results of these calculations are shown in Figure 110. One of these curves shown is appropriate to both the 0.5 lb/hr H_2 and variable H_2 flow-rate cases, since maximum engine power is achieved on the schedule with 0.5 lb/hr H_2. The other curve shown is for the maximum hydrogen-generator flow-rate case, that containing 1.5 lbm/hr of hydrogen in the product gas.

SECTION IV

CONCLUDING REMARKS

Detailed summary discussions are presented at the conclusion of Sections IIB., IIC., IID., for the experimental work and in Sections IIIB., IIIC., IIID., and IIIE for the analytical work. Remarks of a summary nature also appear in the Executive Summary section, and in the Introductory section, Section I.

From these various sources, concluding remarks based on particularly significant findings are presented below.

A catalytic hydrogen generator has demonstrated hydrogen yields of 89-98% of theoretically possible values over a hydrogen flowrate range of 0.4 to 2.1 lbm/hr. No water or steam was required for this performance. The catalyst volume used was later determined to be larger than required indicating that a further economy of operation and design/manufacturing is possible. The operating temperature of the generator provides a satisfactory safety margin and will allow the use of inexpensive structural materials. Equilibrium hydrogen output was achieved in approximately 60 seconds with sufficient output stream energy content to achieve a V-8 engine start after 20 seconds.

A hydrogen generator/V-8 engine combination was operated smoothly with no evidence of deleterious effects on engine hardware and no evidence of safety problems as a result of the presence of the hydrogen gas.

The trends of increased engine efficiency and decreased NO_x emissions in the ultra-lean regime, which were observed with bottled hydrogen, were also observed with hydrogen-gas-generator products.

The trend of increasing hydrocarbon emissions with ultra-lean combustion, reported by several investigators, was observed with the hydrogen-enriched

fuels. Increasing amounts of hydrogen has a beneficial result on the problem but under no operating conditions were the HC emissions below the equivalent EPA 1978 standard.

Large quantities of CO emissions were observed in conjunction with use of the hydrogen-generator products. CO emissions were extremely low when pure hydrogen was used and, hence, the obvious conclusion is the CO contained in the generator products is not completely oxidized in the engine combustion chamber

Brake specific fuel consumption (including the losses associated with the gas generator) decreases of 6 - 15% from the stock engine were observed over most of the engine BMEP - RPM operating regime.

Critical compression ratio tests using a CFR test engine indicate that compression ratio increases to a value of ~10:1 are possible in the ultra-lean combustion region and that thermal efficiency will also increase with increasing values of the compression ratio. Increased compression ratio resulted in no significant change in either the NO_x or unburned hydrocarbon emissions.

The integration of a hydrogen generator with an unmodified V-8 engine having a 8.5:1 compression ratio is predicted to improve fuel economy 15% with NO_x emissions of 0.5 gm/mi over the FDC. This performance is relative to an unmodified but otherwise identical 1973 Chevrolet Impala. The integration of a hydrogen generator with a V-8 engine having a 10:1 compression ratio and an improved equipment lean limit is predicted to improve fuel economy 25% with NO_x emission of 0.2 gm/mi on the FDC relative to an unmodified 1973 Chevrolet Impala.

A model of the hydrogen generator and its attendant accessories has been developed to produce an estimate of the loads this subsystem will impose on the rest of the vehicle system. The maximum additional loads imposed on the engine by the incorporation of a hydrogen generator are estimated to be from 1.6 to 2.3 HP at maximum hydrogen-generator flowrate.

An analytical technique for correlating and replicating the data produced during test of a hydrogen generator/engine system has been developed and verified. This technique provides the means for examining the future potential of the hydrogen-enriched fuels concept.

A model permitting simulation of the performance of a vehicle on the Urban Federal Driving Cycle was develcped and shown to predict, from steady-state engine data, the mileage and NO_x emissions of a vehicle driven over the cycle to within 14% and 8%, respectively, when compared to vehicle, chassis-dynamometer results.

The hydrogen generator contains a high temperature reaction and has the potential of increasing the already high vehicle underhood temperatures. To estimate the magnitude of this temperature increase, a brief analysis was performed. At the minimum hydrogen-generator flowrate, this temperature increase is estimated to be less than $4^{\circ}F$, and at the maximum flowrate to be less than $10^{\circ}F$.

REFERENCES

1. Chemical Engineering, Vol. 24, January 3, 1966.

2. Nitrogen, Vol. 37, No. 5, 1966.

3. Gordon, Sanford, et al., Computer Program for Calculation of Complex Chemical Equilibrium Composition. NASA Lewis Research Center Report SP 273, 1971.

4. "ASTM Manual of Engine Test Methods for Rating Fuels," American Society for Testing Materials, March 1948.

5. Hoehn, F. W. and Dowdy, M., "Feasibility Demonstration of a Road Vehicle Fueled with Hydrogen-Enriched Gasoline," presented at 9th IECE Conference, August 26-30, 1974.

6. Stebar, R. F. and Parks, F. B., "Emission Control with Lean Operation Using Hydrogen Supplemented Fuel," SAE 740187, Feb/March 1974.

7. Obert, Edward F., Internal Combustion Engines: Analysis and Practice, pgs. 143-145, 265-268, International Textbook Company, 1953.

8. "Systems and Equipment," ASHRAE Guide and Data Book, 1967.

9. Pedersen, N. F., "The Statistical and Analytical Approach to Determining Pump Performance," presented at Aerospace Fluid Power Conference, Detroit, Michigan, October 28-29, 1963.

10. Dowdy, M., et al., Final Report – Lean Mixture Engines Testing and Evaluation Program: Vol. I. Executive Summary; Vol. II. Comprehensive Discussion; and Vol. III. Appendices; prepared for U.S. Department of Transportation by Jet Propulsion Laboratory; To be published.